Seal Binder Rheology at Intermediate Temperatures and Influence on Stone Orientation

Herline van der Spuy

Thesis presented in the partial fulfilment
of the requirement for the degree of
Master of Engineering(Civil Engineering)
at the University of Stellenbosch

Supervisors: Prof. K.J. Jenkins and Dr. E.S. Goosen

April 2022

Declaration

By submitting this thesis electronically, I declare that the entirety of the work contained therein is my own, original work, that I am the sole author thereof (save to the extent explicitly otherwise stated), that reproduction and publication thereof by Stellenbosch University will not infringe any third party rights and that I have not previously in its entirety or in part submitted it for obtaining any qualification.

Date: April 2022

Acknowledgements

I would like to thank Professor KJ Jenkins for acting as my study leader and mentor during my research. Your guidance and understanding was really unbelievable.

Dr ES Goosen, I would very much like to thank you for all the patience, help and assistance you have provided. It is much appreciated.

I would like to acknowledge the laboratory manager and staff. Mnr GP Nel, who made sure that I had everything that I required in the laboratory.

To my family and friends, I deeply appreciated your patience and support. Especially my sister, Philippa, who supported me all the way, and kept an eye on me.

Thank you to Stellenbosch University for providing the necessary equipment and facility.

I am grateful for all the post graduate students for keeping me motivated and for the great atmosphere in die office.

Abstract

The conditions of seal binders at intermediate temperatures are important to consider when constructing a road. The condition of a binder at construction time influences the performance of the binder in its lifetime. The intermediate temperature conditions of a binder, at construction time, influences the road performance. Previous work has failed to address how the creep and recovery of a binder at intermediate temperatures influences the performance of the binder for the long-term.

The approach to this study was to evaluate different types of binders used in South Africa, and their performance at various temperatures, with the focus on intermediate temperatures. Original and short-term aged conditions were evaluated to cover the property changes from the refinery to the construction period. The creep and recovery characteristics are analysed to determine the behaviour of the binder, and how it could link to stone orientation.

The materials used in this study was an unmodified binder and four modified binders. The modified binders consisted of two elastomers and two rubber binders. The Bending Beam Rheometer was used to obtain data at cold temperatures, and the Dynamic Shear Rheometer for intermediate and high temperatures. The Multiple Stress Creep and Recovery (MSCR) test was used to obtain the non-recoverable creep compliance (J_{nr} and the recovery (%R)).

Results showed that the type and degree of modification significantly influences the performance of binders at intermediate temperatures. The modified binders demonstrated characteristics that would increase the relationship between the binder and stones, which would affect stone orientation in the surface layer.

Opsomming

Die toestand van bitumin-bindmiddels by intermediêre temperature is belangrik om in ag te neem wanneer ’n pad gebou word. Die toestand van ’n bindmiddel tydens konstruksietyd beïnvloed die werkverrigting van die bindmiddel in sy leeftyd. Die intermediêre temperatuurtoestande van ’n bindmiddel, tydens konstruksietyd, beïnvloed die padverrigtinge. Vorige werk het versuim om aan te spreek hoe die kruip en herstel van ’n bindmiddel by intermediêre temperature die werkverrigting van die bindmiddel vir die langtermyn beïnvloed.

Die benadering tot hierdie studie was om verskillende tipes bindmiddels wat in Suid-Afrika gebruik word, en hul werkverrigting by verskillende temperature te evalueer, met die fokus op intermediêre temperature. Oorspronklike en korttermyn-verouderde toestande is geëvalueer om die eienskap-veranderinge van die raffinadery tot die konstruksietydperk te dek. Die kruip- en herstelkenmerke word ontleed om die gedrag van die bindmiddel te bepaal, en hoe dit met kliporiëntasie kan skakel.

Die materiaal wat in hierdie studie gebruik is, was ’n ongemodifiseerde bindmiddel en vier gemodifiseerde bindmiddels. Die gemodifiseerde bindmiddels het bestaan uit twee elastomere en twee rubberbinders. Die Buigbalk Rheometer is gebruik om data by koue temperature te verkry, en die Dynamic Shear Rheometer vir intermediêre en hoë temperature. Die Multiple Stress Creep and Recovery (MSCR)-toets is gebruik om die nie-herstelbare kruip-nakoming (J_{nr} en die herstel (%R)) te verkry.

Resultate het getoon dat die tipe en graad van modifikasie die werkverrigting van bindmiddels by intermediêre temperature aansienlik beïnvloed. Die gemodifiseerde bindmiddels het

kenmerke getoon wat die verhouding tussen die bindmiddel en klippe sou verhoog, wat kliporiëntasie in die oppervlaklaag sou beïnvloed.

Contents

List of Figures

List of Tables

Chapter 1

Introduction

1.1 Background

In South Africa, the traffic volume and vehicle loads have been increasing over the past decade. Pavement performance has become an integral part of pavement management systems. The surfacing layer of the pavement structure consists of either asphalt or seals. Seals are more often applied in South Africa, than asphalt surfacing - especially in rural environments. For example, the surface of flexible pavement network is South Africa includes a seal: asphalt surfacing: asphalt ratio of 80:20. Thus, seal performance is an important function in the South African road system.

The function of a seal is to provide a durable, waterproof and skid-resistance road surface. Over the years, the industry and research have developed many materials and application methods that increased seal performance. As a result, there are a variety of guidelines that have been created for each step in the pavement construction process: the design, construction and maintenance of roads.

South Africa has a wide range of temperatures. For each region, different methods and materials must be utilised to ensure an efficient road surface. The bituminous material which is used in asphalt and seal work has different properties and behaviour at different loading times and temperatures. An important factor to consider is the bitumen's condition from the refinery to

the construction site and the initial trafficking period. A binder's characteristics can change during this time, and it is thus crucial to take the changes into consideration. It cannot be expected of the binder to perform on-site the same as it did in the laboratory environment. Tests that are performed in the laboratory are run under set conditions. On-site, conditions yield significant variability in terms of few main sources, namely materials, climate, traffic and construction.

Rutting is a form of permanent deformation failure of a bituminous surfacing layer. One of the tests that evaluate a binder's rutting potential is the Multiple Stress Creep and Recovery (MSCR) test. Two parameters that come from the MSCR test are the non-recoverable Creep Compliance (J_{nr}) and the percentage recovery (%R). The J_{nr} is a good parameter to use to evaluate a binder's potential to resist permanent deformation. The %R is an indicator to see how much of the binder recovers after an applied load.

Measuring the rutting potential of binders at intermediate temperatures can be useful in the evaluation of binder performance at construction time. The hot binder is exposed to cooler temperatures and this can affect the property changes in the binder. It can also influence the binder's performance and stone embedment.

1.2 Problem Statement

There is a change in binder properties between factory and construction. These changes are often caused by the binder experiencing a range of temperatures. It is well known that temperature is one of the most influential factors regarding binder performance. For example, for every change of 6°C temperature, the binder stiffness typically doubles or halves. The properties of a binder at construction time can influence the performance of the binder in its lifetime. Not accounting for the changes in properties which the binder undergoes, seal surfacing failures will occur more often and result in high maintenance. There is a gap in research in seal rheology and binder performance at intermediate temperatures.

1.3 Objectives

The primary goal of this research project is to investigate the seal binder performance in terms of intermediate temperatures by evaluating the behaviour of three types of seals and their short term aged conditions. To achieve this goal, the following objectives are required:

- Assess low temperature behaviour using the Bending Beam Rheometer in order to evaluate susceptibility to cracking failure.
- Determine the Master Curves from the Dynamic Shear Rheometer and the Bending Beam Rheometer as a means of analysing the behaviour of binders at various temperatures and frequencies.
- Determine the J_{nr} and %R for each binder in its original and aged condition at intermediate temperatures to appraise the changes in permanent deformation characteristics.
- Obtain the durability parameters and evaluate the performance of each type of binder.

1.4 Limitations

This study has a number of limitations related the the research that are associated with technical and practical aspects as outlined below:

- Binders were limited to three types.
- This study is linked to another study regarding stone orientation, and thus bituminous binders were limited to only five.
- Time did not allowed for repetition tests, which could validate results.
- Knowledge related to rubber binder testing is limited as the material is still a novel product that is used in South Africa.
- Due to new testing conditions, some test procedures were adapted. This was done by recommendations from industry.
- The study excludes testing bitumen emulsion types, namely SC-E1, SC-E2 and CAT65.

- Long term ageing is not considered in this study.
- A multiple stress creep and recovery test is conducted at non-standard temperatures rendering results that cannot be measured against guideline limits.

1.5 Report Overview

The outline of this research study is as follows:

- **Chapter 2** focuses on the background and literature of bitumen, the modification of bitumen, bitumen rheology, rheological testing and modelling.
- **Chapter 3** discusses the experimental design and research methodology that was conducted in this study. Descriptions and explanations of test procedures are included in this chapter.
- **Chapter 4** entails the results and analysis procedures that were followed. As well as comparing and discussing the data.
- **Chapter 5** presents the conclusions and recommendations of the research.

Chapter 2

Literature

2.1 Seals

A seal is made up of a layer of bituminous binder that is sprayed onto the road and is thereafter covered with a layer of stones or sand (aggregate). It is important that the layer of aggregate is applied, and rolled, promptly after the sprayed binder. This is to make sure that there is good adhesion between the binder coat and the aggregate. The rolling action orientates the aggregate particles in such a way that it fills up the voids in the binder. This whole process is concluded by opening the road to traffic, which will ensure a reasonably water-resistant, dense pavement surface (TRH3, 2007). There are various types of seals, each with a different combination of various materials. Common seals are the single, double, Cape, and slurry seals. Figure 2.1 and 2.2 illustrates the different types of seals. According to the TRH3 (2007) surfacing seals have three main purposes:

- To provide a protective waterproof layer to the underlying layers of the pavement structure.
- To ensure the road surface can endure the damage caused by traffic and the environment.
- To provide the traffic with a sufficient skid resistance surface, as well as incorporating all possible weather conditions.

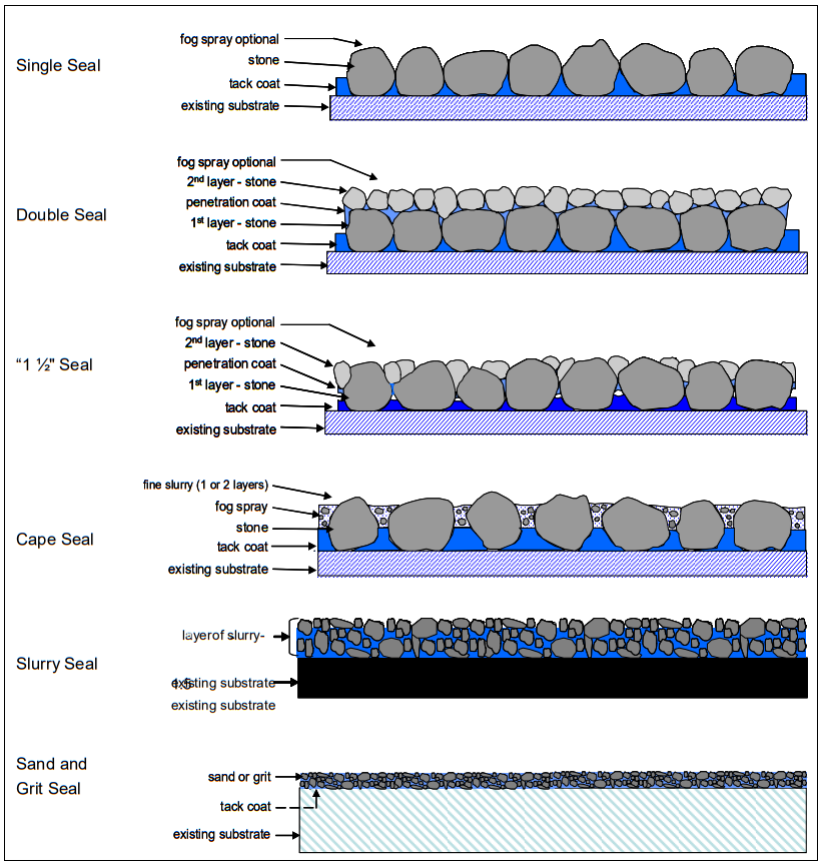

Figure 2.1: An illustration of seal types (TRH3, 2007)

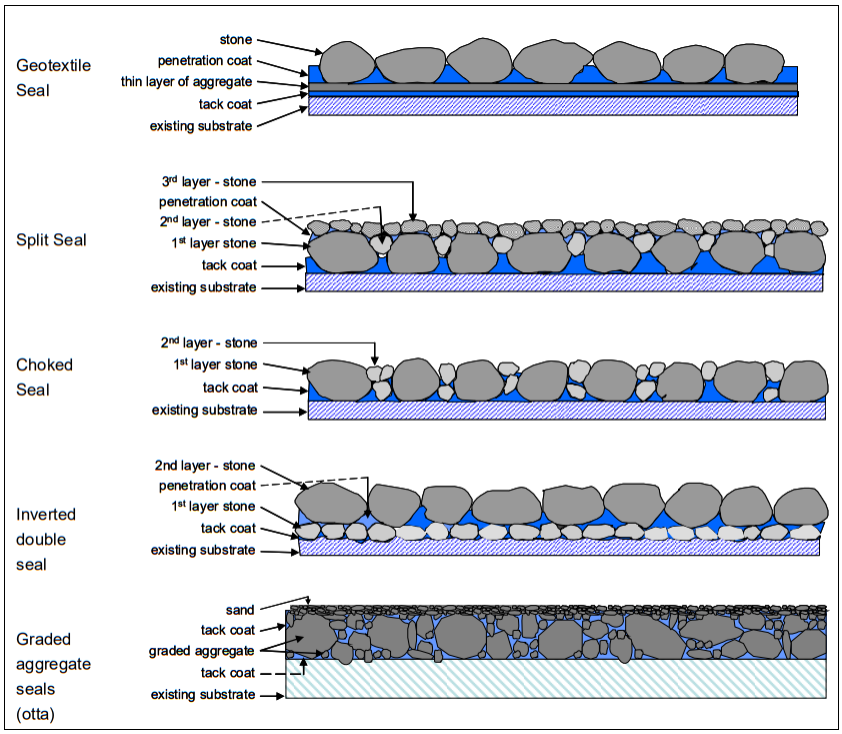

Figure 2.2: An illustration of seal types (TRH3, 2007)

In South Africa, the air temperatures can range from approximately -8°C up to 40°C (TRH3, 2007). A high temperature map of South Africa was created, using the Kriging interpolation method (O'Connell *et al.*, 2015). The data was obtained by utilising ThermalPads (a software developed by the CSIR), and temperature prediction algorithms that were developed by (Viljoen, 2001). Figure 2.3 and 2.4 display maps of isotherms of South Africa, as well as a main isotherm band that represents the SUPERPAVE grading classification. The north-western half of South Africa has a seven-day mean maximum temperature of 64°C and the south-eastern as 58°C. Generally road and air temperatures are affected by the altitude. From the south of the country to the north, the temperature increases slightly. The type and grade of a binder are set out by the road surface temperatures, which are, in turn, affected by the air temperatures (TRH3, 2007).

Factors relevant to this study that influence the performance of seals are:

- Pavement structure and condition
- Traffic
- Road geometry
- Design
- Materials

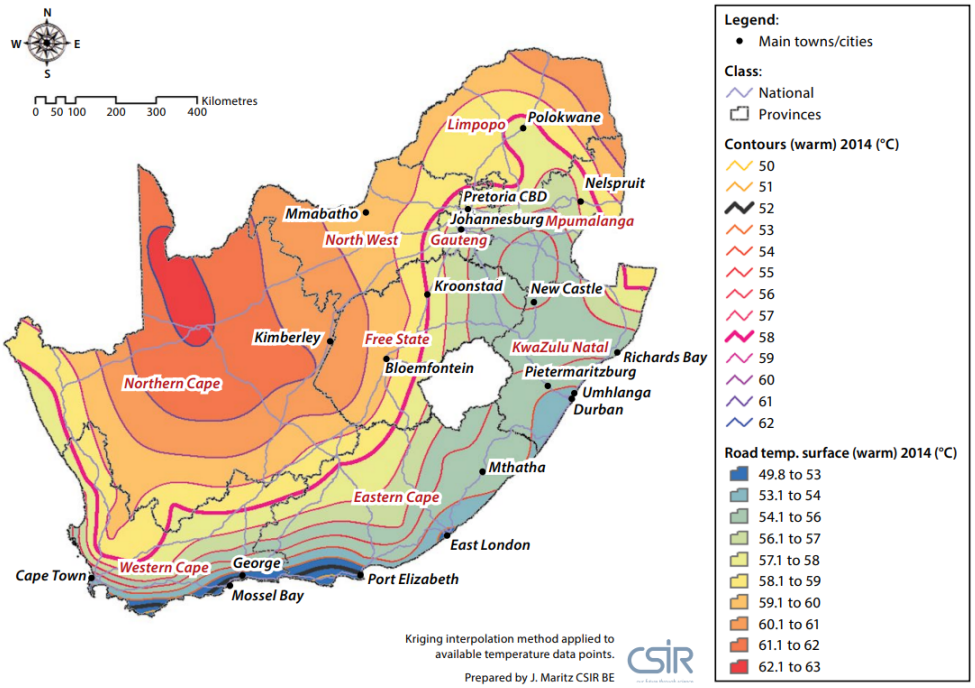

Figure 2.3: High pavement temperatures in South Africa (O'Connell *et al.*, 2015)

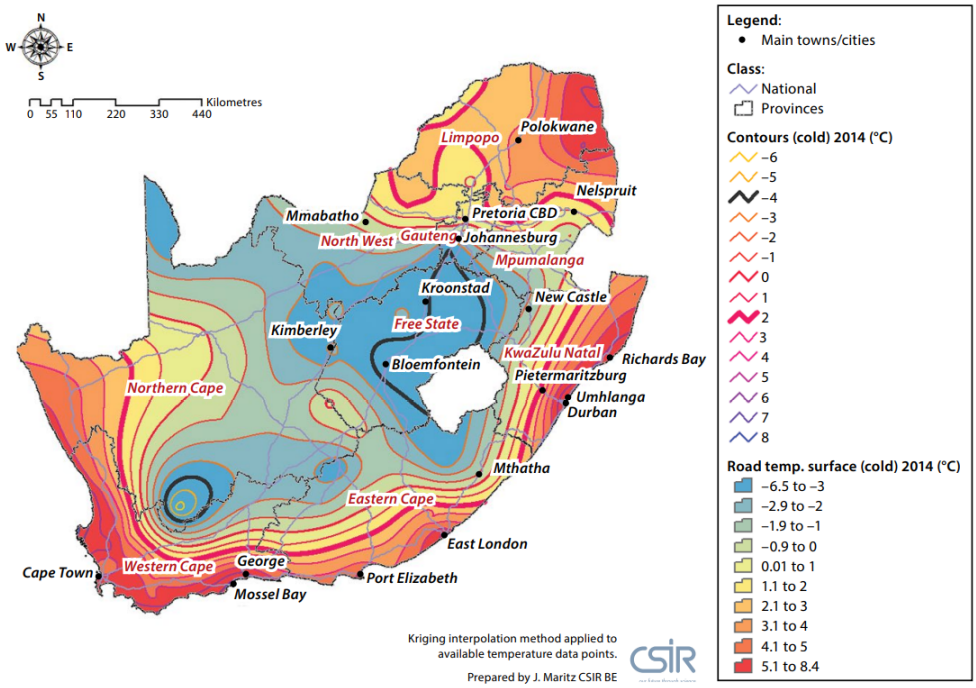

Figure 2.4: Cold temperatures of pavements in South Africa (O'Connell *et al.*, 2015)

2.1.1 Pavement Structure and Condition

Satisfactory seal performance is irrelevant if the supporting layers fail. Thus, to a certain extent, seal performance is governed by the structural sufficiency of the pavement layers below it, especially under the influence of traffic. A seal's function is to mainly provide an adequate wearing course and be water-resistant.

In the pavement structure, it is beneficial that the surfacing layer has flexural properties. In cold temperatures, when the seal is rigid, there is a higher risk of cracking. Together with traffic, temperature changes, moisture conditions, and some chemical reactions, the seal experiences variability in its rheological properties. These constant changes contribute to the binder's likelihood of shrinkage, and consequently, cracking failure (TRH3, 2007).

The type of material that is used as the base of a pavement structure, as well as the degree of compaction, affects the performance of the base. Thus, the resistance of aggregate penetration is dependent on the selection of base material and compaction thereof. High binder application rates can lead to the embedment of the surfacing aggregate into the base. This reduces the voids in the seal, and in turn, can result in bleeding or hydroplaning i.e. loss of skid resistance.

Along with aggregate embedment, aggregate orientation also plays a major role in the performance of seals. Stone orientation is discussed in further detail in Section 2.2.

2.1.2 Traffic

Traffic is one of the key factors that impact on seal binder performance. Traffic can be controlled by increasing or decreasing the speed limits, by designing a road network system that balances the number of vehicles on the road, and by dedicating lanes to vehicles with large loads. Undoubtedly, heavy vehicles have a larger impact on the seal binder than lighter vehicles. And as such, the type, number, and combination of different vehicles all contribute to how the seal will behave. Road geometry is interrelated to the influence of traffic, but other traffic factors that also play a role are (TRH3, 2007):

- **Volume:** The number of vehicles on the road, have an impact on various aspects of the seal. The wearing and polishing of the aggregate particles have the effect of reducing the skid resistance. The embedment of the stones results in the reduction of voids in the seal and consequently causes bleeding. Although, it is reported that there is a minimum num-

ber of vehicles that the seal requires per day. This is believed to keep the binder active and flexible.

- **Loading and vehicle type:** Naturally, heavy vehicles will have a larger impact on the road, especially concerning the embedment. The influence of the unbalanced weight of a heavy vehicle turning at an intersection can damage the surfacing, particularly when there are repeated loads. Surfacing failures such as debonding or ravelling are typical distresses that happen at turns or curves of the road.

- **Tyre pressures:** High tyre pressures influence the road, in the sense that there is a larger vertical stress that is induced on the surface. It was found that over the years, the average heavy vehicle tyre pressure has increased from 520 kPa to 700 kPa.

- **Speed and traffic distribution:** Slow-moving traffic (categorised as less than 40 km/h) will have a different effect on the surface than fast-moving traffic. Slow traffic will cause longer periods of loading, and in turn higher horizontal stresses, this is especially damaging to the surfacing with heavy vehicles. The load of vehicles is distributed to structural layers from the wheel paths. On a narrow road, there is little lateral movement of traffic and the load is concentrated to a specific wheel path. Wider roads offer more space for vehicles to move and subsequently, multiple wheels paths and greater load distribution.

2.1.3 Road Geometry

Road geometry encompasses elements such as gradient, sharp curves, intersections and road width. Steep slopes inadvertently cause slower moving traffic. As discussed above, slow-moving traffic can cause distress such as bleeding. The traction force of vehicles also result in debonding or flushing on the surface. Horizontal stresses are induced by sharp curves or turns at intersections. These stresses can lead to the ravelling or slippage of the surfacing. Vehicles that take sharp turns around corners can also contribute to the stone loss. As mentioned before, the width of the road is important to distribute the load from the wheel paths.

2.1.4 Design

The design process is an important factor that affects seal performance. The design of a seal should incorporate and accommodate all probable scenarios that can occur in the environment.

2.1.5 Materials

A seal consists of two materials: Aggregate and binder. Both materials have their own functions that contribute to the seal's performance.

Aggregate

The aggregate in the surfacing has four main functions (TRH3, 2007):

- It provides the surface with skid-resistance.
- It transfers the wheel load from the surfacing layer to the underlying pavement layers, as well as providing protection against the abrasion of the moving vehicles.
- To provide the binder with protection against the harmful ultra-violet rays of the sun.
- It provides the seal with a structure to allow for the binder's elastic behaviour, as well as providing enough voids which will prevent the binder from flushing to the surface.

The factors that affect the performance of the seal, regarding aggregates, according to the TRH3 (2007) are:

- **Spread rate:** As the aggregate provides protection to the substrate from the damage of the moving vehicles, a good spread rate is vital. It is expected that the aggregate should lie in a shoulder-to-shoulder formation, in a single layer in a uniform mosaic pattern.
- **The shape and size:** The shape of the aggregate influences the stability of the seal. A more angular aggregate will provide better interlocking abilities and more points of contact. This will ensure that the aggregate provides a good protective layer against traffic abrasion. The size of the stone particles affects how much of the binder will fill the voids. A smaller aggregate size has a greater possibility of the binder filling the voids.

- **Porosity and absorption:** A porous aggregate refers to the aggregate absorbing the binder's lighter fractions. This can then have the consequence of the binder being too brittle to retain the aggregate on the road.

- **The cleanness, dust content and adhesion characteristics:** It is essential that an aggregate has good adhesion characteristics. It will ensure that the bond between the binder and aggregate can hold throughout the expected lifetime of the seal. If an aggregate is not clean, or when dust is present, the adhesion abilities are adversely affected.

- **Strength, durability and wearing characteristics:** As mentioned previously, an aggregate's function is to provide strength and durability to protect the lower pavement layers. An aggregate is thus expected to be hard enough to provide ample protection against the abrasion of traffic. The hardness of the aggregate also affects the rate of wearing that takes place.

Bitumen Binder

A crucial characteristic that contributes to a seal's performance is adhesion. The level of adhesion between binder and aggregate can make or break a seal. Alongside the adhesion other important factors of the binder that contribute to the seal's performance are:

- **Binder type:** There are various binders that can be used in the construction of seals. They consist of penetration grade bitumen, bitumen emulsions, cut-back bitumens and modified bitumens. Each of these are selected based on the specific conditions and which seal would ensure the best performance.

- **The application rate of the binder:** There is a minimum and maximum amount of binder that should be applied for the construction of seals. For the seal to have optimal performance, the type of binder and volume of binder, as well as the aggregate shape and size should be determined pre-construction, while also considering the type of traffic and environmental conditions. Too little binder will cause the stones to be unstable and will not bind to the underlying surface. When the maximum amount of binder is exceeded, and the voids are overfilled after compaction, flushing and bleeding can occur, which in turn will reduce skid resistance.

- **The grade of the binder:** The selection of the proper grade of conventional binder is important to ensure optimum performance of the seal. The selection process is dictated by the climate conditions at construction time, as well as the long-term ambient temperatures which the binder will experience.
- **The viscosity of the binder at the time of application:** To ensure a uniform application rate, the viscosity of the binder should be appropriate. As viscosity varies with temperature, and each grade of binder has its own temperature/viscosity curve, the selection of binder is based on its viscosity properties.

2.2 Stone Orientation

The embedment and orientation of aggregates in seals during the construction period play a major role in the performance of the seal. The orientation of the aggregate in seals is generally dependent on the adhesion between the binder and stone particles (Van Zyl and Jenkins). After compaction is done by a steel wheel or pneumatic tyres, the aggregate particles orientate themselves further by the initial trafficking (Von Benecke, 2021). The factors on which orientation is based, are (Von Benecke, 2021):

- Spread rate of the aggregate.
- The type of aggregate.
- Aggregate application rate.
- The type of compaction.
- The number of roller passes during construction or compaction blows.

In addition to the rheological factors:

- Binder rheology.
- Binder type.
- Temperature of the binder in service.

- The relationship between temperature and viscosity of the binder.
- Binder application rate.

2.3 Bitumen Binder

A bituminous material is a low-grade crude oil. Crude oil is a viscous liquid that originates from the earth, and it is a fossil fuel. Bitumen is the result of crude oil that has been chemically and physically changed through various processes. Bitumen is described as a dark brown to black in colour material and can be in a state of very viscous to very solid (Read and Whiteoak, 2014). The process of creating bitumen starts with the fractional distillation of crude oil. The material in the distillation column is in two states, liquid, which resides at the bottom of the column and vapour which is at the top of the column. The lightest fraction in the distillation column is removed through side-streams at the top. The heaviest fraction, which is at the bottom, is removed with a pipe. This fraction from the distilled crude oil is known as the long residue. The long residue is directed into a vacuum distillation column, where it undergoes further distillation, the material is then referred to as a short residue. Bitumen can be manufactured straight from the distillation process if it complies with the correct specifications. The physical properties of the bitumen can be altered if required. This is done by 'air blowing'. It is an oxidation process that involves the passing of air over the material at a temperature range of approximately 240 - 320°C. The effect of exposing the short residue to air currents is that it transforms some of the low molecular weight maltenes into higher molecular weight asphaltenes. This reaction causes a reduction in the penetration of the bituminous material and an increase in the softening point, which improves the bitumen's low temperature susceptibility. Figure 2.5 illustrates the process of crude oil to bitumen (Read and Whiteoak, 2014).

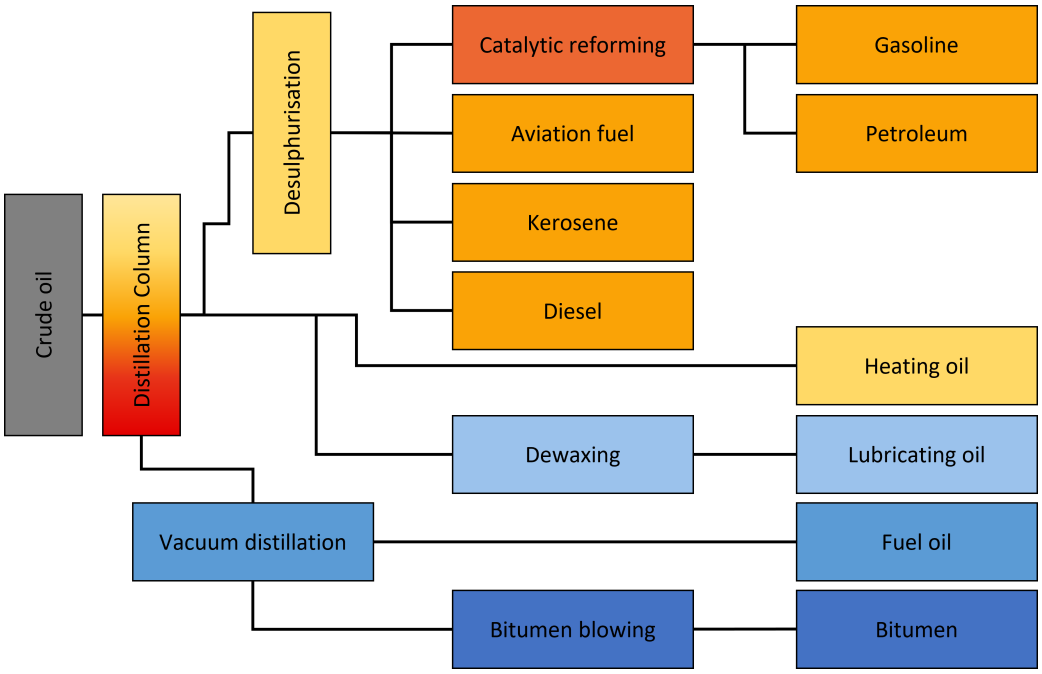

Figure 2.5: A diagram depicting the process of bitumen. (Adapted from Read and Whiteoak, 2014)

Bitumen technology has improved greatly over time. There are two bitumen binder types that are used. Unmodified and modified binders. The modification of binders has increased the performance of seals.

The reason for the modification of the bitumen binder was developed when the unmodified binder proved to be unreliable and a lot of maintenance was done, which in turn was costly (TRH3, 2007). The modification of bitumen binder is common as it has more superior properties than unmodified binders (TRH3, 2007).

The primary four types of bitumen are:

- Penetration Grade
- Bitumen Emulsion
- Modified Binders
- Cutback Bitumen

2.4 Composition

Bitumen has a very intricate chemical network. The composition of bitumen is dominated by carbon and hydrogen chemical elements. See Table 2.1 for the chemical composition. The complexity of the composition of bitumen can be broken down into two broad chemical groups, the asphaltenes and the maltenes. The maltenes are further divided into saturates, aromatics and resins. Figure 2.6 shows the bitumen composition.

Table 2.1: Typical chemical elements in bitumen (Read and Whiteoak, 2014)

Chemical Element	% in bitumen
Carbon	82 - 88
Hydrogen	8 - 11
Sulphur	0 - 6
Oxygen	0 - 1.5
Nitrogen	0 - 1

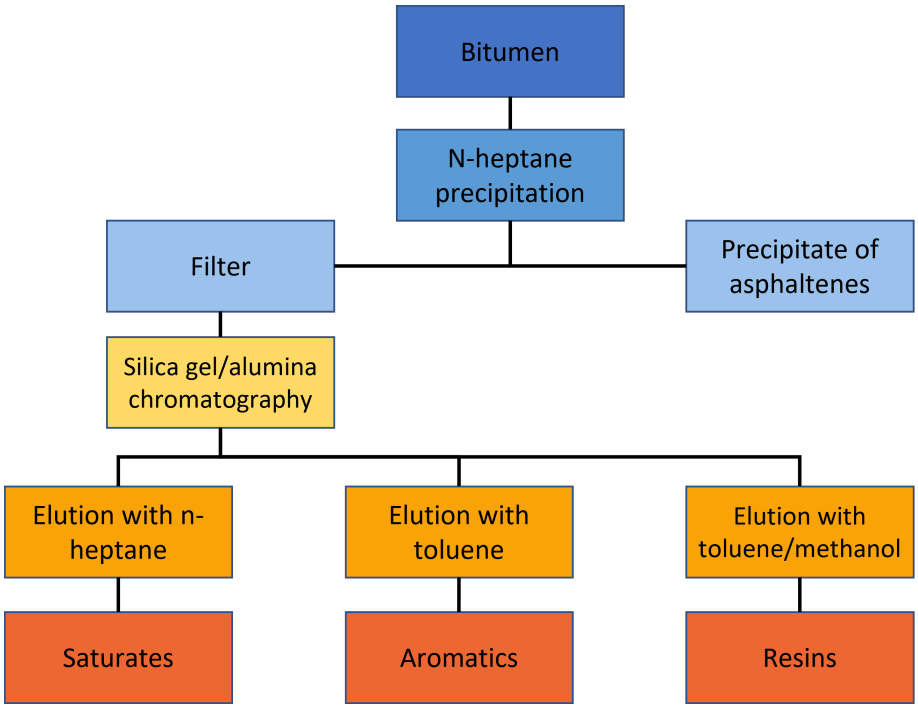

Figure 2.6: A schematic of the composition of bitumen. (Adapted from Read and Whiteoak, 2014)

2.4.1 Asphaltenes

Asphaltenes are regarded to be complex and highly polar aromatic materials, which have high molecular weight. Figure 2.7 displays the structure of an asphaltene molecule. This group is described as insoluble black or brown amorphous solids (Hunter *et al.*, 2015). They contain nitrogen, sulphur and oxygen atoms, along with carbon and hydrogen atoms. The particle size of the asphaltenes ranges between 2 - 5 nm. The content of asphaltene has a large impact on the rheological characteristics of bituminous material. The asphaltenes make up about 5 - 25% of the bitumen. With an increasing asphaltene content, the binder becomes more viscous and will have a lower penetration, but a high softening point (Hunter *et al.*, 2015).

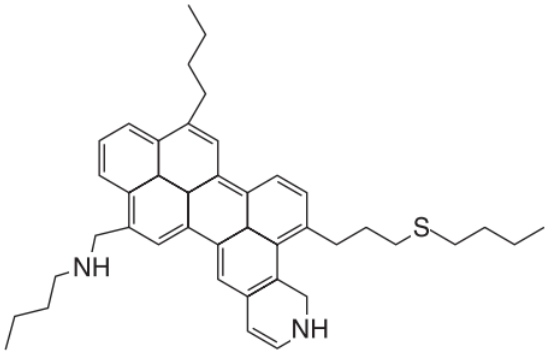

Figure 2.7: A schematic of asphaltene in bitumen (Read and Whiteoak, 2014)

2.4.2 Saturates

Saturates are straw-coloured or colourless non-polar viscous oils. They comprise of compounds, called aliphatic hydrocarbons and cycloaliphatic, that are straight and branched-chained. The saturates forms about 5 - 20% of the bitumen (Read and Whiteoak, 2014). Figure 2.8 shows the structure of a saturate molecule.

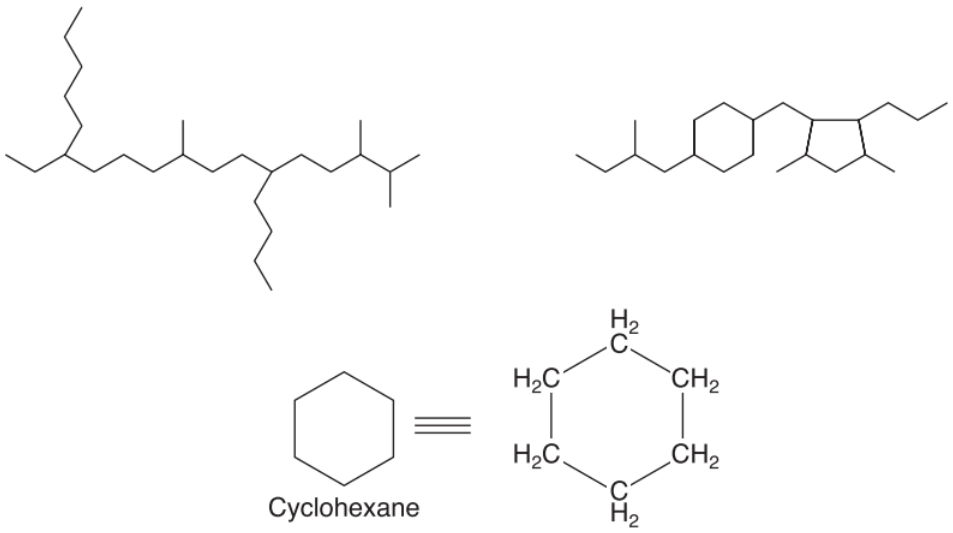

Figure 2.8: A schematic of the saturate particle (Read and Whiteoak, 2014)

2.4.3 Aromatics

Aromatics, which are dark-brown viscous liquids, constitute approximately 40 - 65% of the total bitumen. For the peptised asphaltenes, they represent a large percentage of the dispersion medium. They also have the lowest molecular weight naphthenic aromatic compounds in bituminous material (Hunter *et al.*, 2015). Figure 2.9 displays a representation of the structure of an aromatic molecule.

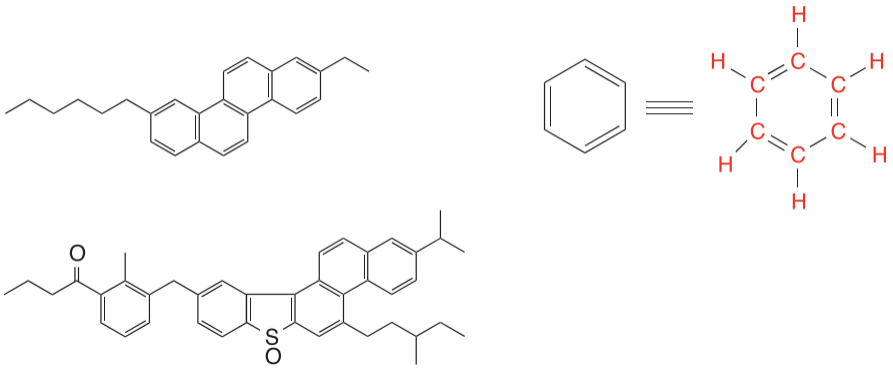

Figure 2.9: A schematic of the aromatic molecule (Read and Whiteoak, 2014)

2.4.4 Resins

Resins, which are dark brown in colour, are dispersing agents for asphaltenes. They are soluble in n-heptane and mostly constitutes hydrogen and carbon, also containing a bit of sulphur, oxygen and nitrogen atoms. Resins can be solid or semi-solid and are strongly adhesive, due to their polar nature (Read and Whiteoak, 2014).

2.5 Bitumen Structure

There are models created that attempt to represent the structure of bitumen molecules. The models are described as a colloidal system that comprises of maltenes and asphaltenes. Where the maltenes represent the continuous phase, and the asphaltenes the dispersed phase. The system consists of high molecular weight asphaltene micelles, which is dispersed in lower molecular weight maltenes. The micelles are described as the asphaltenes that are clustered in addition to an absorbed layer of high molecular weight aromatic resins. There are two boundary types of bitumen, namely a sol-type and a gel-type. In the sol-type bitumen, the asphaltene micelles have good mobility in the bitumen due to the sufficient amount of aromatics and resins. In gel-type bitumen, due to the lack of sufficient aromatics or resins, the micelles tend to group together and will form an uneven disconnected asphaltene structure (Read and Whiteoak, 2014). Figures 2.10 and 2.11 illustrates a sol- and gel-type bitumen, respectively.

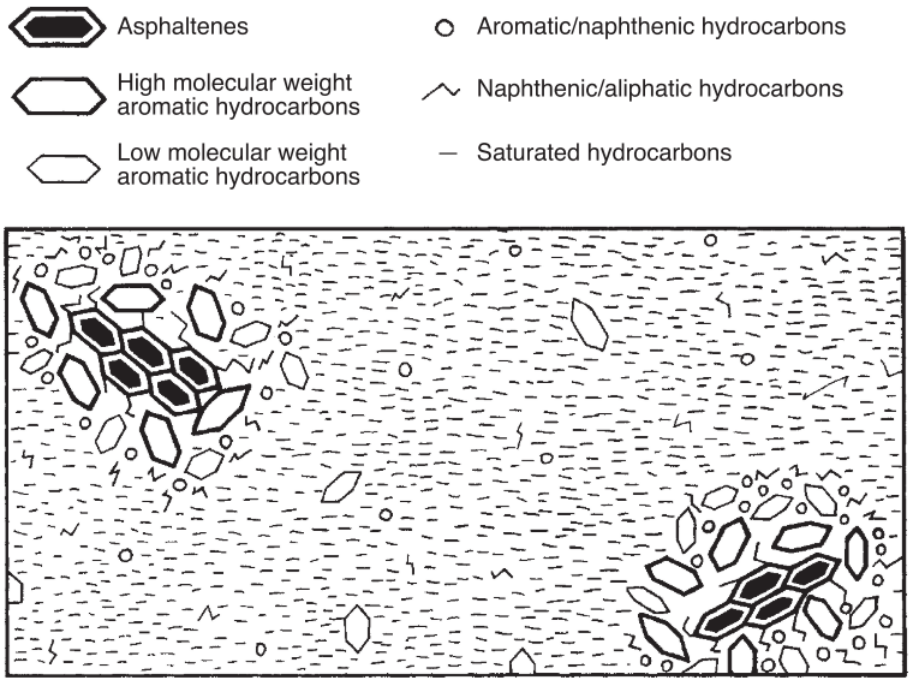

Figure 2.10: A schematic representation of a sol-type bitumen (Read and Whiteoak, 2014)

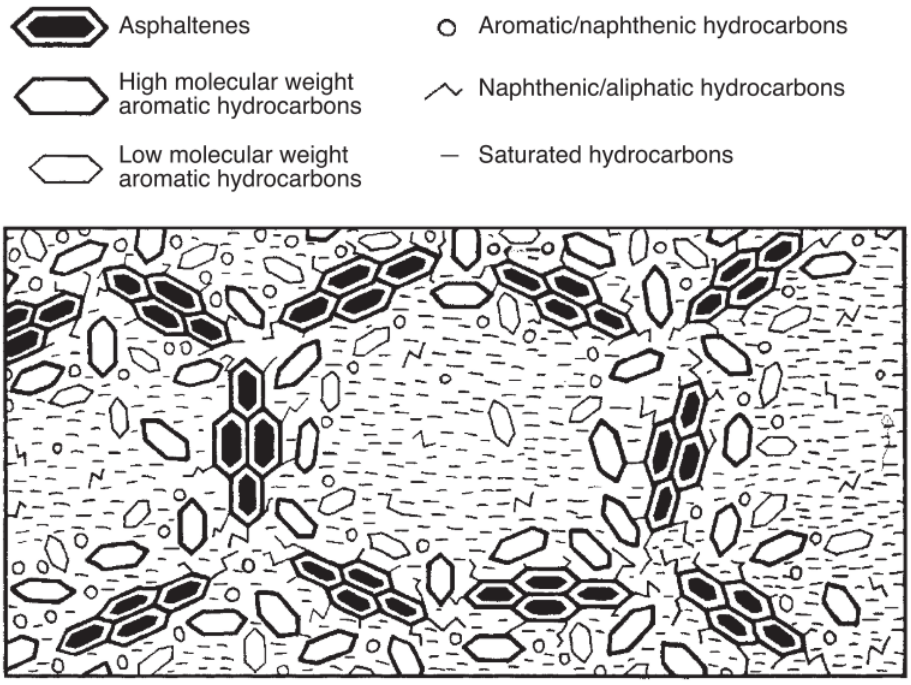

Figure 2.11: A schematic representation of a gel-type bitumen (Read and Whiteoak, 2014)

2.6 Unmodified Binders

Unmodified binders are extracted from the earth, and adjusted to use as a workable material for asphalt and seals. It is not modified. The penetration grade bitumens are described by the penetration and softening point tests (Read and Whiteoak, 2014). For example, the PEN 70/100 bitumen has a penetration that spans from 70 to 100.

2.7 Modified Binder

A polymer modified binder (PMB) is not classified according to the softening point. This is because the amount of the polymer that is added to the bitumen influences the softening point. Modified binders are divided into two groups: Homogenous and non-homogenous.
Homogenous binders are defined as a mix of bitumen and polymers, where on a microscopic level, it cannot be detected that the two phases behave differently. It acts as one phase material (TG 1, 2015). Examples of commonly used homogenous modified binders are:

- SBS
- SBR
- Natural rubber
- EVA

More details on the homogenous binders that are used, can be found in the Technical Guidelines 1. Non-homogenous binders are the exact opposite of homogenous binders and two phases are detectable. Depending on the phase, the binder will behave differently when a test is performed. Bitumen rubber is an example of a non-homogenous binder.

2.7.1 Styrene-Butadiene-Styrene (SBS)

The SBS binder is regarded as thermoplastic rubber. There are two classifications; a linear block copolymer or a radial block copolymer. The linear polymer is more workable, as it does not

result in a higher softening point and viscosity compared to the radial polymer. The glass transition point (T_g) is used to characterise the polymer. A cross-linking bond ensures that the particles provide high elasticity. The softening point of the elastomer is characterised by its asphaltene content, where a high amount of asphaltene induces a low softening point (TG 1, 2015). Figure 2.12 is showing how an increased SBS content affects softening point, taking into account asphaltene content. The higher the asphaltene content, the more SBS is required to increase the softening point.

There is a link between the deformation resistance and the elastic recovery of the material. It was found that the chance of deformation is decreased when there is an increase in elastic recovery, and the cohesive strength also increases. The addition of the SBS elastomer ensures flexible behaviour at low temperatures, and thus enhances the binder's resistance to cracking. The SBS elastomer is also generally more preferred than the SBR.

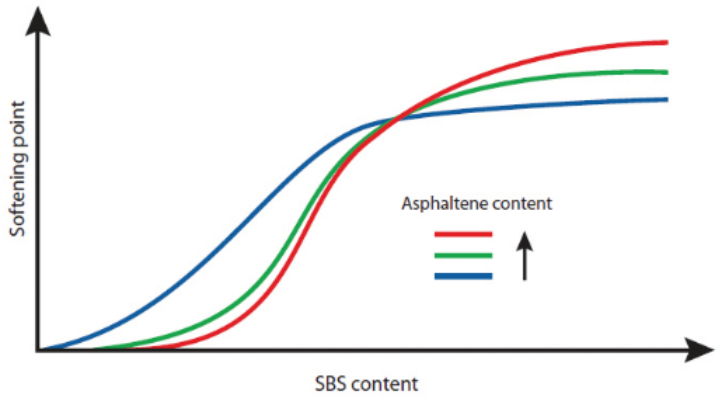

Figure 2.12: The different asphaltent contents on the softening point with the SBS (TG 1, 2015)

2.7.2 Styrene-Butadiene-Rubber (SBR)

Depending on the grade of the binder, SBR is made up of styrene-butadiene polymer which is emulsified with a solids content mainly larger than 50%. The butadiene is the component that bestows the binder its elasticity, thus making the binder more flexible (TG 1, 2015). The styrene component ensures the stiffness and strength of the binder. The SBR has similar chemistry and mechanical binding mechanism to that of the SBS. The SBR polymer improves multiple properties of the binder. Such as the adhesion between the binder and the aggregate when sealing, and the flexibility and elasticity.

2.7.3 Natural Rubber Latex

Natural rubber latex is a modifier that contributes to the improvement of the elasticity of the bitumen. It comprises of polymerised isoprene monomers (TG 1, 2015). This monomer is generally used when modifying cold bitumen, as it is sensitive to heat. It is a useful binder to use when sealing fine cracks that have a width of less than 3 mm. This is due to the addition of latex to an emulsion.

2.7.4 Ethylene-Vinyl-Acetate (EVA)

This modifier is a polymeric plastomer. It consists of two monomers, namely ethylene and vinyl-acetate. These two monomers form long crystalline molecular strings which detach when there is an increase in temperature above the binder's glass transition point. The EVA properties are controlled by the following parameters (TG 1, 2015):

- Molecular weight: It is standard practice to measure the melt flow index (MFI) for EVA's; The lower the viscosity and molecular weight, the higher the MFI.
- Vinyl-Acetate (VA) content: The proportion of the rubbery regions get higher as the VA content increases. The proportion of the crystalline regions also lower when the VA content increases. Thus, when there is an increase in VA content, there is an increase in flexibility and a decrease in stiffness.

Compared to the SBS and SBR, the EVA bitumen have improved safer handling, workability, has higher thermal stability and delayed deterioration (TG 1, 2015). It also contributes to the binder's resistance to rutting in hot-mix asphalt.

2.7.5 Non-Homogeneous Binders

Bitumen rubber is a two-phase product, which has the flow-like characteristics of bitumen and the stiffness and elasticity properties of a rubber tyre (TG 1, 2015). The binder consists of bitumen and rubber crumbs. The rubber crumbs have specific grading, composition and morphology. One of the reasons why bitumen rubber is favoured is because the crumbs are obtained from the recycling and processing of rubber tyres. It is noteworthy that the type of tyres that are used vary and depends on the make and source of the tyre.

2.7.6 Modified Binder Classification System

The classification system was created with the intent to describe a binder based on its performance. The system was developed to cover four main criteria. The type of application and temperature, the type of modifier used and a number. To describe classes of modified binders, the following codes are utilised (TG 1, 2015):

Type of application:

- Asphalt (A)
- Crack Sealant (C)
- Spray Seal (S)

Type of binder system:

- Emulsion: If the material is an emulsion, the letter C would follow directly after the application type.
- Hot applied: No letter is used.

Predominant type of modified used:

- Elastomer (E)
- Plastomer (P)
- Rubber (R)
- Hydrocarbon (H)

Level of Modification:

- The level of modification is denoted with a number. The number is based on the softening point. As the number increases, so does the softening point.

There is an additional code that indicates whether a fluxing agent or cutter may be permitted. If the binder application does not allow the fluxing agent, nor the cutter, then brackets with the letter t should be added after the classification. Table 2.13 shows the different classes of modified binders according to their application.

Modified Binder Class	Application - Spray Seal
S-E1	Spray seal - hot applied elastomer modified
S-E2	Spray seal - hot applied elastomer modified
S-R1	Spray seal - hot applied bitumen-rubber
S-R2	Spray seal - hot applied bitumen-rubber
SC-E11	Spray seal - emulsion elastomer modified
SC-E21	Spray seal - emulsion elastomer modified
	Application - Premixed Asphalt
A-E1	Asphalt - elastomer modified
A-E2	Asphalt - elastomer modified
A-P12	Asphalt - plastomer modified
A-H1	Asphalt - hydrocarbon modified
A-H22	Asphalt - hydrocarbon modified
A-R1	Asphalt - bitumen-runner
A-R2	Asphalt - bitumen-runner
AC-E1	Microsurfacing - emulsion elastomer modified
AC-E2	Microsurfacing - emulsion elastomer modified
	Application - Crack Sealant
C-E1	Crack sealant - hot applied elastomer modified
CC-E1	Crack sealant - emulsion elastomer modified
C-R1	Crack sealant hot applied bitumen rubber
C-R2	Crack sealant hot applied bitumen rubber

Figure 2.13: The modified binder classification system (TG 1, 2015)

2.8 Rheological Properties

The behavioural characteristics of bitumen. The important characteristics that are important to consider are:

- Rheology
- Elasticity
- Cohesion
- Adhesion
- Ageing and Durability

2.8.1 Flow Behaviour

Bitumen is a material mostly used in pavement construction. It is in the top layer of the pavement. It is a thermo-plastic, visco-elastic fluid. At low temperatures or slow loading times, the behaviour is like an elastic solid, with a glassy-like appearance. And at a higher temperature or faster loading times, the behaviour is as a viscous fluid. From this, stress is a factor to which the material responds, and is dependent on the applied load and the temperature. The parameters used in the rheology of bitumen, are mainly stress, strain, loading time and temperatures (Read and Whiteoak, 2014).

2.8.2 Elasticity

Elasticity is a characteristic that is considered when analysing a binder's potential recovery. When a load applied is removed, and the binder recovers to its initial shape, it is described as the elastic behaviour of the binder. Elasticity is linked to the binders ability to absorb large stresses. The elastic property of bitumen can be modified by the addition of polymers. The elastic potential of a modified binder will depend on the type of modifier and the degree to which the modifier is applied (TG 1, 2015).

2.8.3 Cohesion

Cohesion is the term used to describe the amount of tensile stress that is required to break the molecular bonds of the bitumen particles. Cohesive strength is thus linked to crack resistance. The strength of the bituminous binder is increased with the addition of modifiers, such as polymers and rubber crumbs. Therefore, a higher tensile force is required to break the bonds of the bituminous binders molecules, than it is without. A cohesive failure results in cracking, as illustrated in Figure 2.14.

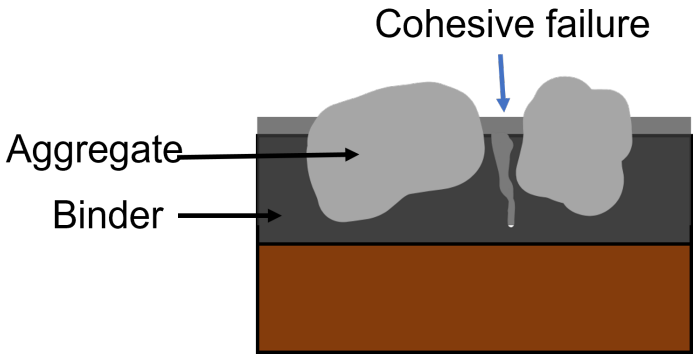

Figure 2.14: Cohesive failure. Adapted from (Gerber, 2016)

2.8.4 Adhesion

The term adhesion is used to measure the strength between the binder and the aggregate. The adhesive property of the binder-aggregate interaction is mainly dependent on the chemical and physical nature of the bituminous material and aggregate type. Adhesive failure occurs when there is a weak bond and the aggregate detaches from the binder. Figure 2.15 illustrates how adhesive failure occurs. The following factors can contribute to adhesive failure:

- Properties of the aggregate, such as mineralogy, surface texture, etc.
- Presence of moisture or dust
- Level of modification of the binder that can affect the adhesion strength.
- Road and air temperatures

There are two factors that cause adhesive failures of seals that relate to temperature:

- In conditions of cold temperatures, a decrease in adhesion is caused by the increase in stiffness.
- The higher the degree of modification in homogeneous modified binders, the more water aversion, stiffness, and the associated risk of adhesion failure increases.

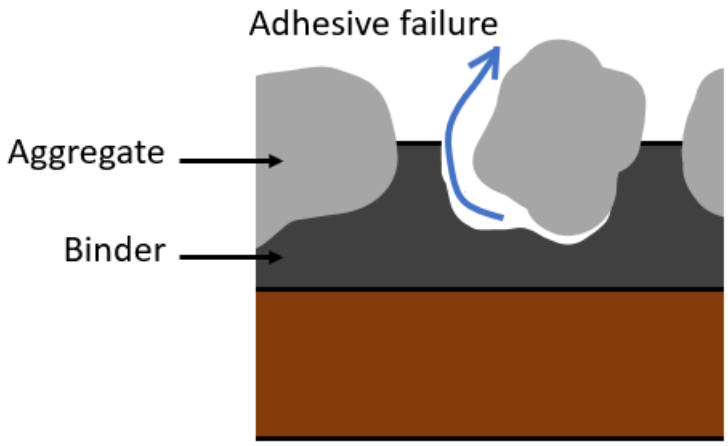

Figure 2.15: Adhesion failure. (Adapted from Gerber, 2016)

2.8.5 Ageing and Durability

The term ageing in rheology is used to describe the changes that a bitumen property undergoes from storage, mixing to laying and in-service (Read and Whiteoak, 2014). Durability is linked to ageing, as it describes the binder's ability to resist the effects of ageing (TG 1, 2015). There are many factors that influences the change in visco-elastic behaviour of a bituminous material. The two most common factors that affect this change (ageing) are temperature- and time-related conditions (TG 1, 2015). When there is an increase in stiffness and a decrease in the binder's elastic properties, it is called hardening. The hardening of a binder throughout its life on the road is referred to as in-service ageing. The factors that influence the hardening of a binder are:

- Oxidation
- Physical hardening
- Exudation
- Loss of volatiles

Temperature susceptibility is one of the most important properties of a bituminous material. The susceptibility of a binder to temperature affects its ability to perform. A binder's temperature susceptibility is described as the level of variation in its viscosity (TG 1, 2015). It is generally

represented by the Softening Point and the Fraass Brittle Point, for high and low temperatures respectively. The range between these two points is referred to as the service temperature of the binder. These two endpoints of the range are also referred to as the extreme points, and are dependent on the crude source of the bitumen, as well as the grade of the bitumen. Figure 2.16 describes the relationship between the consistency and temperature of the bitumen.

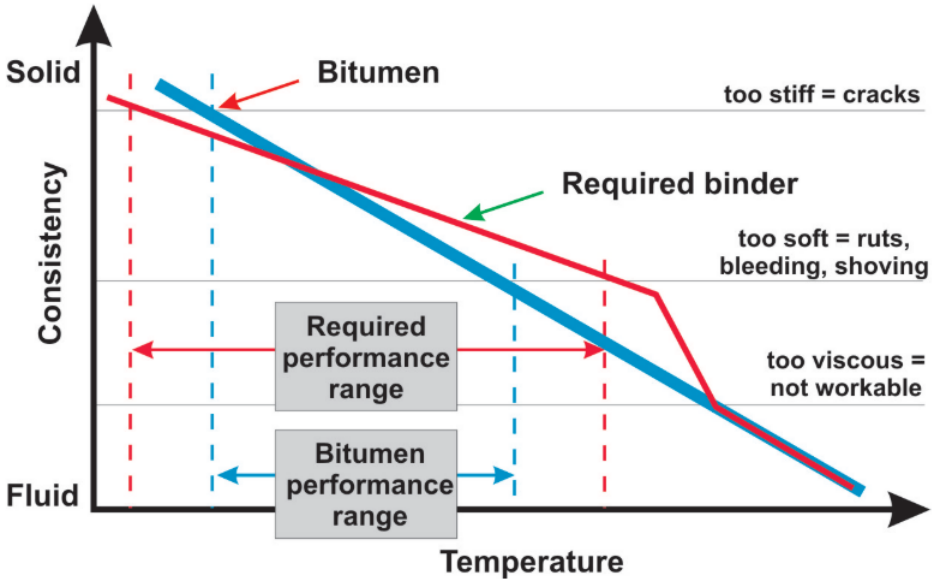

Figure 2.16: A diagram describing the performance of bitumen depending on viscosity and temperature (TG 1, 2015)

2.9 Apparatus and Tests

It is important to understand how a binder will perform under certain conditions. In the field, the binder is exposed to various temperatures and traffic. The effect of ageing also plays a role in the long term performance of a seal. The following factors are important to know before selecting the appropriate binder:

- The high-temperature performance and rutting potential.
- The intermediate temperature performance, where fatigue cracking occurs.
- The low-temperature performance and cracking potential.

Each of these factors can be tested in different apparatuses. The Dynamic Shear Rheometer (DSR) is used for high to intermediate temperatures, the Bending Beam Rheometer (BBR) is used for very low temperatures and the Rolling Thin Film Oven (RTFO) is used to induce short-term ageing. The purpose of each device is to determine the rheological properties of the binder under specified conditions.

2.9.1 DSR

The Dynamic Shear Rheometer (DSR) is a device that can measure the rheological properties of a binder at different frequencies and temperatures. It is used to conduct visco-elastic tests on a material (Read and Whiteoak, 2014). The test applies to binders that have a dynamic shear modulus ranging between 100 Pa to 10 MPa. This range is generally obtained at 10 rad/s, between the temperatures 4 and 88°C. The test is performed at various frequencies. A load cell is an instrument that measures the force sustained by the specimen as a result of the moving plate. The movements of the load cell are recorded with a computer.

In this experiment, a twisting rod, attached to a flat disk moves in a sinusoidal pattern, as shown in Figure 2.17. Beneath the flat disk is the specimen, which is place on a plate parallel to the disk of the rod.

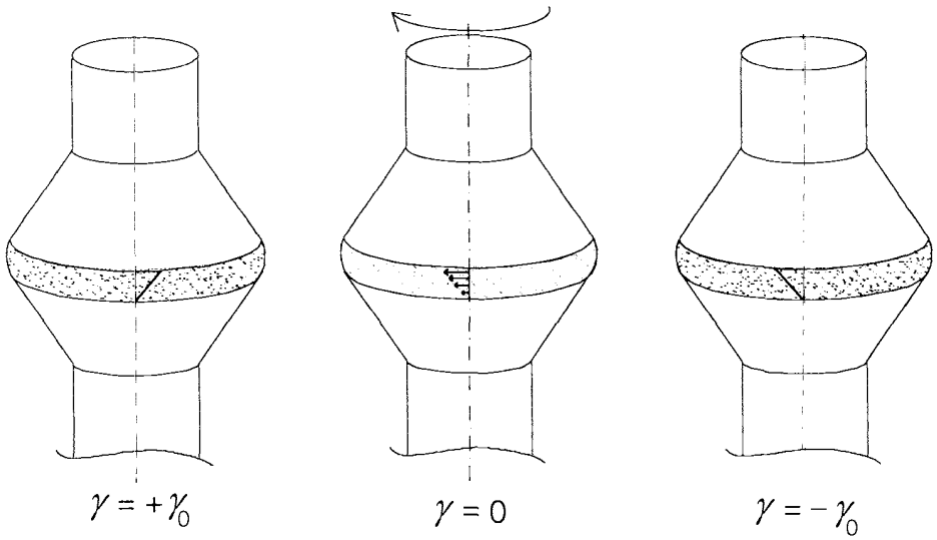

Figure 2.17: Measurement of strain in the DSR (Shaw and MacKnight, 2005)

During the test, a sinusoidal strain is applied to the sample, the resulting stress is then monitored as a function of frequency. This method is referred to as 'strain-controlled', which is more

common than the 'stress-controlled' technique. In the stress-controlled testing, sinusoidal varying stress is applied, and then the responded strain is obtained. The signals are recorded over an angle of 2π. The difference between these two signals is then compared. This difference is called the phase angle, denoted as δ. When the signals are exactly in-phase, a.k.a. $\delta = 0$, the specimen is considered to be perfectly elastic (Shaw and MacKnight, 2005). Figure 2.18 shows how the strain and stress sinusoidal signals are obtained as a function of time:

$$\gamma(t) = \gamma_0 \, sin(\omega t) \tag{2.1}$$

$$\sigma(t) = \sigma_0 \, sin(\omega t + \delta) \tag{2.2}$$

where,

γ(t) = shear strain as a function of time

σ(t) = stress as a function of time

γ_0 = shear strain amplitude

σ_0 = stress amplitude

ω = frequency

t = time

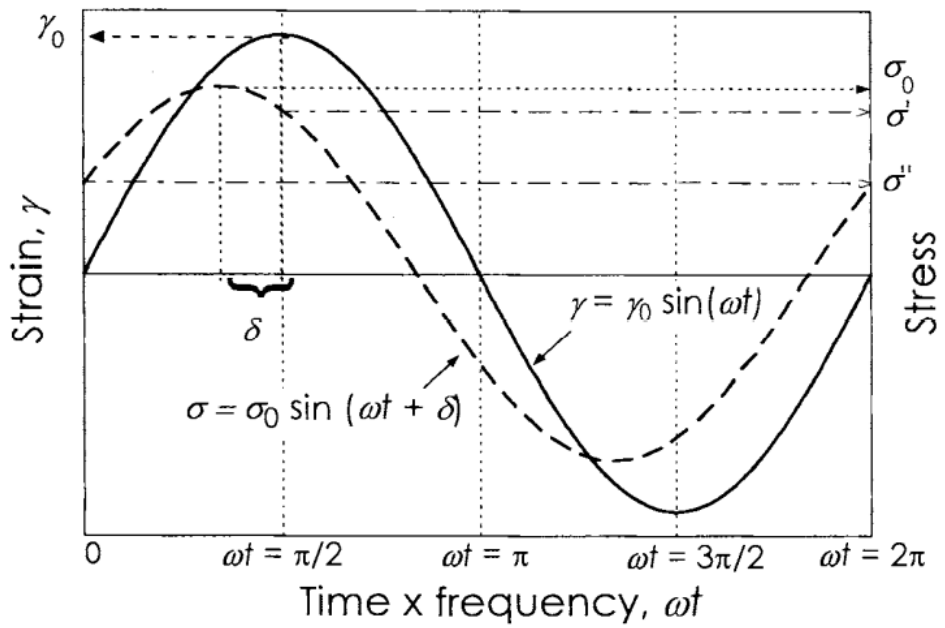

Figure 2.18: Sinusoidal loading and corresponding stress and strain response (Shaw and MacKnight, 2005)

From the figure, it can be seen that the maximum strain rate is obtained at zero strain, due to a sine wave having its maximum rate of change at this point. Therefore, the stress at zero strain is due to the specimen responding only to the strain rate, and the material would be purely viscous. And consequently, the strain reaches its maximum, which is at $\omega t = \pi/2$, the strain rate approaches zero. Therefore the strain rate would be only responding to the strain, and would thus be an elastic material (Shaw and MacKnight, 2005).

$$G' = \frac{\sigma_0}{\gamma_0} cos\,\delta \tag{2.3}$$

$$G'' = \frac{\sigma_0}{\gamma_0} sin\delta \tag{2.4}$$

According to Mturi *et al.* (2011), the dynamic complex modulus is calculated as follows:

$$G^*(\omega) = \frac{|\tau(\omega)|}{|\gamma(\omega)|} \tag{2.5}$$

Other parameters can also be determine from the dynamic testing, such as :

$$J^* = \frac{1}{G^*} \tag{2.6}$$

$$\eta^* = \frac{G^*}{\omega} \tag{2.7}$$

where,

J* = dynamic complex compliance modulus

η^* = dynamic complex shear viscosity

The tests that are performed on the DSR, are frequency and strain sweeps, as well as creep recovery tests.

2.9.2 Strain Sweeps

A strain sweep is a test conducted to determine the linear viscoelastic region (LVE) of a material. According to ASTM D7175-08, the linear region is described as being the range in strains, at which the complex modulus is 95% or more of the initial strain value. Thus, tests conducted in the LVE region will give accurate results. If testing occurs outside of the LVE region, certain simplifications and assumptions are no longer valid. Such as the time-temperature superposition principle. The frequency sweep tests, as well as the creep and recovery tests, should therefore be conducted in the LVE region.

2.9.3 Frequency Sweeps

A frequency sweep is a test that is oscillatory and is performed at variable frequencies. During the process, the amplitude and testing temperature remains constant. Due to the frequency being the inverse value of time, the frequency sweeps are used to analyse time-dependent shear behaviour. As stated before, a strain sweep is often conducted before a frequency sweep to ensure the test stays within the LVE region. The results from the frequency sweep tests are used to construct master curves, which are utilised to analyse the rheological properties of a binder at various temperatures and frequencies. In the ASTM D7175-08 standard, oscillatory loading frequencies range between 1 - 160 rad/s.

2.9.4 MSCR

A creep and recovery test is a useful test to determine the elastic response in a bituminous binder, as well as the change in elastic response at two separate stress levels (ASTM D 7405-10a, 2010). The test produces two main parameters that are used to analyse a binder's rheological properties concerning creep and recovery. The non-recoverable creep compliance (J_{nr}) and the percentage recovery (%R). The Jnr acts as an indicator of the resistance of a binder to plastic deformation under a repeated load (ASTM D7405-10a, 2010). With a low J_{nr}, the bitumen is able to absorb higher stress levels and the susceptibility to plastic deformation is lower. Creep and recovery tests are done to obtain the following (Gierhart, 2011):

- The rutting performance of the binder is evaluated.
- The most economic use of modifiers to improve binder performance.

During the Multiple Stress Creep and Recovery (MSCR) test, a one second load is applied to the sample and then the load is lifted and the sample is left to recover for nine seconds. This is repeated for 10 cycles, thus the test runs for 100 seconds. The load that is applied is often 0.1 kPa, followed by 3.2 kPa for the next ten cycles (ASTM D 7405-10a, 2010). Figure 2.19 displays a typical strain versus time diagram from an MSCR test. Figure 2.20 displays the creep and recovery phases in 10 seconds.

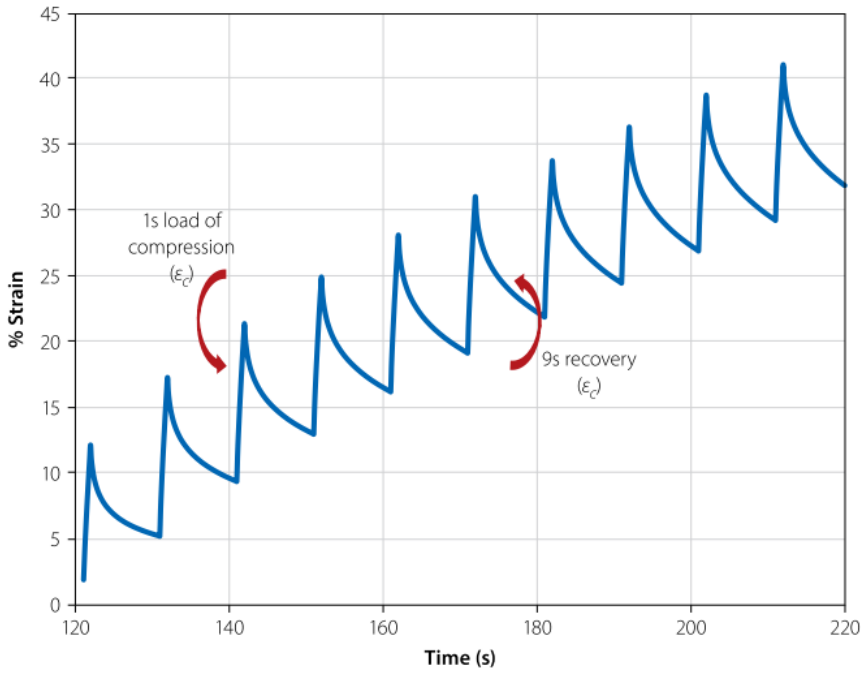

Figure 2.19: An example of a typical MSCR test result (Bredenhann *et al.*, 2019)

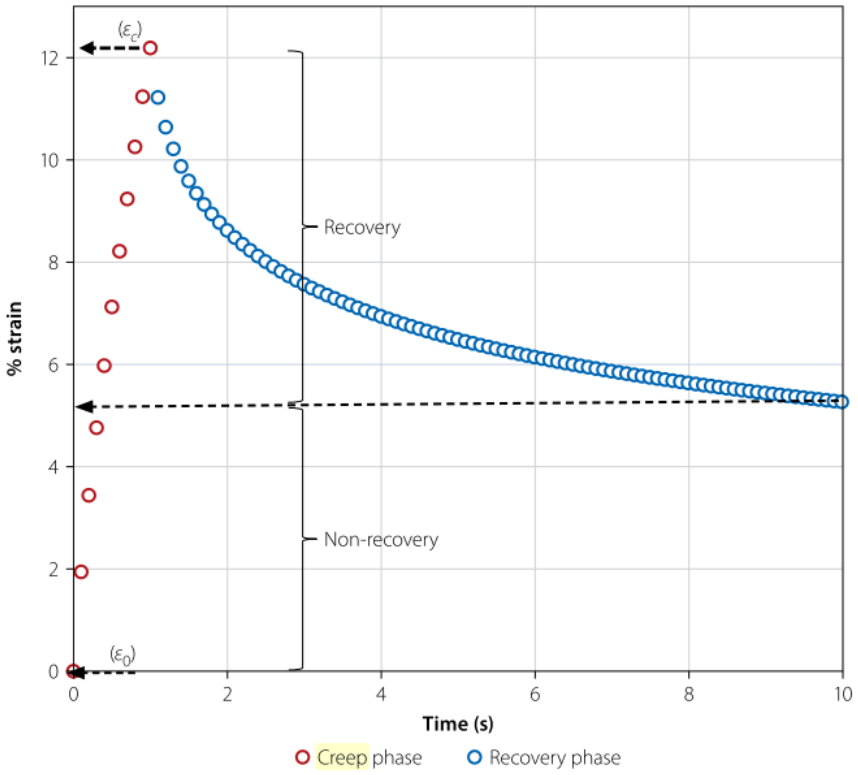

Figure 2.20: Creep and recovery phase (Bredenhann *et al.*, 2019)

From this test, the J_{nr} is calculated as:

$$J_{nr} = \frac{Average\ non-recoverable\ shear\ strain}{Applied\ shear\ stress} \tag{2.8}$$

As the J_{nr} provides the rut resistance of the binder, the %R is an indicator of the presence of polymers in the binder. The %R is as follows:

$$\%R = \frac{\epsilon_0 - \epsilon_r}{\epsilon_0} \tag{2.9}$$

where,

ε_0 = initial strain in the creep stage

ε_r = final strain after recovery

2.9.5 BBR

As bitumen becomes brittle at low temperatures and tends to fracture, it is important to assess a binder's properties to be able to predict performance. The BBR is used to determine the deflection that a beam of bitumen will experience when put under a constant load, at low temperatures. This test evaluates the bitumen's potential to cracking at low service temperatures. It tests the binders resistance to deformation when subjected to a load at a specified temperature (SABITA, 2017). In this test, a beam of bitumen is placed on two supports and a load is applied. Figure 2.21 displays how the beam deflects with time and how the stiffness decreases.

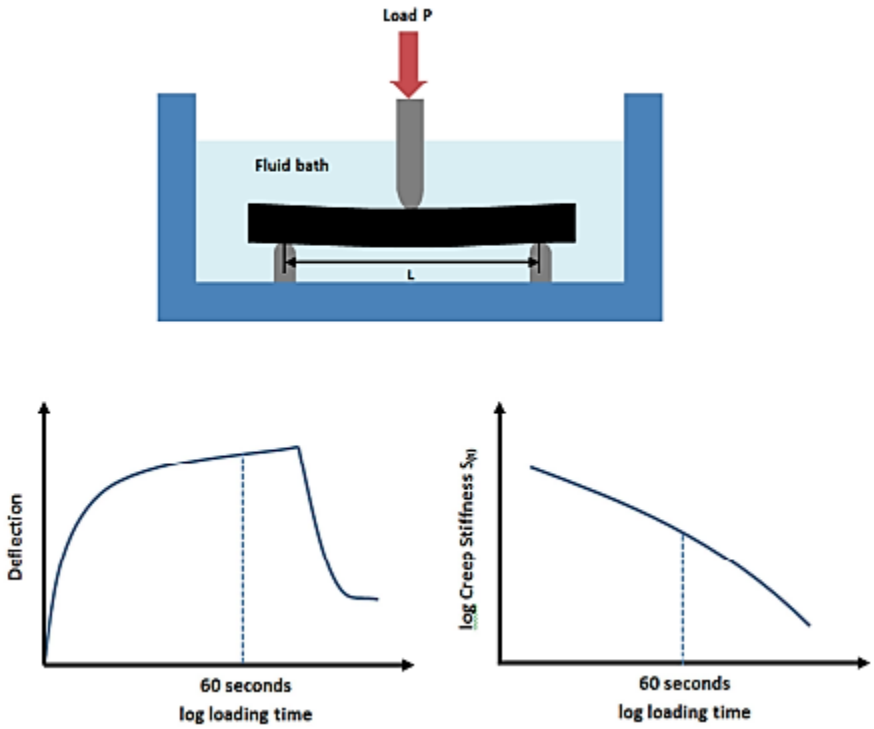

Figure 2.21: A schematic of the bending beam rheometer (SABITA, 2017)

The two parameters that are derived from this test are the stiffness (S) and the relaxation parameter or creep rate (m). A bitumen beam is placed on the supports and a constant creep load of ±980 mN is applied. The beam is placed in a fluid bath at testing temperature. The test is conducted for a period of 240s. The BBR testing utilises the elastic beam theory and the elastic-viscoelastic correspondence principle, to correlate the creep stiffness with time (SABITA, 2017).

$$S(t) = \frac{PL^3}{4bh^3\delta(t)} \tag{2.10}$$

where,

S(t) = Creep stiffness at time t (MPa)

P = Test load, usually of 100g (N)

L, b and h = length, width and thickness of beam (mm)

δ(t) = deflection at time t (mm)

2.9.6 RTFOT

It is important to test bitumen characteristics at different stages of its life, to enable the rate of ageing to be evaluated. The different ages of bitumen tend to exude different performance behaviours. There are two categories for a binder's age, namely short-term ageing and long-term ageing. Long term ageing is simulated by a Pressure Ageing Vessel. Short-term ageing is a term used to described a binder's characteristics at the time of mixing, transportation and application processes (Nicholls, 2005). The RTFO is an oven that simulates these conditions of which the binder undergoes. In the RTFO there is a rotating wheel with 8 cylindrical containers. Figure 2.22 displays a picture of the RTFO. Each of these containers is filled with 35g of the bituminous binder. The wheel is lodged vertically and rotates at a rate of 15 revs/min (Nicholls, 2005). Air is blown on the rotating wheel. In each of the containers, there is a thin film of bitumen which is kept at 163°C and the test is conducted for 75 min. With the effect of air and heat on the binder, short-term ageing is stimulated on the binder.

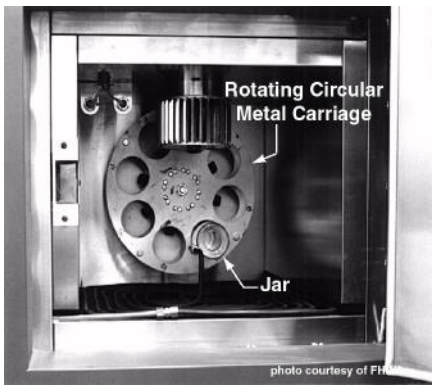

Figure 2.22: The Rolling Thin Film Oven (Pavement Interactive, 2012)

2.10 Flow Behaviour of Bitumen

Elastic behaviour of bitumen is a description given to a material when the material displays the ability to return to its original form after a load is applied to temporarily deform the material. Bitumen displays elasticity at low temperatures and high loading frequencies. The relationship was captured by Robert Hooke in 1660 and is referred to as Hooke's Law. Hooke's Law states that, under a uniaxial load, a linear elastic stress-strain in a homogenous, isotropic material,

will behave as:

$$\sigma = E\,\epsilon \tag{2.11}$$

Where,

σ = normal stress

E = Young's Modulus and

ε = normal strain

When the material is subjected to a shear load, the relationship is:

$$\tau = G\gamma \tag{2.12}$$

Where,

τ = normal strain

G = shear stiffness modulus and

γ = the shear strain

A relationship between the equations 2.11 and 2.12 was developed:

$$G = \frac{E}{2(1+\upsilon)} \tag{2.13}$$

Where υ is Poisson's ratio. When the material reaches its elastic limit and starts to deform, Hooke's law no longer holds true. The elastic limit is the point to which the material reaches where it starts to permanently deform.

Viscous behaviour is displayed when a material constantly deforms under a load. At high temperatures, it displays a fluid-like behaviour. Shear flow and extensional flow are two basic kinds of flow with relative movement of adjacent particles of the fluid. Shear flow is where the particles move past each other. Extensional flow is where the particles move towards or away from one another. Figure 2.23 displays a schematic of how the particles move.

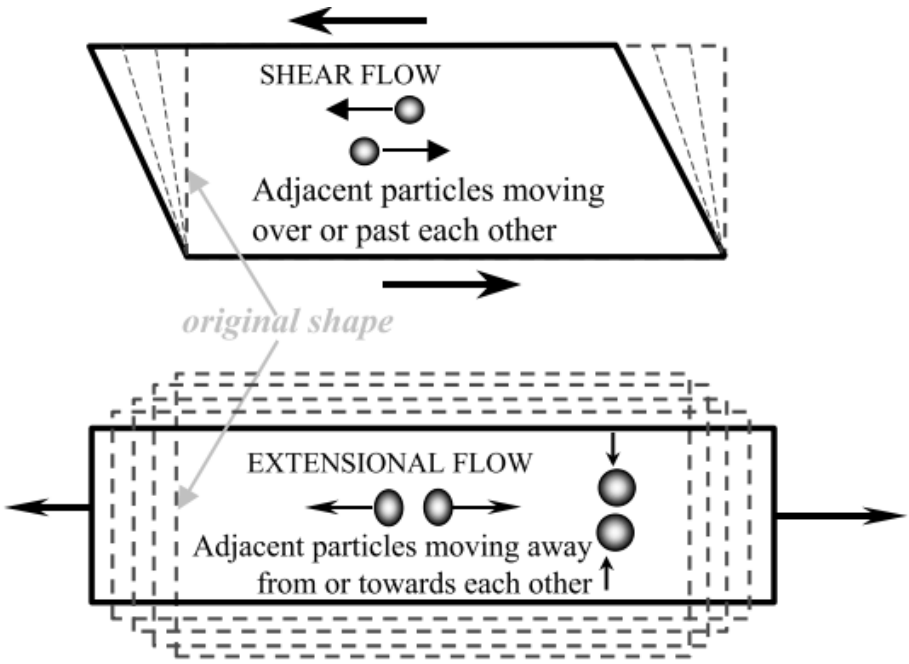

Figure 2.23: The movements of particles in shear and extensional flows (Butt, 2011)

Viscosity (η) is defined as the ratio between the applied shear stress (σ) and the rate of strain (γ), which is essentially the measure of resistance to flow of a liquid (Hunter *et al.*, 2015). Thus, the viscosity equation is, measured in Pa.s:

$$\eta = \frac{\sigma}{\gamma} \tag{2.14}$$

Newtonian fluids are where the viscosity stays constant with deformation rate or time, temperature and pressure may vary (Butt, 2011). The rheological behaviour of low molecular weight fluids is accurately described by this equation (Macosko, 1996).

$$\tau = \mu\gamma \tag{2.15}$$

Where,

τ = shear stress

γ = shear strain rate

μ = dynamic viscosity

Non-Newtonian behaviour is displayed when the liquid reaches a certain high shear rate, depending on the fluid (Hunter *et al.*, 2015). Materials can be classified according to the behaviour they display when applied a load. There are two types, namely shear thickening (fluids are termed as dilatant) and shear thinning (fluids are termed as pseudoplastic). Models can be used to describe the behaviour of liquids under various shear conditions. The power model is one of the basic models that is used (Hiber and Chiang, 1992):

$$\eta = m \cdot \gamma^{(n-1)} \tag{2.16}$$

Where m and n are positive constants for any given model. When n < 1, then the viscosity decreases and the liquid is pseudoplastic, when n > 1, then the viscosity increases and the liquid is dilatant. At n = 1, the fluid is Newtonian. Figure 2.24 displays the shear stress and viscosity behaviour of fluids.

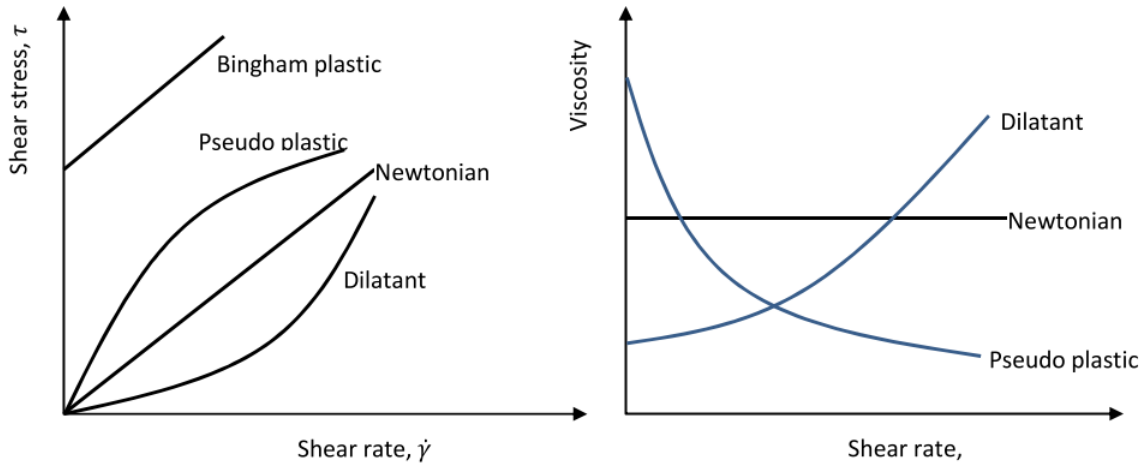

Figure 2.24: The types of fluids (Asiimwe *et al.*, 2014)

2.10.1 Viscoelastic Modelling

To understand viscoelastic behaviour, mechanical models are used as a representation. They are constructed from elements such as dashpots and springs, which represent the viscous and elastic elements respectively. The dashpot in series obeys Newton's law, where the spring in series obeys Hooke's law. In Hooke's model, the force is proportional to the extension, and in Newton's law the force is proportional to the rate of extension (Mainardi and Spada, 2011).

Hooke's model:

$$\sigma(t) = E\epsilon(t) \tag{2.17}$$

and the Newton model:

$$\sigma(t) = b_1 \cdot \frac{d\epsilon}{dt} \tag{2.18}$$

where,

E = elastic modulus

$\sigma(t)$ = stress as a function of time

$\varepsilon(t)$ = strain as a function of time

b_1 = viscosity constant

Figure 2.25 displays the spring for Hooke's law and the dashpot for Newton's law, as well as a graph of how each law is portrayed in terms of strain.

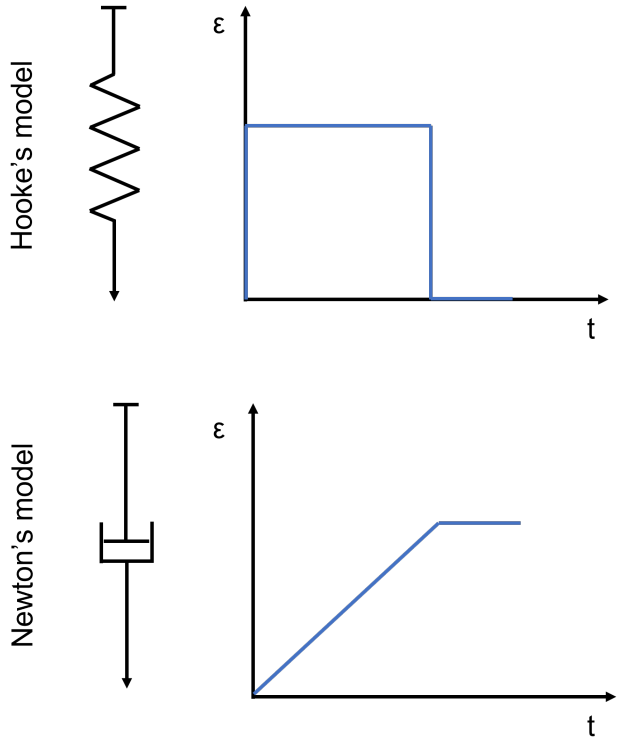

Figure 2.25: The spring and dashpot elements (Butt, 2011)

The Maxwell model is represented by a spring and a dashpot in series. The model shows that when a constant load is applied, linear deformation takes place. When the load is removed, the material will relax slightly, but due to permanent deformation, will not recover fully. The spring represents the part where the material will recover and the dashpot where it will deform. When the two elements are set in parallel, it is the Kelvin-Voigt model. The model shows an exponential strain creep, but no stress relaxation. Figure 2.26 displays both the Maxwell and Kelvin-Voigt models. The equation for the Maxwell and Kelvin-Vogit models are:

$$\sigma(t) + a_1 \cdot \frac{d\sigma}{dt} = b_1 \cdot \frac{d\epsilon}{dt} \tag{2.19}$$

$$\sigma(t) = E\epsilon(t) + b_1 \cdot \frac{d\epsilon}{dt} \tag{2.20}$$

where,

$a_1, b_1 =$ Creep or Relaxation coefficients

.

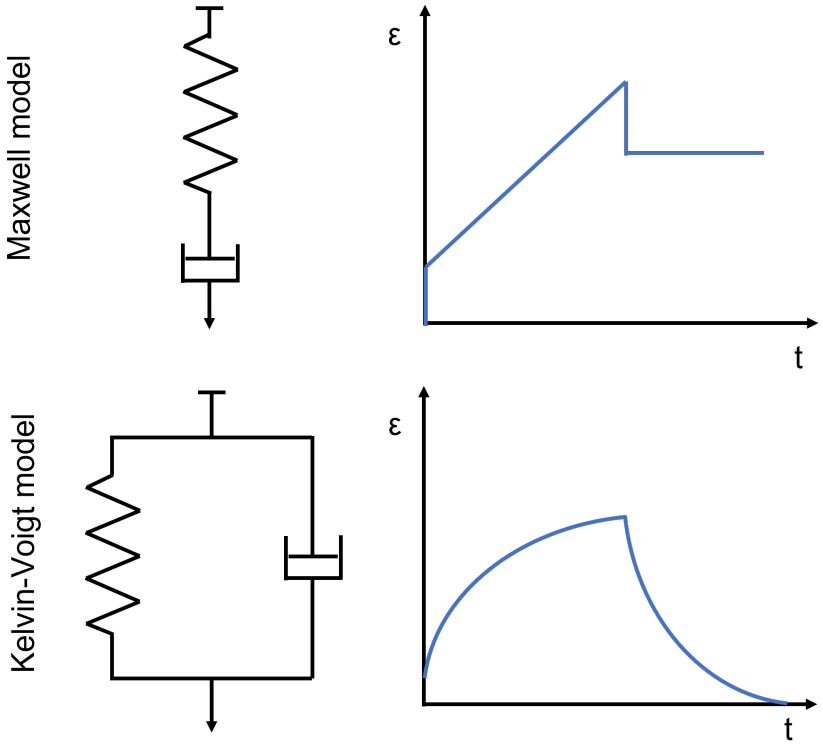

Figure 2.26: The Maxwell and Kelvin Voigt models (Butt, 2011)

The Burger model is a combination of the Maxwell and Kelvin-Voigt model, a four-element model. These models allow for a creep representation and a relaxation representation. The Burger model is the model that best describes the behaviour of the material, and is the most common model used in the study of rheology (Mainardi and Spada, 2011).

$$[1 + a_1 \cdot \frac{d}{dt} + a_2 \cdot \frac{d^2}{dt^2}] \cdot \sigma(t) = [b_1 \cdot \frac{d}{dt} + b_2 \cdot \frac{d^2}{dt^2}] \cdot \epsilon(t) \tag{2.21}$$

In the Burger model, it is clear that the spring will deform, as it is unrestrained, and this is an immediate elastic response. The Kelvin-Voigt shows that there will be a delayed elastic response, as the spring is inhibited by the dashpot. The alone standing dashpot will then show a steady state of deformation. Figure 2.27 displays the model behaviour.

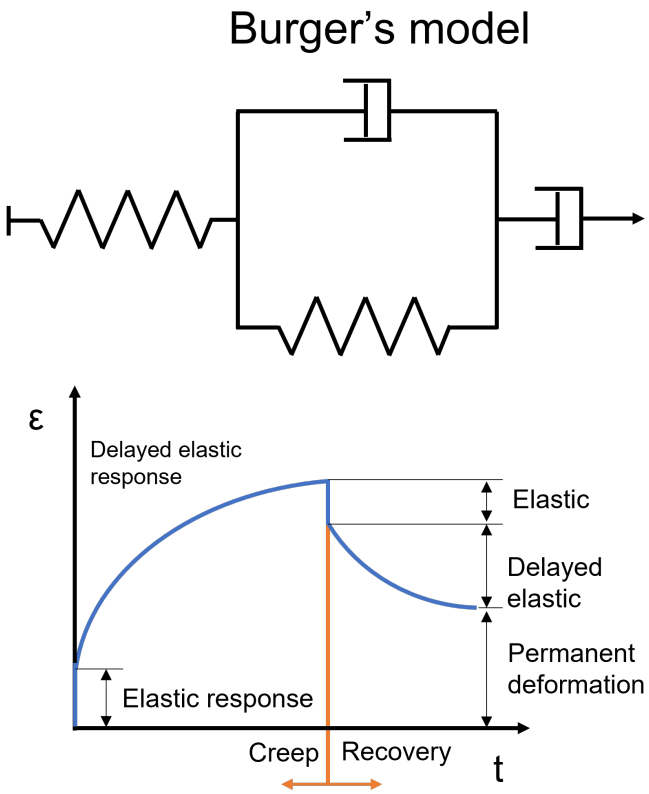

Figure 2.27: Burger's model. (Adapted from Hunter *et al.*, 2015)

2.11 Analysis

There are various methods that can be used to relay the characteristics and performance properties of bitumen. The methods start with raw data received from testing on an apparatus, to manipulating and converting the data to workable figures. Equations are used to engineer various diagrams and charts. These charts are then used to evaluate the binder's performance potential and can be utilised to make decisions.

2.12 Master Curves

A master curve is a useful tool that is utilised to describe the visco-elastic nature of a binder (Rowe and Sharrock, 2011). The stiffness of a material, at multiple temperatures, over a range of frequencies are referred to as isotherms. These isotherms are used to construct a master curve. The isotherms are vital to the construction of a master curve, as they can shift the various temperature curves into one single smooth curve (hence the master curve). The curve is based on one reference temperature that is chosen. This reference temperature (T_{ref}) is used to analyse the data further and determine the behaviour of the material. To shift these isotherms to the reference temperature, a shift factor a_T is used. At the reference temperature, the shift factor is equal to one. The frequency scale on the master curve is a logarithmic reduced frequency. Figure 2.28 displays how isotherms are shifted to form a master curve. To calculate the reduced frequencies, Equation (2.22) (Hunter *et al.*, 2015) is used:

$$log\, f_r = log\, f + log\, a(T) \tag{2.22}$$

where,

f_r = reduced frequency (rad/s)

f = frequency (rad/s)

$a(T)$ = shift factor

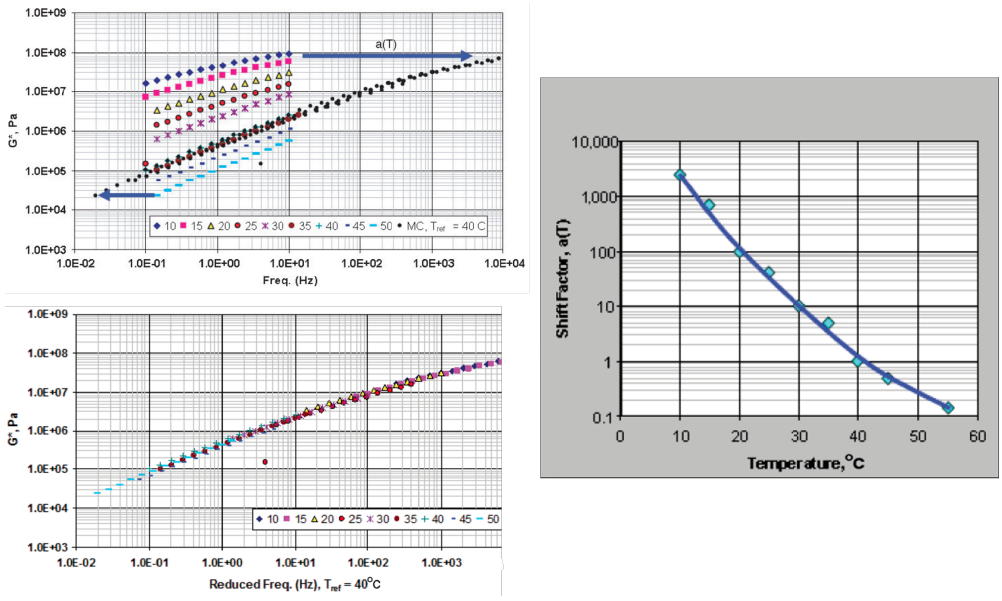

Figure 2.28: A shift factor applied to isotherms to create a master curve (Rowe and Sharrock, 2011)

2.12.1 Shift Factors

The shift factor is a ratio between the reduced frequency and the frequency. The master curve consists of the complex modulus (G*) vs the reduced frequency and also the phase angle (δ) vs the reduced frequency. There are many shift factors equations that have been developed in history.

- Arrhenius
- Williams-Landel-Ferry
- Kaelble
- Modified Kaelble

The Williams, Landel and Ferry (WLF), the Kaelble, the modified Kaelble and the Arrhenius equations are some of the most popular used equations. From the master curve, one can observe the viscoelastic behaviour.

The **Arrhenius** equation is another method of determining the shift factor for a master curve. The equation is constructed as:

$$log a_{\mathrm{T}} = C(\frac{1}{T} - \frac{1}{T_{\mathrm{ref}}}) \tag{2.23}$$

Where,

a_T = shift factor

C = constant

T = testing temperature

T_{ref} = reference temperature

The constant is a fitting parameter which is equal to:

$$C = \frac{0.4347 E_a}{R} \tag{2.24}$$

Where E_a is the activation energy (J/mol) and R is the ideal gas constant (8.314 J/mol.K) (Yusoff *et al.*, 2011*b*). In literature, there are other values suggested for the constant C, such as 10920, 13060 and 7680 K. The Arrhenius equation has been found to produce a better fit of master curves for low temperatures (Yusoff *et al.*, 2011*b*). Rowe and Sharrock's research in 2011, showed that the Arrhenius equation best describes the behaviour below the glass transition.

The **Williams-Landel-Ferry** equation for determining the shift factors is:

$$log a_T = \frac{-C_1(T - T_{ref})}{C_2 + (T - T_{ref})} \tag{2.25}$$

Where C_1 and C_2 are both empirical constants. (Rowe and Sharrock, 2011) concluded that the WLF equation produces a better fit at temperatures close to the glassy temperature and that the equation is also applicable at higher temperatures (Yusoff *et al.*, 2011*b*).

The **Kaelble** shift equation is a modification of the WLF equation.

$$log a_T = \frac{-C_1(T - T_d)}{C_2 + |T - T_d|} \tag{2.26}$$

Where T_d is the defining temperature. Kaelble introduced a magnitude term, which changed the hyperbolic shape into a sigmoidal one (Rowe and Sharrock, 2011). This modification produced an inflection point in the curve at the defining temperature. Above the inflection point, the curve was found to be similar to the WLF curve. It was found that the Kaelble equation, at low temperatures, produces imprecise data compared to the WLF equation. This is due to the equation suggesting that the reference temperature and the defining temperature are the same. The equation was altered to accommodate this.

The **Modified Kaelble** equation adjusted the Kaelble equation to accommodate the error that appears at low temperatures:

$$log a_T = -C_1\left(\frac{T - T_d}{C_2 + |T - T_d|} - \frac{T_{ref} - T_d}{C_2 + |T_{ref} - T_d|}\right) \tag{2.27}$$

The solution was to separate the defining temperature from the reference temperature, and this was done by adding a constant term. In 2011, Rowe and Sharrock's results showed that the root mean square error reduces significantly from the Arrhenius to the Modified Kaelble. It was concluded that the Kaelble method provided a better fit compared to the WLF and Arrhenius methods (Rowe and Sharrock, 2011). Figure 2.29 gives an example of how the shift factor models are compared.

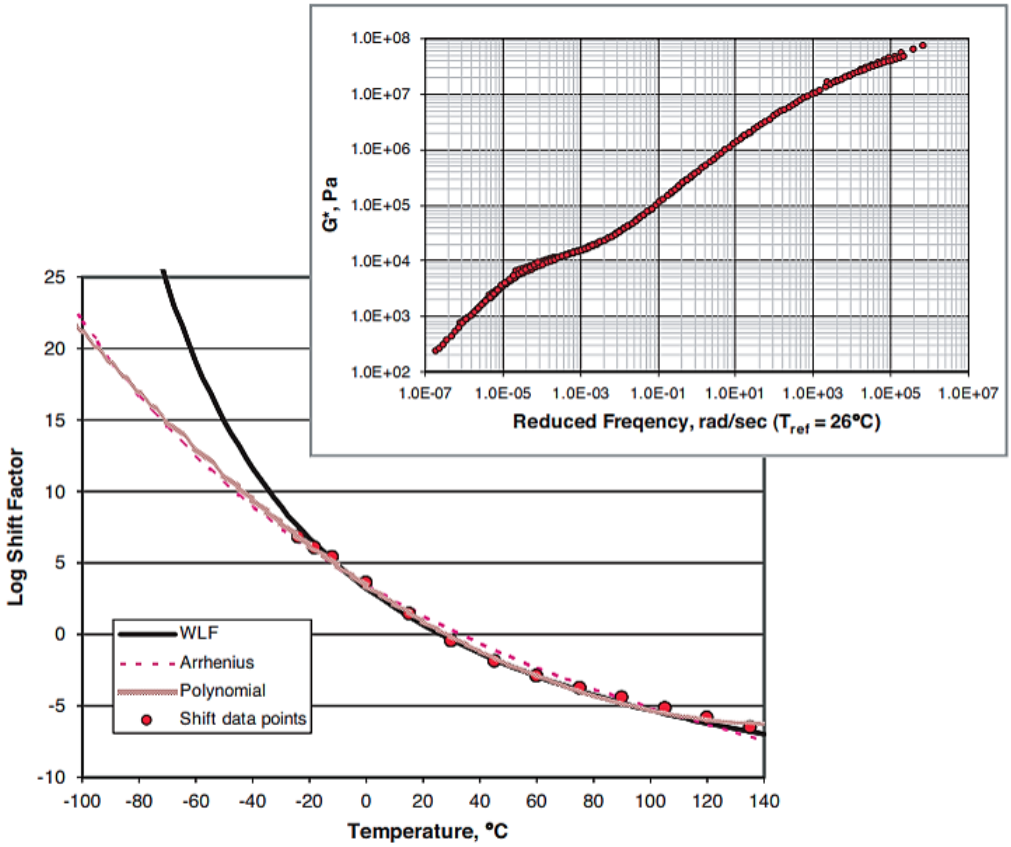

Figure 2.29: The comparisons between Kaelble, Arrhenius and WLF for a SBS modified binder (Rowe and Sharrock, 2011)

2.12.2 Mathematical Models

There are various mathematical models that are used to describe the characteristics of bituminous binders. The benefit of using models to describe the rheological behaviour of a binder is to provide rational parameters (Anderson and Marasteanu, 2010). These rational parameters can link the binder and the mixture behaviour, and develop a relationship to express the ageing process. Some of the most commonly used empirical models which are used to evaluate the properties of bituminous binders are:

- The Christensen-Anderson (CA) model
- The Christensen-Anderson-Marasteanu (CAM) model
- The Standard Sigmoidal (SS) model
- The Discrete Relaxation Spectrum.

There are four main parameters that were recognised by (Christensen and Anderson, 1992), to characterise the properties of bituminous binders, which are abstracted from the master curve. A visual explanation of the model can be seen in Figure 2.30. These parameters are:

- Glassy modulus (G_g) - The glassy modulus is the upper limit of the complex or stiffness modulus at high frequencies and low temperatures. The glassy modulus generally ranges from 0.6 GPa to 1.5 GPa, but a value of 1 GPa is commonly assumed.

- Steady-state viscosity (η_0) - The steady-state or Newtonian viscosity is described as the limit of the complex shear viscosity (η^*), as the phase angle approaches 90°, which nears viscous behaviour.

- Cross-over frequency (ω_c) - The cross-over frequency is where the tan of $\delta$is equal to one (also where G' = G"), for any given temperature.

- Rheological Index (R) - The rheological index is a parameter that can indicate the rheologic type and is bitumen specific. It is the difference between the upper limit of the complex modulus (or the glassy modulus) and the complex modulus at the crossover frequency. The rheological index is not a measure of temperature, but a measure of the shear rate dependency of the material, which can indicate cracking behaviour.

The CA model:

In Christensen and Anderson's model, there are three equations that the model comprises of.

$$|G^*| = G_g(1 + (\frac{w_c}{w})^{\frac{(log2)}{R}})^{\frac{-R}{log2}} \tag{2.28}$$

$$\delta = \frac{90}{(1 + (\frac{w_c}{w})^{\frac{(log2)}{R}})} \tag{2.29}$$

where,

G* = complex modulus (Pa)

ω = frequency (rad/s)

δ = phase angle (°)

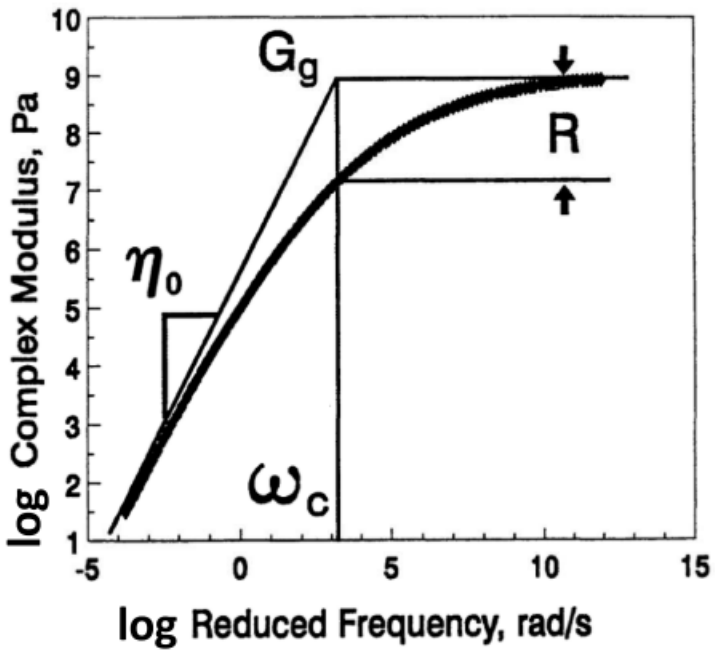

Figure 2.30: A visual explanation of the CA model (Anderson *et al.*, 1994)

From these two equations above, Christensen and Anderson combined them to create the third equation of the model, the rheological index:

$$R = \frac{(log2) \cdot log(\frac{|G*(\omega_C)|}{G_g}}{log(1 - \frac{\delta(\omega_C)}{90})} \tag{2.30}$$

Although the R equation is useful to obtain the rheological index, it was found that it is impossible to use at $\delta = 90°$. From research it was found that the CA model produces a lack of fit to the master curve in the region of high temperatures and longer loading times (Da Silva *et al.*, 2004). Refer to Figure 2.31.

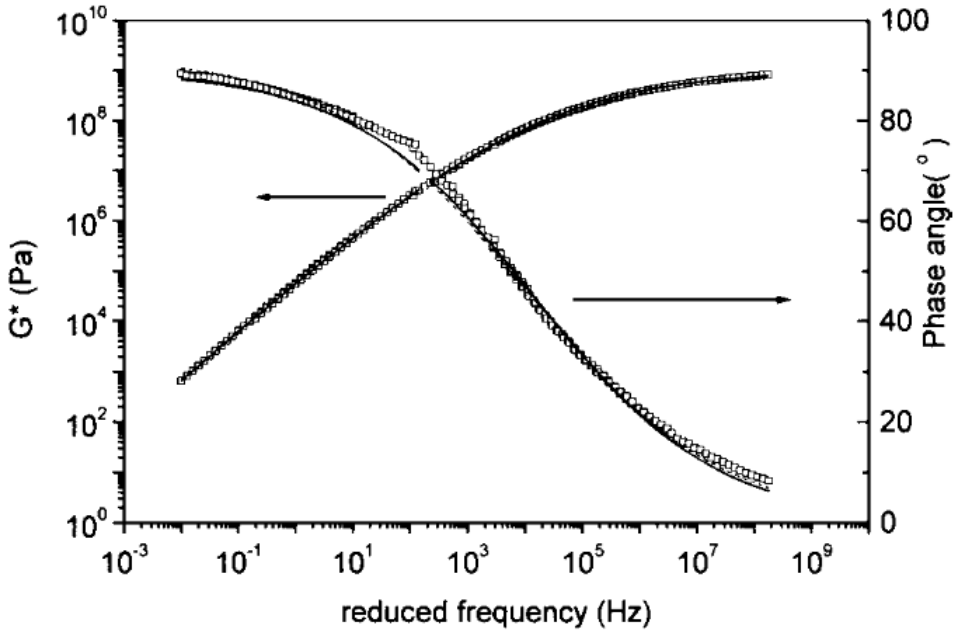

Figure 2.31: The master curve constructed by the use of the CA model (Da Silva *et al.*, 2004)

A study done by (Yusoff *et al.*, 2013) concluded that the CA model struggles to provide an accurate representation of the binder behaviour of EVA. In the study, the G_g was taken as 10^9 Pa for in shear and as $3x10^9$ Pa for in extension or in flexure in the CA model, where the cross-over frequency and the R-value is fitted (Anderson *et al.*, 1994). The CA model shows accurate behaviour when the phase angle is between 10° and 70° (Yusoff *et al.*, 2011*a*). It is recommended that the CA model be used when the applications in stiffness (G*) are ≥ 100 kPa.

CAM Model:

The CAM model is an adjusted version of the CA model. Anderson and Marasteanu attempted to improve some of the previous model's elements, such as the descriptions of unmodified and PMB bitumen materials, which lack accurate representation at low and high frequencies (Yusoff *et al.*, 2011*b*). The equations of the CA model were modified and the following equations were proposed:

$$|G*| = G_g(1 + (\frac{w_c}{w})^v)^{-\frac{\omega}{v}} \tag{2.31}$$

$$\delta = \frac{90\omega}{(1 + (\frac{w_c}{w})^v)} \tag{2.32}$$

Where ν= log(2/R), and the other symbols still remain as defined previously. An additional parameter was introduced, the ωparameter. This parameter tackles the issue of how the tempo of |G*| converges into the 45° and G_g asymptotes, as the frequency reaches zero or infinity (Marateanu and Anderson, 1996). Marasteanu and Anderson had tested 38 modified and unmodified bitumen binders in their model. It was found that the difference in the data between the CA model and the CAM model ranged between 10 - 35% respectively (Yusoff *et al.*, 2011*b*). (Da Silva *et al.*, 2004) modelled pure asphalt binders using the CA model and the CAM model. It was concluded that the CAM model does accommodate the PMB binders, where the CA lacks, yet the fit at the extreme temperatures is still not addressed.

Standard Sigmoidal Model:

The Sigmoidal model is a dynamic modulus function, which is used to describe the rate dependency of the modulus master curve. The model was introduced in the Mechanistic-Empirical Pavement Design Guide (ME PDG), which was developed in the National Cooperative Highway Research Program (NCHRP) project A-37A. It is a symmetrical four-parameter model, which has undergone modification to present the equation:

$$log|G*(\omega)| = min + \frac{max - min}{1 + e^{\beta+\gamma(log\omega)}} \tag{2.33}$$

where,

min = lower horizontal asymptote

max = upper horizontal asymptote

ω = the reduced frequency

β controls the horisontal position of the inflection point

γ = the slope of the curve

A graphical representation is presented below in Figure 2.32:

From the equation above, (Rowe, 2009) created an equation to determine the phase angle.

$$\delta(\omega) = -90 \cdot \alpha \cdot \gamma \cdot \frac{e^{\beta+\gamma(log\omega)}}{[1 + e^{\beta+\gamma(log\omega)}]^2} \tag{2.34}$$

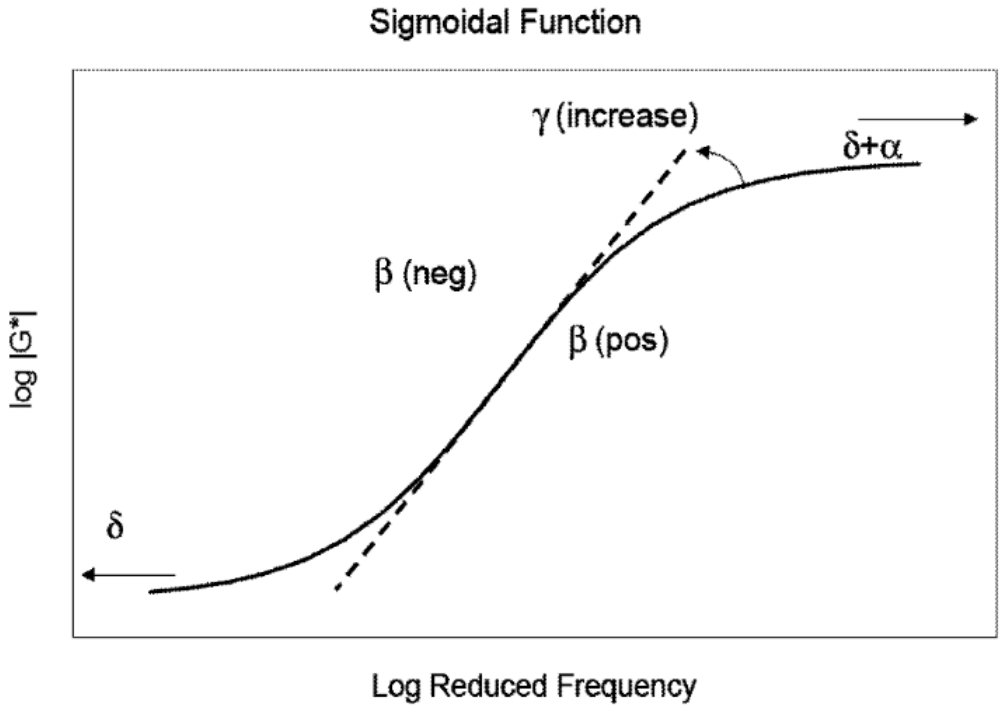

Figure 2.32: The definition of the sigmoidal model (Yusoff *et al.*, 2011*a*)

There are three fitting parameters, ß, min and γ. ß and γ are the two parameters that describe the shape between the inflection point and the asymptotes. To obtain an estimate of the fitting parameters, an optimisation process is used. Microsoft's Excel Solver function is used for this purpose. Although it requires initial input values, the solver function replaces the tedious method of initial guesswork. For a study done by (Yusoff *et al.*, 2013) had initial values of β= -1, min = 1 and γ= 1. The study observed that at low frequencies and or high temperatures, the G* of asphalt is small, dues to the min values that are all negative. The γindicated no effect on the slope of the master curve from intermediate and high temperatures, with or without ageing the values were consistent. The βincreases with age for the unmodified binders, yet decreases when the binder contains EVA and SBS polymers (Al-Haddad, 2015). The studies concluded that the SS model does not have the ability to correlate the LVE rheological properties of the highly modified binders, even if the age did not influence the accuracy (Yusoff *et al.*, 2013).

The Discrete Relaxation Spectrum

(Baumgaertel and Winter, 1992) describes the discrete relaxation spectrum as a summation of discrete terms, where each term has a characteristic time constant, λ_i. The advantage of the discrete spectrum is that the model can be used to predict a broad range of linear viscoelastic material functions. The model has a variety of ways to "discretising a specific continuous spectrum". The model is dependent on discrete relaxation modes. The mode refers to a decaying time function. The Maxwell modes are well known and are considered easy to use in calculations. The relaxation modulus from the discrete spectrum is defined as:

$$G(t) = G_e + \Sigma^n g_i \exp \frac{-t}{\lambda_i} \tag{2.35}$$

where,

t = time (s)

g_i = relaxation strength of discrete relaxation mode

G_e = equilibrium modulus

λ_i = discrete relaxation time

The discrete relaxation spectrum, or the generalised Maxwell model, is based on the mechanical model of Maxwell, which is a spring and a dashpot in parallel, see section 2.5.

$$G'(\omega) = G_e + \Sigma^n g_i \frac{(\omega\lambda_i)^2}{1 + (\omega\lambda_i)^2} \tag{2.36}$$

$$G''(\omega) = \Sigma^n g_i \frac{\omega\lambda_i}{1 + (\omega\lambda_i)^2} \tag{2.37}$$

This model has been proved useful is modelling flow behaviour.

2.13 Durability Parameters

Durability is a significant property that contributes to the behaviour and performance of a bitumen binder. Ageing is a term used to explain the rheological changes that a binder experiences over time. The cause of the change in properties is due to external/environmental factors, such as traffic climate changes. Durability is defined as the ability of a binder to resist the effects of ageing (TG 1, 2015). Some durability parameters that are used are:

- Glover-Rowe (G-R)
- Critical temperature difference (ΔT_C)
- Visco-elastic transition (VET) stiffness and temperature
- Rheological Index (R-value)
- Ageing ratios

2.13.1 ΔT_c

With the G-R parameter, the ΔT_c, is another parameter that is useful to measure the relaxation and stiffness properties of a binder at intermediate and low temperatures. The presentation of the parameters are seen on a black space diagram (G* vs δ). With a soft binder, the phase angle will have a high value, whereas with a hard binder, the phase angle will have a low value. The G-R parameter provides limits to show where cracking would occur. The ΔT_c parameter is used to describe low-temperature cracking, and is defined as (Rowe *et al.*, 2014):

$$\Delta T_c = T_{c,S(60)} - T_{c,m(60)} \tag{2.38}$$

$$T_{c,S(60)} = T_1 + \frac{log300 - logS(60)_1}{logS(60)_1 - logS(60)_2} \cdot (T_1 - T_2) - 10 \tag{2.39}$$

$$T_{c,m(60)} = T_1 + \frac{0.3 - m(60)_1}{m(60)_1 - m(60)_2} \cdot (T_1 - T_2) - 10 \tag{2.40}$$

ΔT_c is determine by the difference of two critical temperatures, the temperature at S(60) = 300 MPa and m(60) = 0.3. A graphical concept of $T_{C,S}$ and $T_{C,m}$ can be seen in Figure 2.33. The values of the two critical temperatures can be determined by interpolation (Anderson *et al.*, 2011). A limit of $\Delta T_c > -5°C$ is specified by the SA Performance Grade Specification. The low temperature specification of S ≤ 300 MPa and m ≥ 0.3, was converted by (Rowe *et al.*, 2014) to G* ≤ 111 MPa and δ ≥ 26.2°, respectively, to allow for a better representation of the low temperatures on the Black Space Diagram.

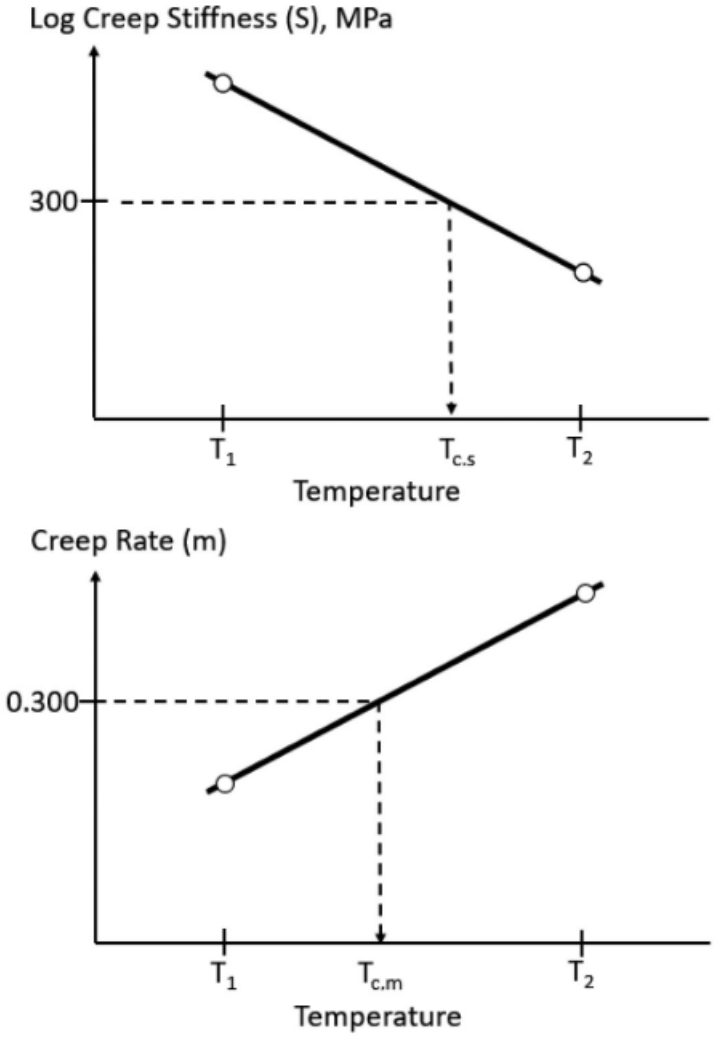

Figure 2.33: ΔT_c illustration (Asphalt Institute, 2019)

2.13.2 Glover-Rowe Parameter

A study where fourteen unmodified binders were tested, showed that the extensional flow of a binder can be represented by an elongation model, using a visco-elastic Maxwell element (Glover *et al.*, 2005). From this model, two rheological parameters became apparent. The dynamic shear modulus (storage modulus) G' and the ratio of the dynamic viscosity to the storage modulus η'/G'. The Glover parameter developed as:

$$Glover\ Parameter = \frac{G'}{\eta'/G'} \tag{2.41}$$

The G' and η' values are measured in a DSR at 15°C at a rate of 0.005 rad/s. Two limits were proposed by Glover, where crack limits of 3 and 5 cm, correspond to a crack warning of 0.003 MPa/s and a crack limit of 0.0009 MPa/s. (Rowe *et al.*, 2014) showed that the Glover parameter van also be expressed as:

$$\frac{G * cos^2\delta}{sin\delta} = Glover - Rowe\ Parameter \tag{2.42}$$

The limiting values of crack initiation is at G-R ≥ 180 kPa and significant cracking at G-R ≥ 600 kPa, where for both the frequency is 0.005 rad/s and temperature at 15°C. Thermal cracking was found to be at G-R ≤ 184 MPa, where the frequency is at 0.01667 rad/s and the temperature varies (Mensching *et al.*, 2015). Fatigue cracking takes place at G* sinδ ≤ 5 MPa where the temperature is also not consistent and the frequency is 10 rad/s. Cracking does depend on the environment. Figure 2.34 displays the cracking limits.

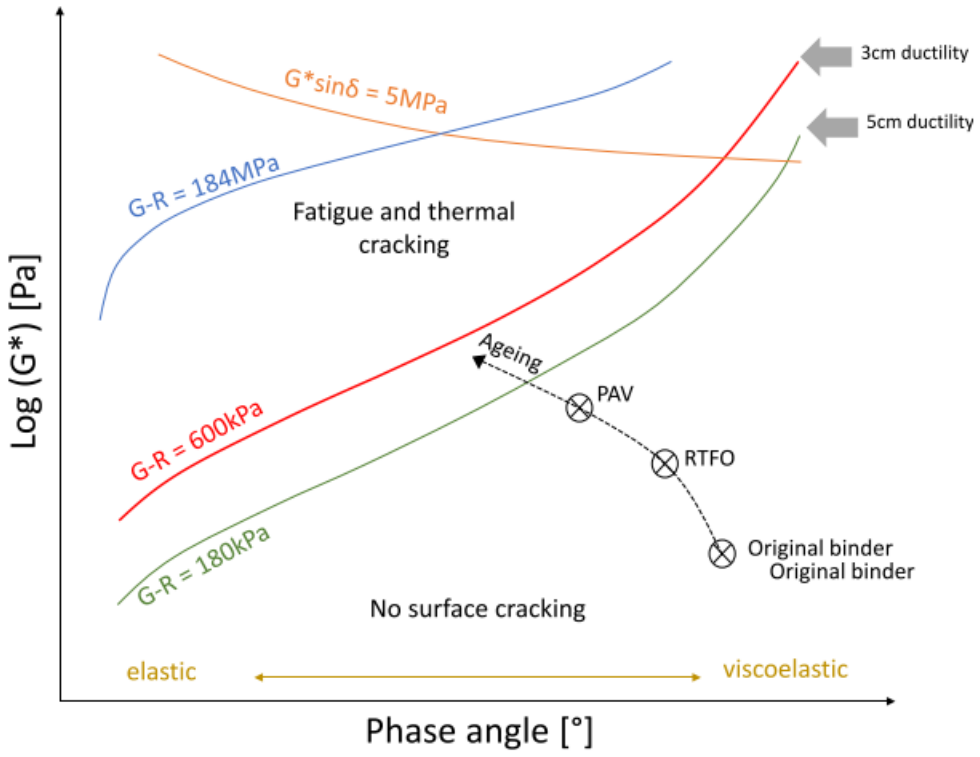

Figure 2.34: Black Space Diagram with G-R parameters. (Adapted from Rowe *et al.*, 2014)

2.13.3 Visco-Elastic Transition Temperature

The Viscous to Elastic Transition temperature (T_{VET}) is the temperature at which the storage modulus is equal to the loss modulus (G' = G"). The T_{VET} is obtained where the $\delta$is 45°. This temperature is useful as it is the temperature where there is an equal proportion of the elastic and viscous component of the bituminous material (Widyatmoko *et al.*, 2005). Widyatmoko stated that bituminous material displays a more viscous behaviour at low temperature when the T_{VET} is lower. There was found that a strong correlation exists between the T_{VET} and the visual surface cracking, in France on many sites (Migliori *et al.*, 1999). A new parameter was introduced during the study done by Widyatmoko, namely the complex modulus at the visco-elastic transition temperature (G^*_{VET}). This parameter was found to be a useful tool to demonstrate the changes in bitumen properties during different levels of ageing. Results from the tests showed that as T_{VET} increases, the age of the binder also increases, but the G^*_{VET} decreases (Widyatmoko *et al.*, 2005). Figure 2.35 shows how the higher the stiffness, the lower the T_{VET}.

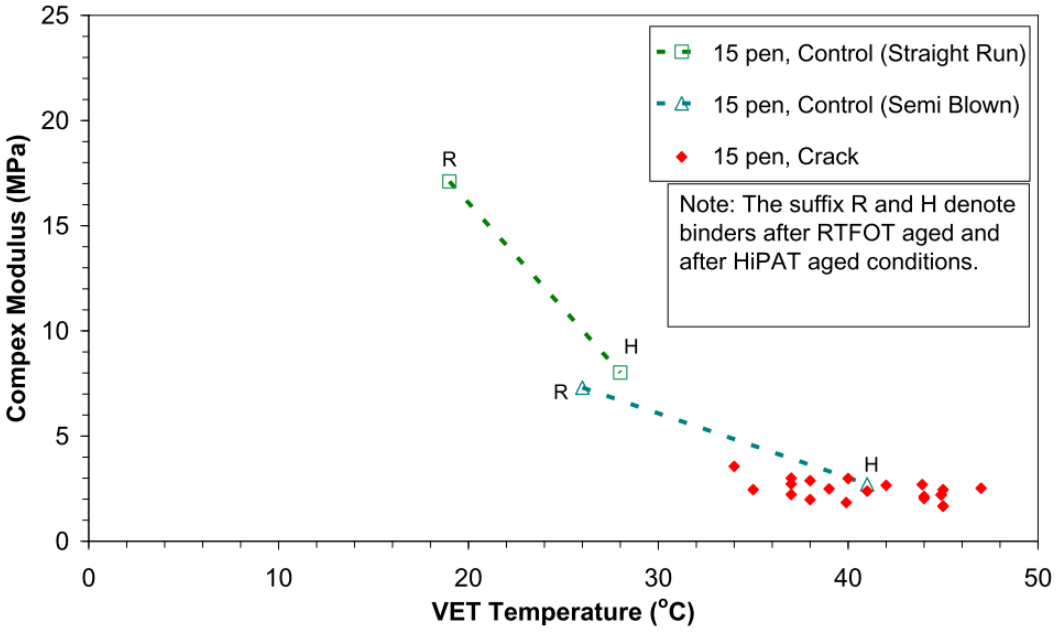

Figure 2.35: G* vs T_{VET} (Widyatmoko *et al.*, 2005)

2.14 Section Summary

A summary of important points from the literature:

- There various types of binders that can be used. The composition of each binder contributes to its performance. Literature shows discusses how a modifier can improve characteristics such as water and skid resistance. The viscoelastic properties are improved to withstand environment factors and repetitive traffic loads.

- The bond between the seal and aggregate is crucial to the performance of the seal. This bond is important to understand the behaviour of stone orientation in seal binders. Characteristics of seal binders such as cohesion and adhesion, are related to cracking and stone loss failures.

- Rheological apparatuses are key to obtaining the test data. The DSR and BBR have shown that the combined test data can provide enough data for the construction of the Master Curve. The RTFO test is a respectable oven that simulates short-term ageing. The ageing of bitumen binder is beneficial to understand long-term performance of seal binders.

- The rheological modelling of bitumen binders is important to the construction of the Master Curves, and Black Space diagrams. These diagrams assist in the analysis of binder behaviour, so as to understand the temperature-related performance. Shift factors contribute to the construction of the Master Curve, and it is thus significant to have an accurate function to allow for a accurate as possible curve. Literature has shown the the Modified Kaelble is a common shift factor function that can provide precise results. The mathematical models, such as the CA and Discrete Spectrum models, are equations that can accurately represent the data. From these models, further calculations can be conducted.

- The MSCR test is an essential test than can provide information on the creep and recovery properties of the bitumen binder. Stone orientation behaviour can be derived from this test. Rutting failure is an example of what the MSCR test evaluates.

- Durability parameters provided information regarding the possible failures that binders can experience. The G-R parameter and the ΔT_c are significant tools to assess the durability of a binder.

Chapter 3

Methodology

This chapter aims to explain how testing was conducted and what methods were used to analyse the data. To establish the approach in which analysis could be carried out, tests were performed on the selected binders in their original form and after short term ageing. The materials used in this study were obtained from a refinery, TOSAS.

The objective of this chapter is to:

- Convey what materials were used,
- Explain the procedures utilised to obtain rheological properties and,
- The methods used to analyse the rheological properties of the bituminous binders.

3.1 Materials Used

This study conducted tests on unmodified and modified binders. Only one unmodified binder was used. Two types of modified binders were used, namely a polymer modified binder (PMB) and a bitumen rubber binder. Table 3.1 displays the specific bituminous binders that were tested. These binder were conducted at two ages, the original binder condition (i.e. unaged binders) and short-term aged binders (i.e. aged binders.)

Table 3.1: Binders used in this study

Unmodified Binder	
Penetration Grade	PEN 70/100
Modified Binder	
Polymer Modified Binder	S-E1
	S-E2
Bitumen Rubber	S-R1
	S-R2

3.2 Testing and Conditioning Devices

There are three devices used in this study to obtain the rheological properties for analysis, namely a conditioning device and two testing devices. Two testing devices were used to test the binders in their original state and after ageing. The Dynamic Shear Rheometer (DSR) and the Bending Beam Rheometer (BBR) have been used to test the binders in their original and aged states at high and low temperatures, respectively. The short term ageing of the binder was necessary to simulate binder properties in a construction environment. The conditioning device was utilised to age the binders. The Rolling Thin Film Oven (RTFO) allowed for the binder to simulate short term ageing.

The Anton Paar MCR 302 Dynamic Shear Rheometer at the University of Stellenbosch, was used to conduct the tests at high and intermediate temperatures. Temperatuers that were used in the DSR testing ranged between 10°C and 70°C. The Canon Thermoelectrically-cooled Bending Beam Rheometer was used to do rheological testing at low temperatures. Test temperatures on the BBR ranged between -12°C to -36°C. The ageing of the binder was conducted in the Rolling Thin Film Oven (RTFO). All these devices were used at the University of Stellenbosch. For each test, the ASTM standards were followed.

3.3 Experimental Design

Below, in Figure 3.1, is the experimental procedure followed for this study. Each binder is tested without ageing in the testing devices, DSR and the BBR. Each binder is also aged for short term ageing, and then tested again in the DSR and BBR.

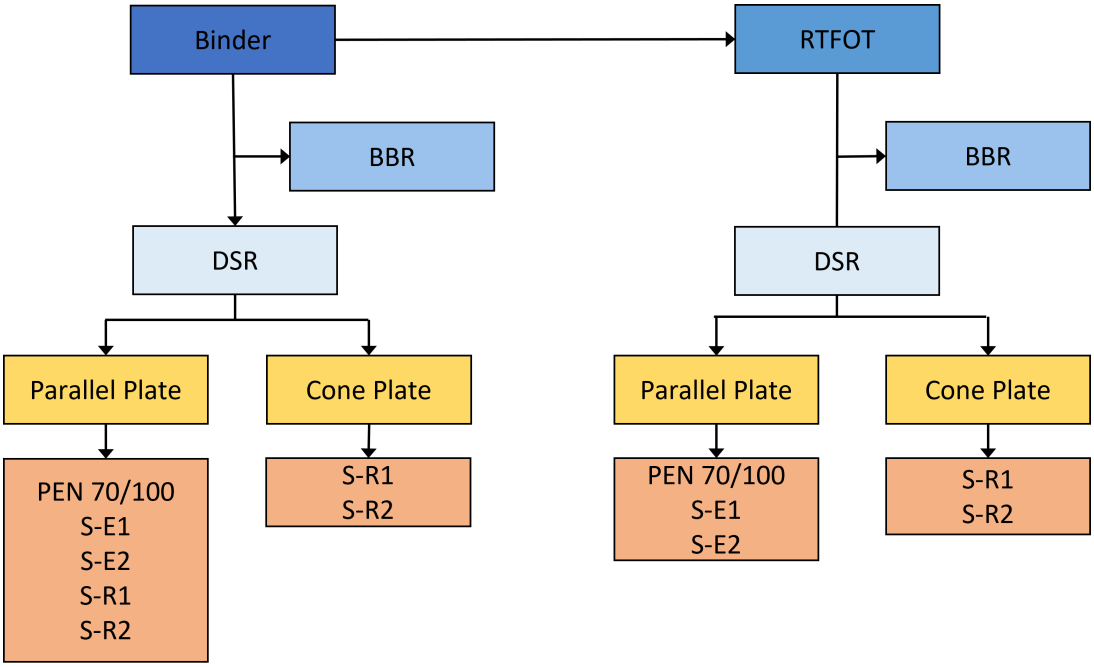

Figure 3.1: Experimental design of how each binder was tested

3.3.1 Objectives of the testing procedure

The objective of this study is to analyse the rheological properties of binders at intermediate temperatures.

This analysis will evaluate and present the rheological properties of five binders before and after ageing. The analysis assesses bitumen binders performance and rheological properties at intermediate temperatures, in terms of creep and recovery. The analysis will evaluate how the binder properties at intermediate temperatures perform at construction temperature.

3.4 Test Procedure

The rheological properties of a binder are obtained through testing the materials in a Dynamic Shear Rheometer (DSR) and a Bending Beam Rheometer (BBR). The ageing process is done in a Rolling Thin Film Oven (RTFO). Samples are prepared according to each individual device's ASTM guide. Some of the materials are handled differently, due to the material properties.

3.4.1 Sample Preparation

The DSR samples and the BBR samples are prepared individually and according to each device's specifications.

3.4.1.1 DSR sample

The DSR has a standard preparation for the samples in the ASTM D 7175-08 (2013) procedure. Circular silicone moulds are created for the samples. Different mould sizes are created to accommodate the testing at different temperatures. For the high temperature testing, the silicone mould dimensions are 25 mm in diameter, with a thickness of 1 mm. For the intermediate temperatures, the moulds are 8 mm in diameter and 2 mm in thickness. Temperature interval for each plate configuration is directly related to the measured stiffness. This relates to machine compliance and accuracy. Figure 3.2 shows the pouring of the silicone mix and how the mix is left to set. When the moulds are cast, there should be slight a overflow, so as to ensure that the sample is not too small for testing. Figure 3.3 shows how the binder is poured into the silicone moulds. Figure 3.4 displays the PEN 70/100 binder and the S-R1 binder, respectively. One can see the rubber crumbs in Figure 3.4.

Figure 3.2: Pouring the silicon mix into the moulds

Figure 3.3: Pouring the binder into the moulds

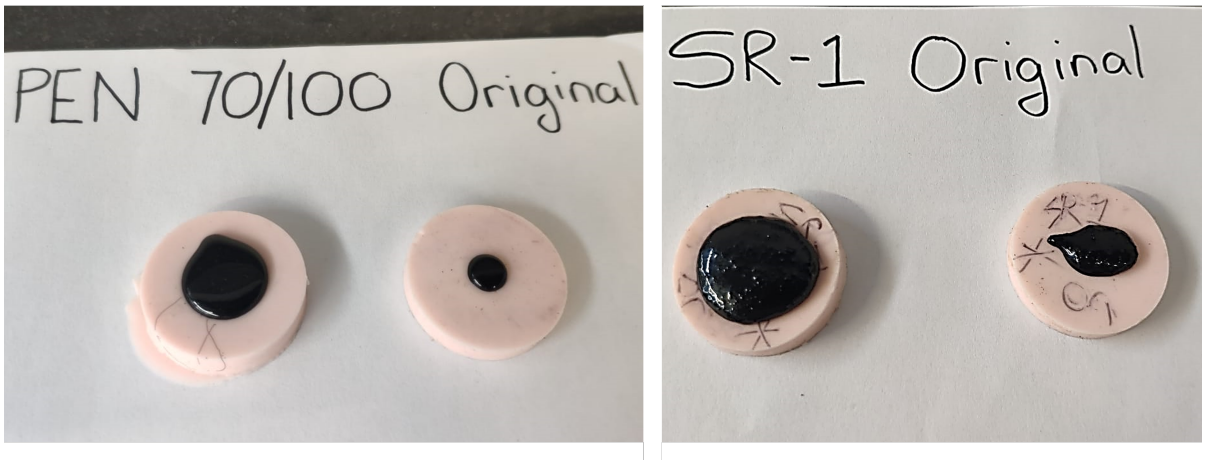

Figure 3.4: PEN 70/100 and S-R1 in silicone moulds

3.4.1.2 BBR samples

The BBR sample preparation followed the standard procedure set out in the ASTM D 6648-08 (2008). The BBR moulds that were used consisted of stainless steel bars, O-rings and plastic strips. The beam mould was constructed according to specifications. Figure 3.5 shows a constructed beam mould. The specimen moulds have interior dimensions of 6.35 ±0.05 mm wide, 127 mm ±5 mm long and 12.7 mm ±0.05 mm deep.

The mould is prepared and the binder is heated in the oven for one hour at 170°C. This ensures the binder is fluid enough to pour easily. The binder is then poured into the moulds, slowly to ensure no air bubbles are present in the mould, see Figure 3.5. The binder should overflow a bit. The sample is then left to cool for about 45 to 60 minutes. After the sample has cooled sufficiently the excess binder is trimmed off with a heated spatula or trimming tool. Figure 3.6 shows the specimen before and after trimming.

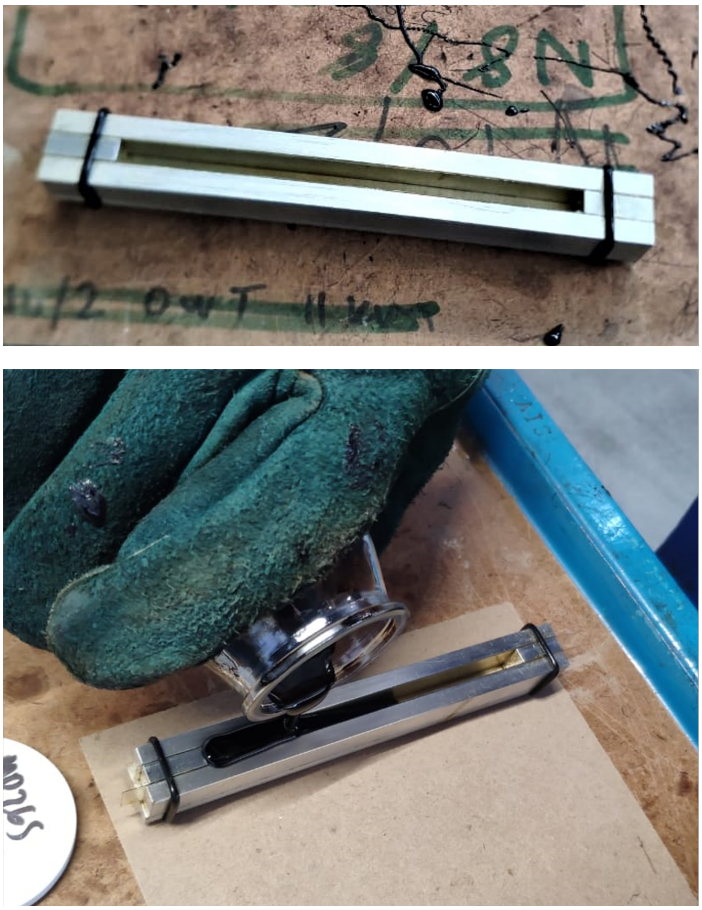

Figure 3.5: The empty constructed beam and the slow pouring of the binder into the beam

Figure 3.6: On the left is an untrimmed specimen and to the right is a trimmed specimen beam

The rubber binder is difficult to trim, due to the binder having a high elasticity. The trimming tool had to be heated to a very high temperature. Even then the rubber beam had voids. Figure 3.7 displays how the rubber proved to be difficult when trimming. Beams that showed imperfections, visible air bubbles or distortion were not used for testing.

Before demoulding, the specimen is placed in a cold bath, for 5 minutes, long enough for the beam to stiffen, so that the specimen can be readily disassembled. When disassembling the beam, it is important to not bend the specimen in the process. Figure 3.8 shows a beam that has been perfectly set and formed and can be tested. Figure 3.9 shows a beam that acquired air bubbles when it was poured. The voids indicate there was air entrapped when pouring. Pouring might have been too fast or the binder was not heated enough to pour easily. The beams that were accepted for testing were then placed in a cold bath at testing temperature for 60 minutes. The beams were then ready to be tested.

Figure 3.7: Trimming rubber beam

Figure 3.8: Beam after demoulding

Figure 3.9: Beam with voids

3.4.2 Ageing

The RFTO was used to age the binders and represent short-term ageing. The procedure to age unmodified binders differs from that of modified binders. The unmodified binders followed the procedure set out by the ASTM D 2872-04 (2004). The modified binders follow the TG1 Method MB-2 for the sample preparation and Method MB-2 for the ageing process in the RTFO. Short term ageing approximates the seal condition at construction. Figure 3.10 shows both the containers into which the binder is placed. The unmodified binder using the glass bottle and the modified binders using the brass container.

3.4.2.1 Unmodified binders

The RTFO was preheated to a temperature of 163 ± 05°C for at least 16 hours before testing. The sample preparation for the unmodified binder was to heat the binder in an oven of 150°C for the minimum time required for the binder to be completely fluid. About 35 ± 0.5g was poured into the glass bottles and immediately rotated horizontally, to pre-coat the inner surface of the bottle. The samples were then placed on a cooling rack for a minimum of 60 minutes to a maximum of 180 minutes. The samples were inserted in the rotary and rotated with a constant airflow of 4000 ± 200 mL/min for 85 minutes. The samples were then removed and the residue scraped out into a glass container and immediately sealed. The residue had to be tested within 72 hours after ageing.

3.4.2.2 Modified binders

The PMB binders and the rubber binders have similar preparation methods. Unlike the unmodified binder, the modified binders used a brass container. Both binders were placed in an oven with a temperature of 180°C for two hours. Thereafter the binder was removed from the oven and placed on a heating plate. The PMB binder was stirred for 30 minutes and the temperature of the heat source is kept at ±170°C. After the 30 minutes the sample was homogenised, and ready for testing. The rubber binder was place on a heat source and stirred for 5 min while keeping the temperature of the heating plate at ±170°C. After the binder was homogenised, the binder was ready for testing. A roller was placed in the container before closing the container with the lid. Figure 3.11 displays the rollers that were placed in the containers. Both the PMB

and rubber binders follow the same procedure for ageing. The oven was preheated to a temperature of 163 ±0.5°C for only 2 hours before testing. 40 grams of binder was poured into the brass containers. The containers were placed in the rotary, without turning on rotation or allowing airflow for 30 minutes. Thereafter turn on rotation, with the airflow for 60 minutes. The residue had to be tested within 24 hours of ageing.

Figure 3.10: The brass container and the glass bottle for the RTFO

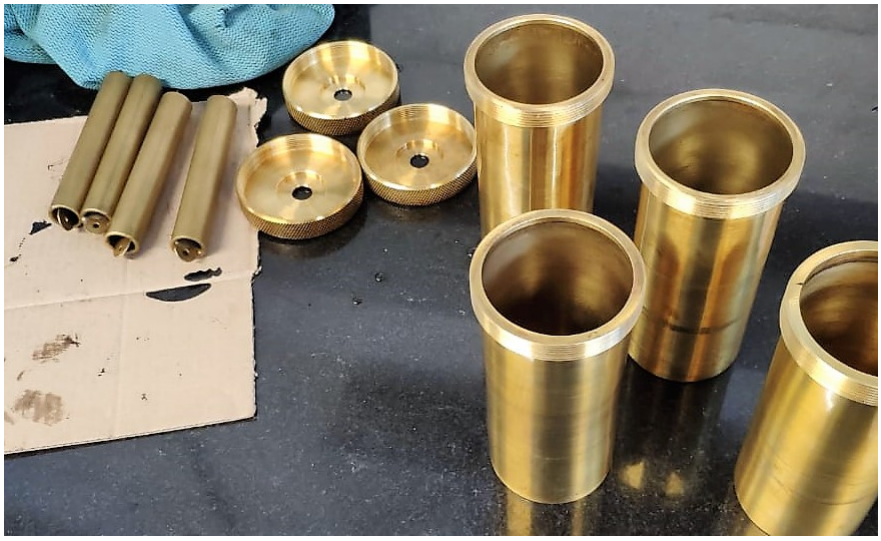

Figure 3.11: Brass containers, with rollers and lids

The RTFO in which the ageing test was conducted, proved to have trouble staying at a constant temperature. The oven took a long time to reach the desired testing temperature and when the oven door was opened, there was a large decrease in temperature. To counter this temperature loss, it was decided that the oven's temperature was set to 180°C before the containers were inserted. Which was 20°C higher than the testing temperature. Thus, when the oven door was opened to place the containers in the rotary, the temperature would drop to 160 ±2°C. When the oven door was closed, the oven temperature was immediately set to the testing temperature of 163°C. This ensured that when the samples were in the oven, they were tested at the correct temperature. Table 3.2 shows the significant temperature decrease and why adaptions were required.

Table 3.2: RTFO temperature fluctuations with time

Time (minutes)	**Temperature (°C)**
0	163.5
Door opened for ± 30s	160.3
Door closed	159.5
5	147.5
6	148
10	150.5
15	153.6
20	157.3
25	159.6
30	161.5
35	162.8

3.5 Testing

Additional tests were conducted after initial testing for further research on plate configurations. The rubber binders original conditions were tested on a cone plate (CP) and parallel plate (PP) configuration in the DSR, Table 3.3.

Table 3.3: The plate configurations used for testing

Binder		Plate
PEN 70/100	Original	PP
	Aged	
S-E1	Original	PP
	Aged	
S-E2	Original	PP
	Aged	
S-R1	Original	PP
	Original	CP
	Aged	CP
S-R2	Original	PP
	Original	CP
	Aged	PP

3.5.1 DSR Testing

On the Dynamic Shear Rheometer, two tests were carried out. Namely the frequency sweep and the multiple stress creep and recovery tests.

3.5.1.1 Frequency Sweeps

The frequency sweeps testing procedure was conducted according to the ASTM D7175. The frequency sweep for the lower temperatures, made use of 8 mm parallel plates. The higher temperatures used a 25 mm parallel plates. Overlapping temperatures of 25°C and 35°C were chosen so as to ensure the data is correlated with one another.

The DSR is switched on, and the compressor is set at 5 bar, with the cooling unit at 5°C. The zero gap for the DSR is set at different temperatures for the different sizes. The 8 mm's zero gap is at 20°C and the 25 mm at 50°C. Thereafter the parallel plate is heated to 60°C to ensure sufficient bonding between the sample and the plate, when the sample is placed on the plate, the mould is pushed into an arch, which releases the sample and then sticks to the plate due to the high temperature. As the plates are set at the specified gap, the sample bulges. It is important to trim the sample, as to ensure that the test is performed on the specified dimensions to provide reliable results. The tests are performed at various temperatures for each plate. See Tables 3.4 and 3.5 for the frequency range and temperatures.

Table 3.4: Frequency Sweep test conditions for the 8 mm plate

Plate	8 mm						
Temperature (°C)	10		15		25		35
Frequency (rad/s)	0.251	0.316	0.398	0.501	0.63	0.794	0.999
	1.26	1.58	1.99	2.51	3.16	3.98	5.01
	6.3	7.94	9.99	12.6	15.8	19.9	25.1
Strain (%)	1						

Table 3.5: Frequency Sweep test conditions for the 25 mm plate

Plate	25 mm						
Temperature (°C)	25		35		45	60	70
Frequency (rad/s)	0.251	0.316	0.398	0.501	0.63	0.794	0.999
	1.26	1.58	1.99	2.51	3.16	3.98	5.01
	6.3	7.94	9.99	12.6	15.8	19.9	25.1
Strain (%)	1						

3.5.1.2 MSCR

The MSCR is also performed on the DSR. This is a test where the creep and recovery potential of the binder is tested. The MSCR test for this study required the testing temperature to be at 22°C, 28°C and 34°C. These are the intermediate temperatures determined by the Performance Grade Specifications. The load applied was 3.2 kPa and the test was run for 10 cycles of 10 seconds each. The MSCR test is usually conducted at high temperatures, which then makes use of the 25 mm parallel plate. But as this study focuses on intermediate temperatures, the MSCR test was conducted on an 8 mm parallel plate, which were used when the DSR performs lower temperatures tests. The gap size of 2 mm for the 8 mm plates were used for the PEN 70/100, S-E1 and S-E2 binders. Yet for the rubber binders, a modification had to be made. The ASTM procedure was followed and stated that if the particle size is larger than 250µm, then the gap size is determined by multiplying the particle size of the rubber, by 4. And as the rubber particle size was 600 µm (according to Johannes Lambert), the gap size for the rubber particle was set for 2.4 mm. The temperatures at which testing was conducted was 22°C, 28°C and 34°C.

3.5.2 BBR Testing

A calibration of the beam was done before placing the beam in the BBR. The beam was placed on the supports and the prompts on the BBR were followed. The test runs for 240s where a 980 ±50 mN load was placed on the beam. The testing temperatures for this study ranged between -12°C and -36°C. The BBR calculates the stiffness and the m-value of the beam, as well as the deflection while the beam is being loaded. The load is applied for the loading times of 8, 15, 30, 60, 120 and 240 seconds. The stiffness and m-values are determined from the values at 60 seconds.

3.6 Data Analyses

The data analysis consists of various stages. The raw data was gathered from the various testing devices and provided as input to the RHEA software for analysis. Microsoft Excel was used to manipulate the data to be used in the RHEA software. Figure 3.12 shows the stages by which the data analysis was carried out.

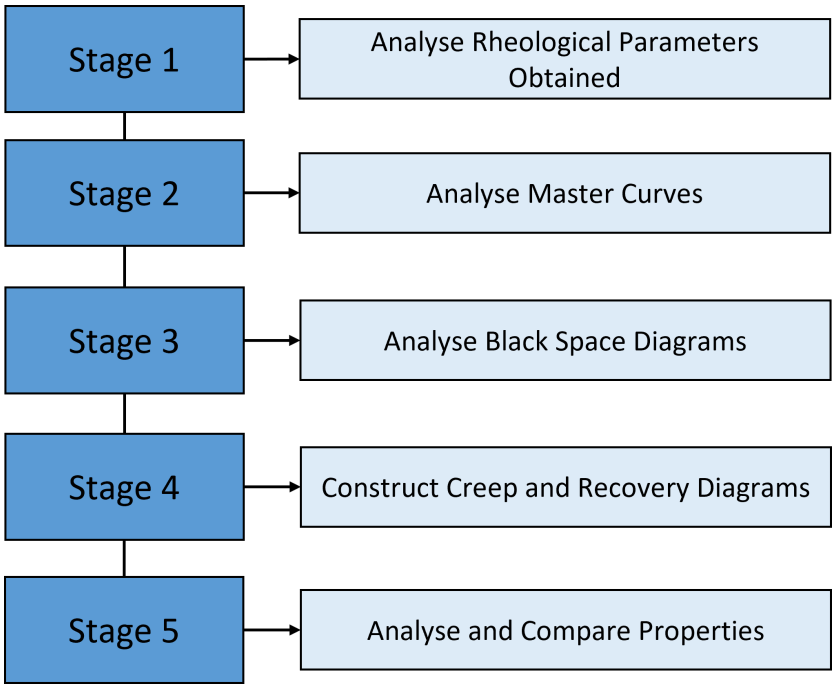

Figure 3.12: The stages of the data analysis

3.6.1 Analyse Rheological Properties

The first stage was to analyse the rheological parameters obtained. The basic parameters were acquired from the testing devices and the RHEA software. These basic parameters were used for further analysis. Below are the parameters that are used.

- Storage Modulus (G')
- Loss Modulus (G")
- Complex Modulus (G*)
- Phase Angle (δ)
- Strain (%)

3.6.2 Analyse Master Curve

The data obtained from the BBR was uploaded into the RHEA software and converted to DSR data. The data from the frequency sweeps, combined with the converted BBR data, was used by RHEA to construct the master curves. RHEA creates isotherms for each temperature. The reference temperature to which the isotherms were shifted was chosen as 15°C, to allow for the G-R parameter to be calculated. The mathematical models discussed in Chapter 2, (CA, CAM, DS), were used to plot a function on the master curve so as to allow for any data point to be calculated within the master curve temperature range.

3.6.3 Analyse Black Space Diagrams

The Black Space Diagrams were created from the data by RHEA software. The Black Space Diagram shows the viscous and elastic behaviour of the binder. The G-R parameter plots G* vs delta on the Black Space diagrams, thus eliminating temperature and loading time.

3.6.4 Construct Creep and Recovery Diagrams

The creep and recovery analyses were conducted in Microsoft Excel. The strain values obtained from the DSR allowed for the calculation of the creep compliance and the percentage recovery of each binder at each of the different temperatures.

3.6.5 Analyse and compare parameters

The last stage was the analysing of the data and obtaining the parameters listed below:

- Glover-Rowe (G-R)
- Viscoelastic Transition temperature (T_{VET})
- Viscoelastic Modulus (G_{VET})
- Critical temperature difference (ΔT_C)
- Creep Compliance (J_{nr})
- Percentage Recovery (%R)

- Maximum temperature of PG specifications (T_{max})
- Shift factor (a_T)

Each binder's parameters were summarised and compared to the other parameters. The original binders were compared to their aged counterparts. And all binders were compared with one another to evaluate the behaviour of the viscous and elastic components and how each plays a role in the performance of the binder.

Chapter 4

Results

This chapter will follow the procedure set out in Chapter 3. The chapter will convey the results obtained from the testing. The first stage will discuss the low-temperature analysis, such as the BBR results and the ΔT_c parameter. The next stage will discuss the creation of the master curves and the analysis thereof. Stage 3 will analyse the Black Space diagram and Stage 4 the MSCR test results. The last stage will discuss the durability parameters.

4.1 BBR Analysis

The cracking of seal binders may occur due to fatigue or in extreme weather conditions, such as very low climates. The possibility of a binder cracking is important in the decision on which binder should be selected for the specific road. To evaluate the performance of a seal binder at low temperatures, tests were conducted on the BBR. The BBR gives test results in terms of the stiffness (S) and the relaxation parameter (m-value). It can then be converted into workable data to analyse with the DSR test results. By conducting a low-temperature analysis, the range of temperatures is increased and can be used for a better analysis of the binder properties. In addition, the BBR results provide an anchor at the high (G*) end of the Master Curve, assisting with the accuracy of the models.

4.1.1 BBR results

A typical output from a BBR test is presented in Table 4.1.

Table 4.1: BBR test results for the PEN 70/100 Original (unaged) @ -12°C

Time (s)	Force (mN)	Deflection (mm)	Measured Stiffness (MPa)	Estimated Stiffness (MPa)	Difference (%)	m-value
8	988	0.546	206.14	205.89	0	0.414
15	985	0.716	156.72	157.17	0	0.445
30	986	0.984	114.15	114.09	0	0.479
60	**986**	**1.389**	**80.87**	**80.88**	**0**	**0.513**
120	988	2.006	56.11	55.99	-0.178	0.548
240	984	2.963	37.83	37.86	0.265	0.582

To compare each binder's performance at low temperatures, a mutual temperature of -24°C was selected. The results for the other temperatures can be found in the appendices. In Figure 4.1, the deflection versus time diagram is displayed for the binders at -24°C. The rubber binders have higher deflections compared to the PEN 70/100 and the elastomers. The deflection of the aged rubber binders are much higher than that of the unaged. Whereas with the aged elastomers and PEN 70/100, the deflections are lower than for the unaged binders.

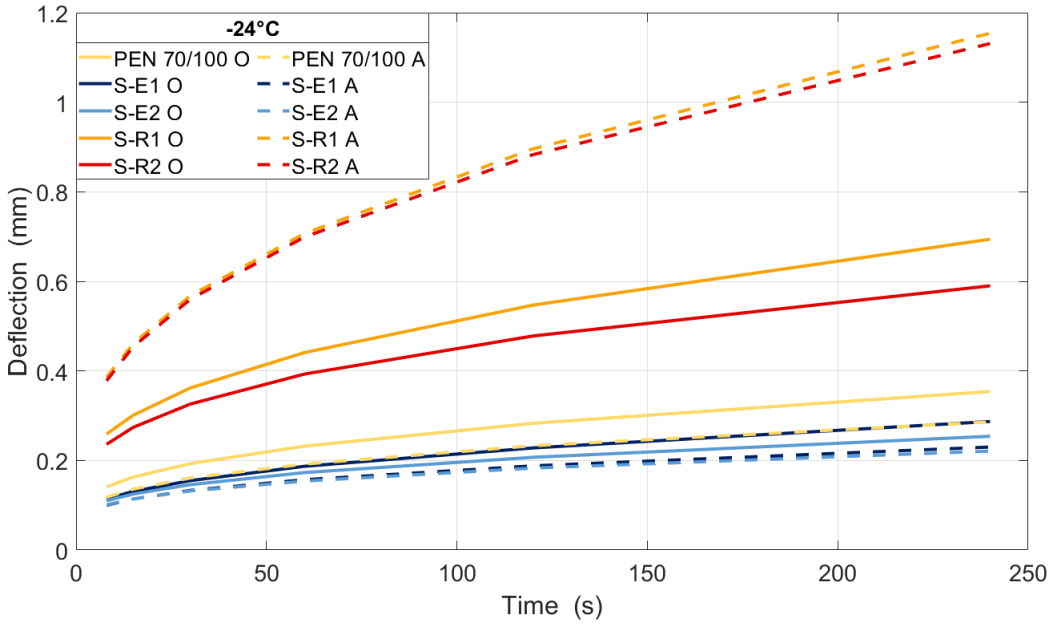

Figure 4.1: BBR deflection versus Time for all the binders at -24°C

Figure 4.2 displays the stiffness of the binders versus time. From this figure, it is clear that at -24°C, the rubber binders have the lowest stiffness and the elastomers have the highest stiffness. This can be due to the rubber modification contributing to the rubber being able to resist the effect of cold temperatures increasing stiffness. The rubber binders also display a decrease in stiffness with ageing. The alteration of the binder's nature with the addition of rubber improves the rubber binders performance at cold temperatures. Regarding the elastomers, the stiffness increases with age. From these results it is clear that the type of modification has a great influence on low temperature performance of the seals.

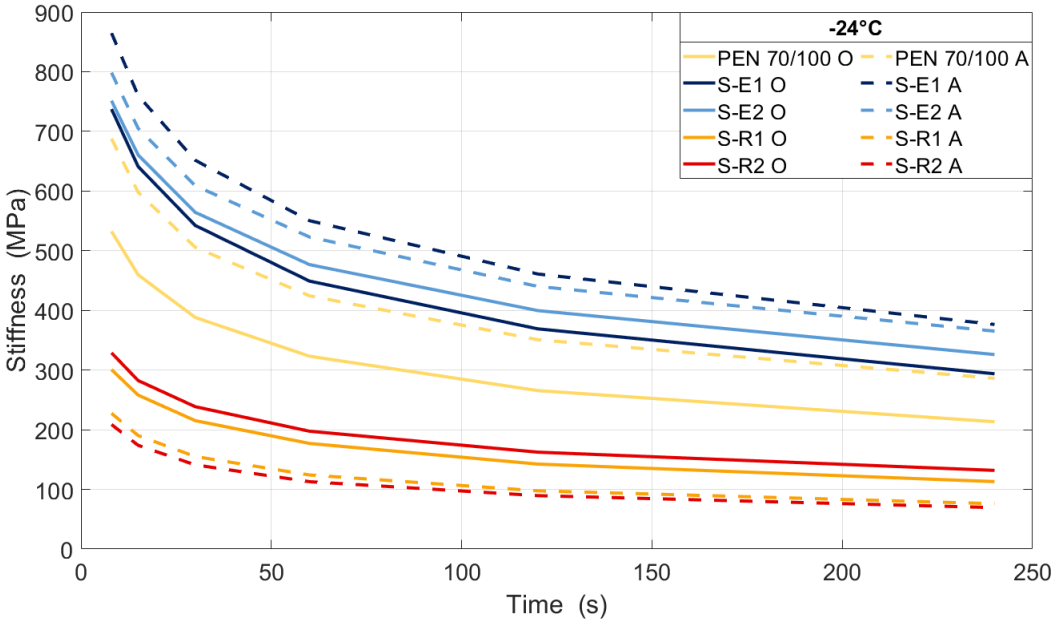

Figure 4.2: BBR stiffness versus Time for all binders at -24°C

According to Wang *et al.* (2019)'s research, at a temperature below 5°C, a liquid styrene-butadiene rubber (LSBR) modified binder that has a content of not more than 3 wt% of the base asphalt, will have a good anti-ageing performance. The team also concluded that as the LSBR content increases, the stiffness decreases. This supports the results that with an increase in modifier in the rubber, the stiffness decreases, whereas otherwise it would be expected to increase such as in the case of the elastomers.

4.1.2 ΔT_c parameter

To determine the ΔT_c of the binders, a relationship between the stiffness (S) and relaxation parameter (m) is created with time. From this, the S (stiffness) at 60 seconds and the m (slope) at 60 seconds is obtained. With the S(60) and m(60) values obtained for each temperature, the points are plotted against temperature and a trend line is created, see Figure 4.3. The S(60) = 300 MPa and m(60) = 0.3 is used to obtain the temperatures, $T_{c,S}$ and $T_{c,m}$. With these two temperatures, the ΔT_c could be calculated.

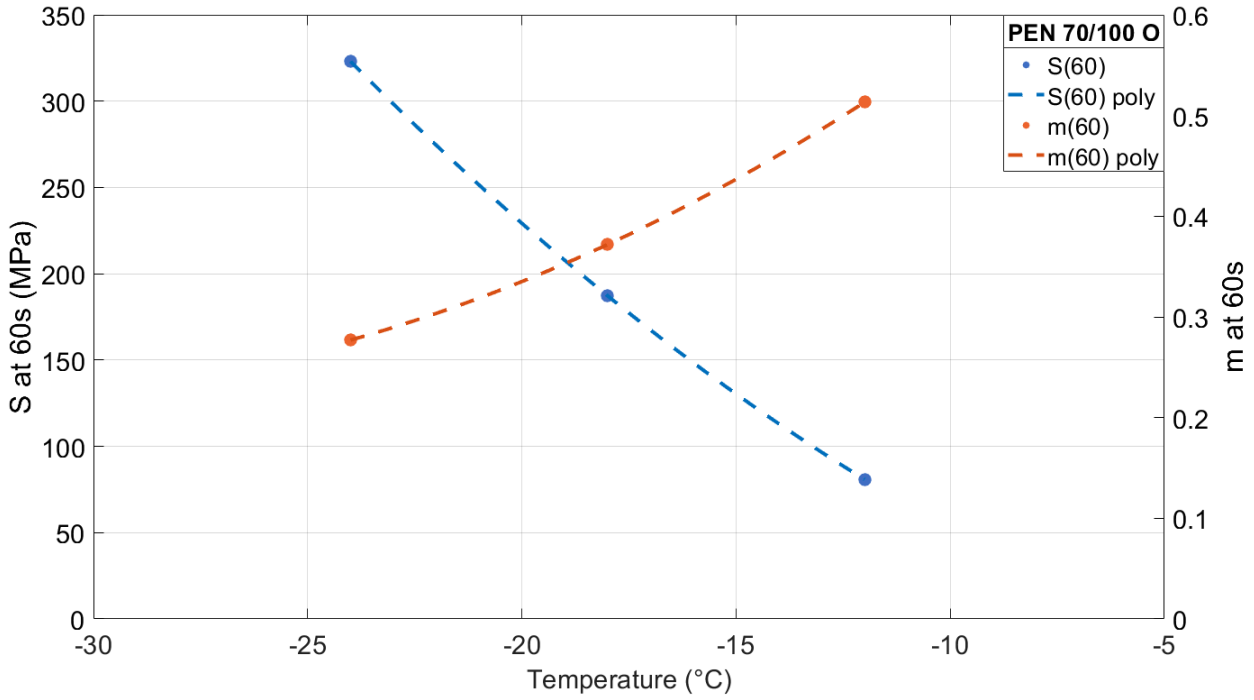

Figure 4.3: Trendlines for S(60) and m(60) for the PEN 70/100 Original (unaged)

Table 4.2 displays the S(60) and m(60) at each of the temperatures. These are then used to calculate the ΔT_c. Table 4.3 displays the ΔT_c for each of the binders. With declining temperatures, when the S limit is reached before the m limit, it is referred to as being S-controlled. There are only three binders that display S-controlled behaviour. It is preferred to have a binder that is S-controlled, as it means that the binder would have less of a chance of displaying thermal cracking and that the relaxation properties are still intact. The Performance Grade Specifications require a binder to have a ΔT_c of $\geq$ -5°C. Figure 4.3 displays a chart presenting the data.

Table 4.2: BBR data for the PEN 70/100 Original (unaged)

Temperature (°C)	**S60 (MPa)**	**m60**
-12	80.88	0.51
-18	187.25	0.37
-24	323.03	0.28
T_S (°C)	**T_m (°C)**	**ΔT_c (°C)**
-23.19	-22.55	-0.64

It is generally anticipated that the ΔT_c would decrease with age. Yet, these results show that only the elastomers adhere to this. The rubber binders' contradicting results may be due to the elastic component in the rubber and can link to the previous diagram of where stiffness decreases with age. The result is unexpected. As ΔT_c represents a binder's ability to relax, a high value would be favourable.

Table 4.3: ΔT_c for all binders

Binder		**$T_{c,s}$ (°C)**	**$T_{c,m}$ (°C)**	**ΔT_c (°C)**
PEN 70/100	Original	-23.19	-22.55	-0.64
	Aged	-20.88	-21.57	0.70
S-E1	Original	-20.46	-22.58	2.12
	Aged	-17.73	-19.31	1.58
S-E2	Original	-19.92	-19.12	-0.81
	Aged	-18.23	-16.87	-1.36
S-R1	Original	-27.61	-23.82	-3.79
	Aged	-29.21	-26.49	-2.72
S-R2	Original	-29.55	-21.77	-7.78
	Aged	-31.09	-26.71	-4.39

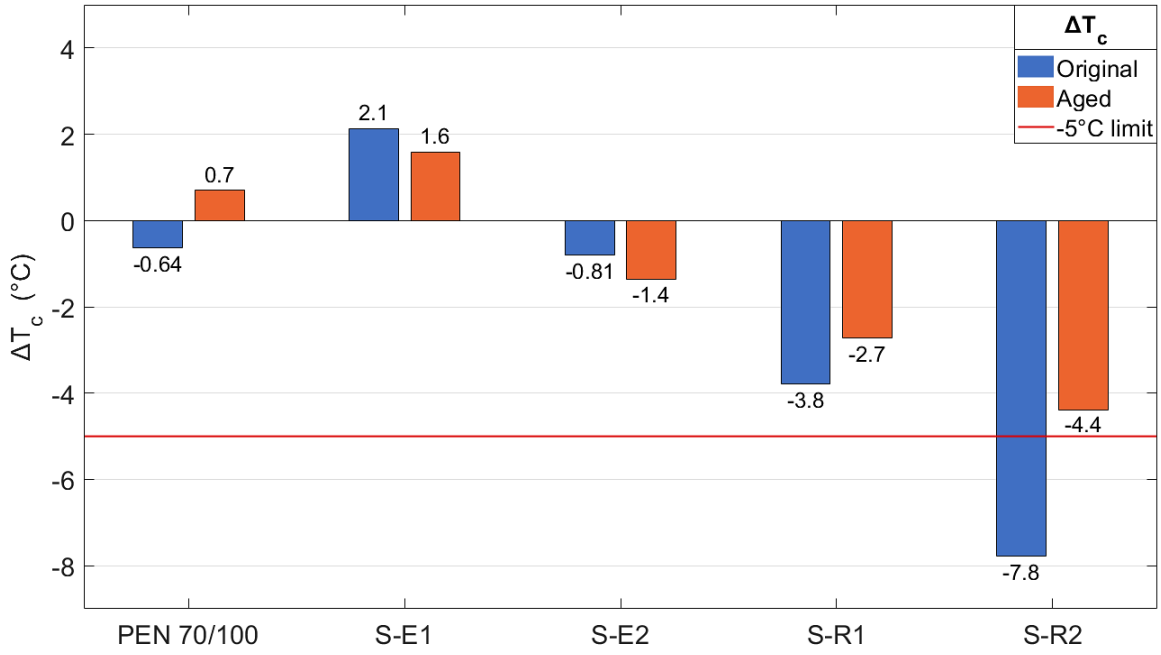

Figure 4.4: ΔT_c for original and aged binders with -5°C limit

4.1.3 Converting the BBR data to DSR data

The BBR data gave the output in stiffness (S) in the time domain (t). These parameters must be converted to shear modulus (G) and angular frequency (ω) in order to construct the master curve. The RHEA Software is used to convert the data from S and m to G* and δ. The conversion is based on the principle $S \simeq 3G^*$ (Christensen and Anderson, 1992) and $\omega t = 2\pi$. The software makes use of the Gordon and Shaw method to free shift the data. Figure 4.5 shows the bending stiffness versus time, which was converted by RHEA to shear stiffness versus frequency. Figure 4.6 shows the converted BBR data as G', G" isotherms. The G', which is the elastic component, shows a constant trend of stiffness increasing with frequency. The G", which represents the viscoelastic component, shows how the stiffness at -24°C stays the same, for the six frequency points. This indicates that the G" decreases the viscoelastic properties and adds to the elasticity of the binder.

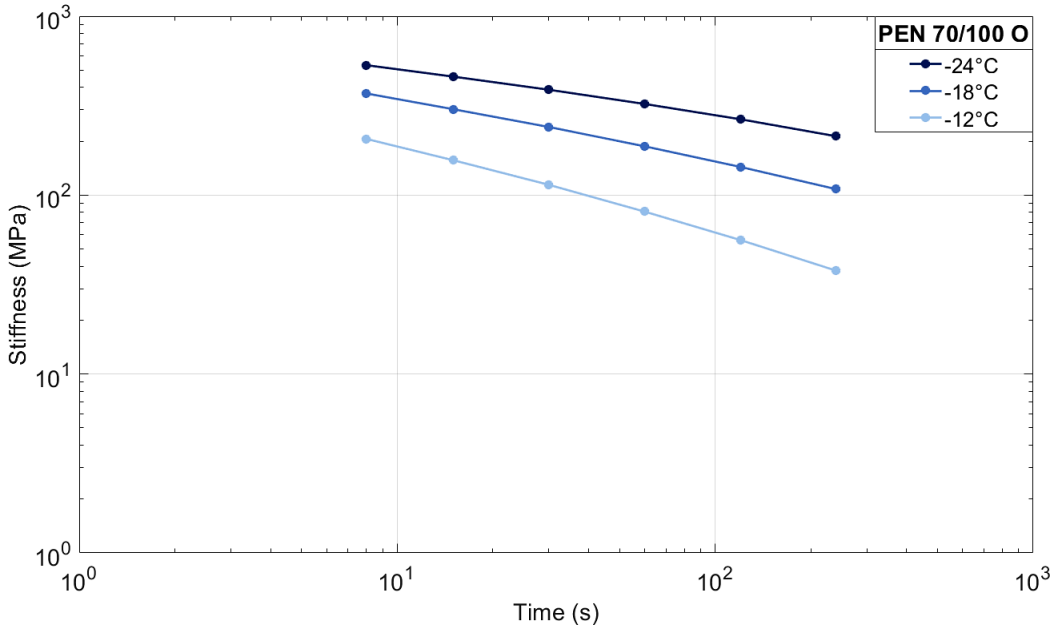

Figure 4.5: The stiffness with time for the PEN 70/100 Original (unaged)

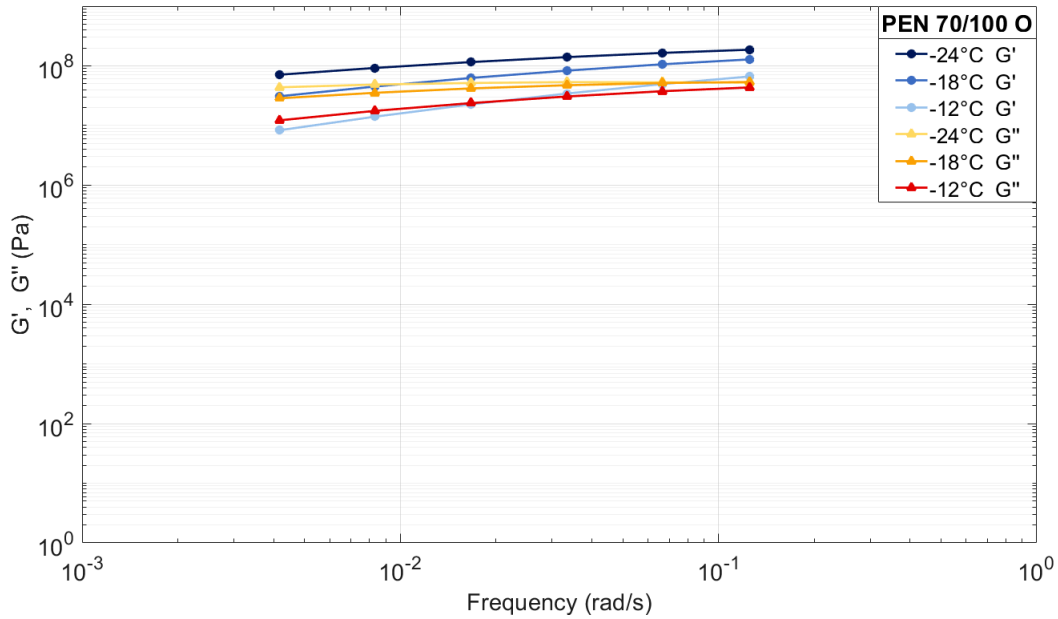

Figure 4.6: The G' and G" vs frequency for the PEN 70/100 Original (unaged)

4.2 Master Curve Analysis

The Master Curve is created by the shifting of isotherms to one temperature, namely a reference temperature. A reference temperature (T_{ref}) was selected to accommodate the calculations of the G-R parameter, which is discussed later in this chapter. Shift factors are used to construct the Master Curves. Various models were utilised to determine the calculation of the shift factors in order to find the best fit for the data. The Master Curve is essential as it allows for the determination of various parameters from one curve.

During the analysis of the rubber binder's DSR data, the results were unexpected and could not be explained. Therefore testing was repeated for the S-R1 and S-R2 original binders, with different plate configurations. With the initial testing, cone plates (CP) were used for the rubber binders. It was suggested that the plate configuration be changed to parallel plates (PP) to evaluate the impact on stiffness from calculation assumptions for these specific geometries. The gap size remained at 2.4 mm for the testing. Due to time constraints, the aged rubber binder was not tested with the PP configuration. In the following analysis, the comparison between the different types of binder's performance are primarily based on the PP results for the rubber binder. However, to evaluate the effect of ageing, the CP testing results are used. Thus, when analysing ageing behaviour, there is consistency between the original and aged binders.

4.2.1 Combined BBR and DSR data

To create the master curve, BBR data and DSR data are combined. The isotherms of the BBR and DSR data for the storage (G') and loss modulus (G") can be seen in Figure 4.7 and Figure 4.8, respectively. There are three models that can be used in the RHEA software to create the master curve and shift the isotherms to the reference temperature of 15°C.

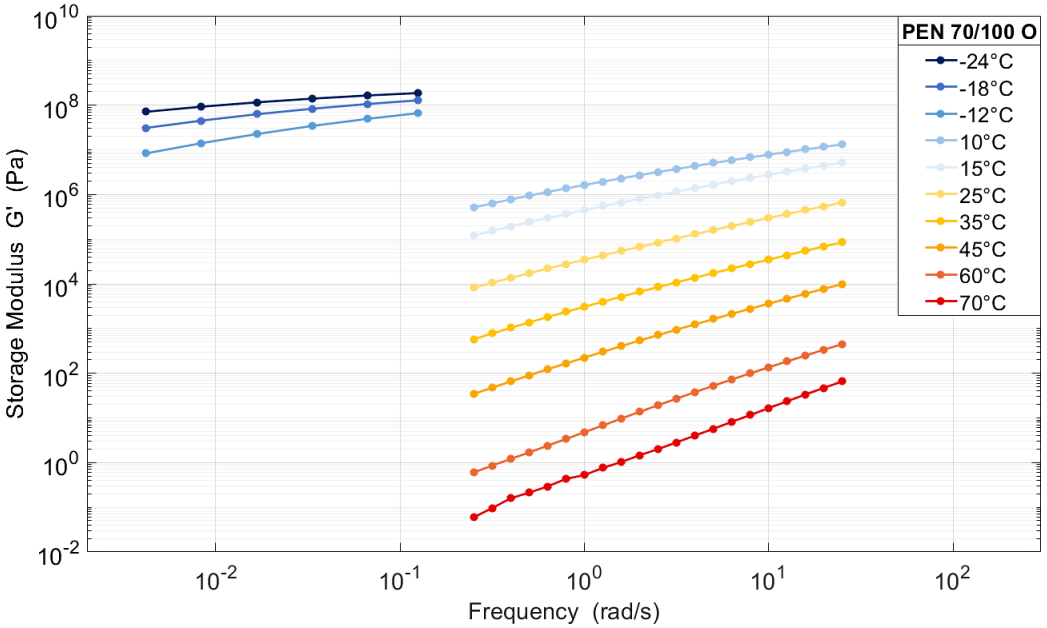

Figure 4.7: Unshifted G' data for PEN 70/100 Original (unaged) isotherms

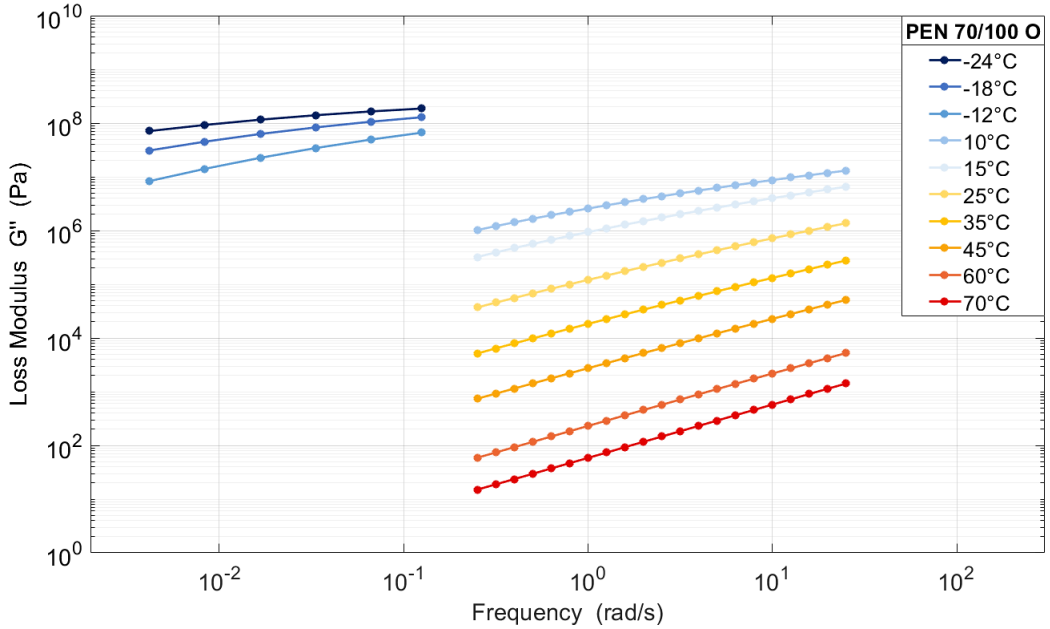

Figure 4.8: Unshifted G" data for PEN 70/100 Original (unaged) isotherms

4.2.2 Shift factors

Shift factors are used to shift the isotherms into one master curve. For each binder tested, three models are constructed: the Arrhenius, the WLF and the Modified Kaelble. The parameters used in the Arrhenius shift factor are presented in Table 4.4. An example of the shift factor fitted to the PEN 70/100 original data is shown in Figure 4.9. Tables 4.5 and 4.6 shows the parameters used in the WLF and Modified Kaelble shift factor functions, respectively. Figure 4.10 displays the WLF and Modified Kaelble shift functions fitted to the free-shifted data points. The shift factor models often struggle to fit the low temperature data points. It is beneficial that the Modified Kaelble is able to fit these points, whereas the WLF does not.

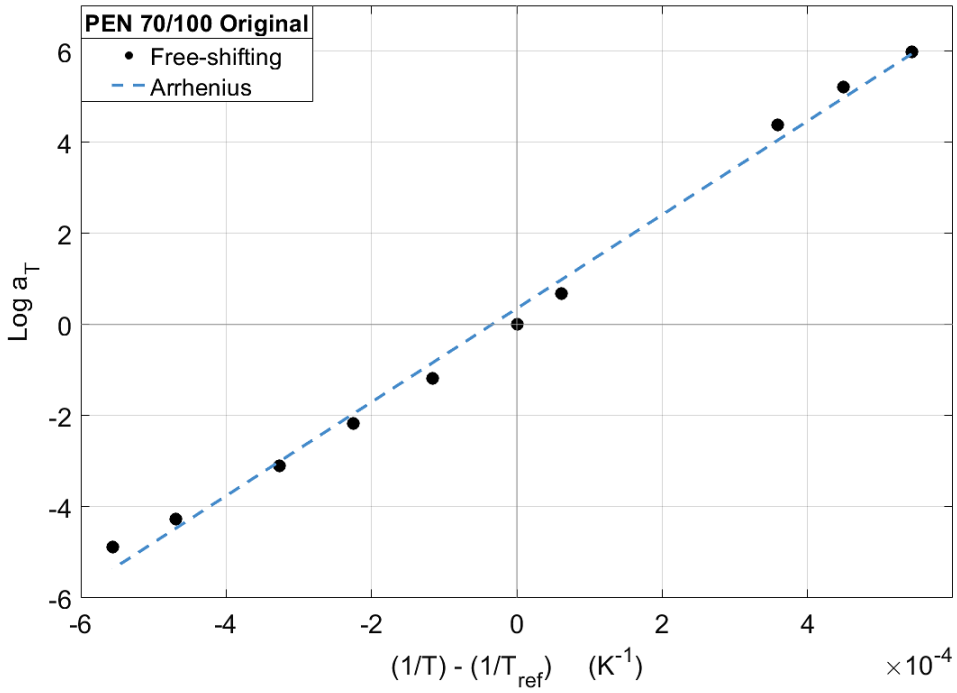

Figure 4.9: The data fitted to the Arrhenius shift factor

Table 4.4: Arrhenius shift factor parameters

Binder		Plate	a_0	a_1	R^2	RMSE ($log a_T$)
PEN 70/100	Original		0.35	1.03E+04	0.99	0.30
	Aged		0.72	1.10E+04	0.98	0.63
S-E1	Original		0.43	1.04E+04	0.99	0.35
	Aged		0.46	1.10E+04	0.99	0.37
S-E2	Original		0.17	1.09E+04	1.00	0.18
	Aged		0.30	1.13E+04	1.00	0.24
S-R1	Original	PP	0.43	1.06E+04	0.99	0.38
	Original	CP	2.08	1.48E+04	0.95	1.34
	Aged	CP	1.73	1.55E+04	0.96	1.34
S-R2	Original	PP	0.44	1.06E+04	0.99	0.36
	Original	CP	2.08	1.48E+04	0.95	1.39
	Aged	CP	2.09	1.51E+04	10.96	1.37

Table 4.5: WLF shift factor parameters

Binder		Plate	C_1	C_2	RMSE ($log a_T$)
PEN 70/100	Original		17.57	140.98	0.25
	Aged		12.46	97.72	0.36
S-E1	Original		16.36	131.21	0.22
	Aged		17.11	129.72	0.22
S-E2	Original		25.58	194.28	0.09
	Aged		22.22	163.21	0.17
S-R1	Original	PP	17.34	141.14	0.18
	Original	CP	8.56	61.36	3.70
	Aged	CP	10.92	69.93	5.50
S-R2	Original	PP	16.77	134.01	0.38
	Original	CP	8.47	60.60	4.14
	Aged	CP	39.57	432.97	4.43

Table 4.6: RMSE for Modified Kaelble with a T_{ref} of 15°C

Binder		Plate	C_1	C_2	T_d (°C)	RMSE ($loga_T$)
PEN 70/100	Original		16.68	89.12	-1	0.03
	Aged		15.65	64.86	-8	0.10
S-E1	Original		16.57	84.55	-3	0.06
	Aged		20.72	99.12	-10	0.03
S-E2	Original		28.94	159.64	-12	0.07
	Aged		25.02	128.71	-9	0.10
S-R1	Original	PP	26.10	106.70	-30	0.09
	Original	CP	13.20	26.64	-6	0.34
	Aged	CP	17.79	40.53	-12	0.10
S-R2	Original	PP	20.20	100.30	-11	0.03
	Original	CP	13.17	26.28	-6	0.28
	Aged	CP	15.21	30.85	-11	0.27

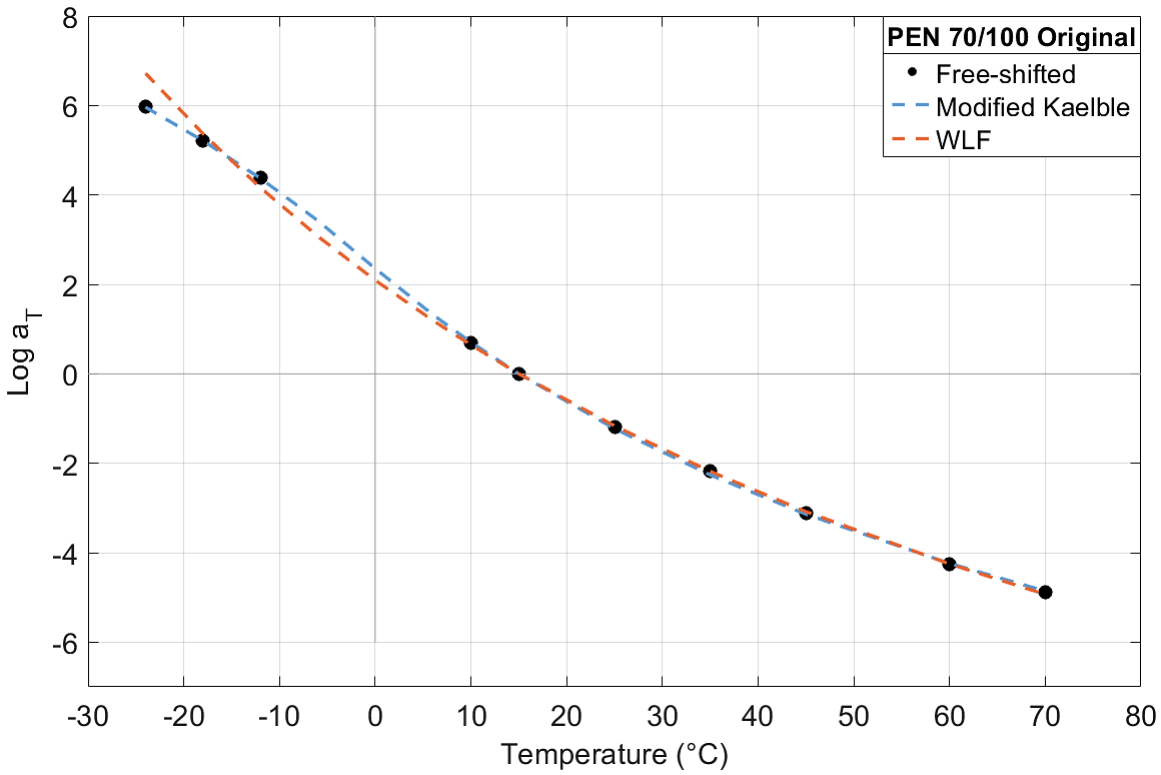

Figure 4.10: Modified Kaelble and WLF of PEN 70/100 Original

The root mean square error (RMSE) in $\log a_T$, was used to determine which model provided the best fit to the data. A low RMSE value indicates a more accurate fit. For each model the RMSE in $\log a_T$ is displayed in Table 4.7. Figure 4.11 gives a representation for the three shift factors for each binder in its original state. This figure presents the parallel plates' results of the rubber. The Arrhenius shift factor clearly has the highest RMSE, followed by the WLF and then the Modified Kaelble, for the reasons explained above. The Modified Kaelble has a significantly low RMSE and was thus used in further analysis and calculations. The aged binders' shift factors follow the same trend as the original state binders. Yet with the aged rubber that was tested with a CP, and not a PP, it is clear that the WLF shift factor equation struggles to find a suitable fit. Figure 4.13 illustrates how the WLF shift function cannot fit the data at low temperatures, this shows how the Modified Kaelble is the better fit for the free-shifted data. Figure 4.12 displays the significant difference between the WLF and the other functions. This shows that the type of plate used in testing has a remarkable influence on the results.

Table 4.7: RMSE for all models with a T_{ref} of 15°C

Binder		Plate	Arrhenius	WLF	Modified Kaelble
PEN 70/100	Original		0.30	0.25	0.03
	Aged		0.63	0.36	0.1
S-E1	Original		0.35	0.22	0.06
	Aged		0.37	0.22	0.03
S-E2	Original		0.18	0.09	0.07
	Aged		0.24	0.17	0.10
S-R1	Original	PP	0.38	0.18	0.09
	Original	CP	1.34	3.70	0.34
	Aged	CP	1.34	5.50	0.10
S-R2	Original	PP	0.36	0.38	0.03
	Original	CP	1.39	4.14	0.28
	Aged	CP	1.37	4.43	0.27

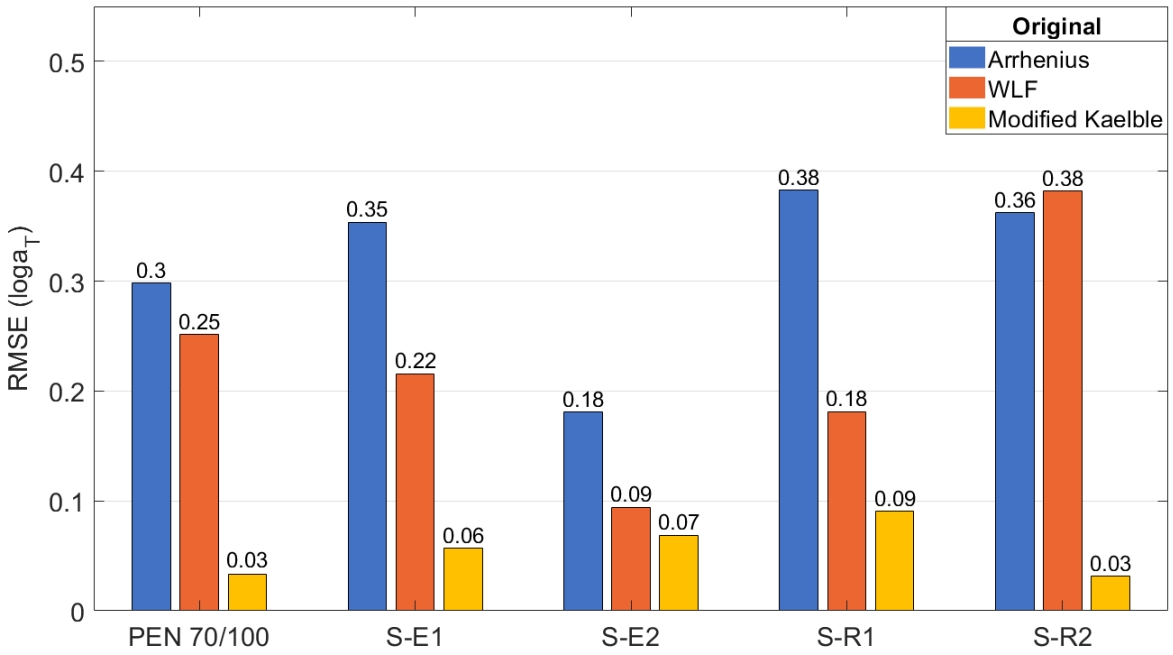

Figure 4.11: RMSE of the shift factors for the binders in original condition, with PP testing data

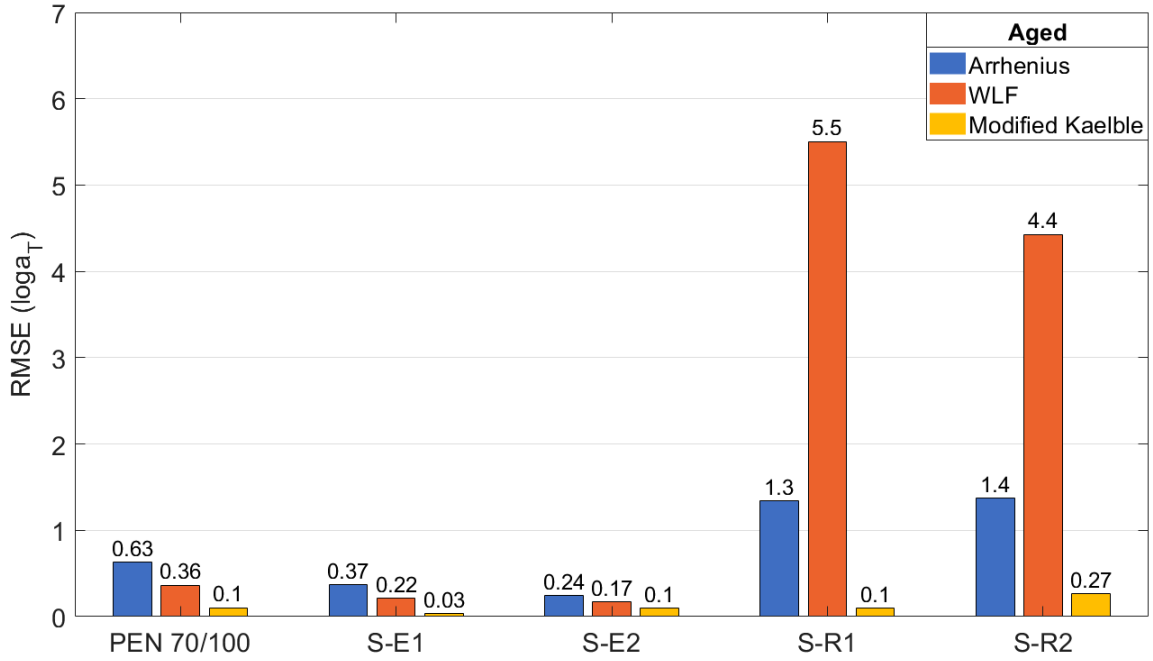

Figure 4.12: RMSE of the shift factors for the binders in aged condition, with CP testing data

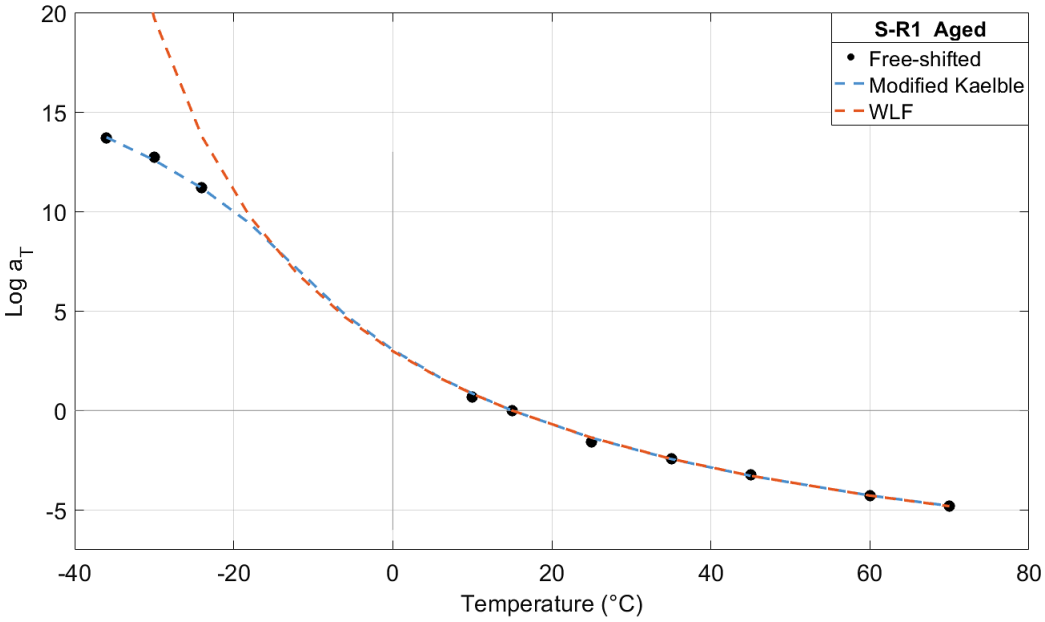

Figure 4.13: WLF and Modified Kaelble shift functions on the S-R1 Aged

4.2.3 Master curve construction

The DSR output, see Table 4.8, gives the necessary parameters to use in the master curves. This output was then used as input for the RHEA software to be processed into workable data. Of the overlapping temperatures at 25°C and 35°C on the 25 mm and 8 mm plates in the DSR, only one temperature's data may be used. To determine which plates' data to use, the theory of when the average of the complex modulus is smaller than 100 000 Pa, the data from the 25 mm plate (isotherm) is used, and when it is larger, then the 8 mm plate's data is used. This is in compliance with the DSR.

Table 4.8: A typical DSR output at 15°C

Point No.	Temp.	ω	G'	G"	Loss Factor	γ	τ	Torque	δ	G*
	(°C)	(rad/s)	(Pa)	(Pa)		(%)	(Pa)	(mN.m	(°)	(Pa)
1	15	0.251	1.21E+05	3.21E+05	2.66	1	3434.9	0.35	69.3	3.44E+05
2	15	0.316	1.54E+05	3.91E+05	2.54	1	4201.5	0.42	68.51	4.20E+05
3	15	0.398	1.93E+05	4.71E+05	2.44	1	5093.2	0.51	67.68	5.09E+05
4	15	0.501	2.41E+05	5.64E+05	2.34	1	6128.6	0.62	66.87	6.13E+05
5	15	0.63	2.98E+05	6.70E+05	2.25	1	7328.6	0.74	66.05	7.33E+05
6	15	0.794	3.66E+05	7.93E+05	2.17	1	8732.8	0.88	65.21	8.73E+05
7	15	0.999	4.48E+05	9.34E+05	2.09	1	10363	1.04	64.37	1.04E+06
8	15	1.26	5.46E+05	1.1E+06	2.01	1	12254	1.23	63.52	1.23E+06
9	15	1.58	6.64E+05	1.28E+06	1.93	1	14445	1.45	62.65	1.44E+06
10	15	1.99	8.03E+05	1.50E+06	1.86	1	16971	1.71	61.77	1.70E+06
11	15	2.51	9.68E+05	1.74E+06	1.8	1	19886	2.00	60.87	1.99E+06
12	15	3.16	1.16E+06	2.01E+06	1.73	1	23235	2.34	59.97	2.32E+06
13	15	3.98	1.39E+06	2.32E+06	1.67	1	27077	2.72	59.05	2.71E+06
14	15	5.01	1.66E+06	2.67E+06	1.61	1	31452	3.16	58.13	3.15E+06
15	15	6.3	1.97E+06	3.06E+06	1.55	1	36428	3.67	57.2	3.64E+06
16	15	7.94	2.34E+06	3.50E+06	1.5	1	42107	4.24	56.27	4.21E+06
17	15	9.99	2.76E+06	3.99E+06	1.45	1	48540	4.88	55.34	4.85E+06
18	15	12.6	3.25E+06	4.53E+06	1.4	1	55801	5.61	54.4	5.58E+06
19	15	15.8	3.81E06	5.14E+06	1.35	1	63984	6.44	53.47	6.39E+06
20	15	19.9	4.45E+06	5.80E+06	1.31	1	73141	7.36	52.53	7.31E+06
21	15	25.1	5.18E+06	6.53E+06	1.26	1	83378	8.39	51.6	8.34E+06

To construct a master curve, the data from the BBR and DSR test results are merged. The merged data then had to be shifted to create a master curve. The Modified Kaelble shift factor was used to construct the Master Curves. Figure 4.14 displays how the shift factor models are used to shift the G' isotherms into a G' Master Curve. The storage and loss moduli are used to determine the complex modulus and phase angle, after shifting.

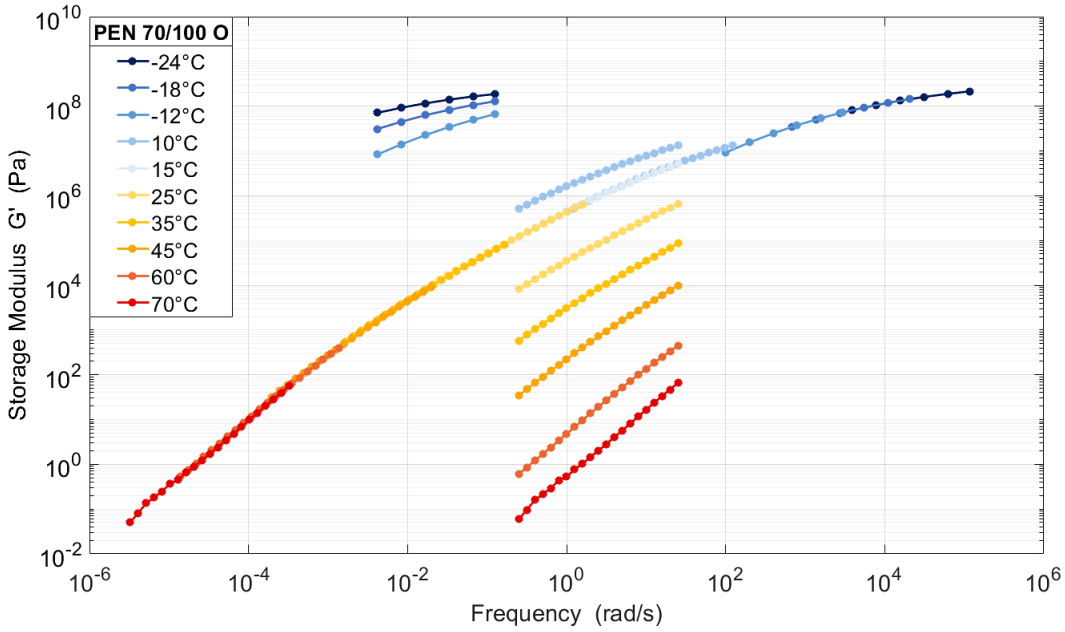

Figure 4.14: Isotherms of the PEN 70/100 Original (unaged) Master Curve G'

Figure 4.15 and 4.16 display the master curves for the complex modulus and the phase angle, respectively. Furthermore, the two curves are combined on one diagram to present the master curves in Figure 4.17. As illustrated in the figure, at low temperatures and high frequencies the G* is high and the δ is low. This is expected as at cold temperatures, bitumen tends to become more elastic, and can be brittle and in turn experience cracking as a result of failure. Further analysis entails the construction of the mathematical models to represent the master curve data and are be used to determine the durability parameters.

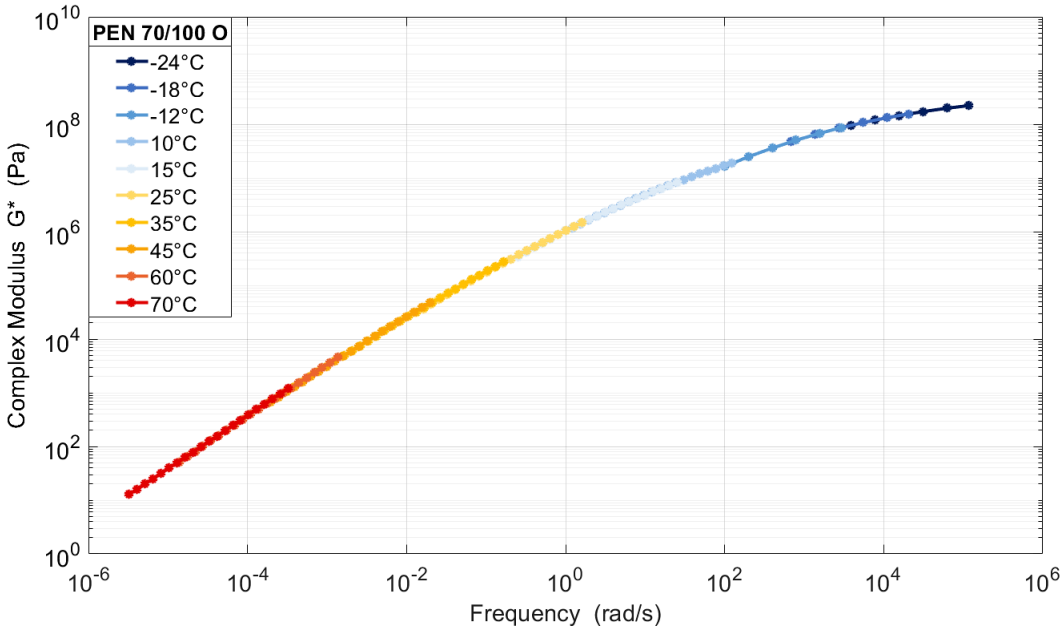

Figure 4.15: Master Curve for the G* of the PEN 70/100 Original (unaged)

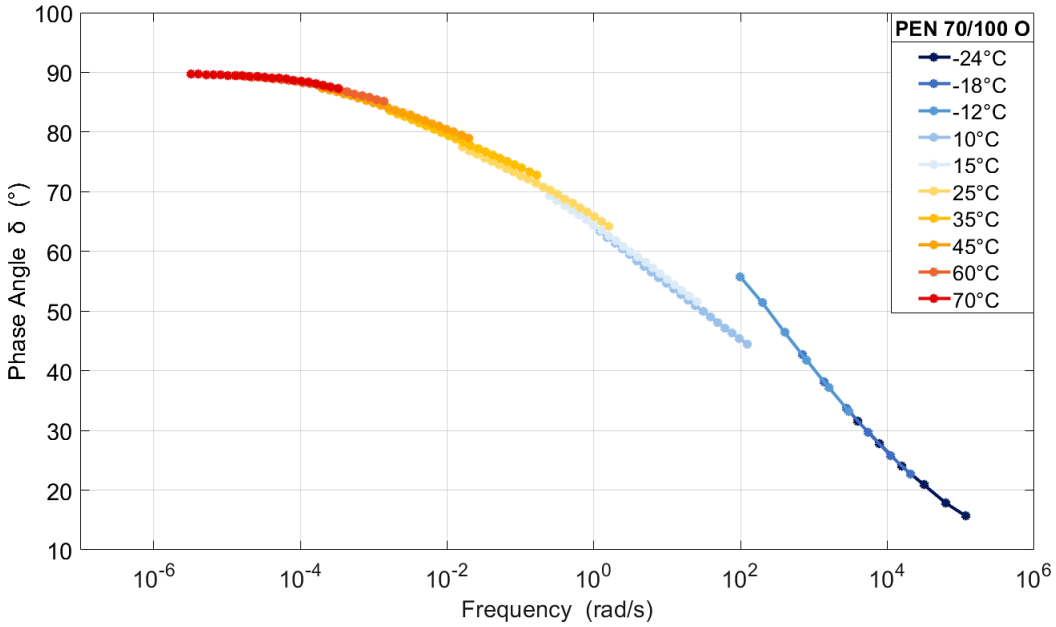

Figure 4.16: Master Curve for the δof the PEN 70/100 Original (unaged)

In Figure 4.18, the master curves for the G* of all the original binders are displayed. It should be noted that the rubber binders' master curves are based on the PP testing in this figure. All the binders converge to the same stiffness level. The level where the curves start to flatten is referred to as the glassy modulus (G_g). The range in which the glassy modulus of a bitumen binder is expected to be near 0.6 GPa and 1.5 GPa. The glassy modulus shows the limit of the G* at high

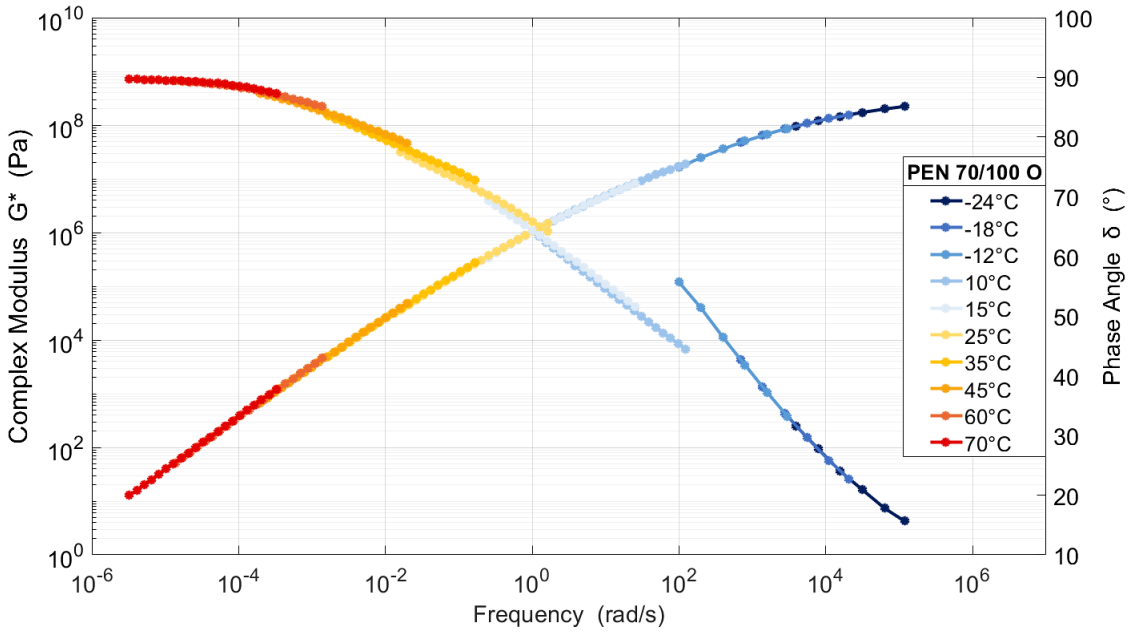

Figure 4.17: Master Curve for the PEN 70/100 Original (unaged)

frequencies and low temperatures. It appears that the current data does not reach the general range and reside below the limit. Figure 4.19 show how the plate configuration differs. The lower stiffness values measured with the CP, cause the BBR data to be shifted further away. The BBR G* values have not changed from Figure 4.18 to Figure 4.19, but the reduced frequencies have changed. This is because the shift model tries to keep the G* on the same trendline.

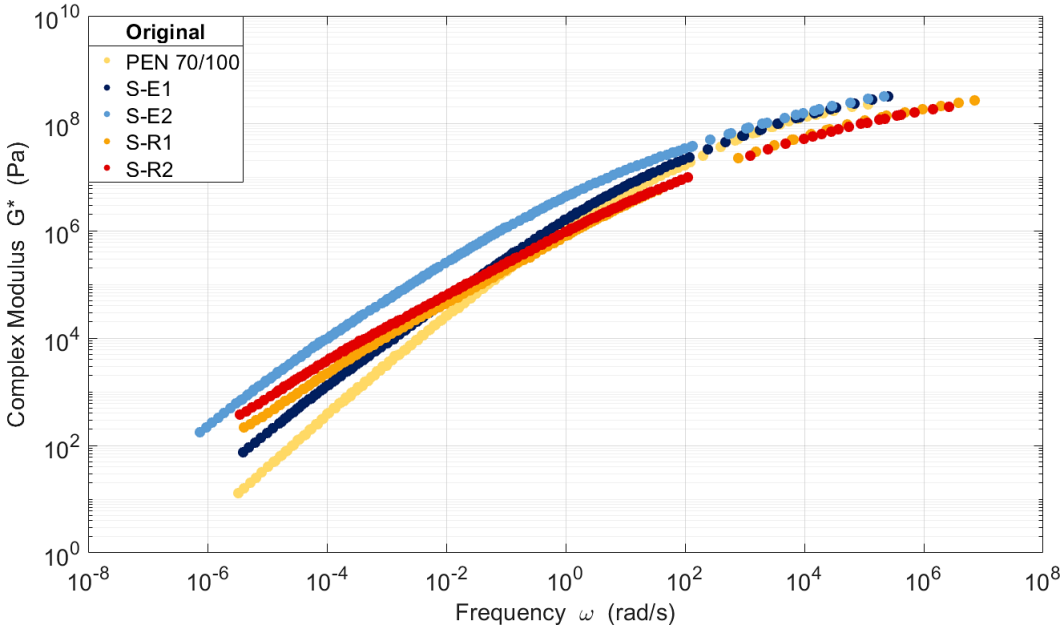

Figure 4.18: Master Curve for the original binders

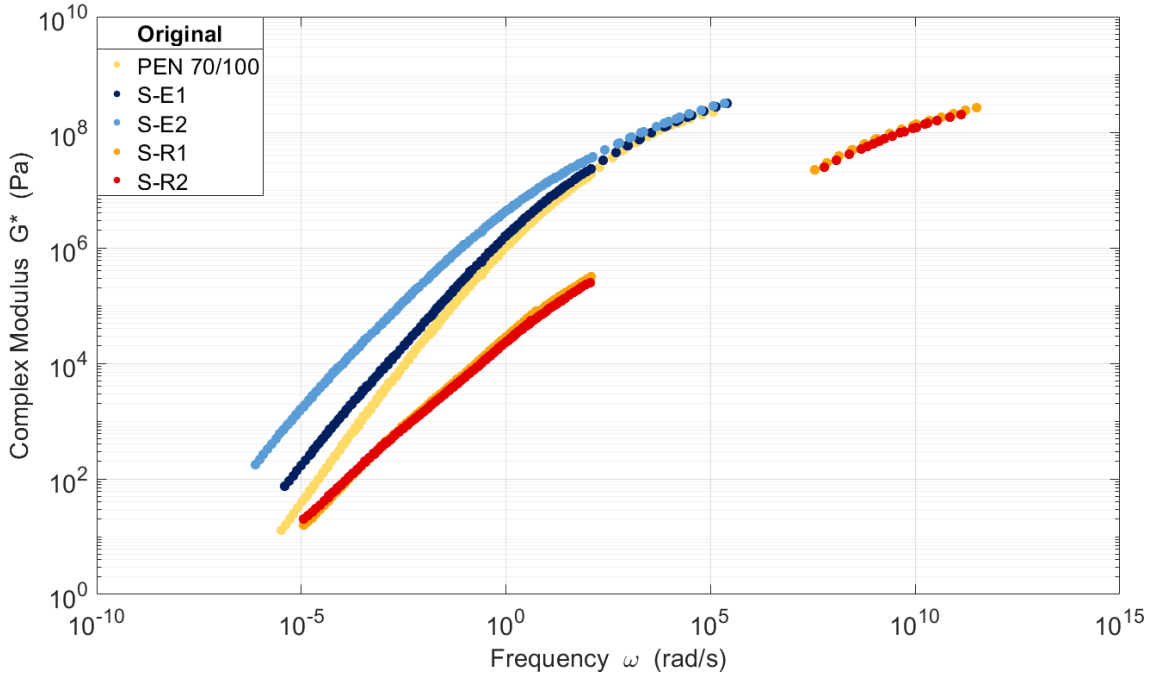

Figure 4.19: Master Curve for the original binders with CP configuration

4.2.4 Mathematical Models

Mathematical models are used to calculate and interpolate binder properties from test data. To differentiate which model provides the optimum results, different models were utilised and applied to the data. The RMSE is an indicator that is used to determine which model provides the best fit. RMSE is determined from the original data and the modelled data. Not all models could fit the data. The RHEA software automatically provided the results of the models that have a good functional fit. The most common model used in the binders was the discrete relaxation spectrum (DS) model, which provided the best fit. The CA model was second best, where only the aged rubber binders were not suited. For the S-R1 aged binder, RHEA displayed as using the GL and SL models, yet the DS model still proves to be the best fit according to the calculated RMSE. This section will give examples of each model for the PEN 70/100, S-E1 and S-R1, as a visual example of how each model fits the data.

CA Model

The CA model could not provide a fit for the aged rubber binders for the CP testing. For the PP testing on the original binders, RHEA provided a CA model function. The CA model parameters are presented in Table 4.9. In Figure 4.20, visually it appears that the CA model fits the data well, regarding the original conditions of the binder. Yet for the phase angle in the PEN 70/100, the CA model does not fit the lower frequencies accurately. Figure 4.20 shows how the model does not cover all the points. Figure 4.21 and 4.22 displays the CA model fitted to the S-E1 and S-R1 original binders.

Table 4.9: Parameters used in the CA model

Binder		Plate	G_o (Pa)	ω_c (rad/s)	β	RMSE (%)
PEN 70/100	Original		7.9E+08	155.2	0.20	3.7
	Aged		5.8E+08	302.75	0.19	9.81
S-E1	Original		2.2E+09	70.13	0.14	6.08
	Aged		2.2E+09	27.58	0.13	4.86
S-E2	Original		2.2E+09	2.56	0.12	2.49
	Aged		2.4E+09	1.3	0.11	2.45
S-R1	Original	PP	2.0E+09	8.78	0.11	13.65
	Original	CP				
	Aged	CP				
S-R2	Original	PP	3.5E+09	2.30	0.09	10.60
	Original	CP				
	Aged	CP				

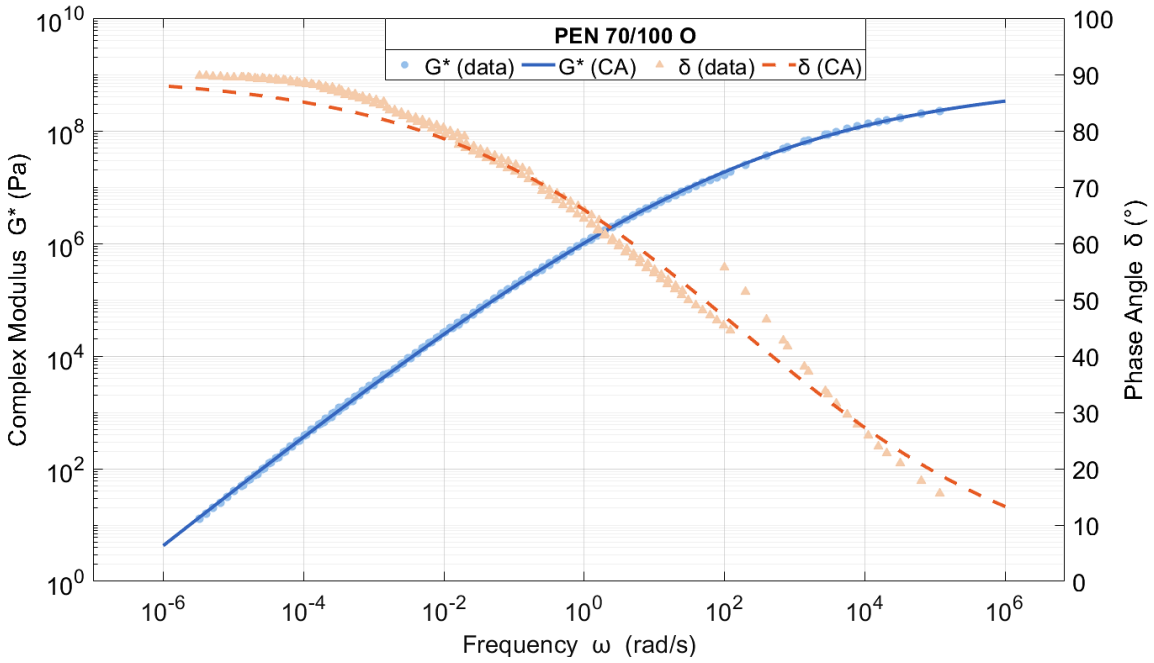

Figure 4.20: Master Curve with the CA model applied to the PEN 70/100 Original (unaged)

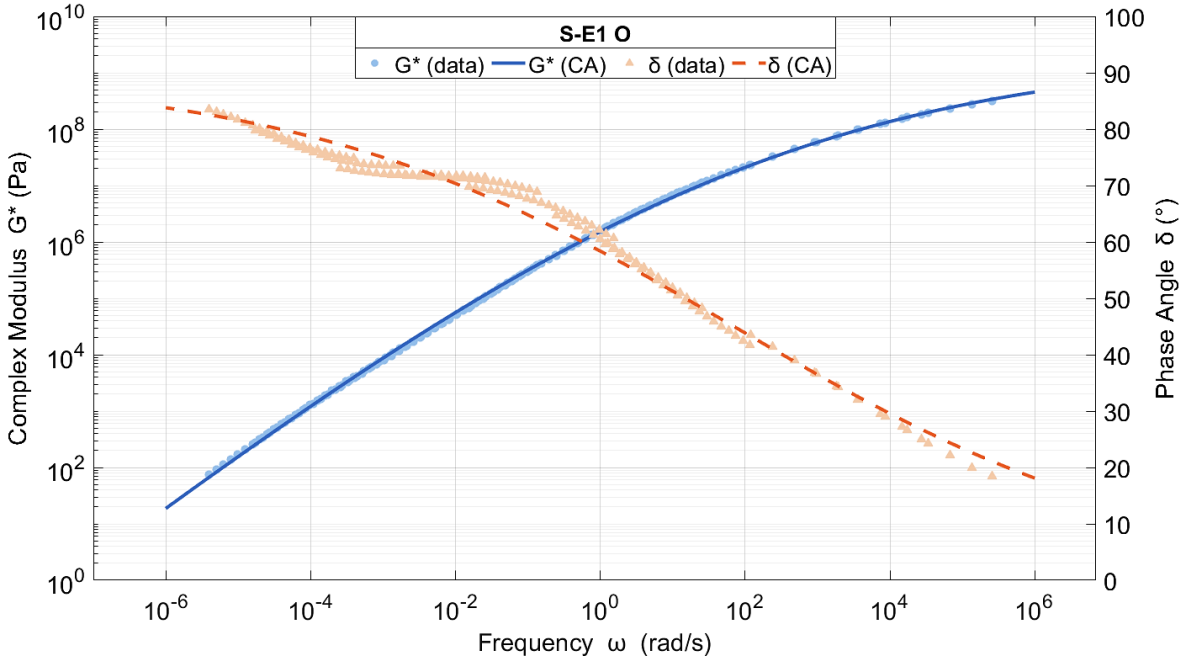

Figure 4.21: Master Curve with the CA model applied to the S-E1 Original (unaged)

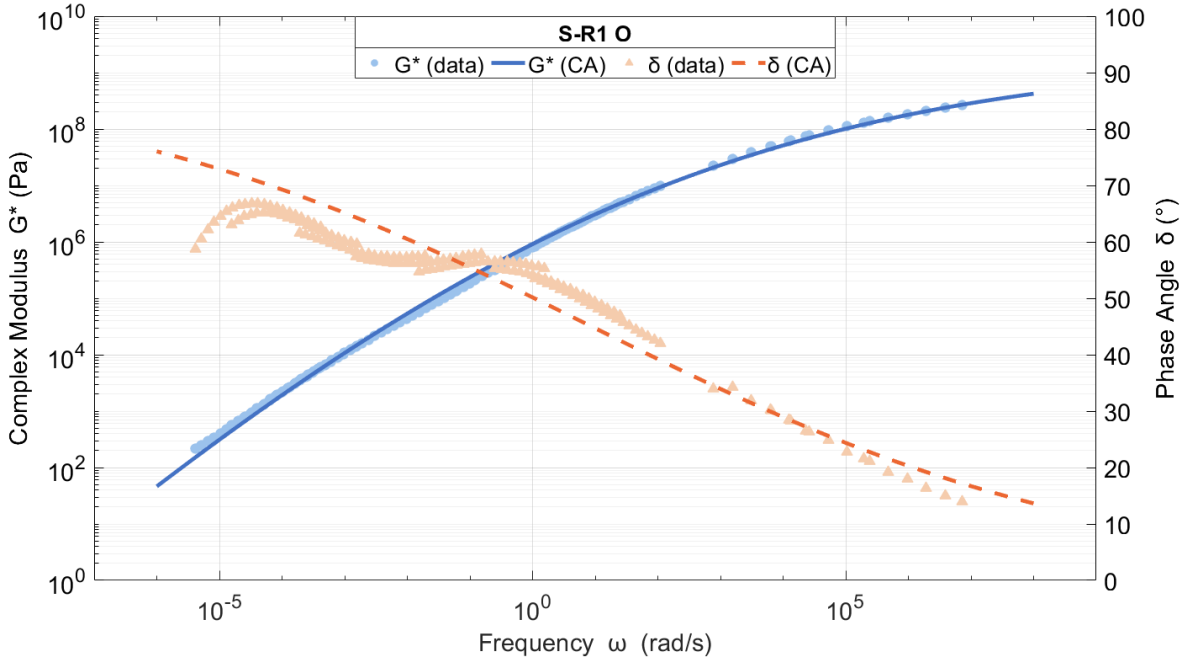

Figure 4.22: Master Curve with the CA model applied to the S-R1 Original (unaged)

GL an SL Model

The S-R1 aged binder was the only case where RHEA software generated a GL and SL model. Table 4.10 displays the values of the parameters used in the GL and SL models. Figure 4.23 illustrates how each model is fitted to the data. Visually, it is apparent that the GL model is not describing the data accurately. Only the G* data at high frequencies are fitted well and the model is completely unsuited to the δ data. The SL curve appears to fit the G* data well, yet struggles to find a good fit for the δ data. It is clear that the GL and SL models are not good fits for the aged S-R1. The RMSE for the GL and SL models are 18.5 and 22% respectively. This will be compared to the other models at the end of this section. It should be noted that the aged data was collected with CP configurations. The observed differences is measured stiffness from the PP data may contribute to the suitability of the models.

Table 4.10: GL and SL parameters

Parameters	GL	SL
min	-1.95	-6.90
max	9.85	9.21
β	-0.62	-0.84
γ	-0.11	-0.16
λ	0.47	-

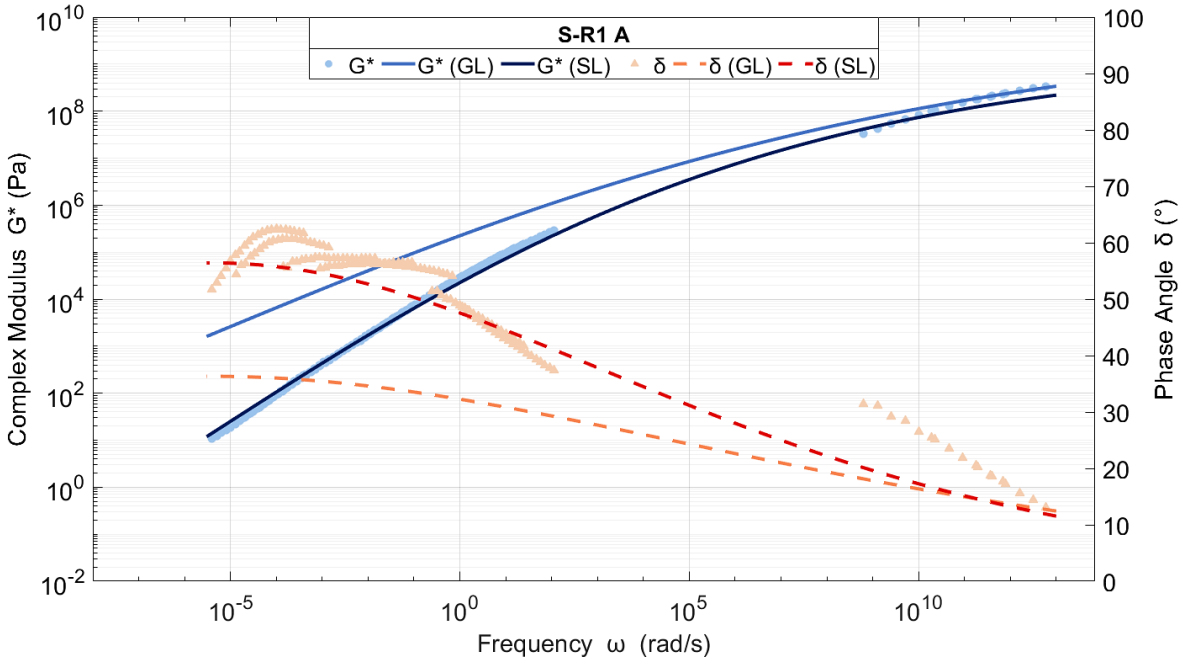

Figure 4.23: Master Curve with the GL and SL model applied to the S-R1 Aged

Discrete Spectrum (DS) Model

The Discrete Spectrum model optimised well for all the binders tested. An example of the mode values of the DS model of the PEN 70/100 original binder is shown in Table 4.11. Figures 4.24, 4.25 and 4.26 illustrate how the DS model is applied to the data. The DS model has a constant called the equilibrium modulus (G_e) which influences the shape of the curve. The RMSE and the G_e of the DS model parameters are displayed in Table 4.12. This constant is greater than zero for only three binders, namely the original and aged S-R1 and the original S-R2 with CP configuration, for the PP testing, the constant is zero for all models. The addition of this value causes the curves at low frequencies to diverge. This can be seen in Figure 4.26, CP tested S-R1

original. Further, it should be noted that the DS model follows all data more precisely - even those points that appear to be outside the LVE behavioural range. When applying the DS model, there is thus a greater need to carefully consider the quality of the test data.

Table 4.11: The strength and relaxation mode values for the PEN 70/100 Original (unaged)

Mode Number i	**Mode Strength g_i (Pa)**	**Mode Relaxation Time λ_i (s)**
1	9.6E+07	1.5E-07
2	6.8+07	6.8E-07
3	1.0E+08	3.4E-06
4	7.8E+07	3.5E-05
5	5.9EE+07	1.9E-04
6	4.1E+07	9.5E-04
7	1.4E+07	6.0E-03
8	5.5E+06	3.2E-02
9	2.0E+06	2.1E-01
10	4.2E+05	1.3E+00
11	9.1E+04	7.1E+00
12	1.6E+04	4.2E+01
13	1.9E+03	2.8E+02
14	1.3E+02	2.0E+03
15	4.0E+00	1.8E+04
16	6.6E-02	2.8E+06

Table 4.12: Parameters used in the DS model

Binder		Plate	G_e (Pa)	RMSE (%)
PEN 70/100	Original			7.63
	Aged			5.2
S-E1	Original			2.61
	Aged			2.34
S-E2	Original			2.57
	Aged			1.88
S-R1	Original	PP		4.44
	Original	CP	5.26	4.21
	Aged	CP	4.46	4.16
S-R2	Original	PP		3.78
	Original	CP	7.25	3.29
	Aged	CP		4.13

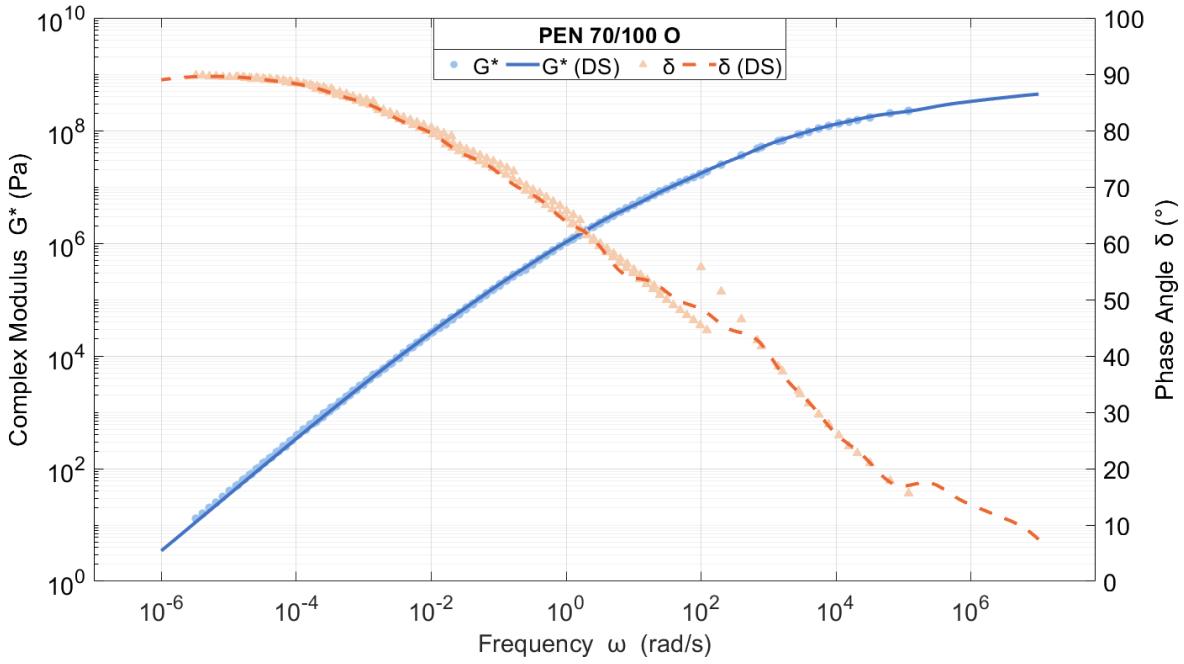

Figure 4.24: DS curve of PEN 70/100 Original (unaged)

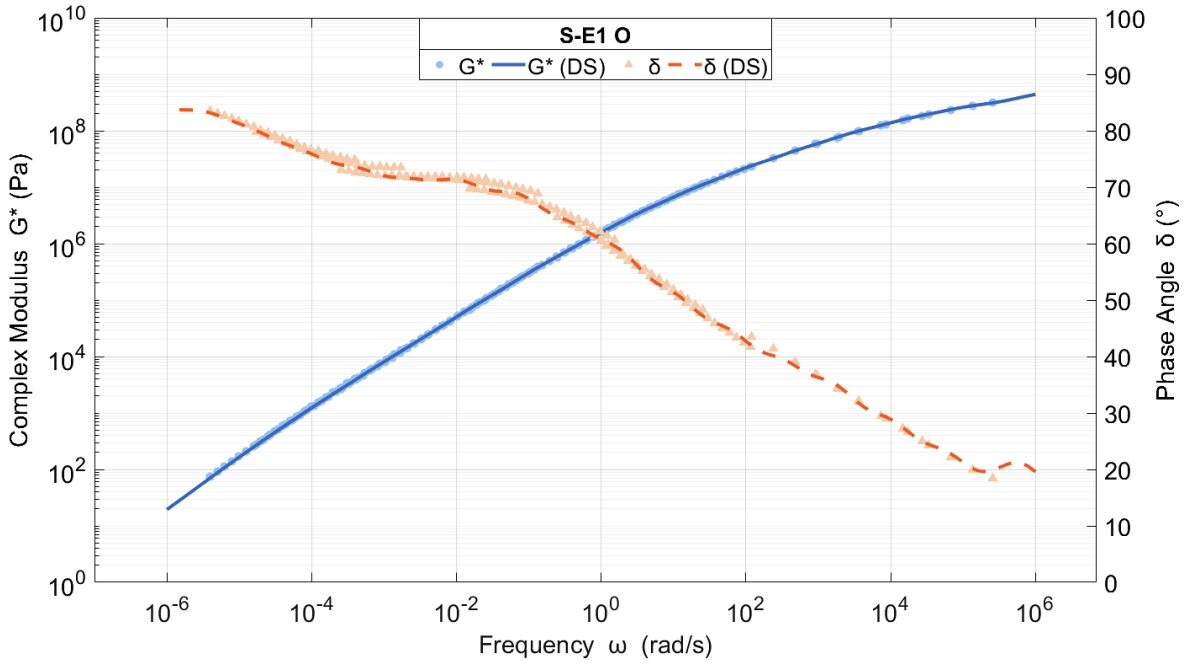

Figure 4.25: DS curve of S-E1 Original (unaged)

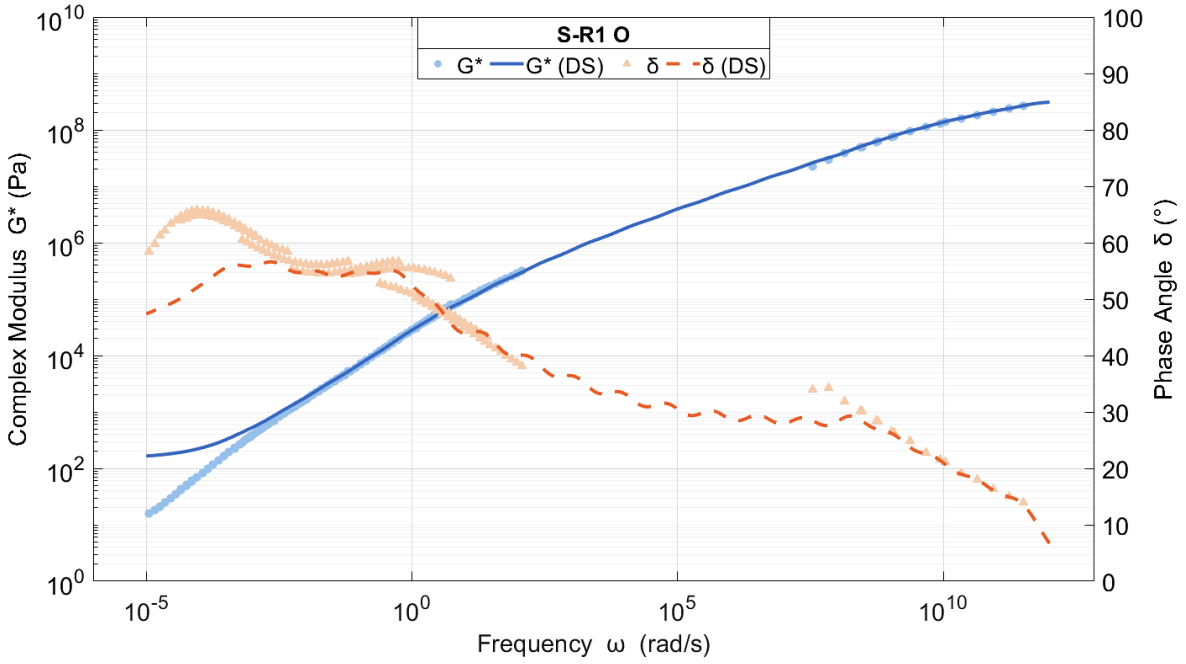

Figure 4.26: DS curve of S-R1 Original (unaged)

Summary

From the information above, it was decided to use the Discrete Spectrum model for further calculations. Table 4.13 shows how the DS model has the lowest RMSE between the models. With the exception of the PEN 70/100 original, but by comparing the CA model and the DS

model in Figure 4.27, it shows how both models have a good fit. Yet by focusing on the δ curve in the high frequency region, it appears that the DS model falls on most of the data points, where the CA model only covers a few data points. At low frequencies, the DS model visually is more suitable than the CA model. Further calculations for the PEN 70/100 original binder will be based on the DS model, due to it illustrating a more appropriate fit for the data than the CA model. Figure 4.28 compares the CA and DS models. The DS model has a more accurate fit on the data than the CA curve. Figure 4.29 displays the GL, SL and DS models. It is clear that the GL and SL curves do not fit the data points as well as the DS model. The graphs where the models are compared for each binder can be found in the appendices.

Table 4.13: RMSE for all models with a T_{ref} of 15°C

Binder		Discrete Spectrum	CA Model	GL	SL
PEN 70/100	Original	7.63	3.79		
	Aged	5.2	9.81		
S-E1	Original	2.61	6.08		
	Aged	2.34	4.86		
S-E2	Original	2.57	2.49		
	Aged	1.88	2.45		
S-R1	Original	4.44	13.65		
	Aged	4.16		18.48	22.02
S-R2	Original	3.78	10.60		
	Aged	4.13			

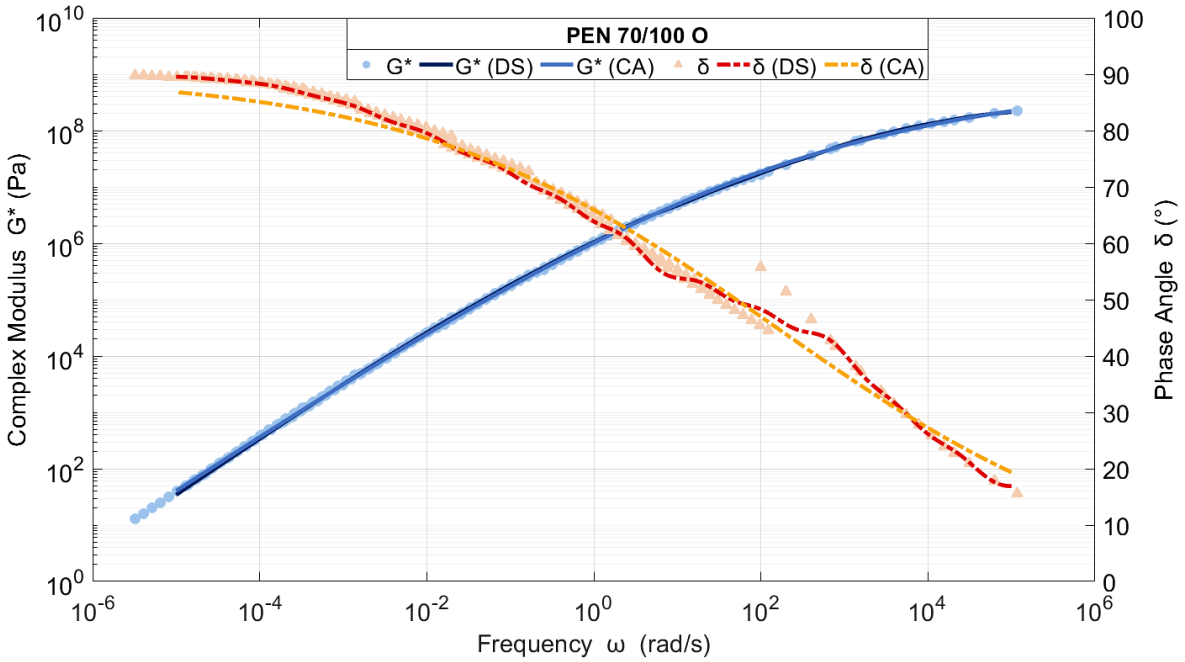

Figure 4.27: Master Curve with the CA and DS model applied to the PEN 70/100 Original (unaged)

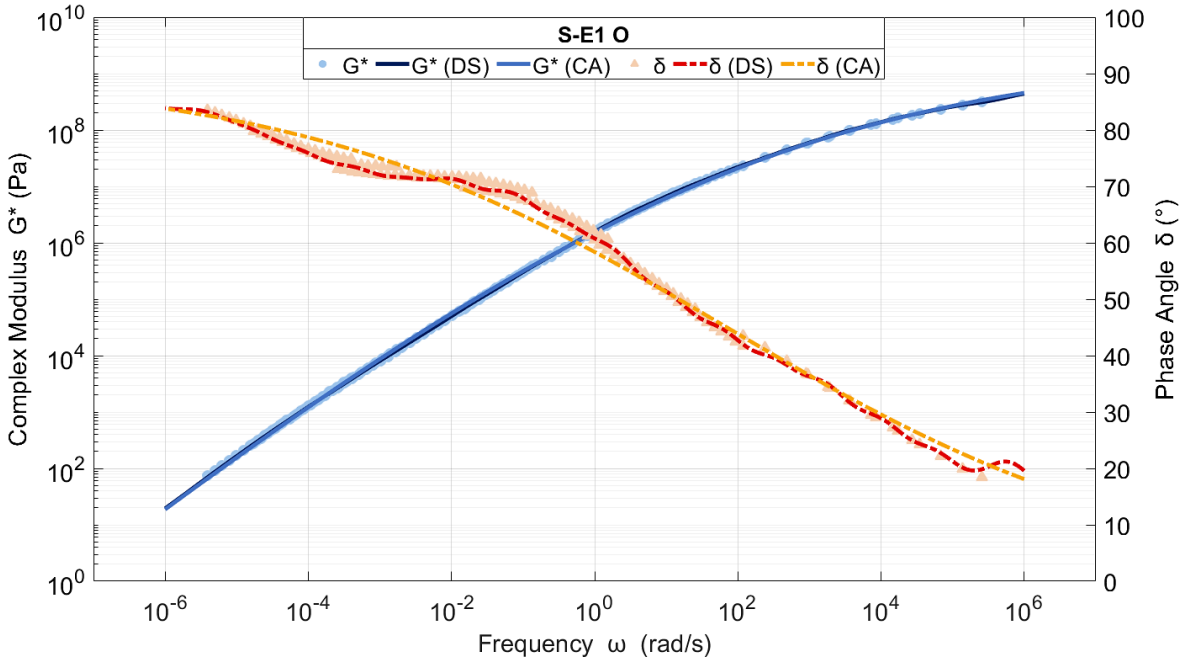

Figure 4.28: Master Curve with the CA and DS model applied to the S-E1 Original (unaged)

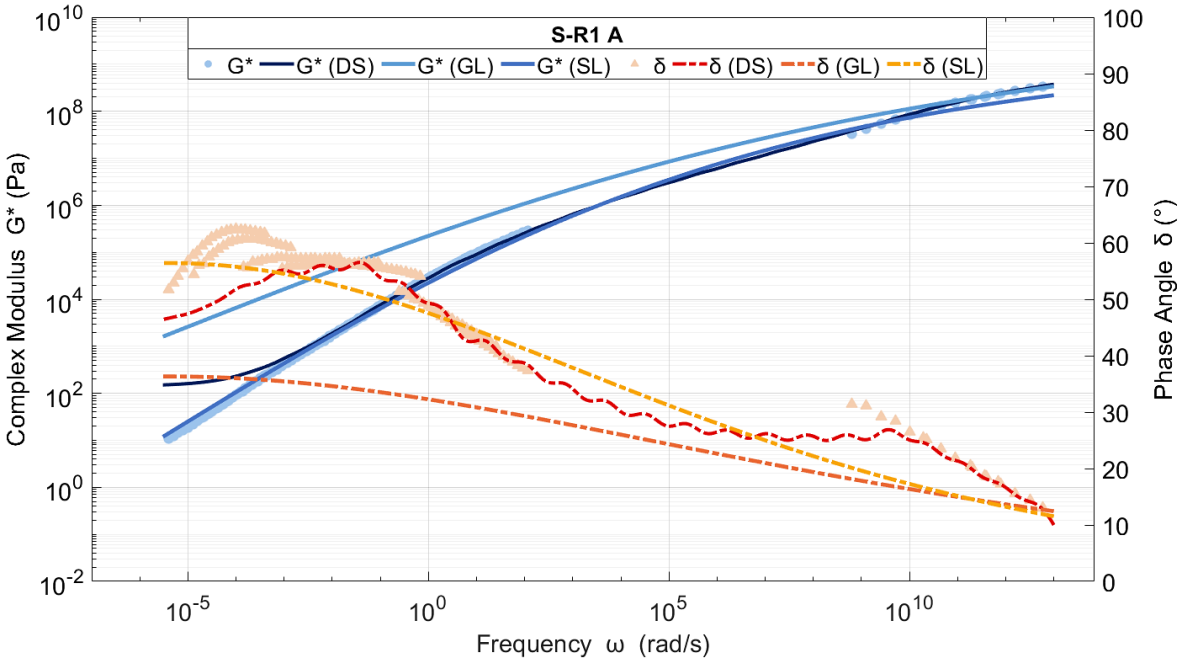

Figure 4.29: Master Curve of S-R1 aged

4.3 Black Space Analysis

This section discusses the Black Space diagrams of the binders. The Black Space diagrams will be used to present the durability parameters, such as the G-R parameter. In a Black Space diagram, the viscoelastic characteristics of a binder are obtained and it is a useful tool to indicate how a binder's modification affects its performance behaviour. In a Black Space, the top left section will display elastic behaviour, as the phase angle is small, whereas the bottom right the binder will display a more viscous behaviour, as the phase angle increases. Figure 4.30 displays the Black Space diagram of the PEN 70/100 original binder's isotherms. As expected, the higher temperatures display more viscous behaviour, where the lower temperatures display elastic behaviour. Figure 4.31 shows that ageing increases the PEN 70/100's elasticity, more so at temperatures below 15°C.

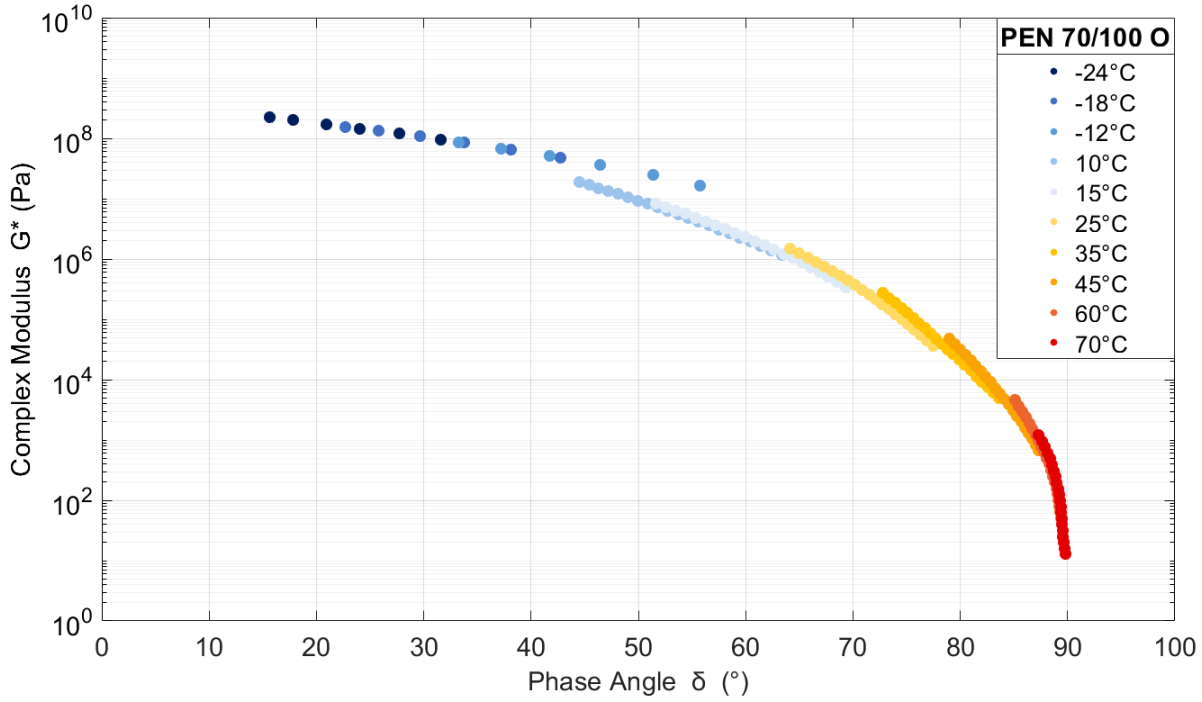

Figure 4.30: Isotherms of the PEN 70/100 Original (unaged)

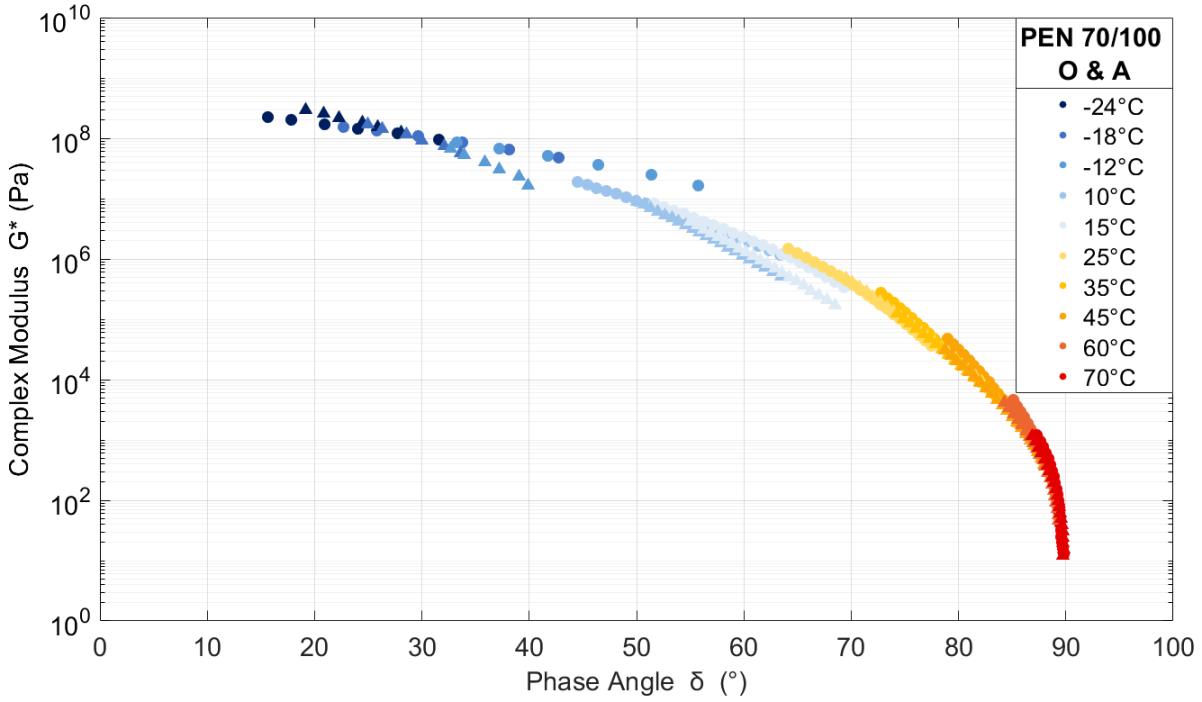

Figure 4.31: Black Space diagram of the isotherms of the PEN 70/100 Original and Aged. The triangle markers indicate the aged binder

Figure 4.32 compares all five binders in their original condition on a Black Space diagram. The figure shows how the addition of a modifier can increase a binder's elasticity. The S-E1 and S-E2 binders demonstrate how the degree of modification improves elasticity by reducing the δ at low stiffness values (or high temperatures). At high δ values, which is associated with high temperatures, the S-E2 binder is located to the left of the S-E1 and PEN 70/100 binder. This supports the previous statement that the degree of modification influences a binder's elastic components. At high temperatures, the rubber exhibits less viscous behaviour than the other binders. There is a significant difference between the shape of the curves. Due to the modification of the PEN 70/100, the elastomers' curves change in shape and appear to have a slight s-shape. The rubber binders have a clear s-shaped curve.

With ageing, the binders display more elastic behaviour. Figure 4.34 displays the original and aged S-R1 with PP and CP testing. By evaluating the CP tested S-R1 data, it can been seen that the aged data moves more to the left on the Black Space diagram.

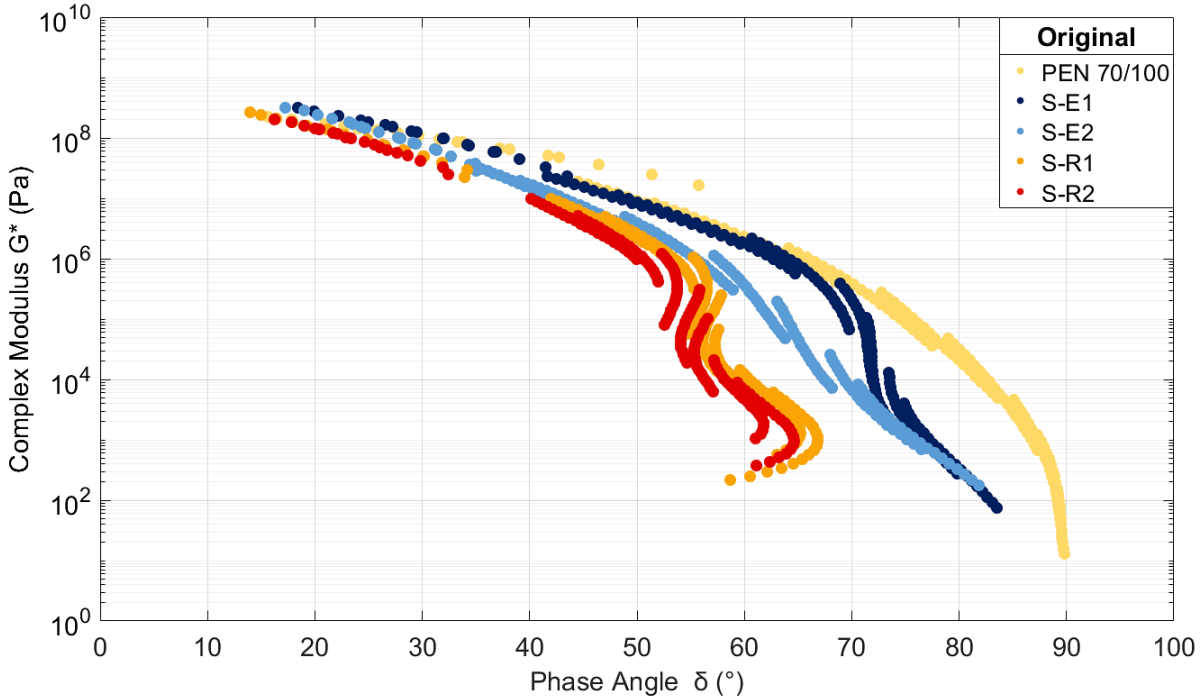

Figure 4.32: Black Space diagrams for all the binders at Original condition with the PP testing

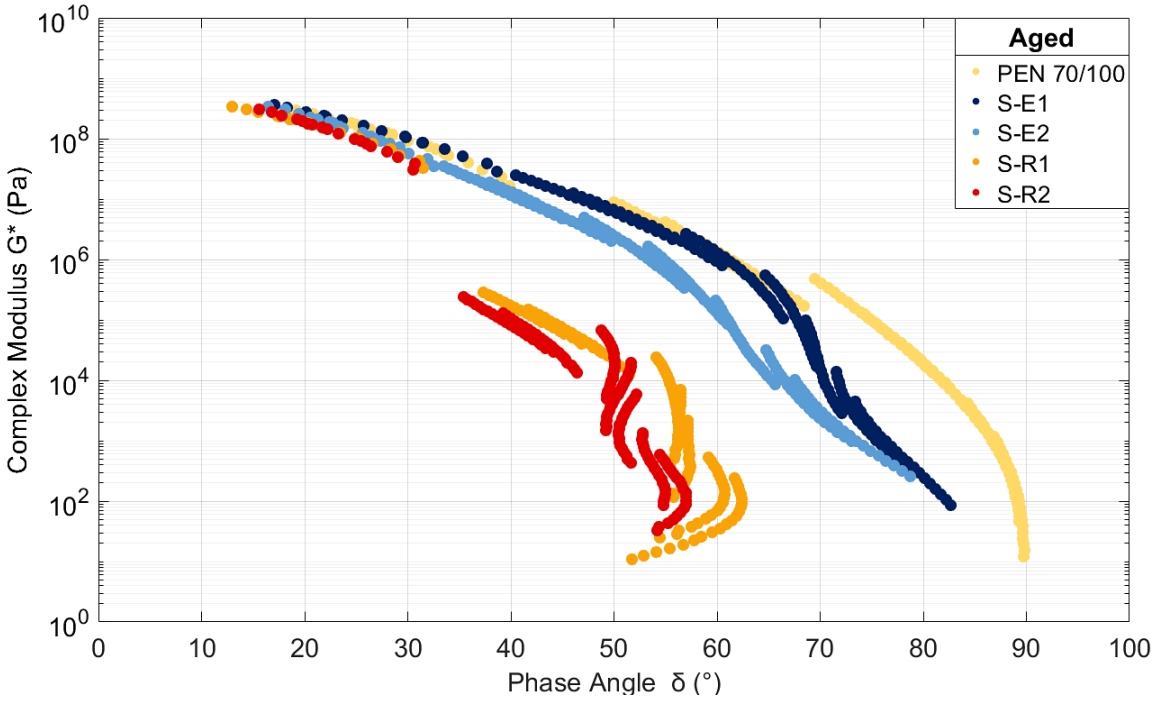

Figure 4.33: Black Space diagrams for all the binders at Aged condition with the PP testing

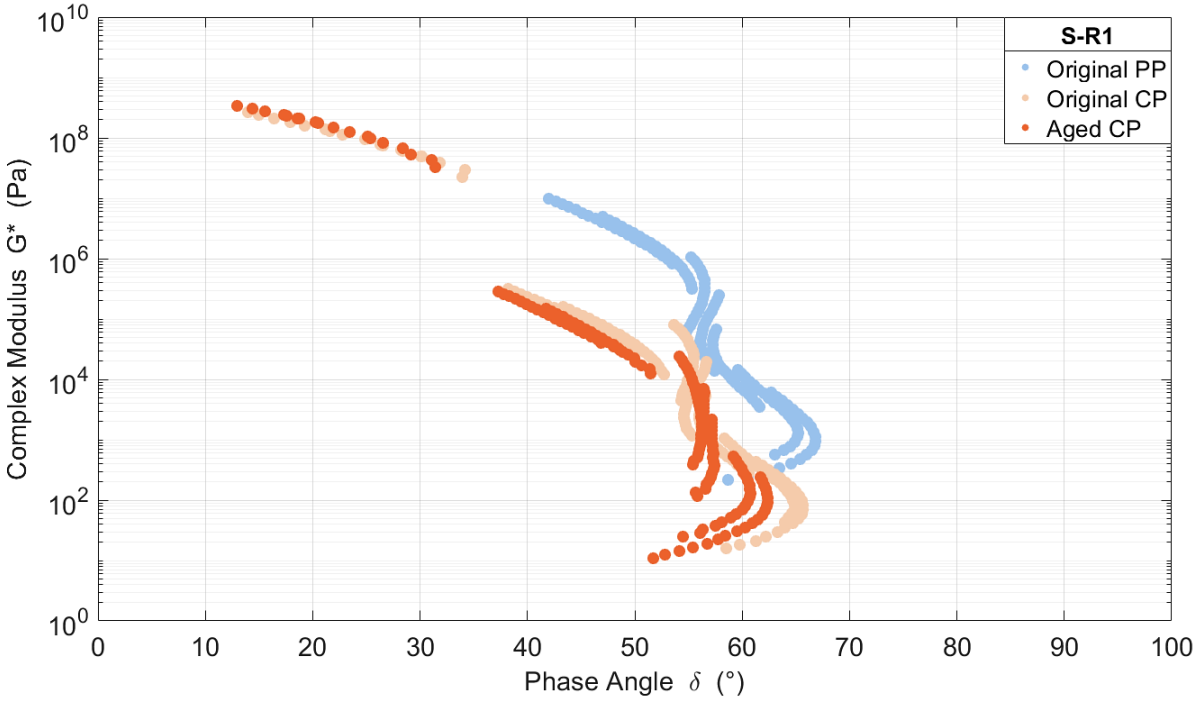

Figure 4.34: Black Space diagram for the S-R1 Original (unaged) binder with CP and PP testing

The CA and DS models applied to the PEN 70/100 original binder can be seen in 4.35. It is clear how the DS follows the data more closely compared to the CA model. Figure 4.36 shows the data of the S-R1 with CP and PP testing with the CA and DS models applied. It is clear that there is a significant difference between the CP and PP data. With the CP testing, there is a vertical gap between the high and low temperature data. This gap occurs at approximately 40°. This result reinforces the fact that CP and PP testing of binders will result in inconsistent data. The PP data does however appear to agree with the BBR data more than the CP data.

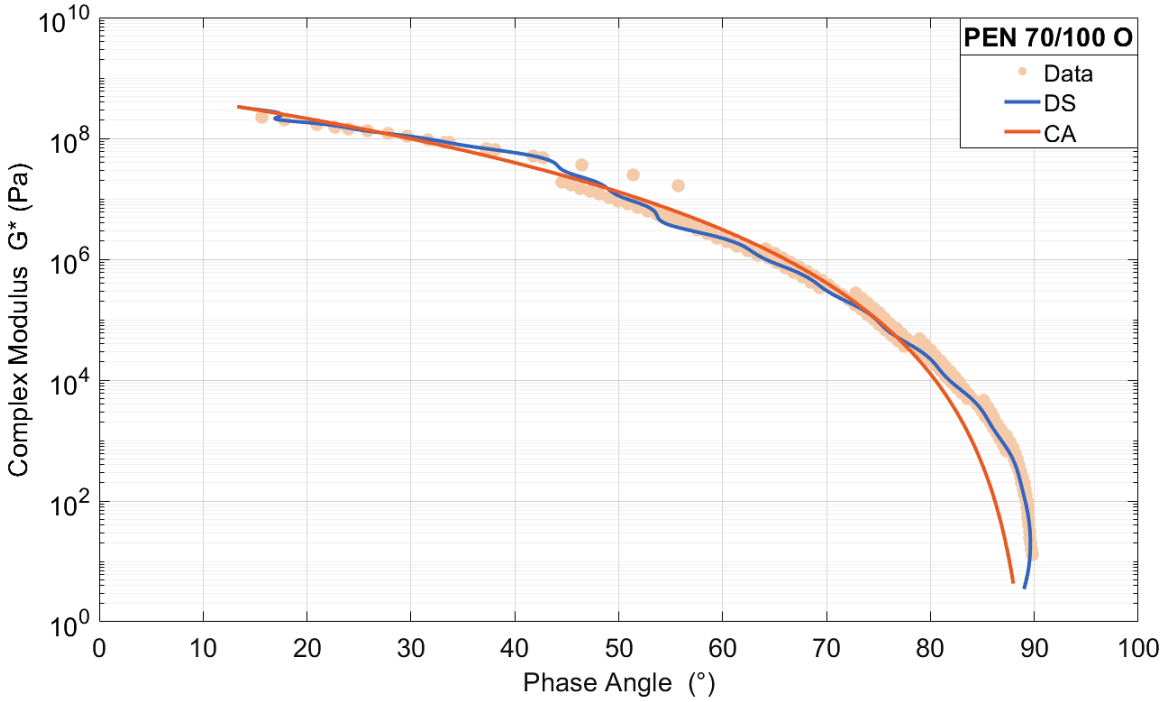

Figure 4.35: Black Space diagrams with the CA and DS models applied to the PEN 70/100 Original (unaged)

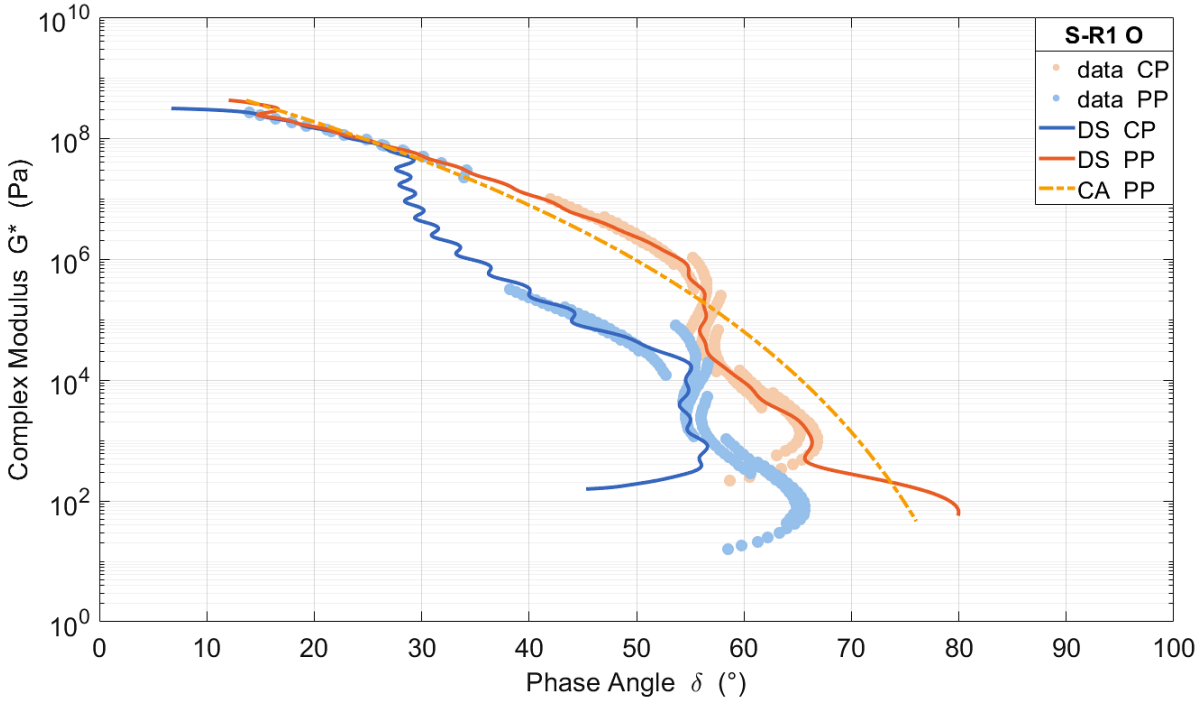

Figure 4.36: Black Space diagrams with the CA and DS models applied to the PEN 70/100 Original (unaged) with CP and PP testing

4.4 MSCR Analysis

The MSCR test is vital to the determination of a binder's recovery potential. This test provides the J_{nr} and %R parameters. These parameters evaluate evaluate a binder's degree of compliance and elastic recovery potential during load repetitions. The J_{nr} evaluates the non-recoverable strain, which is essentially measuring the binder's susceptibility to permanent deformation. The %R measures how much the binder will return to its original shape after a load was applied and removed.

This study focused on the recovery potential of binders at intermediate temperatures as it is believed that higher recovery will counteract stone orientation. The test method is adapted as the standard procedure focuses on high temperatures to investigate rutting susceptibility. The Performance Grade Specifications state that after RTFO ageing, for a 3.2 kPa shear stress, the $J_{nr} \leq 4.5$ at T_{max}. (This is the specification for T_{max} = 58°C, 64°C and 70°C.) Chapter 3 provides further details regarding the necessary changes. As this was a novel test procedure, there is no data to which it can be compared. Yet, basic rheological fundamentals are used in the analysis

of the results. The purpose of testing the binders at intermediate temperatures is to evaluate the binder's properties at construction temperatures. This can be a crucial element to consider, as there are changes in the binder from the refinery to construction and can influence the seal's performance on the road. The binder properties also link to the stone orientation and how the recovery potential of the binder influences the stone orientation. Von Benecke (2021) delves into the influence of stone orientation on seal performance.

Table 4.14: The J_{nr} and %R values for all the binders tested

Binder		**Plate**	**J_{nr} (kPa^{-1})**			**%R**		
			22°C	**28°C**	**34°C**	**22°C**	**28°C**	**34°C**
PEN 70/100	Original		0.30	1.00	3.92	46.2	35.3	23.3
	Aged		0.43	1.81	5.93	46.1	30.8	19.0
S-E1	Original		0.10	0.28	0.58	67.4	63.1	63.0
	Aged		0.07	0.20	0.66	71.2	67.1	62.9
S-E2	Original		0.02	0.06	0.18	80.9	77.8	74.2
	Aged		0.01	0.04	0.13	84.0	80.0	76.6
S-R1	Original	PP	0.09	0.24	0.62	82.86	81.13	79.76
	Original	CP	1.90	5.35	13.35	85.8	84.8	82.4
	Aged	CP	3.18	7.78	13.98	85.2	84.1	83.5
S-R2	Original	PP	0.09	0.11	0.38	85.00	85.69	81.34
	Original	CP	1.90	5.35	13.35	85.8	84.8	82.4
	Aged	CP	1.98	5.75	10.79	87.8	87.3	86.8

Figure 4.37 displays the J_{nr} values for the S-R1 original and aged for different plate configurations. An original sample was tested with the 8 mm CP and a 2.4 mm gap, and another with an 8 mm PP and a 2.4 mm gap size. It is clear that the plate configuration is significant to results. An unaged and aged sample was tested with the CP. From this, it can be seen that the J_{nr} increases with age for the rubber binders, as well as increasing with temperature. J_{nr} value that is more in line with specification values with new configuration. The PP is used to compare the different binders with one another, whereas the CP configuration is used to compare how the rubber binder ages.

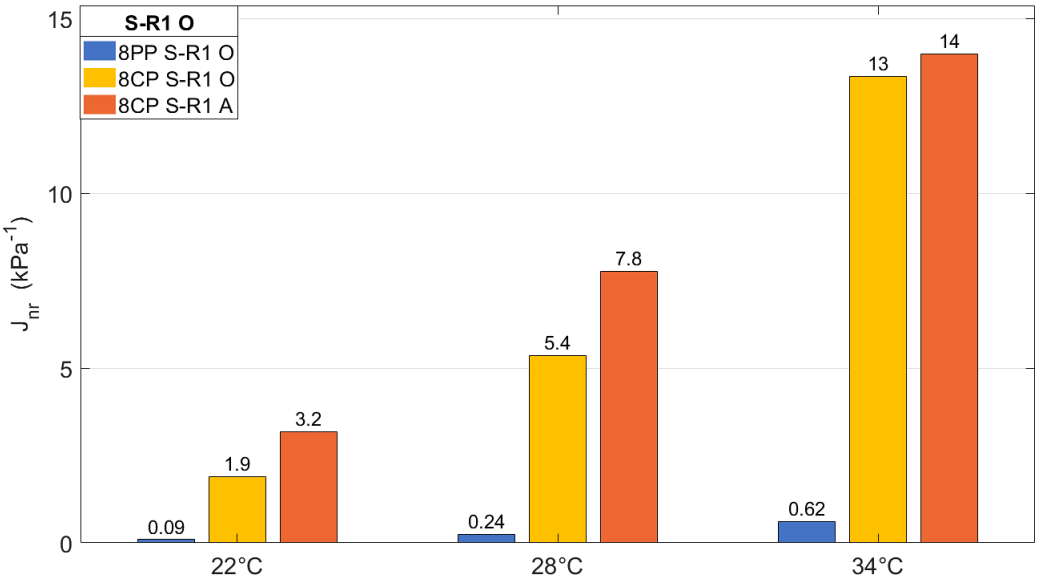

Figure 4.37: Different Plate Configurations for the S-R1 Original (unaged) binder at intermediate temperatures

Figures 4.38, 4.39 and 4.40 show how the PEN 70/100 binder experiences much higher strains than the other binders at each intermediate temperature. From the analysis of the three temperatures, the strain of the binder decreases as modification increases, indicating less permanent deformation. The modification of the PEN 70/100 as polymer modified binders and as rubber binder has a significant reduction in the strain levels at each of these temperatures. Literature has shown that at high temperatures high strain levels are expected. This coincides with the results whereas the temperature increases, the binders experience an increase in strain for a constant applied stress.

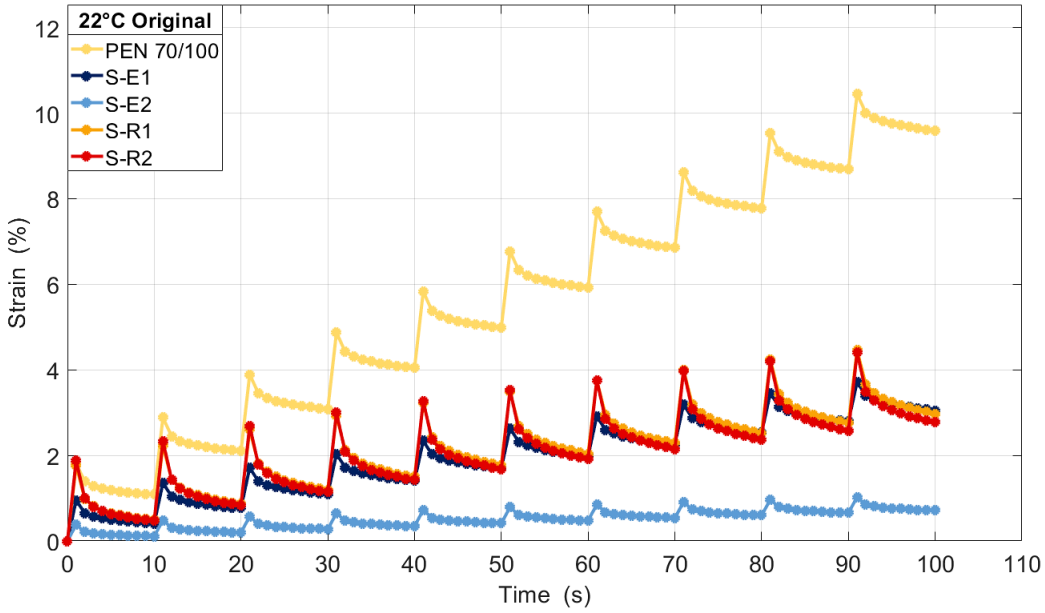

Figure 4.38: MSCR Strain versus Time for Original Binders at 22°C

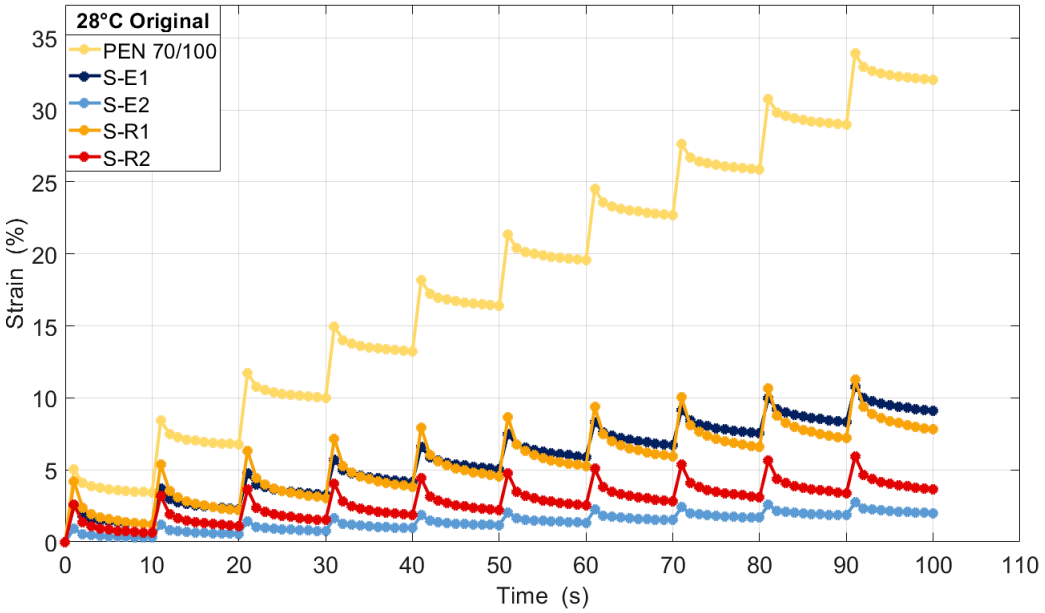

Figure 4.39: MSCR Strain versus Time for Original Binders at 28°C

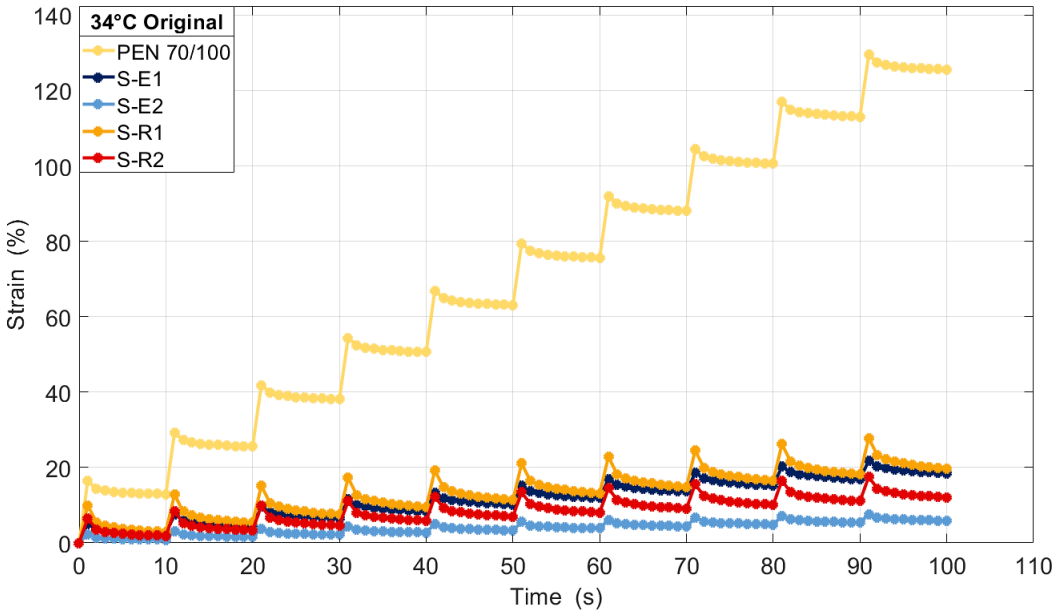

Figure 4.40: MSCR Strain versus Time for Original Binders at 34°C

The Asphalt Institute created a specification to determine whether the binder will have adequate rut resistance. Equation 4.1 displays the boundary line that was developed. Data to the right of the boundary passes the specification and data to the left, fails. At intermediate temperatures, all binders pass the specification. This is expected, as binder will move towards this boundary at high, and away at lower temperatures.

$$\%Recovery = 29.37(J_{nr})^{-0.2633} \tag{4.1}$$

Figures 4.41, 4.42 and 4.43 display the relationship between the % R and the J_{nr}, with the boundary line as an indicator of how well the binder performs.

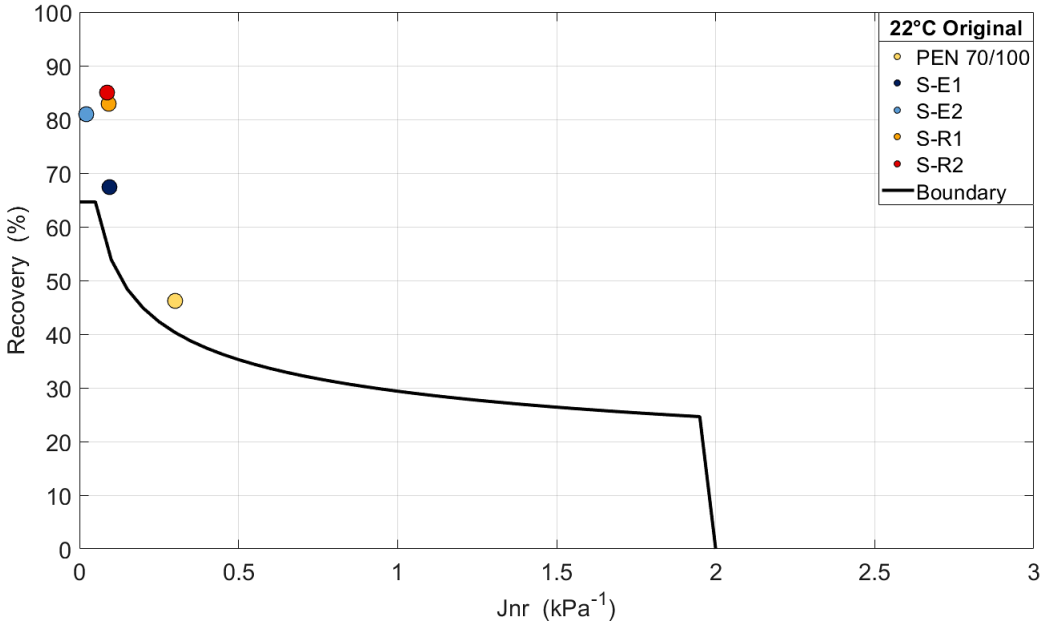

Figure 4.41: The % R versus the J_{nr} for the original binders at 22°C

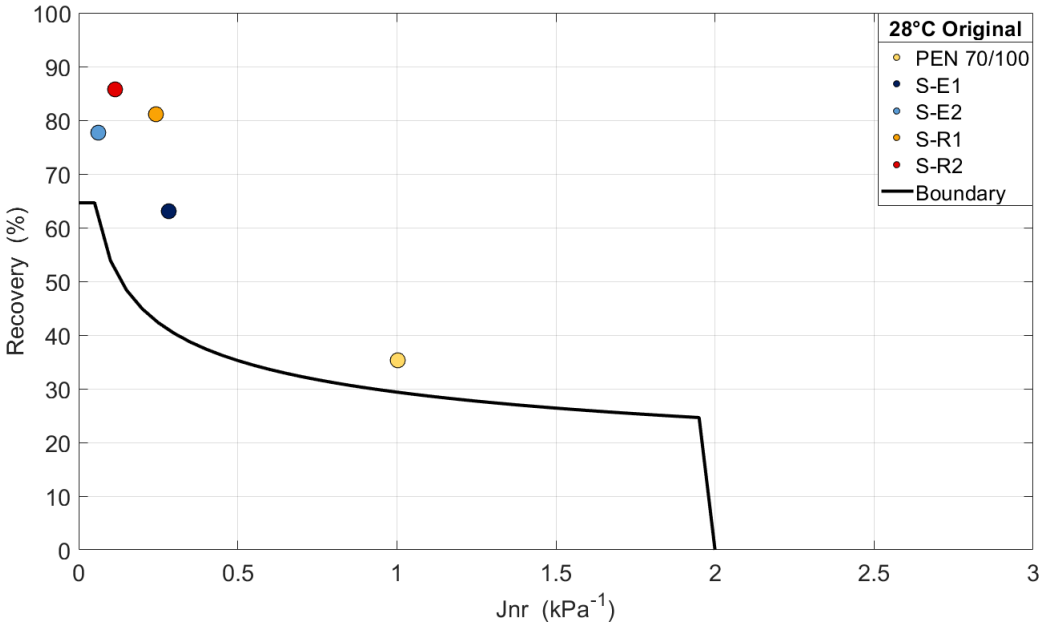

Figure 4.42: The % R versus the J_{nr} for the original binders at 28°C

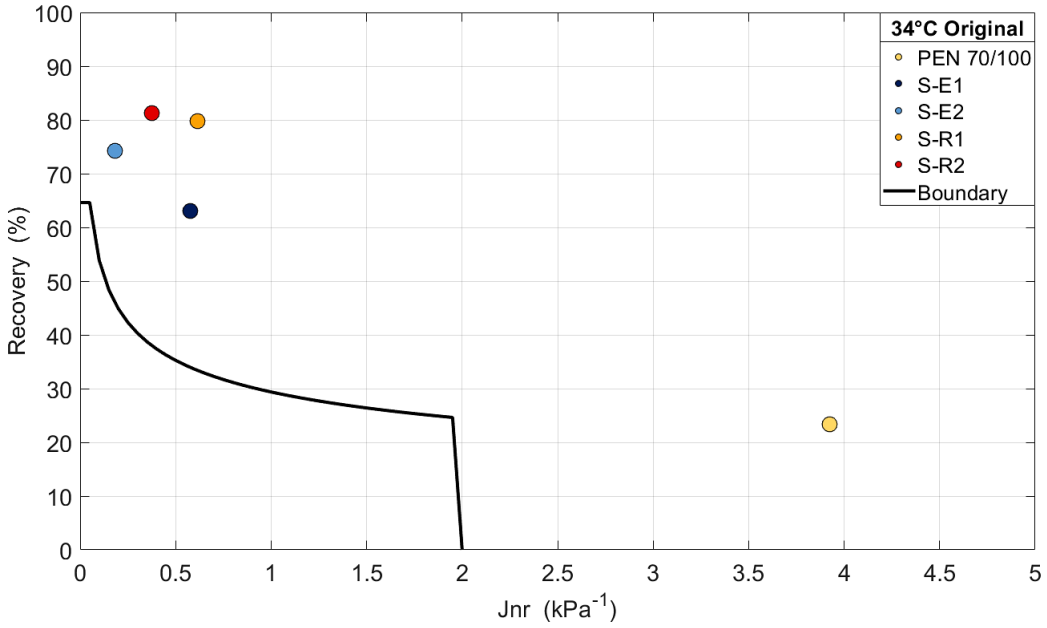

Figure 4.43: The % R versus the J_{nr} for the original binders at 34°C

Analysis of Figure 4.44 shows that an increase in temperature, leads to an increase in J_{nr}. The PEN 70/100 shows large J_{nr} values and low % R. The modified binders have significantly lower J_{nr} values and high recovery. At every intermediate temperature, the S-E2 has the lowest J_{nr}. This means that the binder can absorb more stress, and will not be susceptible to plastic deformation. It is noted that the S-E1 and S-R1 binders both have very similar J_{nr} values at each temperature. The difference between these two binders is the % R. The rubber clearly displays a higher degree of recovery potential than the elastomer, this is due to the rubber's high elasticity component. The PEN 70/100 has a significantly lower % R than the modified binders.

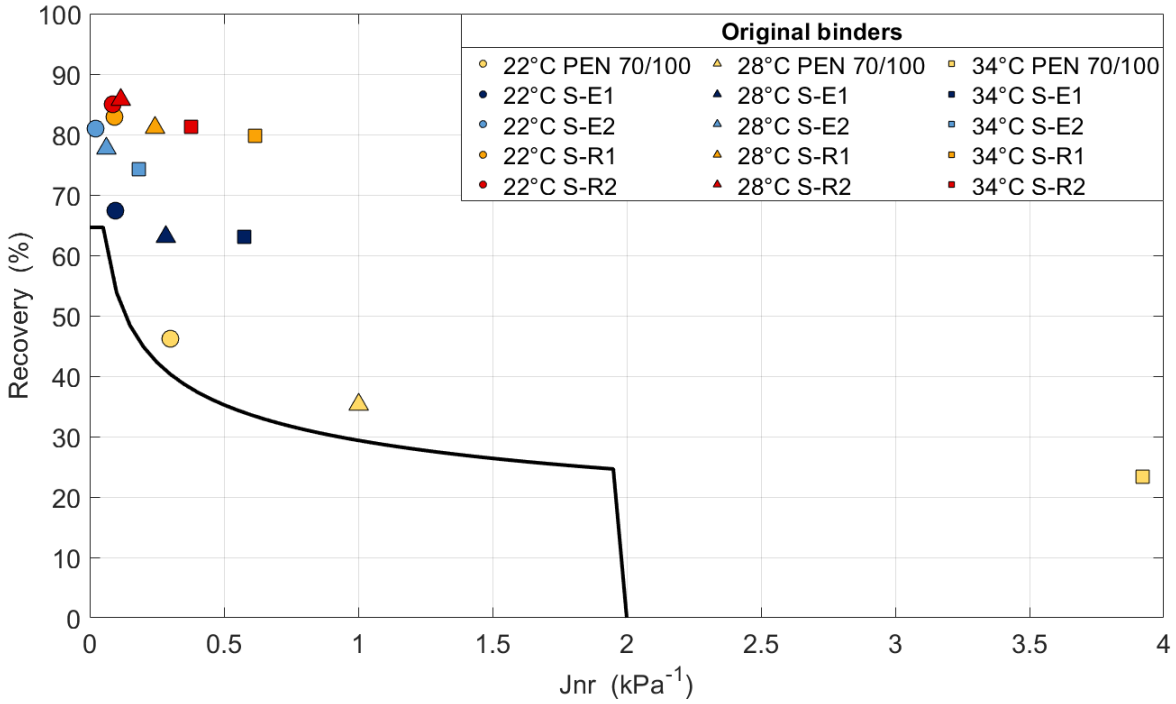

Figure 4.44: % R versus J_{nr} for all original binders at intermediate temperatures

The rubber binders that were tested with cone plates, are used to analyse the effect of ageing on the binders. Figures 4.45, 4.46 and 4.47 also show the relationship between the % R and the J_{nr}, but with the aged binders included. By analysing all three figures, it is clear that with ageing the J_{nr} increases. This is true for the rubber binders and the PEN 70/100. For the elastomers, the J_{nr} appear to remain the same. Interestingly, the elastomers' % R increases slightly with age, whereas the other binders show either a slight decrease, or it remains at a similar value.

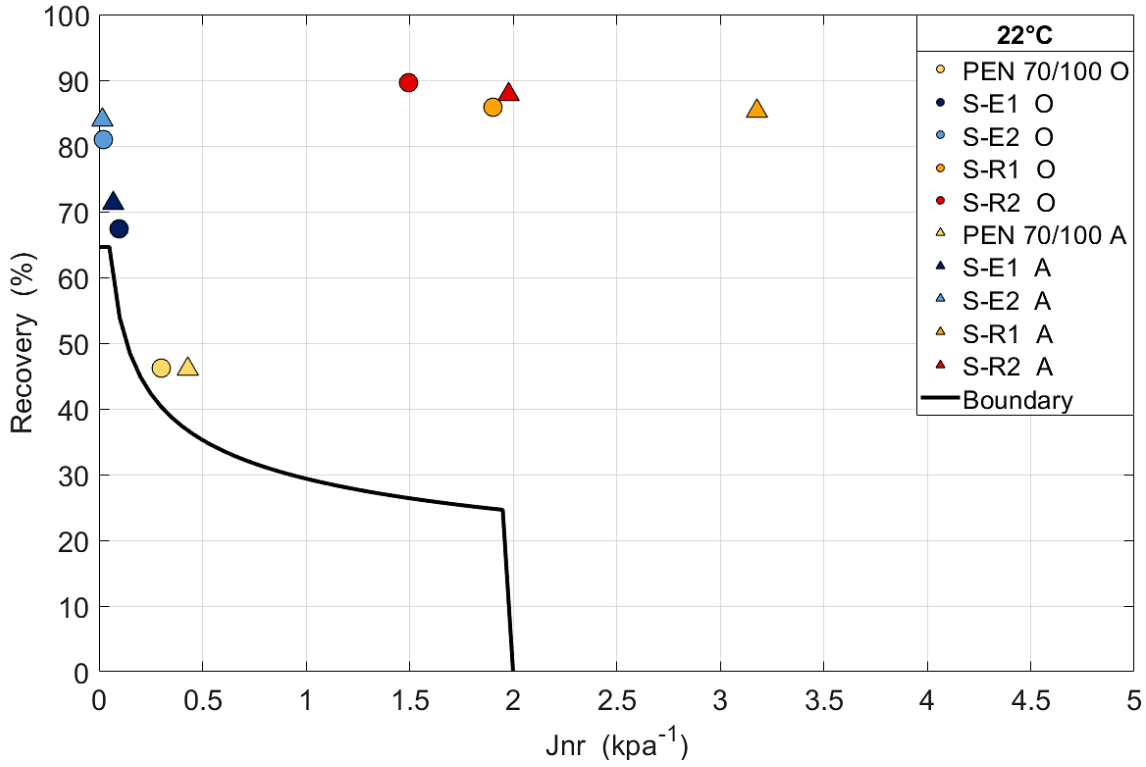

Figure 4.45: The original and aged binders at 22°C for the %R vs J_{nr}

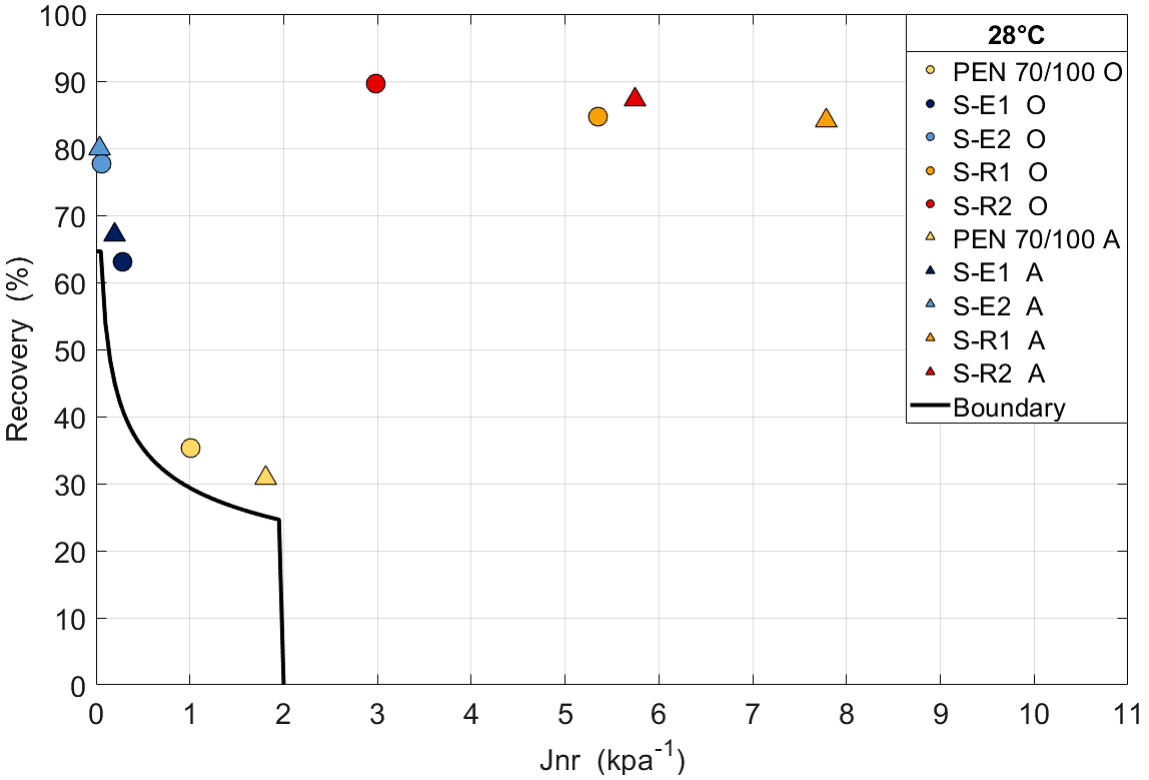

Figure 4.46: The % R vs the J_{nr} at 28°C

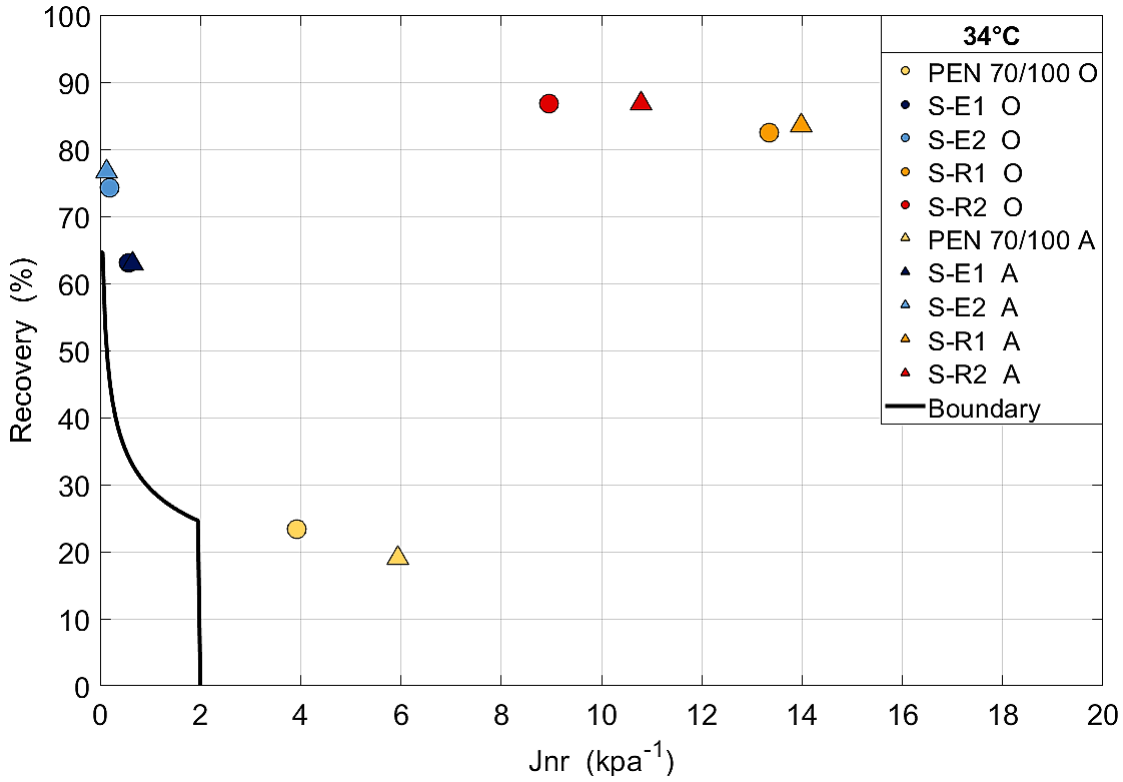

Figure 4.47: The % R vs the J_{nr} at 34°C

4.5 Durability Parameters

The durability parameters that were used in this study, are the G-R parameter and the Visco-Elastic Transition temperature and related parameters.

4.5.1 G-R parameter

The G-R parameter is a useful tool to determine the susceptibility of a binder to cracking. To determine whether a binder has a G-R value that is susceptible to cracking, it is plotted on a Black Space diagram. The results of the G-R parameter were obtained at 0.005 rad/s and a reference temperature of 15°C. In Table 4.15 the G-R parameter, as well as the rheological index is shown.

Table 4.15: The G-R parameter and Rheological index for the binders.

Binders		Plate	G* (Pa)	δ (°)	G-R (kPa)	R
PEN 70/100	Original		1.4E+04	81.01	0.34	1.46
	Aged		6.0E+03	83.82	0.07	1.35
S-E1	Original		2.9E+04	71.26	3.13	2.01
	Aged		4.7E+04	68.40	6.79	2.10
S-E2	Original		1.6E+05	61.84	40.24	2.27
	Aged		1.8E+05	58.78	57.58	2.45
S-R1	Original	PP	2.9E+04	56.60	10.51	3.17
	Original	CP	1.1E+03	56.59	0.4	4.17
	Aged	CP	1.1E+03	57.27	0.39	4.08
S-R2	Original	PP	4.1E+04	54.35	17.25	3.28
	Original	CP	1.0E+03	54.53	0.41	4.47
	Aged	CP	1.4E+03	50.19	0.77	4.96

There are two crack limits related to G-R in the Black Space diagram, onset damage of 180 kPa and a significant cracking limit of 600 kPa. The first limit is linked to the ductility of 5 cm and the second to 3 cm. Thus, when a binder has a G-R value at a high δ and a low G*, the binder will have little to no surface cracking. When the G-R value is in the upper left corner of the Black Space diagram, the binder has a strong possibility of cracking. This is where there is a high G* and a low δ, indicating more elastic behaviour. This is supported by the BBR results of where the cold temperatures such as the -24°C, show a high G* and a low δ in the upper left corner of the Black Space diagram.

In Figure 4.48 the CP and PP testing results are displayed. It can be seen that the G-R for all the binders, fall below the damage onset limit of 180 kPa. By evaluating the PP testing results, the original rubber binder has a similar stiffness to the S-E1 binder, but a significantly lower δ. The lower δ indicates the elastic behaviour of the rubber binders. The modification of the binder is clear in the location of the modified binders to the left of the PEN 70/100. The degree

of modification is also emphasised by the S-E2 and S-R2 lying to the left of the S-E1 and S-R1 binders.

To evaluate the effect of ageing of the rubber binders, the CP testing results are analysed. Binders that have aged, shifts slightly to the upper left corner, to a condition where it is more stiff and elastic. This holds for the S-E1, S-E2 and S-R2. The S-R1 binder has both the unaged and aged condition's G-R on almost the same value. The PEN 70/100, however, shows the G-R parameter moving toward the bottom right of the diagram with age. This result was unexpected and cannot be explained.

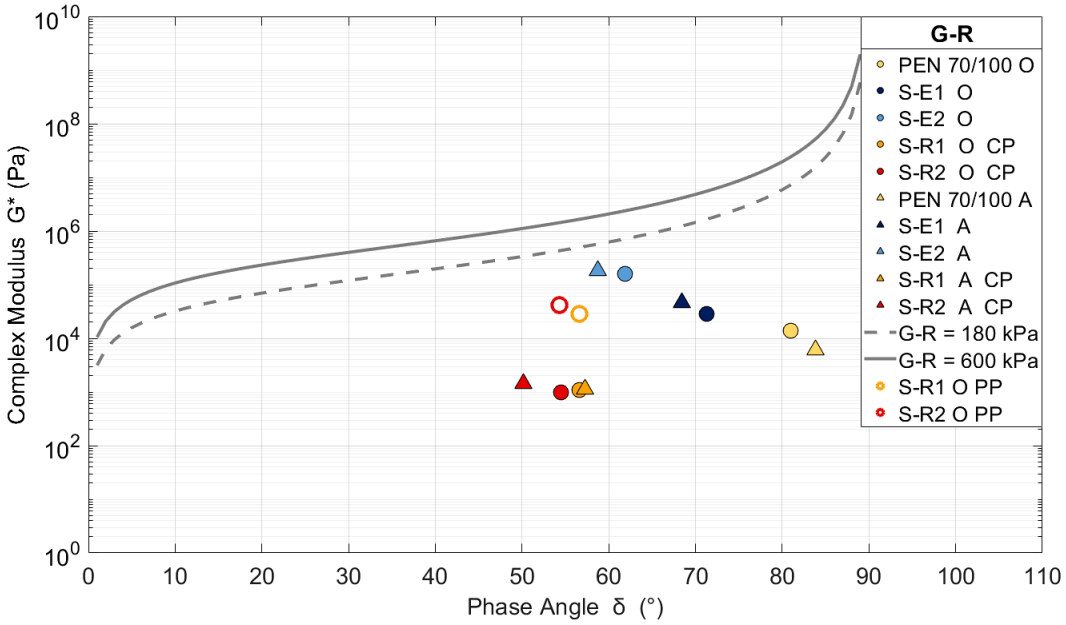

Figure 4.48: G-R values for the Original and Aged binders, including CP and PP testing

Figure 4.49 shows the relationship between the G-R parameter and the rheological index (R). Here, it is more clear that the PEN 70/100 does indeed not perform as expected. It is anticipated that the G-R and R parameters will increase as the binder ages. From Figure 4.50, it is clear that only the S-R2 original binder, surpasses the -5°C, limit. As the ΔT_c is a parameter obtained from the BBR testing, it does not change regarding the CP and PP configuration. The difference can be seen in the G-R values.

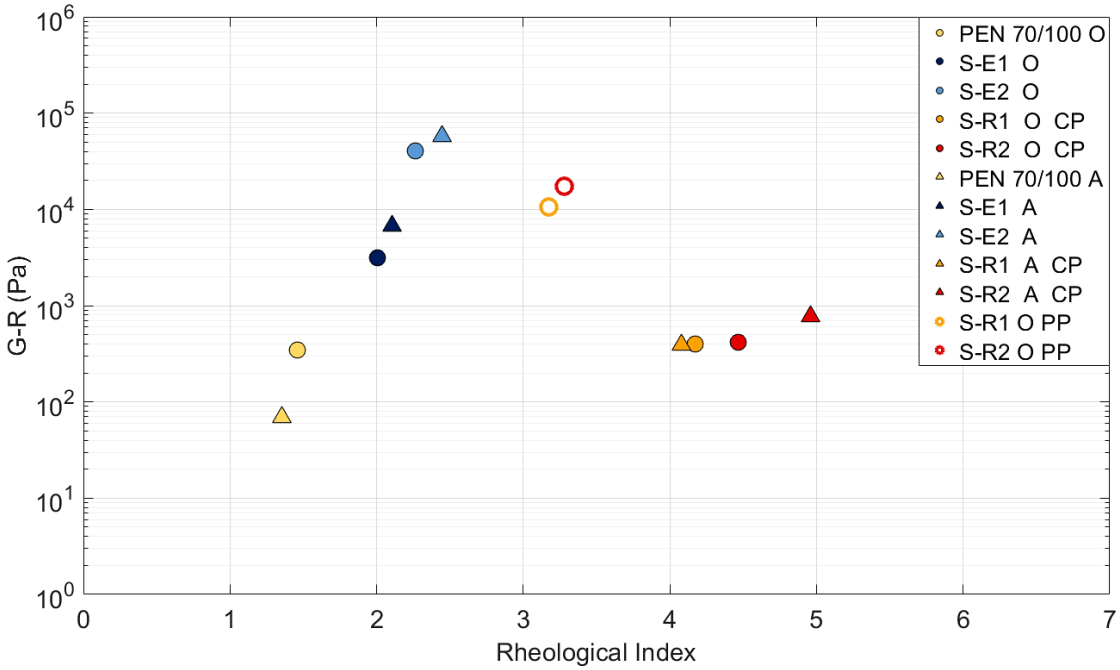

Figure 4.49: G-R vs R

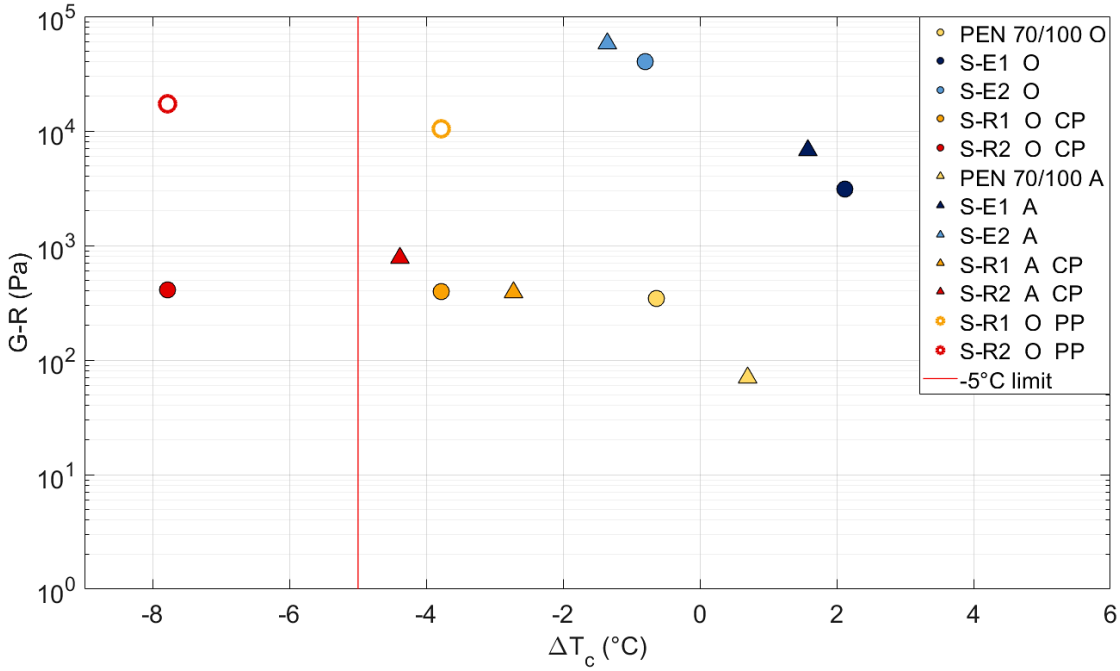

Figure 4.50: G-R vs ΔT_c

4.5.2 T_{VET}

In Table 4.16 the T_{VET} temperatures, crossover frequencies (ω_c) and VET complex modulus (G^*_{VET}) are displayed. The T_{VET} and G^*_{VET} are parameters that are used to evaluate the ageing rate of binders. These parameters are also linked to cracking. The crossover frequency is a measure that evaluates the susceptibility of a binder ageing. As the age increases, the crossover frequency decreases. And thus, in turn, the G^*_{VET} will decrease. From Table 4.16, it can be seen that the unmodified binder has the highest crossover frequency, and the lowest T_{VET}. Whereas the rubber binders have low crossover frequencies, low G^*_{VET}, and high T_{VET}.

Table 4.16: The T_{VET}

Binders		**Plate**	**ω_c at T_{ref}** (rad/s)	**T_{VET}** (°C)	**G^*_{VET}** (Pa)
PEN 70/100	Original		240.19	2.09	2.8E+07
	Aged		130.29	3.65	9.8E+06
S-E1	Original		56.08	5.79	1.7E+07
	Aged		21.08	8.44	1.1E+07
S-E2	Original		2.66	14.82	7.1E+06
	Aged		1.73	16.18	5.7E+06
S-R1	Original	PP	26.50	6.99	5.1E+06
	Original	CP	6.27	12.57	7.7E+04
	Aged	CP	3.56	14.06	5.7E+04
S-R2	Original	PP	9.91	10.47	3.2E+06
	Original	CP	6.90	12.33	6.6E+04
	Aged	CP	1.79	16.04	3.8E+04

Figure 4.51 displays how the T_{VET} will increase with binder age. And that the rubber binders have lower G^*_{VET} values than the other binders for the CP testing. With PP testing, all the original binders fall in the same G^*_{VET} range. There is an increase in T_{VET}, as ageing increases. A higher T_{VET}, indicates that the binder will be more susceptible to cracking. Figure 4.52 reinforces that T_{VET} increases with an increase in age. A slight trend can be seen regarding the results from the PP testing. As the T_{VET} increases, the G-R increases, as well as the ageing. By looking at the CP testing data, the rubber binders fall short of the trend. This stresses the importance of plate geometry when testing.

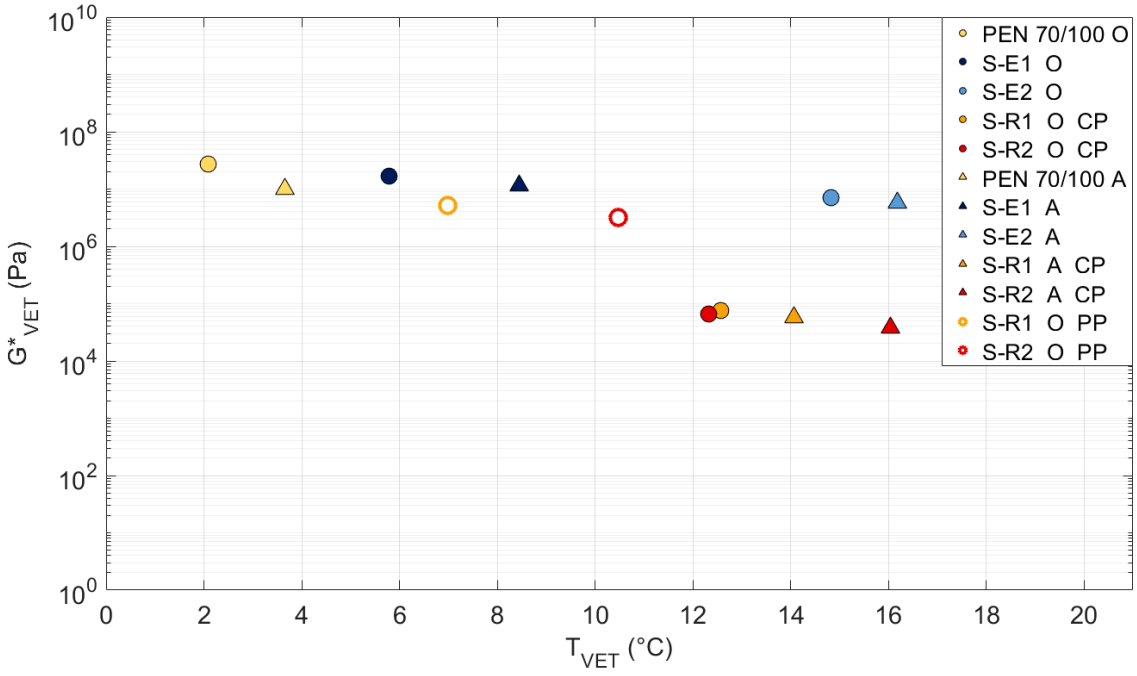

Figure 4.51: G^*_{VET} versus T_{VET}

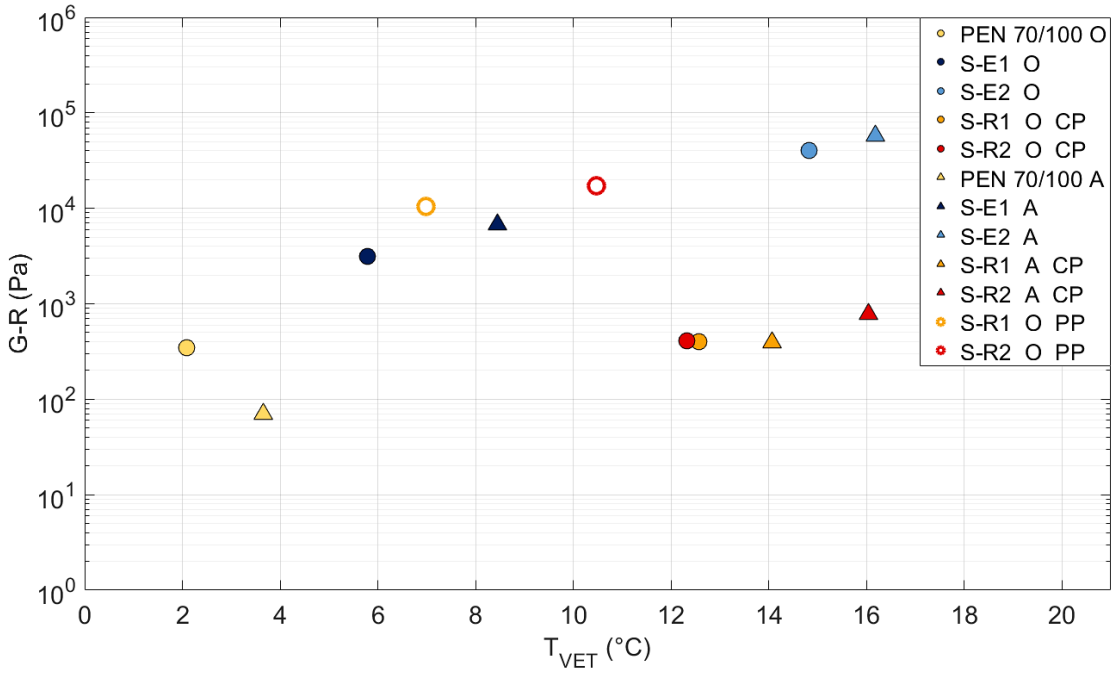

Figure 4.52: G-R versus T_{VET} for the Original and Aged binders, with CP and PP testing data

4.6 Summary

The focus of this chapter was to convey the results from the test procedures discussed in Chapter 3. The PEN 70/100 Original binder was used to indicate how the data analysis was presented. To demonstrate the behaviour of each type of binder, the PEN 70/100, S-E1 and S-R1 Original binders were used. The results for all the binders are provided in the Appendices.
The BBR results included the ΔT_c. The DSR data resulted in the Shift Factors, Master Curves, Black Space diagrams, G-R, R, T_{VET} and G^*_{VET}. The MSCR analysis gave the J_{nr} and % R.

- The S-R2 Original was the only binder that passed the -5°C limit set by the Performance Grade Specifications. This result was not anticipated and cannot be explained. Possible factors contributing to this odd value, can be the trimming of the sample during the testing, or air bubbles were present.

- The Shift Factor models that were used, was the Arrhenius, WLF and Modified Kaelble. The PP testing data showed that the Modified Kaelble shift function provided the best fit for all the binders. The same was true for the CP testing, but the WLF had distinctively high RMSE's regarding the rubber binders.

- The two mathematical models that the RHEA software provided for the binders was the CA and DS models. The S-R1 aged binder, did not have a CA model, but a GL and SL model could be developed. The analysis showed that only the DS model provided a good fit for the data and was used for the calculations of other parameters.
- The MSCR test analysis revealed that the rubber binders had the highest %R, which was anticipated as the rubber binders have high elastic components. The PEN 70/100 binder yielded the lowest % R and the highest J_{nr}.
- The durability parameters showed that the G-R parameters of each binder did not exceed any of the limits set by researchers. The highest G-R value was for the S-E2 Aged binder, which has a value of 57.58 kPa, which is not close to the initial cracking limit of 180 kPa. For the PP testing data, there is a noticeable relationship between the G-R and T_{VET}. With an increase in modification there is an increase in both the G-R and T_{VET}.

Chapter 5

Discussion

This chapter interprets and discusses the findings from Chapter 4. The purpose is to provide a clear perspective of the findings and the consequences of the rheological outcomes.

5.1 BBR results

- The elastomers have higher stiffness values than the PEN 70/100 and rubber binders at -24°C, see Figure 5.1. It would be anticipated that the elastomers have a lower stiffness than the PEN 70/100 depending on the polymer e.g. SBS that is cross-linked versus block based. The relaxation property for the elastomers are similar or lower than the PEN 70/100 in Figure 5.2. The factors that contribute to these unexpected results could be: source, the type of bond in the binder (e.g. cross-linked). It should be noted that South African roads are not expected to reach these extreme temperatures.

- S-E1 original and aged, both have a ΔT_c higher than zero, and display S-controlled behaviour. This means that the relaxation properties when the S(60) value has reached its compliance limit are still valid. Only the S-R2 original binder shows a ΔT_c that exceeds the -5°C limit that the Performance Grade Specifications require, i.e. non-compliance.

- Regarding the ageing in low temperatures. It is expected that the stiffness of the binders increase with age. This is true for the PEN 70/100 and elastomers. Yet, the rubber binders decrease in stiffness with an increase in age. Further research on rubber binder ageing behaviour would assist in explaining this result. Although it is speculated that the com-

bination of ageing and the cold temperatures (which ranged from -24°C to -36°C), altered the properties of the rubber binder.

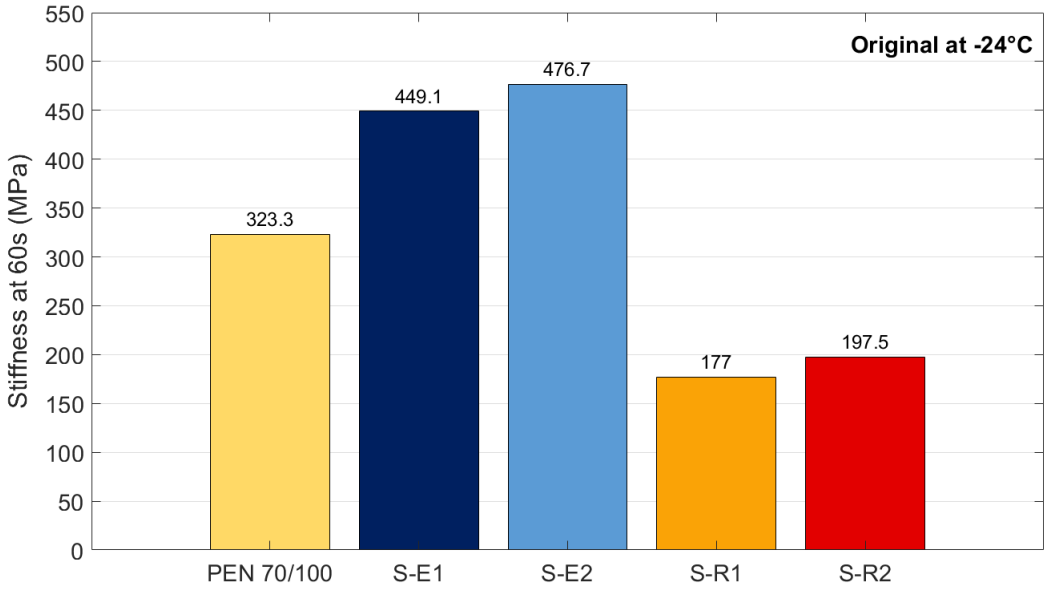

Figure 5.1: Stiffness at 60s for the original binders at -24°C

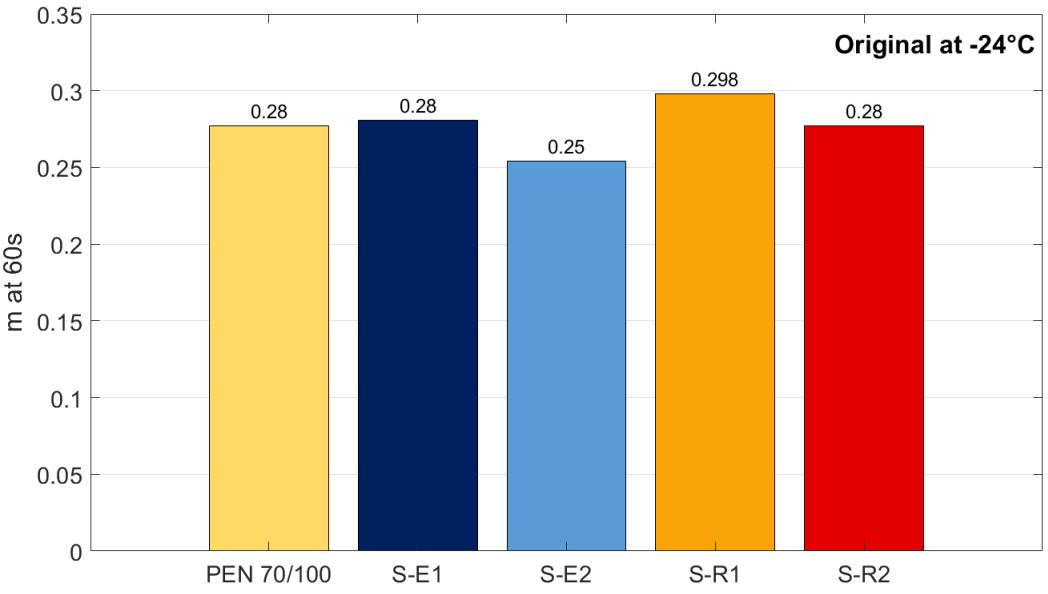

Figure 5.2: m (slope) value at 60s for the original binders at -24°C

5.2 Shift Factors

- The three shift factor functions that were obtained from the RHEA software, are the Arrhenius, WLF and Modified Kaelble functions. The Modified Kaelble was able to best describe both behavioural ranges. This was reflected in the model RMSE.

- WLF struggled to accurately describe low-temperature BBR shift factors. The CP testing revealed that the WLF shift factor function had a very high RMSE. This suggested that the function could not find a suitable fit with the CP tested data.

5.3 Master Curves and Black Space diagrams

Master Curves

- The Master Curves for the PP tested data show that the modified binders have a slightly flatter slope than the unmodified PEN 70/100.

- The analysis showed that the DS model provided the best fit for all the data sets. Figure 5.3 shows the RMSE for each binder for the DS and CA models. Because the DS model is the sum of various components, it has a significantly higher number of degrees of freedom than continuous numerical models, such as the CAM and GL models. The increased degrees of freedom allow the models to follow the data points more closely. This results in significantly lower prediction errors. However, this may also lead to overfitting of data. There is therefore a greater responsibility of the modeller to ensure the data in sound and reflects LVE behaviour.

- The PEN 70/100 showed a 7.63% RMSE for the DS model and a 3.79% RMSE for the CA model. It would be expected that the CA model would provide a better fit, as it has a lower RMSE. Yet visually on the PEN 70/100 Original Master Curve graph with the DS and CA model, the DS model has a more accurate fit for the δ Master Curve.

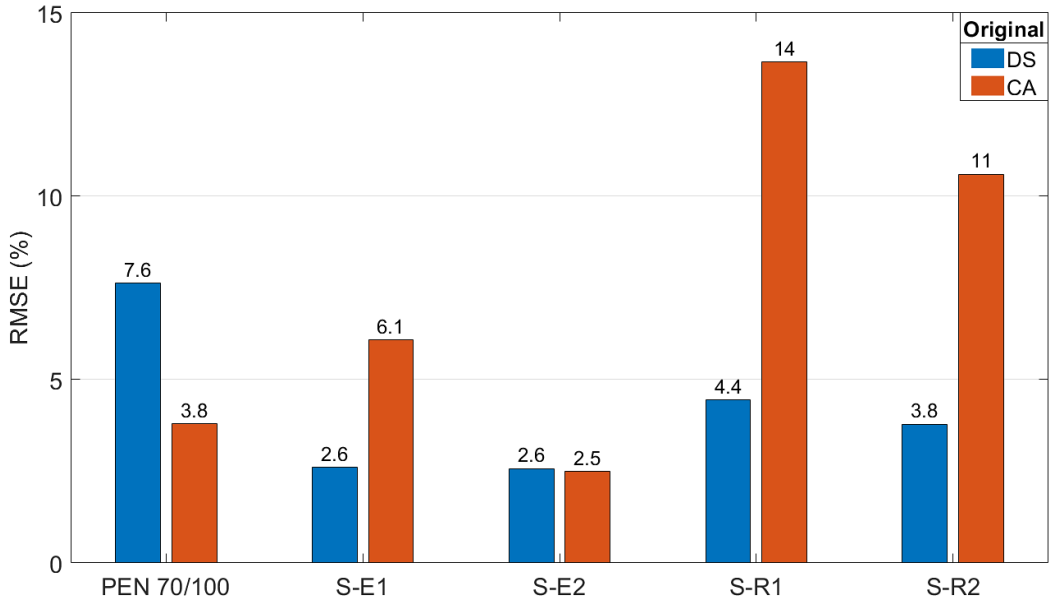

Figure 5.3: RMSE for each binder of each model with PP tested data

Black Space diagrams

- The rubber binders tend to a more elastic behaviour at higher temperatures, due to their non-homogenous nature. A Black Space diagram indicates how the PEN 70/100 modified to S-E1 and S-E2, increases the elasticity of the binders. The adding of crumbed rubber modifier, increases the elasticity even more.

- The Black Space diagram of the S-R1 clearly illustrates the difference between the PP and CP testing. Figure 5.4 demonstrates how the gap between CP and PP testing has an impact on results. This diagram also shows that ageing decreases the δ and in turn increases elasticity. The implications of the gap difference is that incorrect information is received and can lead to early failure of seals.

- During a frequency sweep, the DSR software calculates the binder stiffness based on the torque required to apply a constant strain. The resulting stiffness should be true and independent on specimen geometry. That is the purpose of fundamental measurements.

- For the stiffness to differ (1) the non-homogeneous nature of the rubber binders could influence the stress distribution in the specimen geometries differently or (2) the software assumption for CP calculations are no longer valid for the gap size required for the rubber

binders.

- The G-R parameter evaluates the effect of ageing on the binders. Figure 5.5 confirms that all the binders fall short of the 180 kPa limit. A trend can be seen that with an increase in age, there is an increase in the G-R value, with the exception of the PEN 70/100.

- There is a trend between age and T_{VET}. Figure 5.6 displays that as the age increases, the T_{VET} also increases. A high T_{VET} is associated with cracking, and can also lead to aggregate loss, depending on the creep and recovery parameters. Lower T_{VET} values imply that the binder will generally be prone to more elastic behaviour from these temperatures.

- Interestingly, there is an insignificant difference for T_{VET} of the rubber binders calculated with the CP and PP configurations. Although the shift between DSR and BBR data varied significantly for PP and CP testing, the relative shift between the DSR temperatures remained similar. As a result, the relative shift to temperatures close to the reference temperature also remained similar. T_{VET} for the rubber binders are between 12 and 16°C.

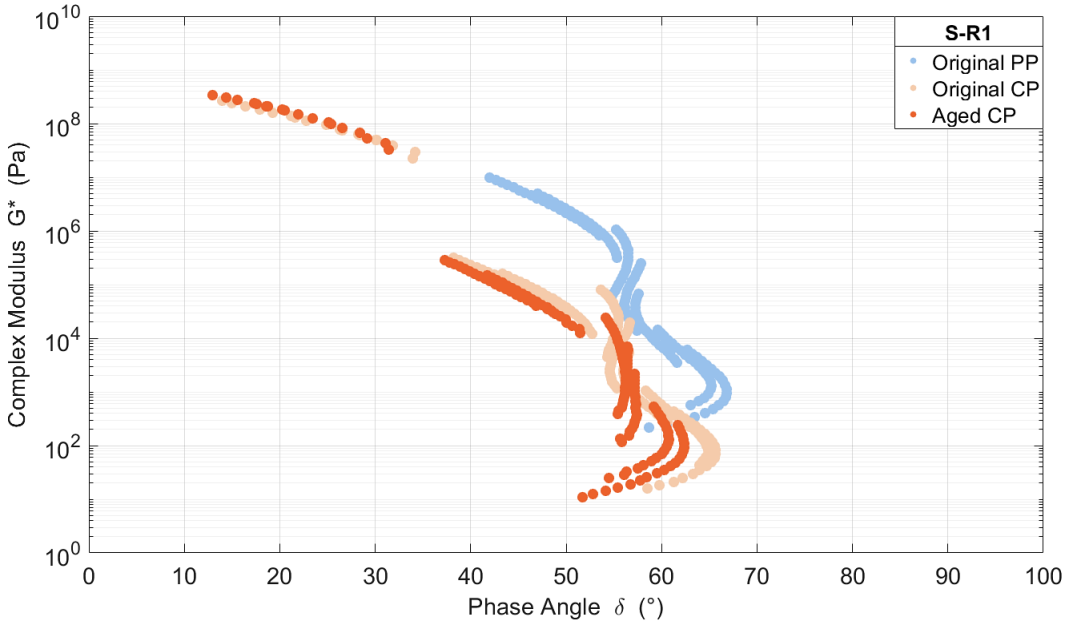

Figure 5.4: Black Space Diagram of the S-R1 different plates

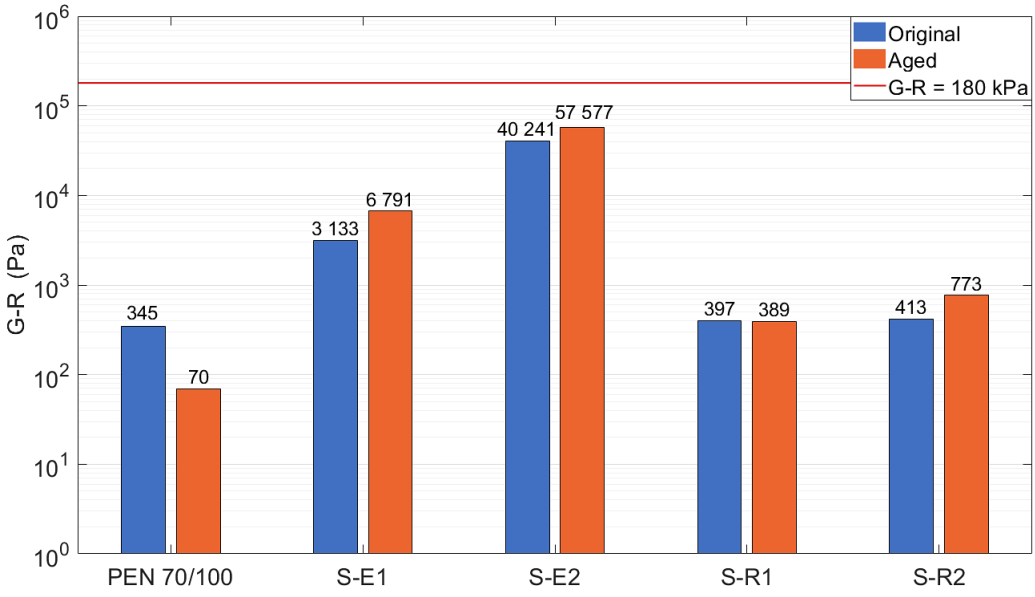

Figure 5.5: G-R of the original and aged binders with CP testing data

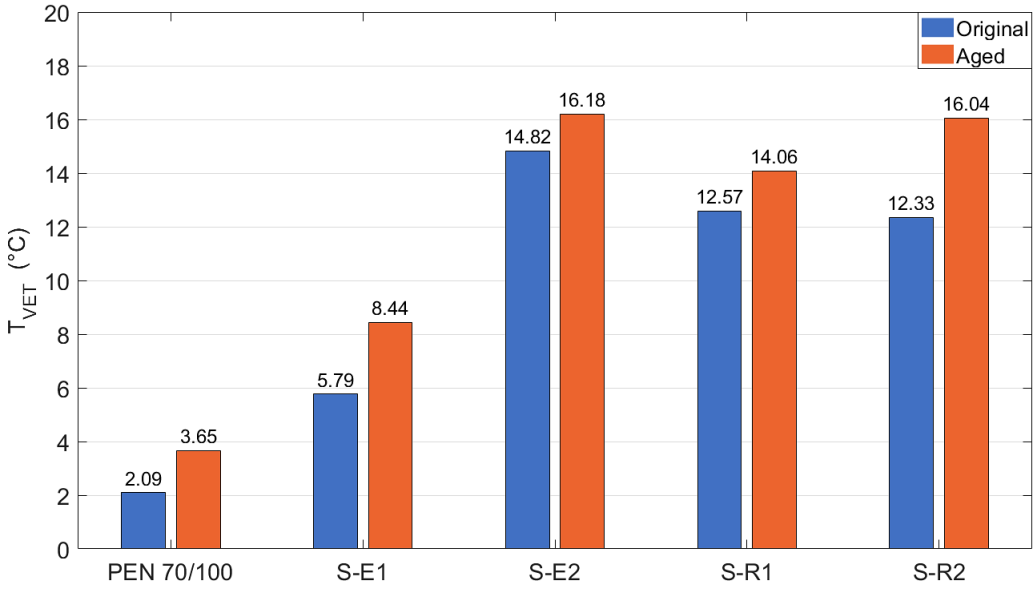

Figure 5.6: T_{VET} for the original and aged binders with CP testing data

5.4 Creep and recovery from MSCR

- The modified binders higher stiffness values, indicated that they can absorb more stress and hence dissipate more energy than the unmodified binder, using the MSCR test.
- Figure 5.7 and 5.8 display the J_{nr} and %R for each original binder at intermediate temperatures. The chart shows the PP testing rubber binder results. Higher J_{nr} values indicate a higher susceptibility to permanent deformation. Even though the elastomers and rubber binders have similar J_{nr} values, the rubber will yield enhanced performance due to the high %R.
- The degree of modification also plays a role and can be seen in the elastomers' J_{nr} results. The S-E1 has a lower %R than the S-E2. The same can be said about the rubber binders, the S-R2 has a slightly higher %R than the S-R1. This is due to the binders having an increase in the amount of modifiers added.
- At intermediate temperatures, short-term ageing does not significantly affect the %R of the modified binders, as opposed to high temperatures. With the exception of the small increase in the elastomers. Overall, the rubber binders have a superior performance at intermediate temperatures regarding creep and recovery, followed by the elastomers. The modification of binders influences the performance of binders, as can be seen by the unmodified PEN 70/100 that underperforms compared to the modified binders.

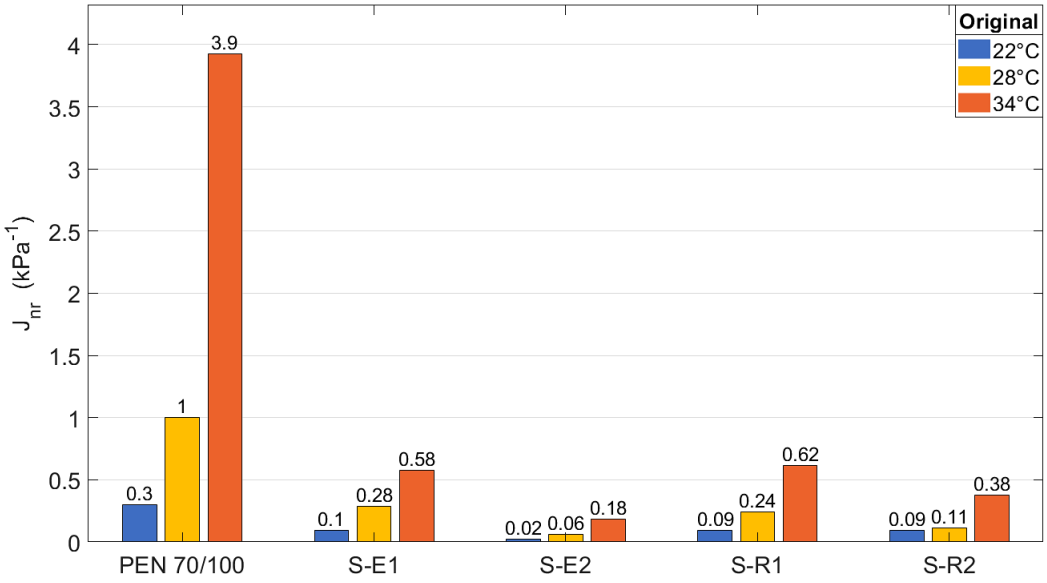

Figure 5.7: The J_{nr} for the original binders (unaged)

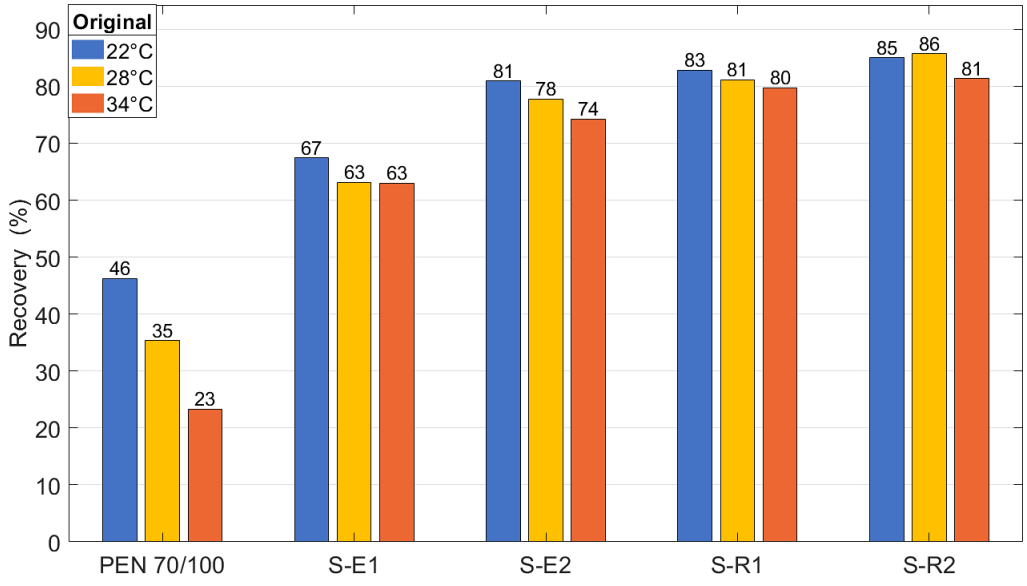

Figure 5.8: % Recovery for the original binders with the PP tested data

Stone Orientation

- Firstly, the concept of stone orientation should be explained, for clarity. As a vehicle's tyre rolls over a seal, it applies forces that create displacement of the stones. After the tyre has passed, there is some rebound. The magnitude of the rebound will influence the volumetrics of the seal i.e. the voids that are available to accommodate the tack or bond coat. If there is only a small rebound (recovery) then the stones orientate onto ALD (average least dimension) and will reduce the voids, leaving less space for the tack coat. This is due to permanent deformation and creates what is defined as stone orientation. If there is very high %R in the binder, then the stones have a higher chance of rebounding to their original position, and are not deforming permanently i.e. retaining the volumetrics of the seal. There are a number of factors that influence stone orientation.

- This study focuses primarily on binder rheology and the role that it plays. Binder application rates must be very accurate to avoid bleeding from over-application or stone loss from under-application. So, this factor is paramount to the quality of seal design and construction.

- Binders that provide a high %R and low plastic deformation will provide seals with extremely low stone orientation. Based on binder rheology data for a limited number of binder types, straight run binder e.g. PEN 70/100 has yielded a higher J_{nr} at intermediate temperatures, which indicates the likelihood of higher strains under load, resulting in significant orientation. On the contrary, lower J_{nr} values provided by the rubber binders S-R1 and S-R2, with higher %R, will experience significantly less stone orientation. The high recovery implies a higher elastic component in the binder leading to a resilient rebound of a seal stone after deforming under traffic loads. A response that is similar to bitumen rubber is that of modified binder.

- Although a low J_{nr} can indicate good performance, the combination of J_{nr} and %R conditions will not be the same for all the binders. This is reflected in the different results of the elastomers and the rubber binders. These result should be analysed with the data obtained from Von Benecke (2021) for further analysis.

Chapter 6

Conclusions and Recommendations

This research project strives to evaluate the rheological properties of seal binders at intermediate temperatures. The goals and objectives, as stated in Section 1.3, of this study were to:

- Assess low-temperature behaviour using the Bending Beam Rheometer in order to evaluate susceptibility to cracking failure.
- Determine the Master Curves from the Dynamic Shear Rheometer and the Bending Beam Rheometer as a means of analysing the behaviour of binders at various temperatures and frequencies.
- Determine the J_{nr} and %R for each binder in its original and aged condition at intermediate temperatures to appraise the changes in permanent deformation characteristics.
- Obtain the durability parameters and evaluate the performance of each type of binder.

6.1 Conclusions

- The rubber binders have lower stiffness at low temperatures, and high relaxation properties, compared to the other binders. Thus, it can be considered that the rubber binders will perform well at extremely cold temperatures.
- The value of ΔT_c of the rubber binders is below zero, indicating that the binders are m-controlled, which is unfavourable. It must also be noted that although a high ΔT_c is de-

sired, even though the rubber binders are non-compliant in certain circumstances, they perform well regarding other criteria.

- At high temperatures, the rubber binders display lower δ values, which indicates higher elasticity. The higher the elasticity, the less chance of rutting occurring.
- The G-R parameter and the T_{VET} increases as the modification of the binder increases. The G-R values were below the crack initiation limit of 180 kPa and all T_{VET} values were significantly lower than the specification intermediate temperatures.
- The modification of a binder greatly reduces the J_{nr} at intermediate temperatures. The degree of modification further decreases the J_{nr}. This means that the S-E2 and S-R2 binders have lower susceptibility to plastic deformation at intermediate temperatures.
- The %R of the PEN 70/100 binder notably decreases with an increase in temperature. The modified binders show a minimal decrease, and the rubber binders show approximately a 1% decrease in %R This shows that the rubber binder retains its elasticity at intermediate temperatures compared to the PEN 70/100.
- The high recovery of the rubber reveals that stone orientation will take place, but once the truck wheel passes on, the stone will rebound to its original position. The low J_{nr} also indicates that the stone will be able to rebound after loading. The elastomers show similar behaviour, but with a lower %R.
- An important finding from this research project revealed that cone plate and parallel plate testing yield significantly different results.

6.2 Recommendations

Recommendations for further research:

- Ageing is a crucial principle in the research of rheological behaviour of bituminous binders. Therefore it is recommended that the short-term ageing process for rubber binders be re-evaluated. It is difficult to obtain a sufficient amount of rubber binder from the bottles after testing. Thus, heating and testing temperatures should be examined.

- It should be considered that the Performance Grade Specifications' limit of $\Delta T_c \geq$ -5°C, may have to be re-examined for the rubber binder.
- The rubber binder cools down significantly faster than the elastomers and unmodified binder. It is suggested that a specific temperature be set to heat the rubber binders in order to pour the binder in to sample moulds, such as the DSR and BBR moulds.
- Due to the rubber binder having a high elasticity, it is difficult to trim the sample when testing on the DSR. So it is recommended that another method of trimming be created. Possibly a mechanical mechanism rather than a hand tool.
- This study found that cone plate and parallel plate testing of rubber binders show different results. It is recommended that further research be conducted in how the geometry of the DSR testing influences the data, and which plate configuration would yield accurate results.
- Regarding DSR testing, there are guidelines, but no gap size specification for rubber binders. As the rubber binders have crumbs in its composition, the gap size should be re-evaluated. For example, a 2 mm gap size would not work for a rubber binder with crumb size of 1 mm. The plates will not measure the shear strain in the binder due to it shearing on the crumbs. However, if the rule of 4 x crumb rubber diameter (600 micron maximum) is used, then a gap of 2.4 mm is proposed.
- It is recommended that there be more testing on rubber binders, so as to fully understand the behaviour of the material, especially at intermediate and low temperatures. Tests to evaluate the viscoelastic properties of the rubber binder should be the focus point.
- It would be beneficial to have more research conducted on the rheological properties of seal binders at intermediate temperatures. As mentioned before, binder properties at construction time temperatures can be important information that links to fatigue cracking.
- In combination with the rheological results of this study which focuses on the rheology of the seal binders, it is recommended that the work of Von Benecke (2021) and Gerber (2021) be taken further and combined with the results presented to assess whether a relationship can be found between J_{nr}, %R and stone orientation at intermediate temperatures.

- The hypothesis underlying these trends makes it important for further investigation of MSCR results tested with a DSR at intermediate temperatures, with actual seal stone orientation measurements during trafficking.

Bibliography

Al-Haddad, A. (2015). Construction of a complex shear modulus master curve for iraqi asphalt binder using a modified sigmoidal fitting. *International Journal of Science, Engineering and Technology Research*, vol. 4, no. 4, pp. 0682–0690.

Anderson, D.A., Christensen, D.W., Bahia, H.U., Dongre, R., Sharma, M., Antle, C.E. and Button, J. (1994). Binder characterization and evaluation, volume 3: Physical characterization. *Strategic Highway Research Program, National Research Council, Washington, DC*.

Anderson, D.A. and Marasteanu, M. (2010). Continuous models for characterizing linear viscoelastic behavior of asphalt binders. In: *ISAP workshop on asphalt binders and mastics*, pp. 16–17.

Anderson, R.M., King, G.N., Hanson, D.I. and Blankenship, P.B. (2011). Evaluation of the relationship between asphalt binder properties and non-load related cracking. *Journal of the Association of Asphalt Paving Technologists*, vol. 80.

Asiimwe, A., Jenkins, K. and Rudman, C. (2014). Surface Run-Off Behaviour of Bitumen Emulsions Used for the Construction of Seals. , no. March, pp. 978–979.

Asphalt Institute (2019). *Use of the Delta Tc parameter to characterize asphalt binder behavior*. ISBN 9781934154779.
Available at: `http://www.asphaltinstitute.org/engineering/delta-tc-technical-document/`

ASTM D 2872-04 (2004). Standard Test Method for Effect of Heat and Air on a Moving Film of Asphalt (Rolling Thin-Film Oven Test). *Annual Book of American Society for Testing Materials Standards*, vol. 4.
Available at: `https://doi.org/10.1520/D2872`

ASTM D 6648-08 (2008). Standard Test Method for Determining the Flexural Creep Stiffness of Asphalt Binder Using the Bending Beam Rheometer. *Annual Book of American Society for Testing Materials*

Standards, vol. 4.

Available at: https://doi.org/10.1520/D6648-08.2

ASTM D 7175-08 (2013). Standard Test Method for Determining the Rheological Properties of Asphalt Binder Using a Dynamic Shear Rheometer. *Annual Book of American Society for Testing Materials Standards*, vol. 4.

Available at: https://doi.org/10.1520/D7175-08.2

ASTM D 7405-10a (2010). Standard Test Method for Multiple Stress Creep and Recovery (MSCR) of Asphalt Binder Using a Dynamic Shear Rheometer. *Annual Book of American Society for Testing Materials Standards*.

Available at: https://doi.org/10.1520/D7405-10A.2

Baumgaertel, M. and Winter, H.H. (1992). Interrelation between continious and discrete time spectra. *J. Nonnewton. Fluid Mech.*, vol. 44, pp. 15–36.

Bredenhann, S.J., Myburgh, P.A., Jenkins, K.J., O'Connell, J.S., Rowe, G.M. and D'Angelo, J. (2019). Implementation of a performance-grade bitumen specification in South Africa. *J. South African Inst. Civ. Eng.*, vol. 61, no. 3, pp. 20–31. ISSN 23098775.

Butt, H.J. (2011). *Controlling the flow of suspensions*, vol. 331. ISBN 0953803201.

Christensen, D. and Anderson, D. (1992). Chemical-physical property relationships for asphalt cements and the dispersed polar fluid model. *Washington, DC*, vol. 37, no. 3, pp. 1279–1291.

Da Silva, L.S., De Camargo Forte, M.M., De Alencastro Vignol, L.D. and Cardozo, N.S.M. (2004). Study of rheological properties of pure and polymer-modified Brazilian asphalt binders. *J. Mater. Sci.*, vol. 39, no. 2, pp. 539–546. ISSN 00222461.

Gerber, A.K.J. (2016). Numerical modelling of performance and failure criteria for surfacing seals. , no. March.

Gierhart, D. (2011). Simple talking points for sharing why your state should be implementing mscr. In: *Southeastern Asphalt User-Producer Group (SEAUPG) Web Meeting*.

Glover, C.J., Davison, R.R., Domke, C.H., Ruan, Y., Juristyarini, P., Knorr, D.B. and Jung, S.H. (2005). Development of a New Method for Assessing Asphalt Binder Durability with Field Validation. vol. 7, no. 2, pp. 1–334.

Hiber, C. and Chiang, H. (1992). *Shear-rate-dependence modelling of polymer melt viscosity*. 2nd edn. Polymer Engineering and Science.

Hunter, R.N., Self, A., Read, J. and Hobson, E. (2015). *The shell bitumen handbook*. ICE Publishing London, UK:.

Macosko, C.W. (1996). *Rheology: Principles, Measurements and Applications*, vol. 86. ISBN 1560815795.

Mainardi, F. and Spada, G. (2011). Creep, relaxation and viscosity properties for basic fractional models in rheology. `1110.3400`.

Marateanu, M. and Anderson, D. (1996). Time-temperature dependency of asphalt binders–an improved model (with discussion). *Journal of the Association of Asphalt Paving Technologists*, vol. 65.

Mensching, D.J., Rowe, G.M., Daniel, J.S. and Bennert, T. (2015). Exploring low-temperature performance in black space. *Road Materials and Pavement Design*, vol. 16, no. sup2, pp. 230–253.

Migliori, F., Ramond, G., Ballie, M., Brule, B., Exmelin, C., Lombardi, B., Samanos, J., Maia, A., Such, C. and Watkins, S. (1999). Correlations between the thermal stress cracking of bituminous mixes and their binders' rheological characteristics. In: *Eurobitume Workshop on Performance Related Properties for Bituminous Binders", Luxemburg*, pp. 3–6.

Mturi, G., O'Connell, J.O. and Zoorob, S.E. (2011). Investigating the Rheological Characters of South African Road Bitumens. *10th Conf. Asph. Pavements South. Africa*, pp. 149–187.

Nicholls, C. (2005). BitVal - Analysis of Available Data for Validation of Bitumen Tests. *Rep. Phase 1 BiTVal Proj.*

O'Connell, J., Mturi, G. and Zoorob, S. (2015). A review of the development of the non-recoverable compliance, jnr, for use in south africa. In: *Proceedings of the 11th Conference on Asphalt Pavements for southern Africa (CAPSA). Rustenburg*.

Pavement Interactive (2012). Rolling thin film oven test.
Available at: `https://pavementinteractive.org/reference-desk/testing/binder-tests/rolling-thin-film-oven/`

Read, J. and Whiteoak, D. (2014). *The Shell bitumen handbook*. ISBN 072773220X.
Available at: `http://books.google.com/books?id=bA1tIkRJL8kC{&}pgis=1`

Rowe, G. (2009). Phase angle determination and interrelationships within bituminous materials. *Adv. Test. Charact. Bitum. Mater.*, , no. 1, pp. 43–52.

Rowe, G.M., King, G. and Anderson, M. (2014). The influence of binder rheology on the cracking of asphalt mixes in airport and highway projects. *J. Test. Eval.*, vol. 42, no. 5. ISSN 00903973.

Rowe, G.M. and Sharrock, M.J. (2011). Alternate shift factor relationship for describing temperature dependency of viscoelastic behavior of asphalt materials. *Transp. Res. Rec.*, , no. 2207, pp. 125–135. ISSN 03611981.

SABITA (2017). Sabita Technical Guideline : The introduction of a performance grade specification for bituminous binders. , no. Version 2.

Shaw, M.T. and MacKnight, W.J. (2005). *Introduction to polymer viscoelasticity*, vol. 43. 3rd edn. ISBN 0471740454.

TG 1 (2015). *The Use Of Modified Bituminous Binder In Road Construction*. July. ISBN 9781874968672.

TRH3 (2007). Design and Construction of Surfacing Seals. Pretoria: South African National Roads Agency. , no. May, p. 267.

Van Zyl, G. and Jenkins, K. (). Overview of Long Term Seal Performance. *Conf. Asph. Pavements South. Africa*, , no. August 2015, pp. 1–13.

Viljoen, A. (2001). Estimating asphalt temperatures from air temperatures and basic sky parameters. *CSIR Transportek, Pretoria*.

Von Benecke, T.C. (2021). Influence of Seal Binders and Rheology on Aggregate Orientation and Embedment Leading to Texture Loss. , no. December.

Wang, M., Li, R., Wen, Y., Pei, J., Xing, X. and Chen, Z. (2019). Rheological and aging behaviors of liquid rubber modified asphalt binders. *Construction and Building Materials*, vol. 227, p. 116719.

Widyatmoko, I., Heslop, M. and Elliott, R. (2005). Viscous to Elastic Transition Temperature and the In Situ Performance of Bituminous and Asphaltic Materials. *J. Inst. Asph. Technol.*, vol. 14, no. May, p. 7.

Yusoff, N.I., Chailleux, E. and Airey, G.D. (2011*a*). A Comparative Study of the Influence of Shift Factor Equations on Master Curve Construction. vol. 4, no. 6, pp. 324–336.

Yusoff, N.I.M., Jakarni, F.M., Nguyen, V.H., Hainin, M.R. and Airey, G.D. (2013). Modelling the rheological properties of bituminous binders using mathematical equations. *Constr. Build. Mater.*, vol. 40, pp. 174–188. ISSN 09500618.
Available at: `http://dx.doi.org/10.1016/j.conbuildmat.2012.09.105`

Yusoff, N.I.M., Shaw, M.T. and Airey, G.D. (2011*b*). Modelling the linear viscoelastic rheological properties of bituminous binders.

Appendices

PEN 70/100 Original

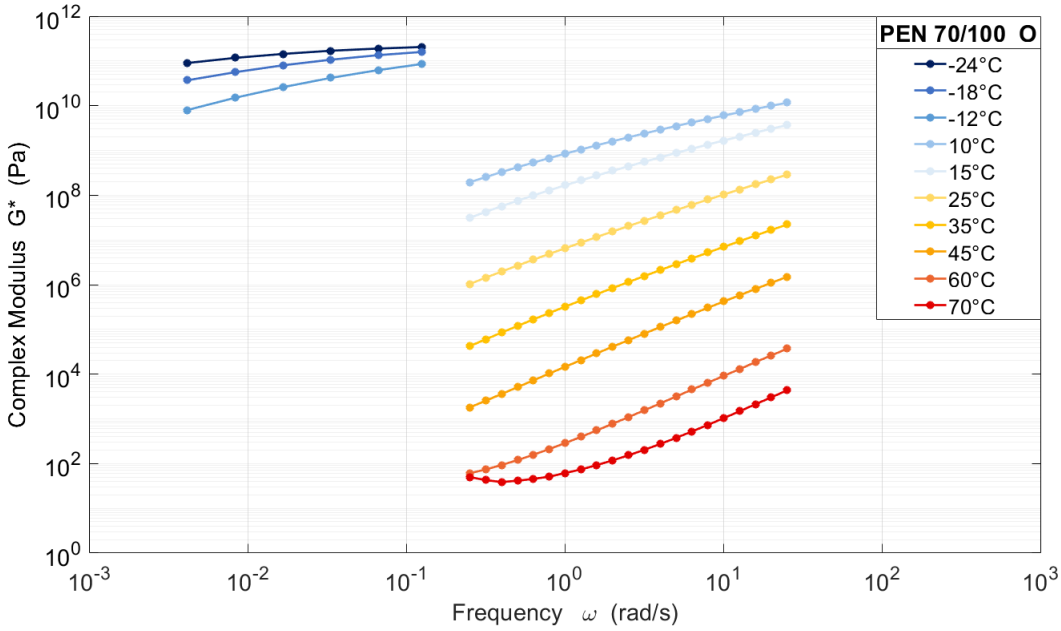

Figure 1: G* vs ω isotherms of the PEN 70/100 Original (unaged)

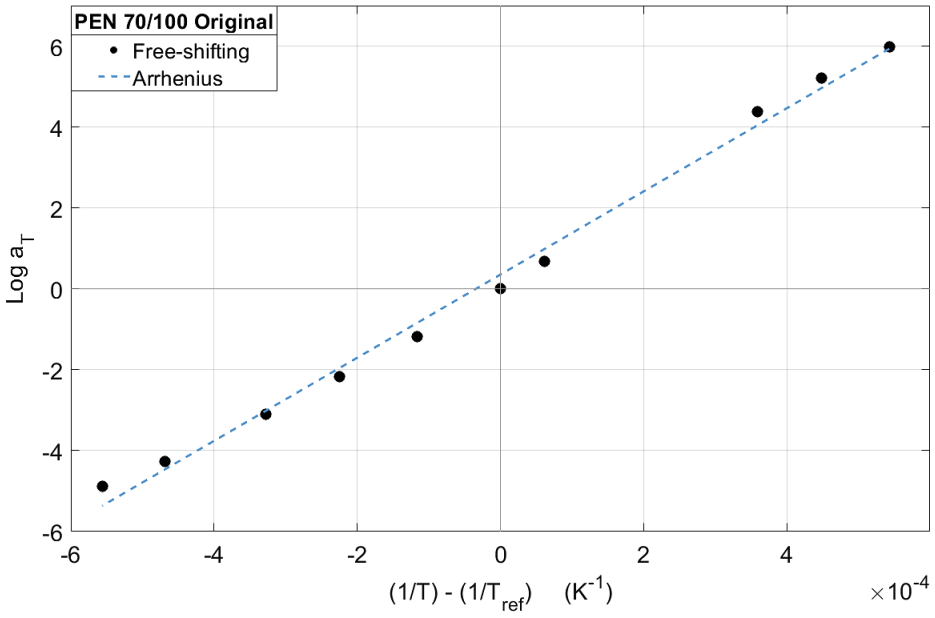

Figure 2: Arrhenius shift factor of the PEN 70/100 Original (unaged)

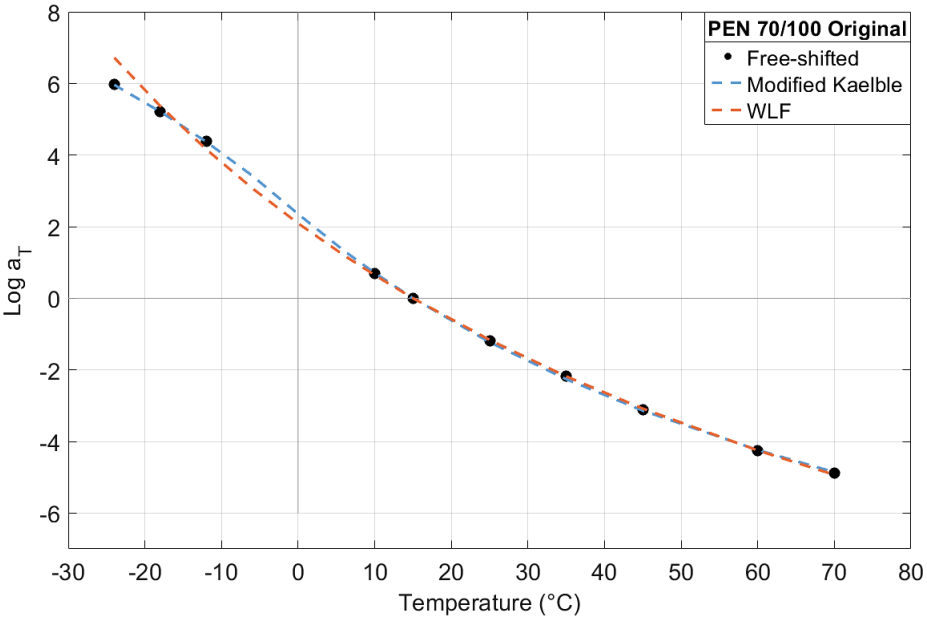

Figure 3: WLF and Modified Kaelble shift factors of the PEN 70/100 Original (unaged)

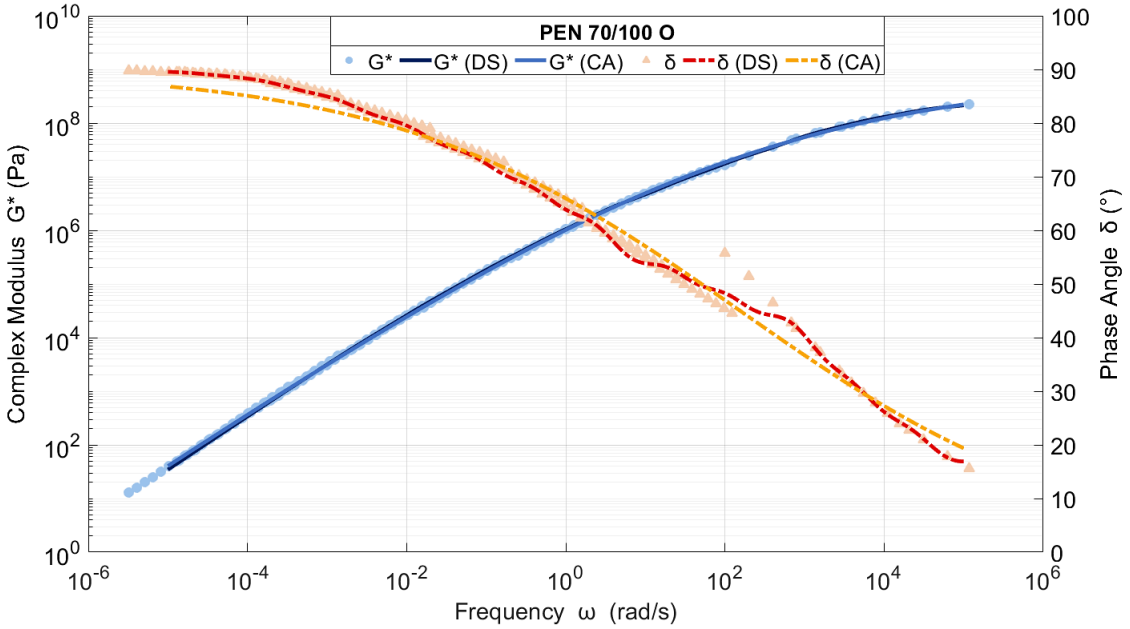

Figure 4: Master Curve with the CA and DS models of the PEN 70/100 Original (unaged)

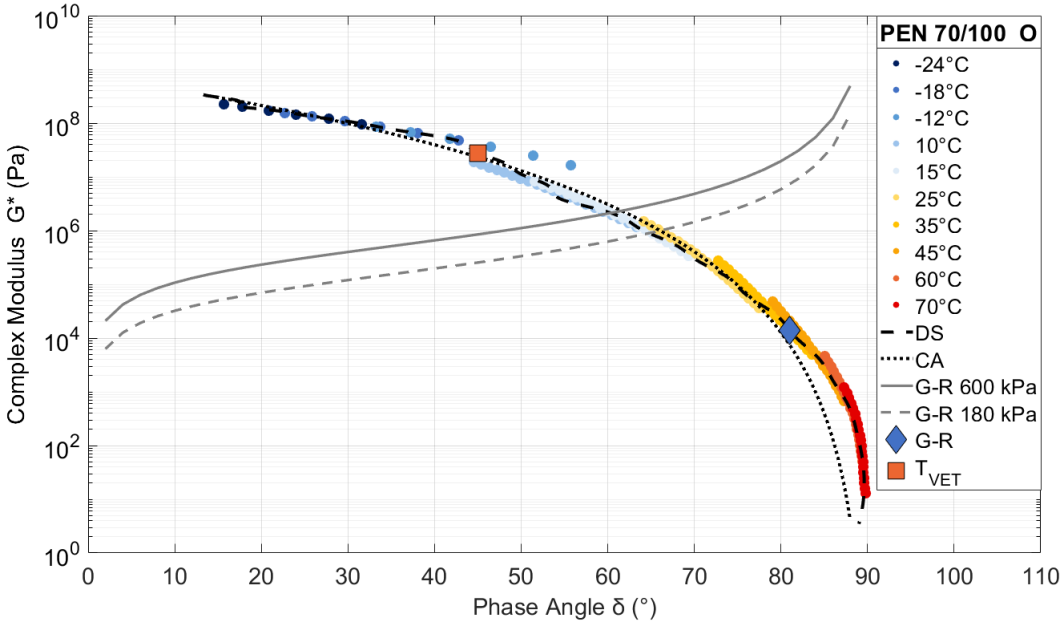

Figure 5: Black Space with the CA and DS models and durability parameters of the PEN 70/100 Original (unaged)

PEN 70/100 Aged

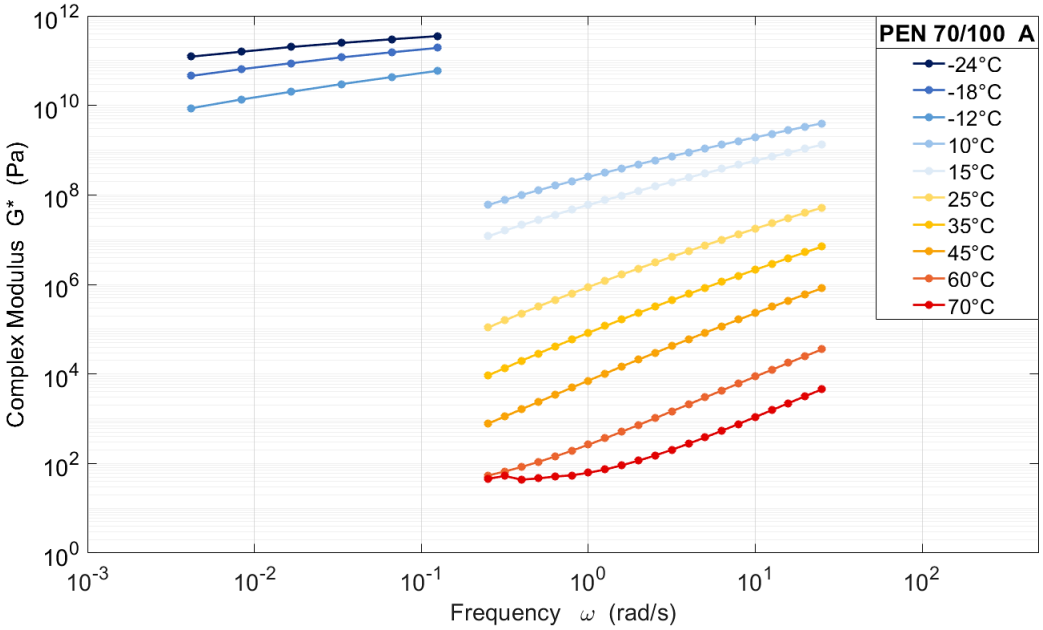

Figure 6: G* vs ω isotherms of the PEN 70/100 Aged

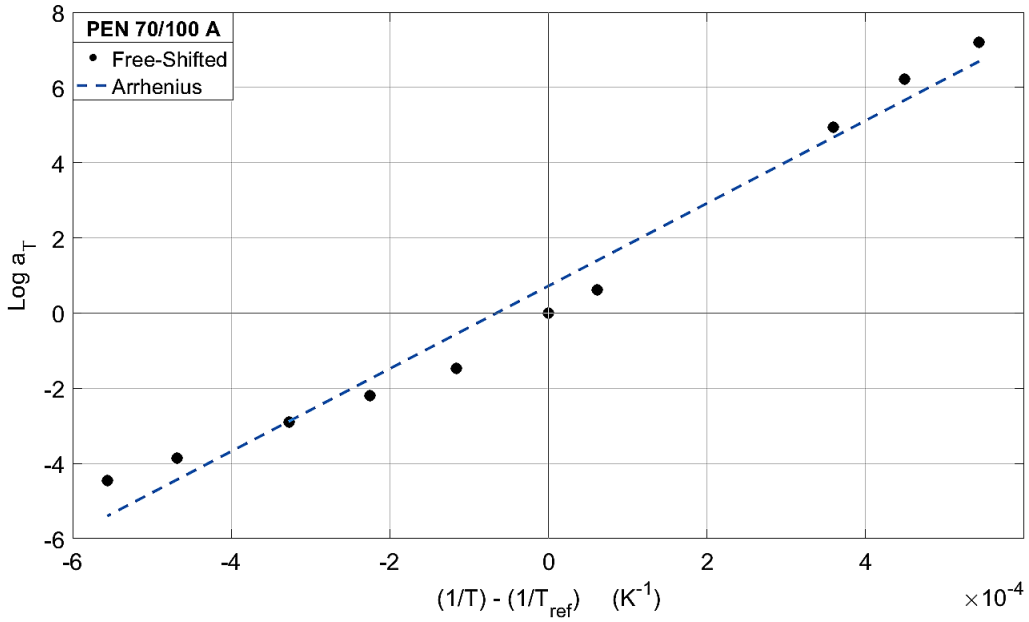

Figure 7: Arrhenius shift factor of the PEN 70/100 Aged

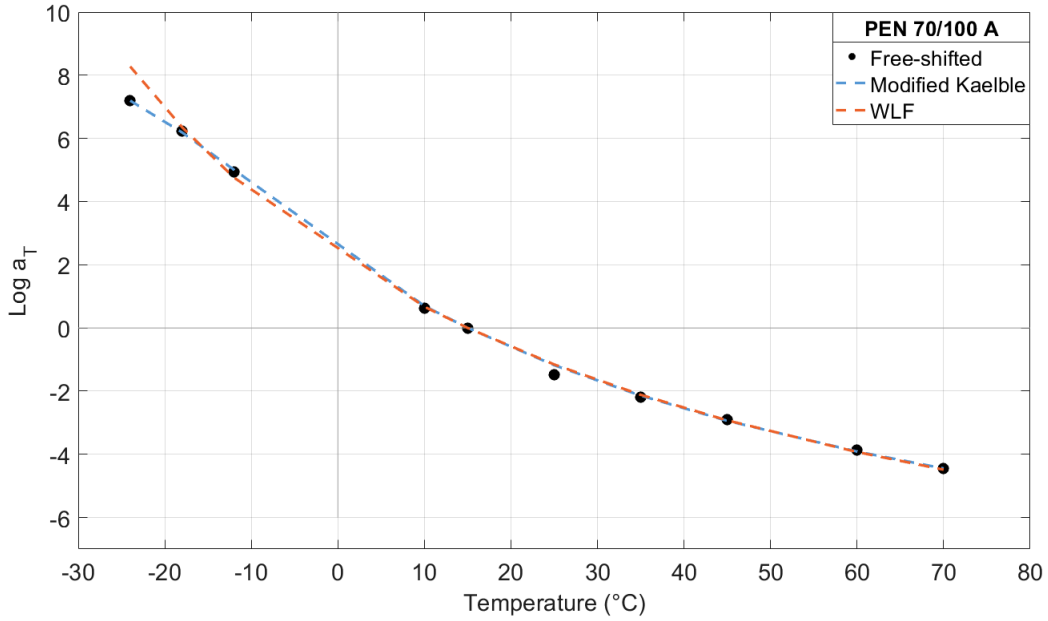

Figure 8: WLF and Modified Kaelble shaft factors of the PEN 70/100 Aged

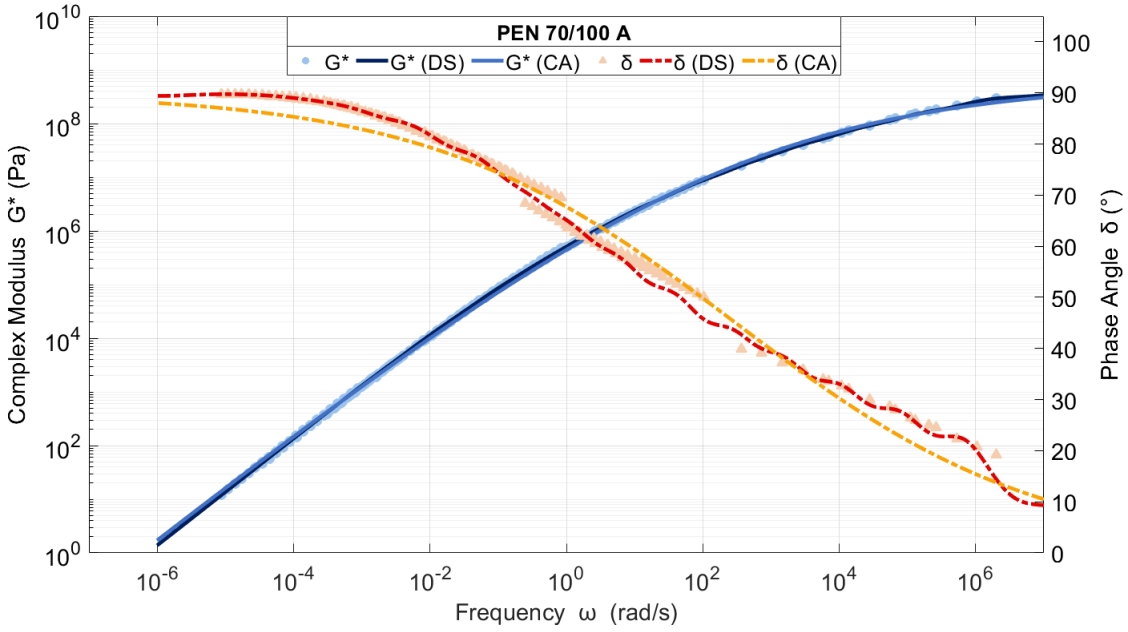

Figure 9: Master Curve with the CA and DS models of the PEN 70/100 Aged

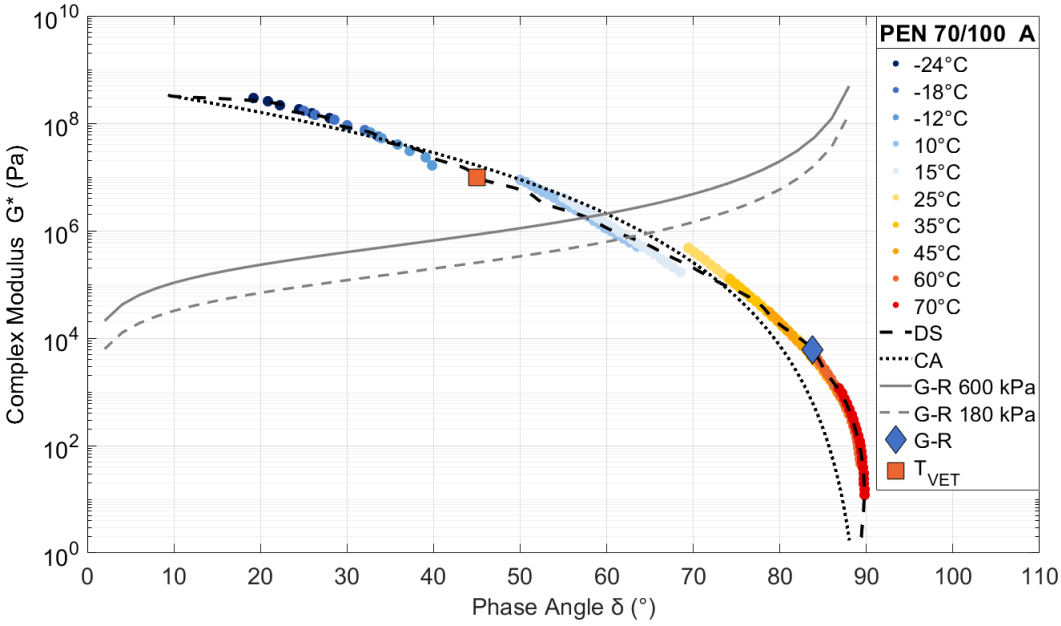

Figure 10: Black Space with the CA and DS models of the PEN 70/100 Aged

S-E1 Original

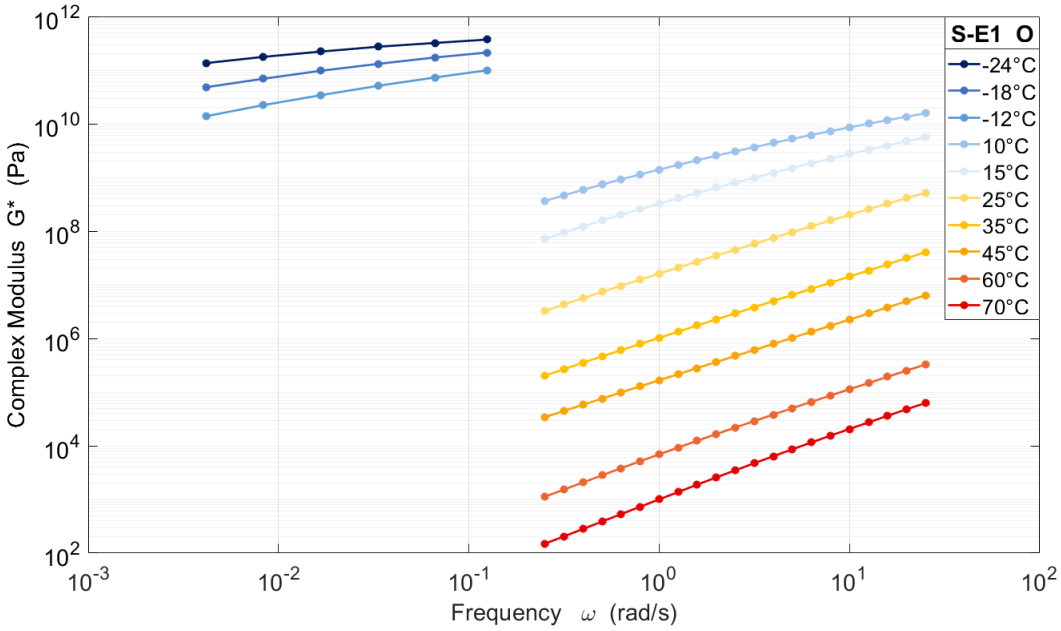

Figure 11: G* vs ω isotherms of the S-E1 Original (unaged)

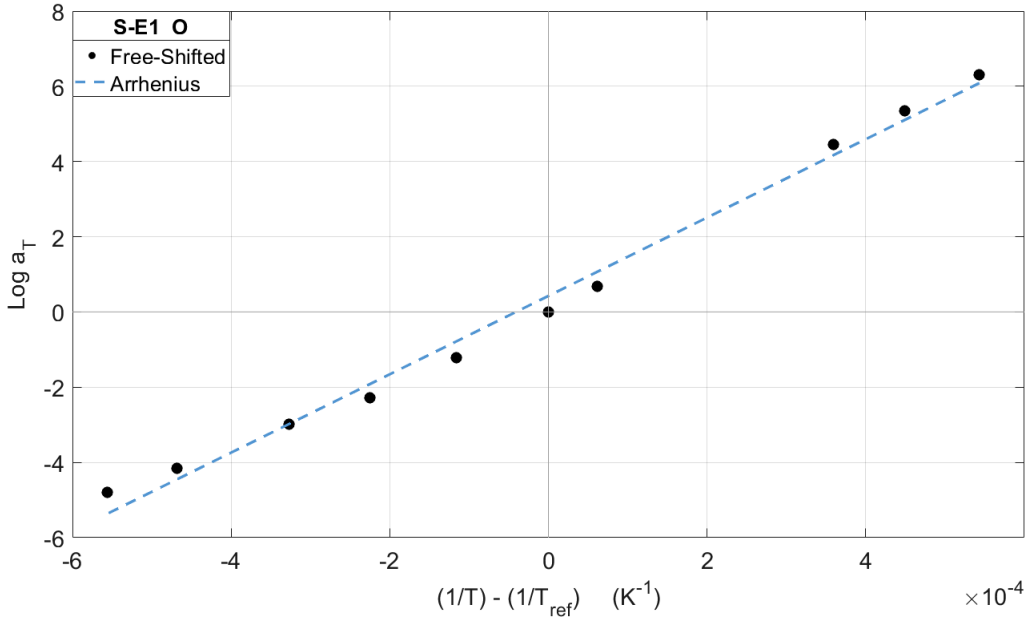

Figure 12: Arrhenius shift factor of the S-E1 Original (unaged)

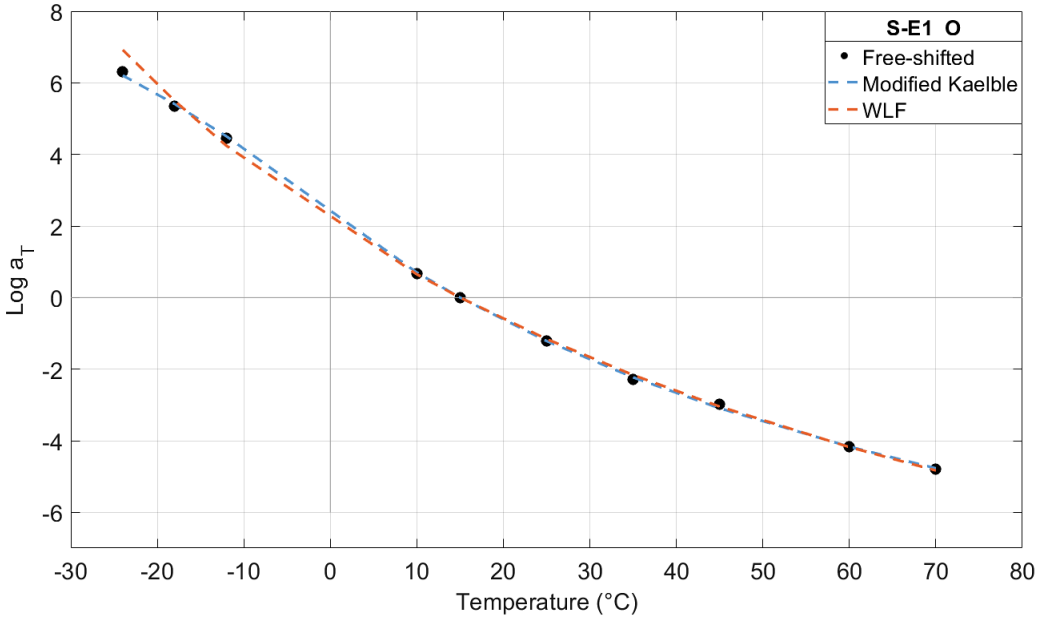

Figure 13: WLF and Modified Kaelble shift factors of the S-E1 Original (unaged)

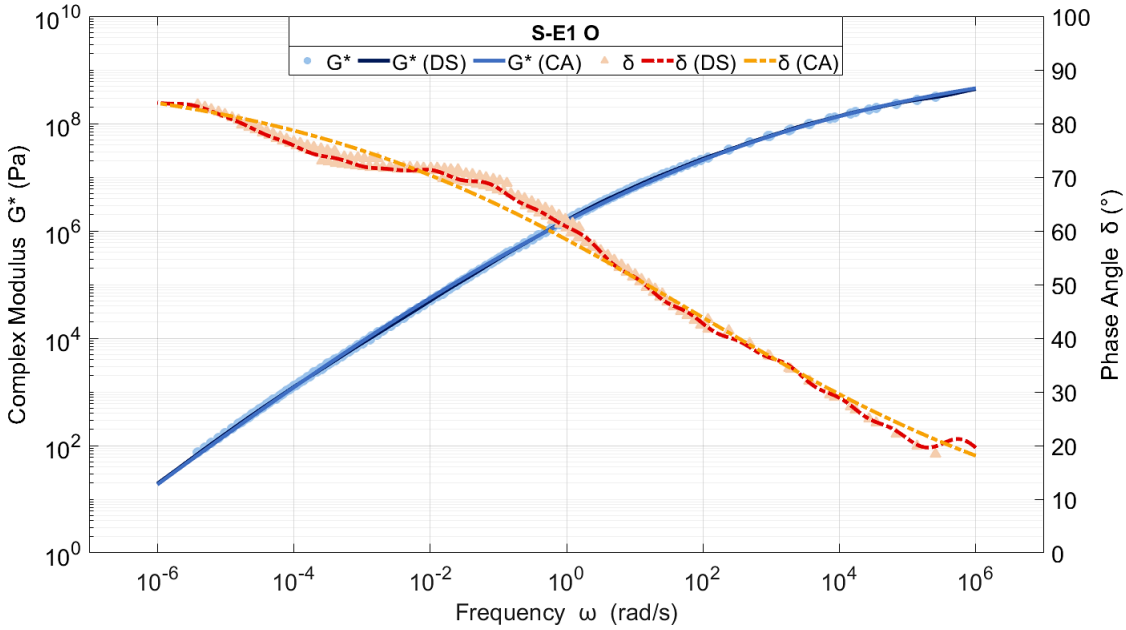

Figure 14: Master Curve with the CA and DS models of the S-E1 Original (unaged)

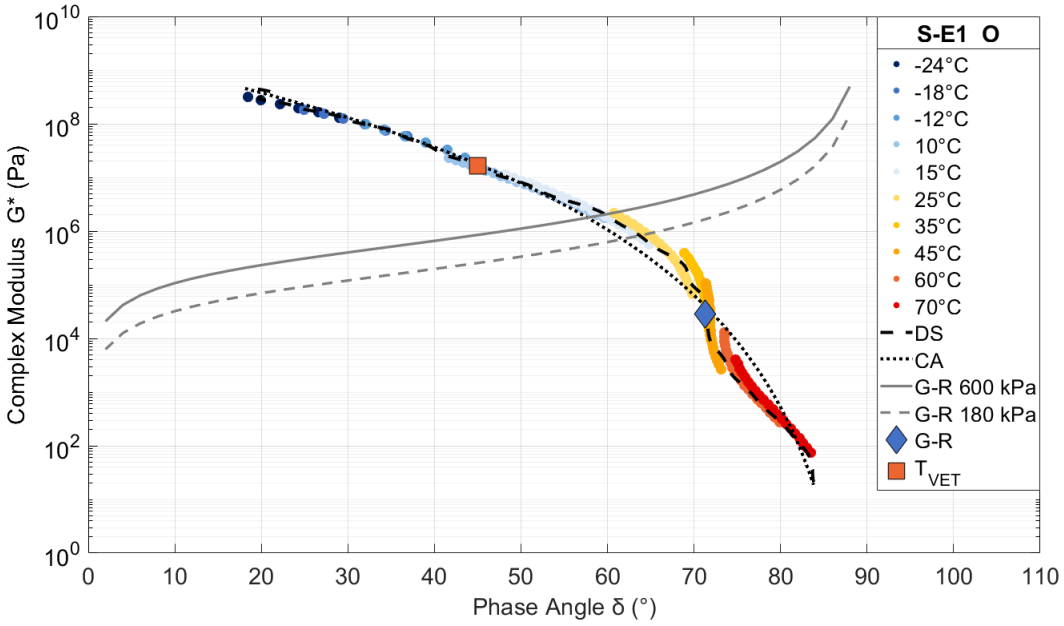

Figure 15: Black Space with the CA and DS model of the S-E1 Original (unaged)

S-E1 Aged

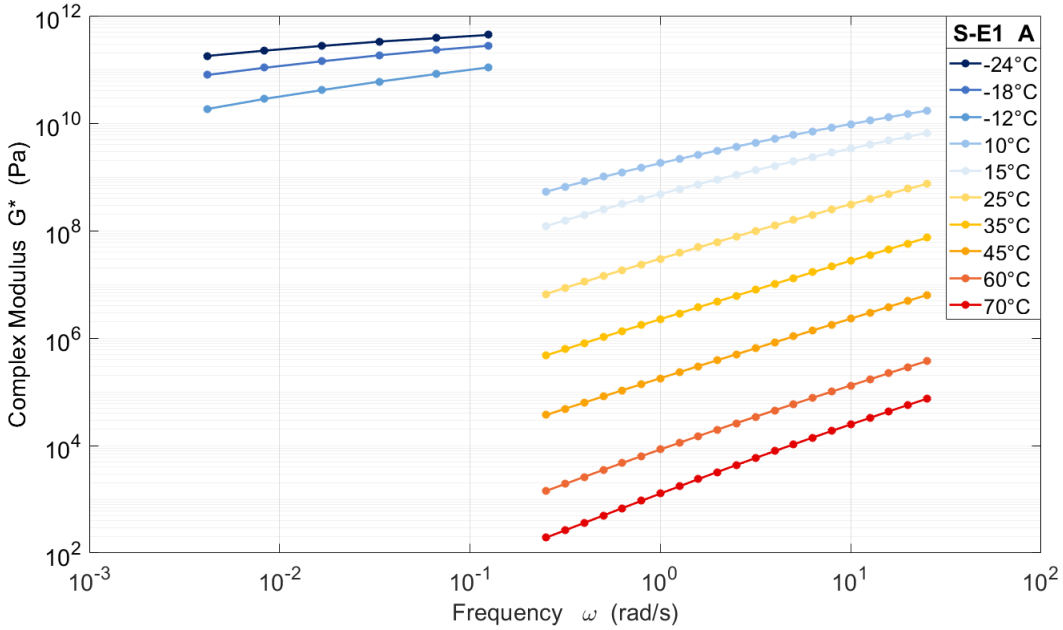

Figure 16: G* vs ω isotherms of the S-E1 Aged

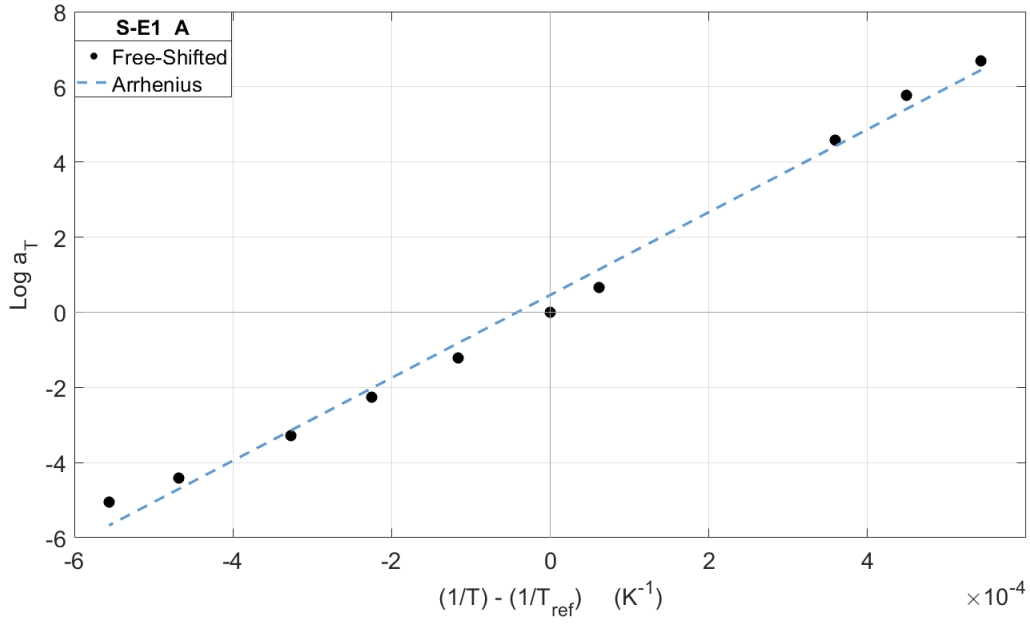

Figure 17: Arrhenius shift factor of the S-E1 Aged

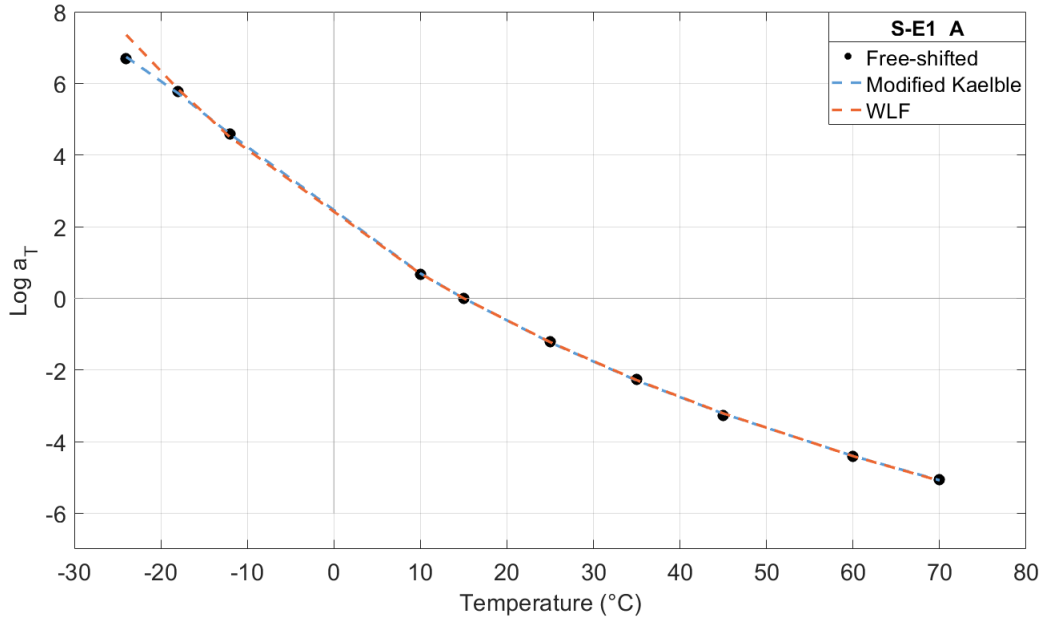

Figure 18: WLF and Modified Kaelble shift factors of the S-E1 Aged

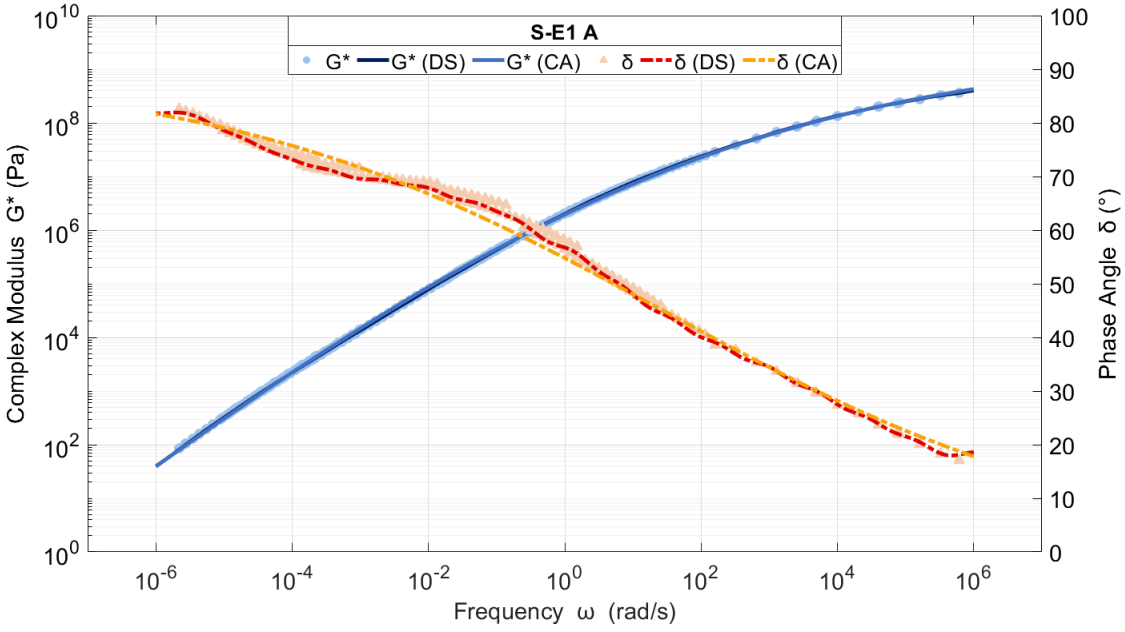

Figure 19: Master Curves with the CA and DS model of the S-E1 Aged

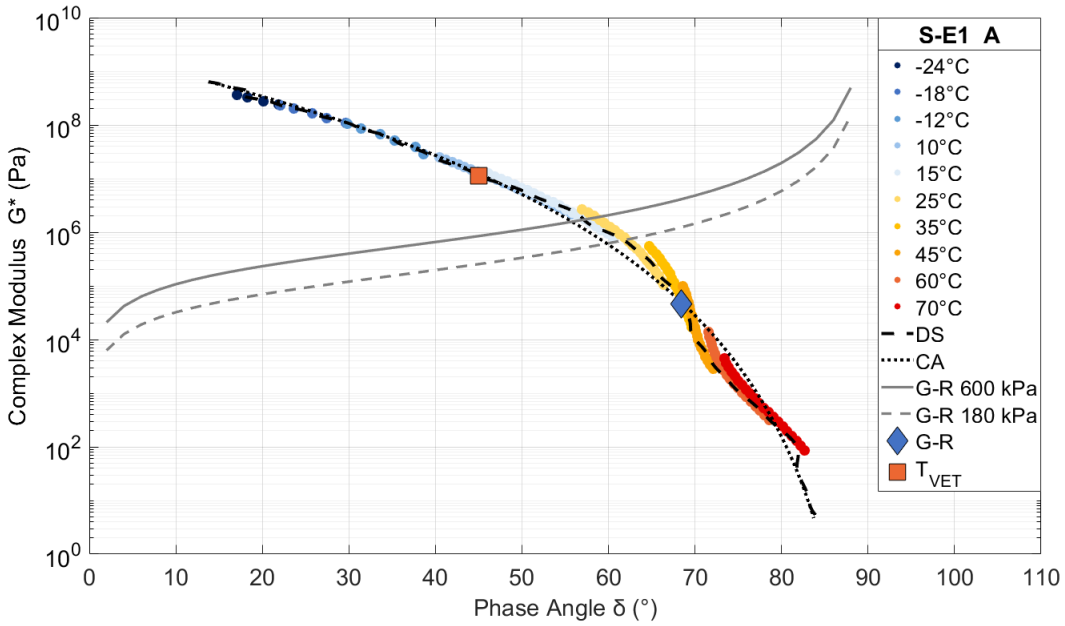

Figure 20: Black Space with the CA and DS models of the S-E1 Aged

S-E2 Original

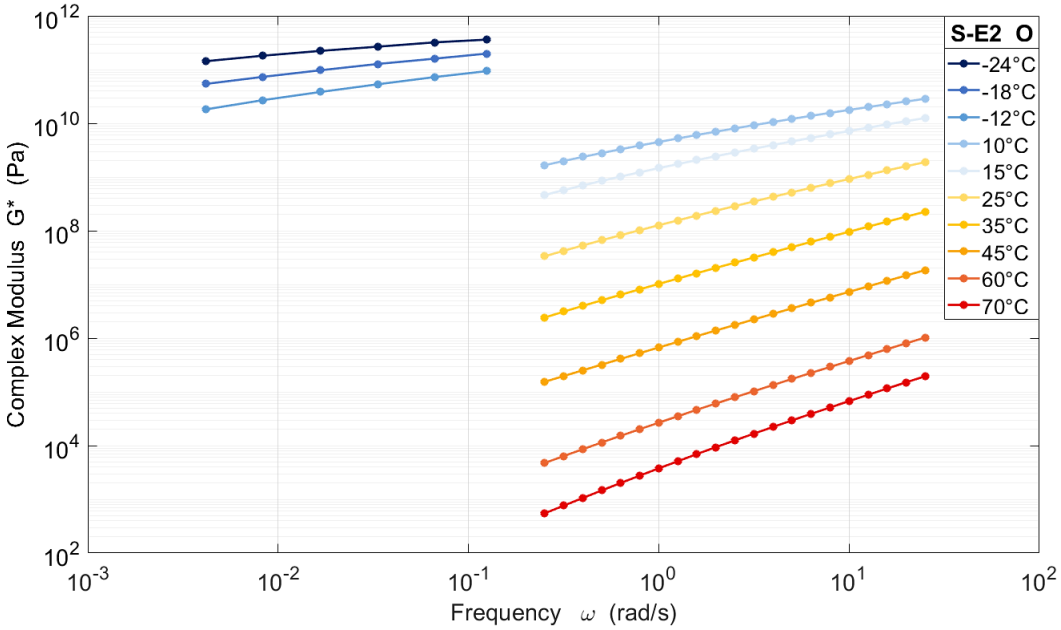

Figure 21: G* vs ω isotherms of the S-E2 Original (unaged)

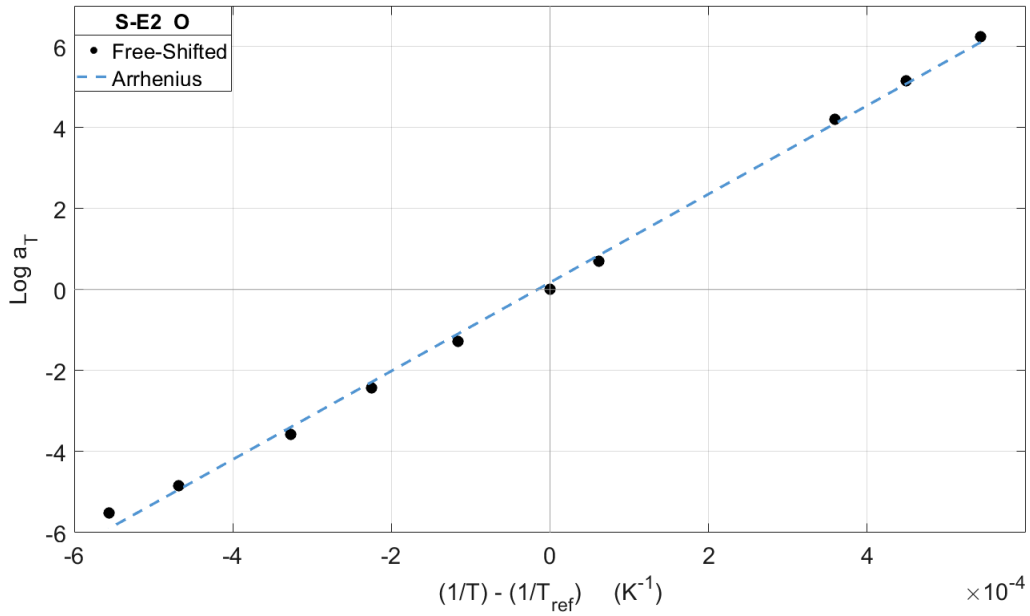

Figure 22: Arrhenius shift factor for the S-E2 Original (unaged)

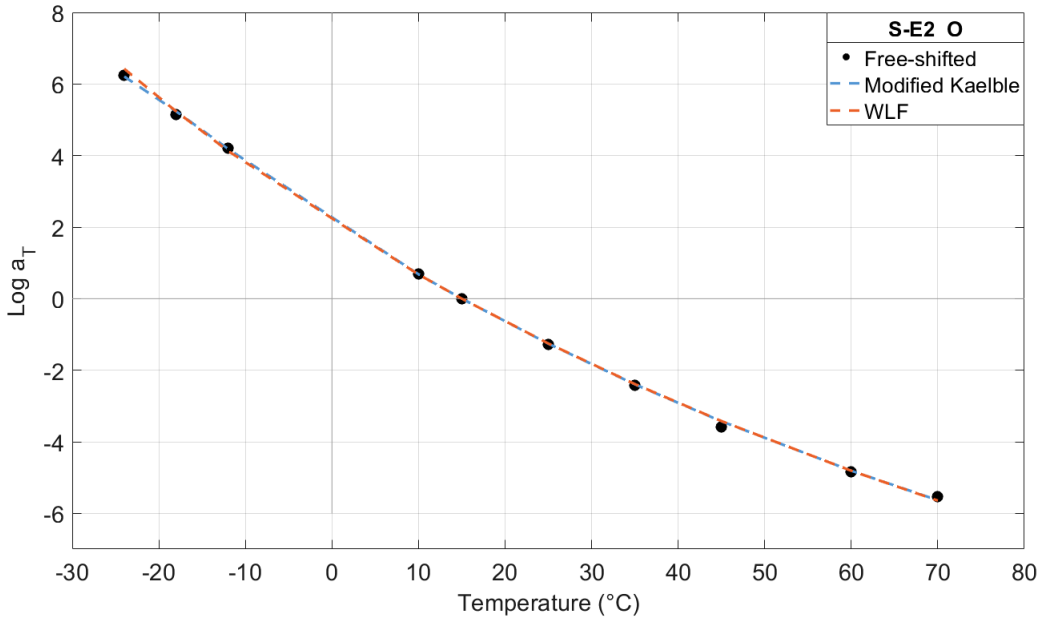

Figure 23: WLF and Modified Kaelble shift factors for the S-E2 Original (unaged)

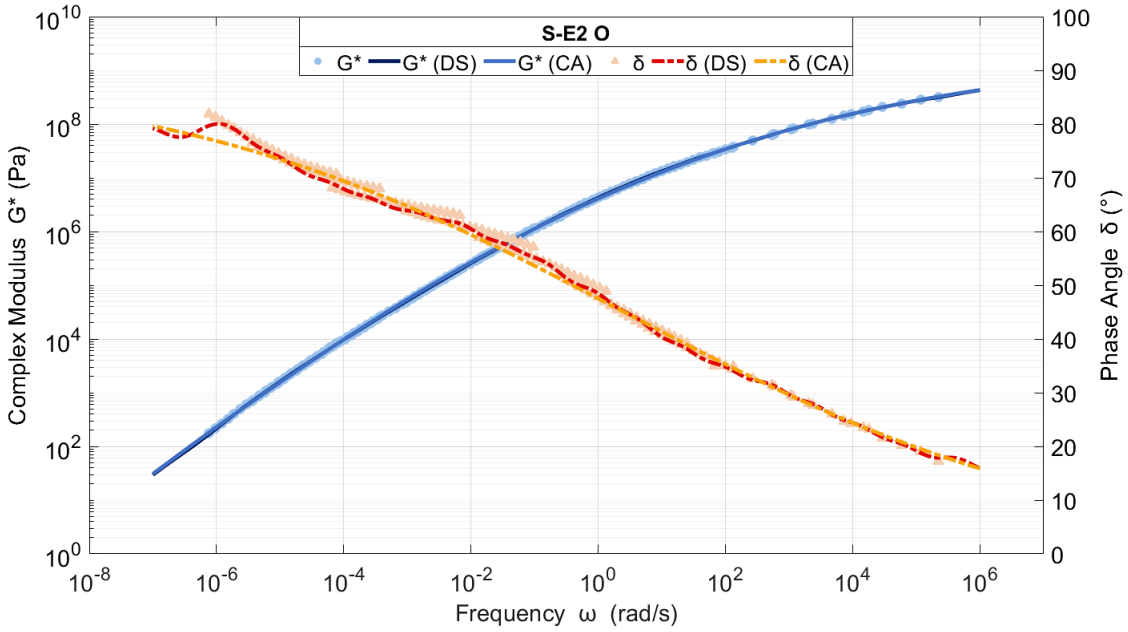

Figure 24: Master Curves with CA and DS models for the S-E2 Original (unaged)

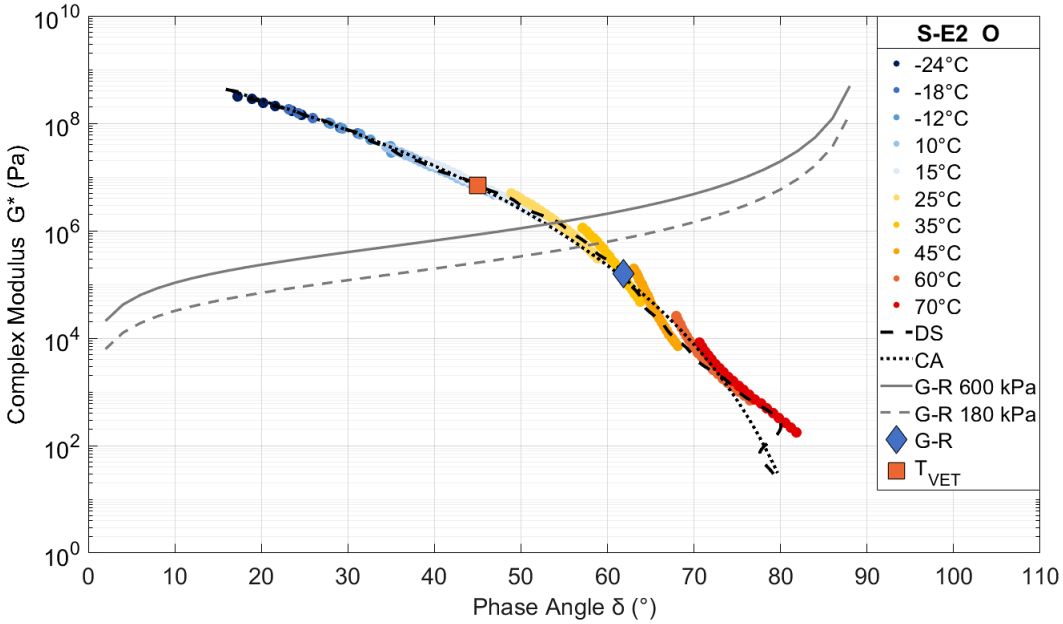

Figure 25: Black Space with the CA and DS models of the S-E2 Original (unaged)

S-E2 Aged

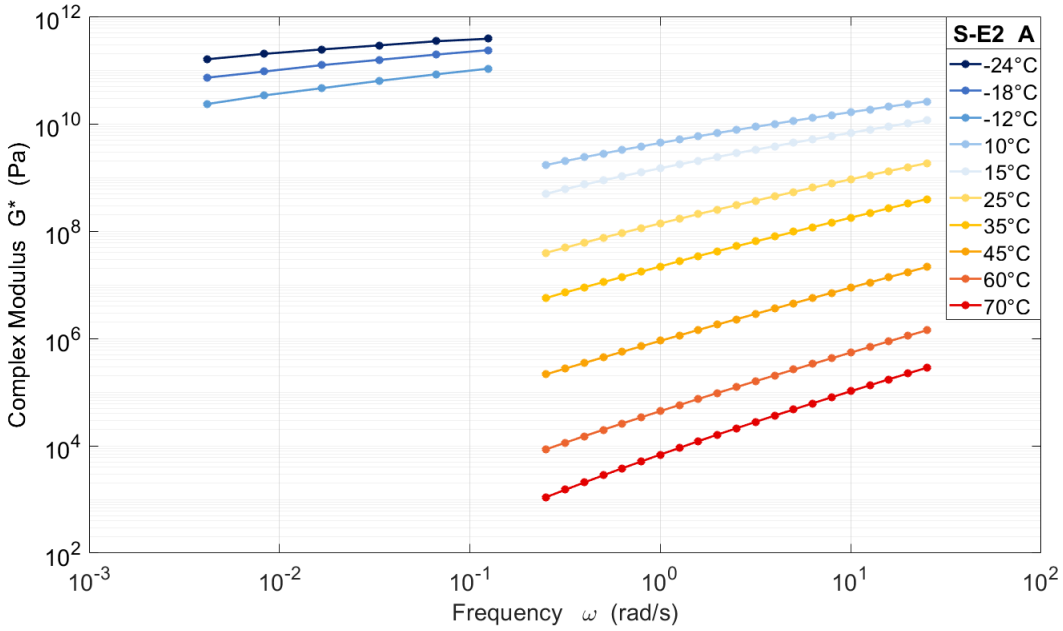

Figure 26: G* vs ω isotherms of the S-E2 Aged

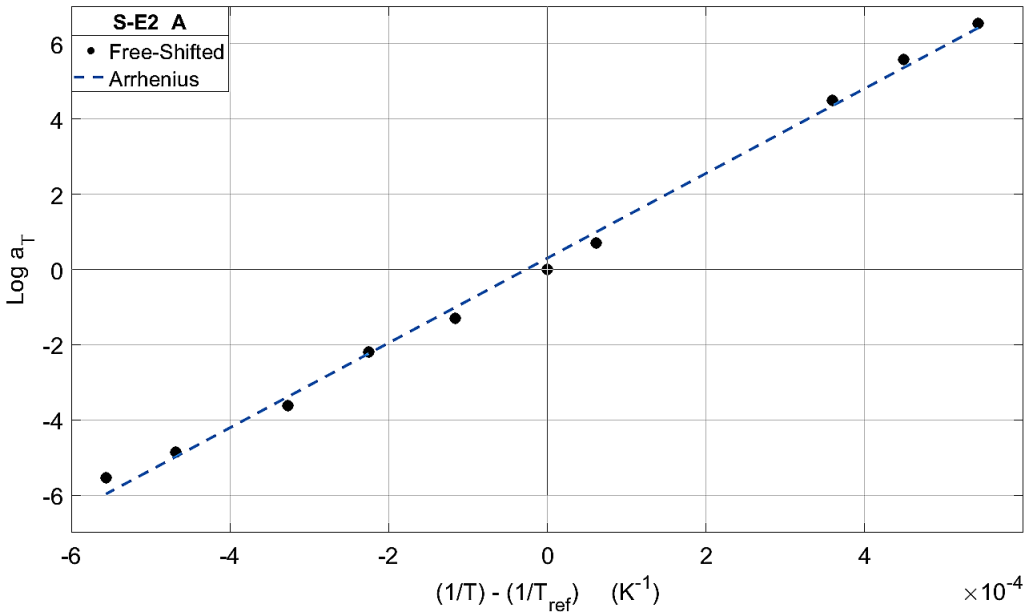

Figure 27: Arrhenius shift factor of the S-E2 Aged

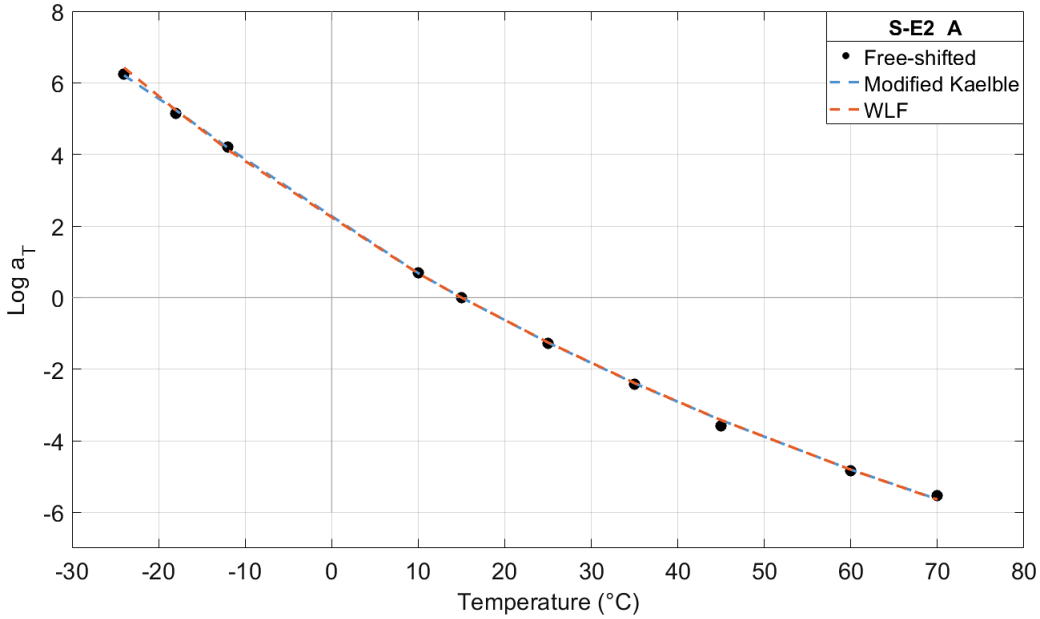

Figure 28: WLF and Modified Kaelble shift factors of the S-E2 Aged

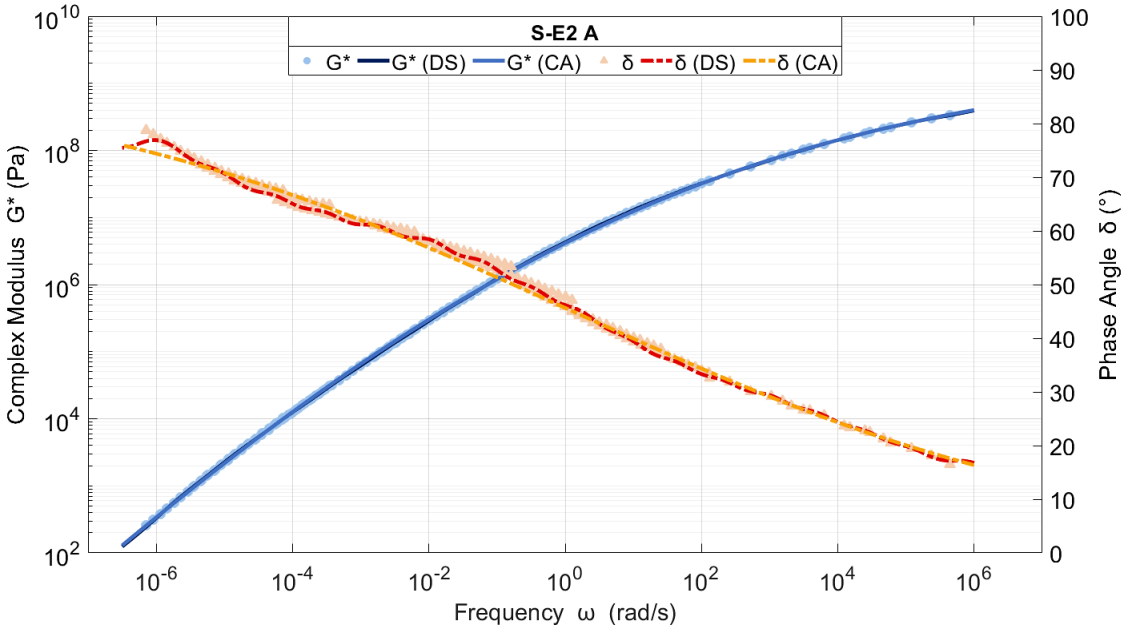

Figure 29: Master Curves with the CA and DS models for the S-E2 Aged

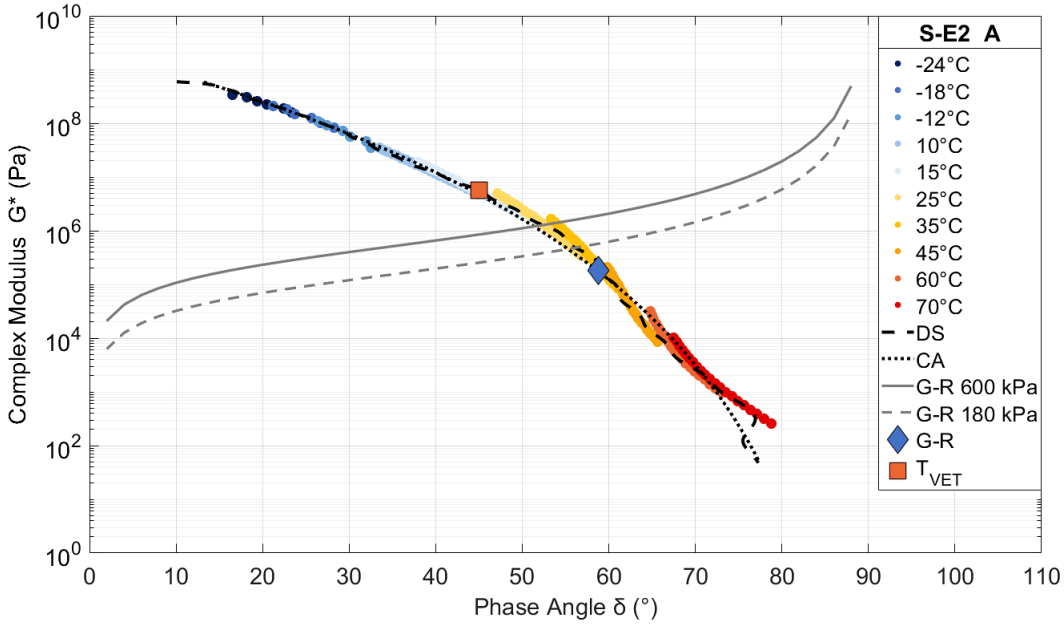

Figure 30: Black Space with the CA and DS models for the S-E2 Aged

S-R1 Original (Parallel Plate)

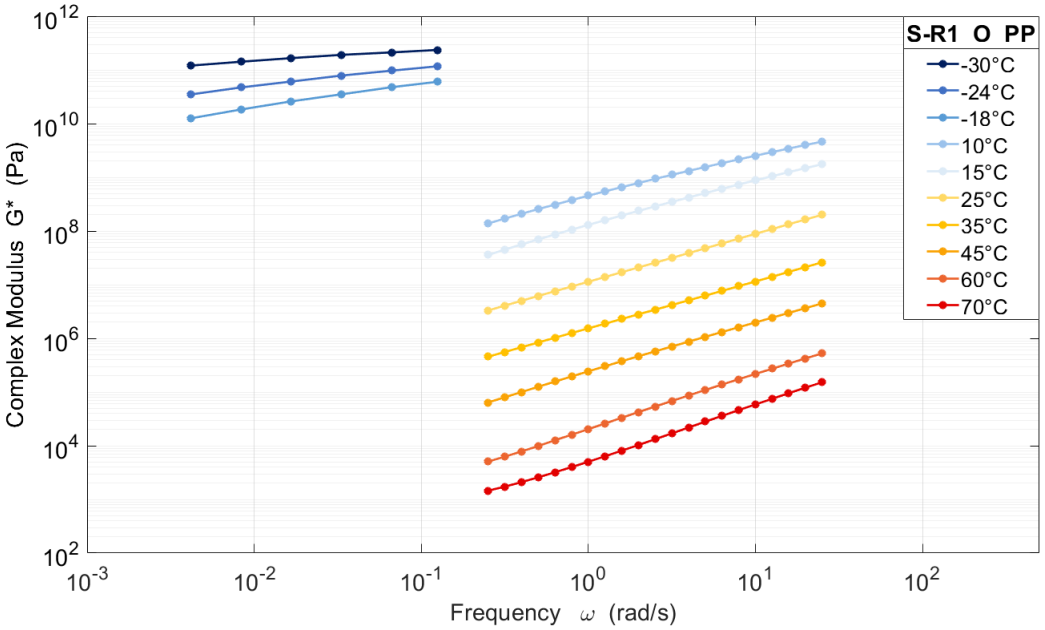

Figure 31: G* vs ω isotherms for the S-R1 Original (unaged) PP

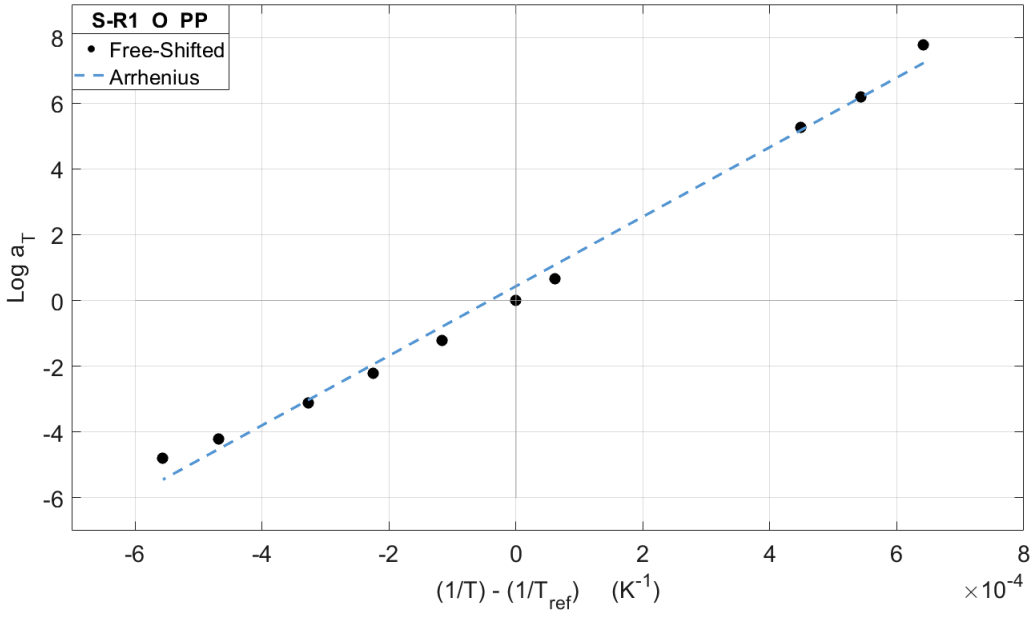

Figure 32: Arrhenius shift factor for the S-R1 Original (unaged) PP

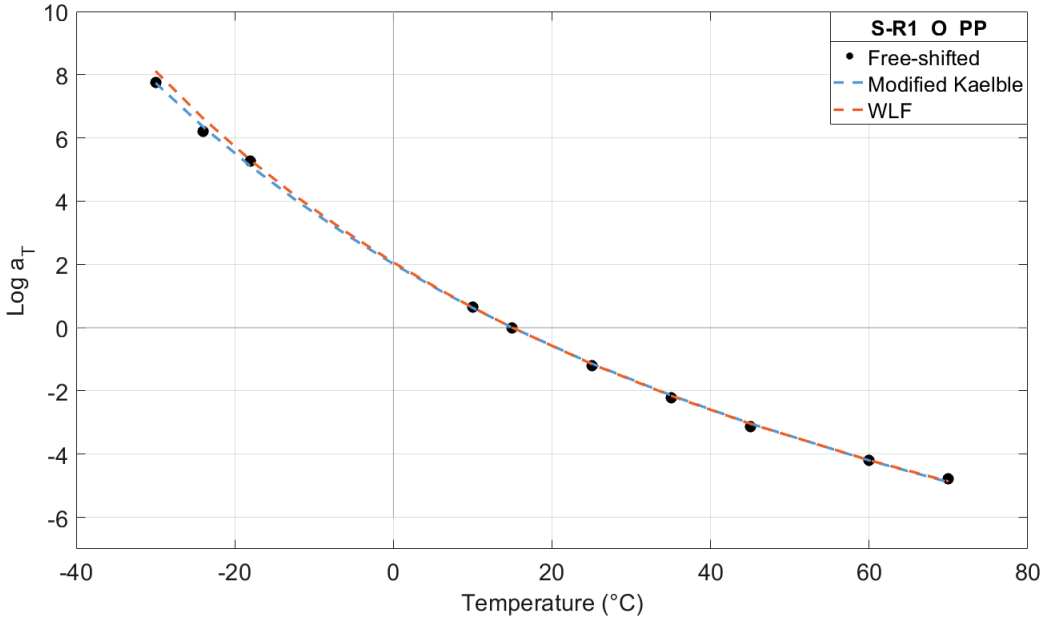

Figure 33: WLF and Modified Kaelble shift factors for the S-R1 Original (unaged) PP

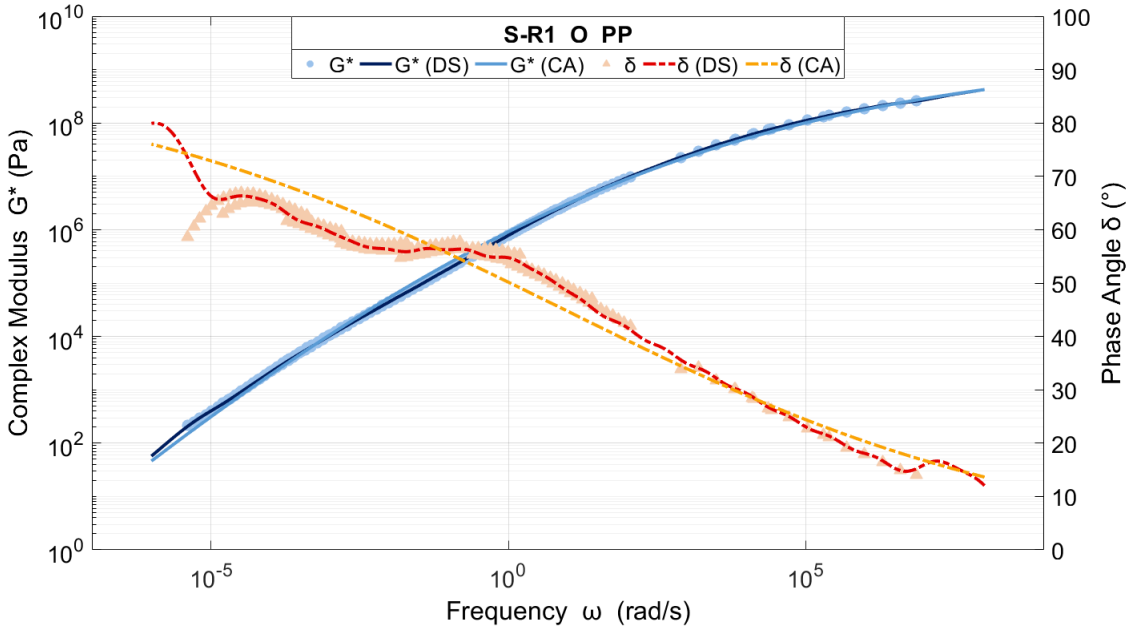

Figure 34: Master Curves with the CA and DS models for the S-R1 Original (unaged) PP

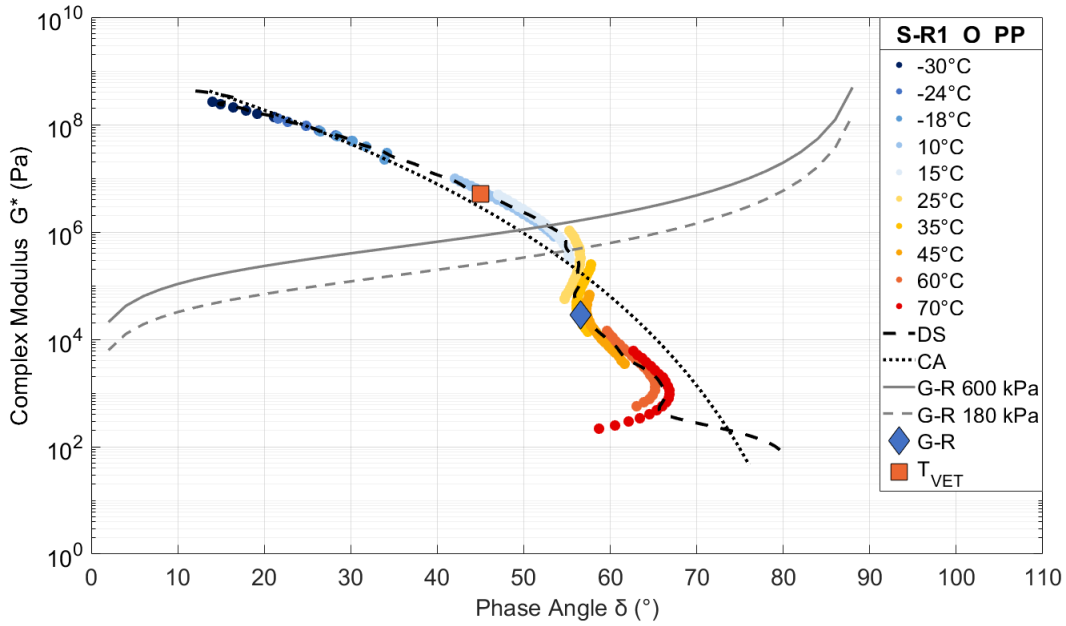

Figure 35: Black Space with the CA and DS models for the S-R1 Original (unaged) PP

S-R1 Original (Cone Plate)

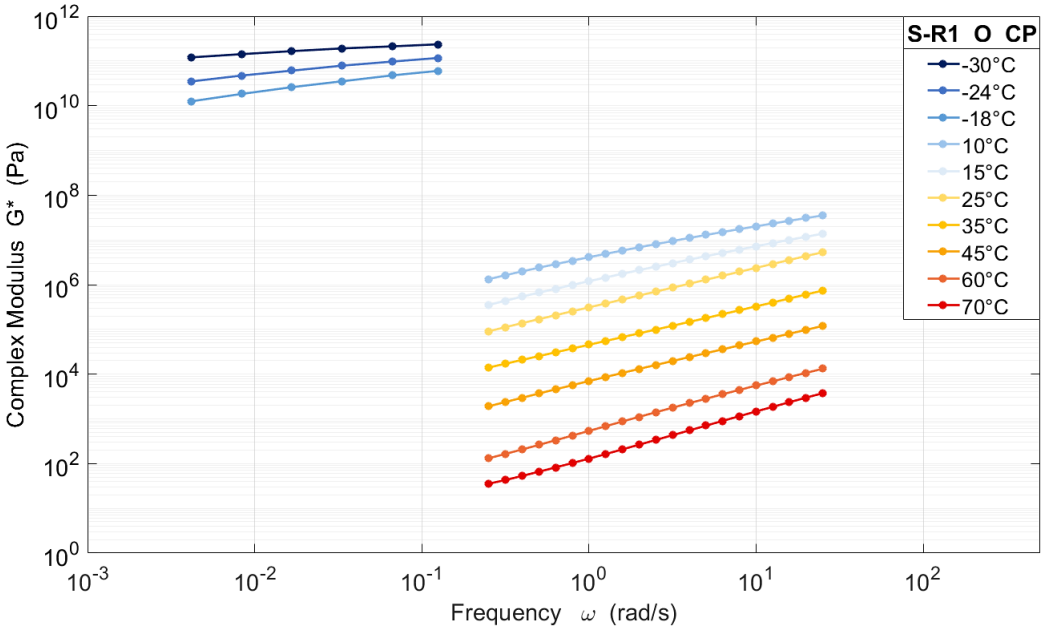

Figure 36: G* vs ω isotherms for the S-R1 Original (unaged) CP

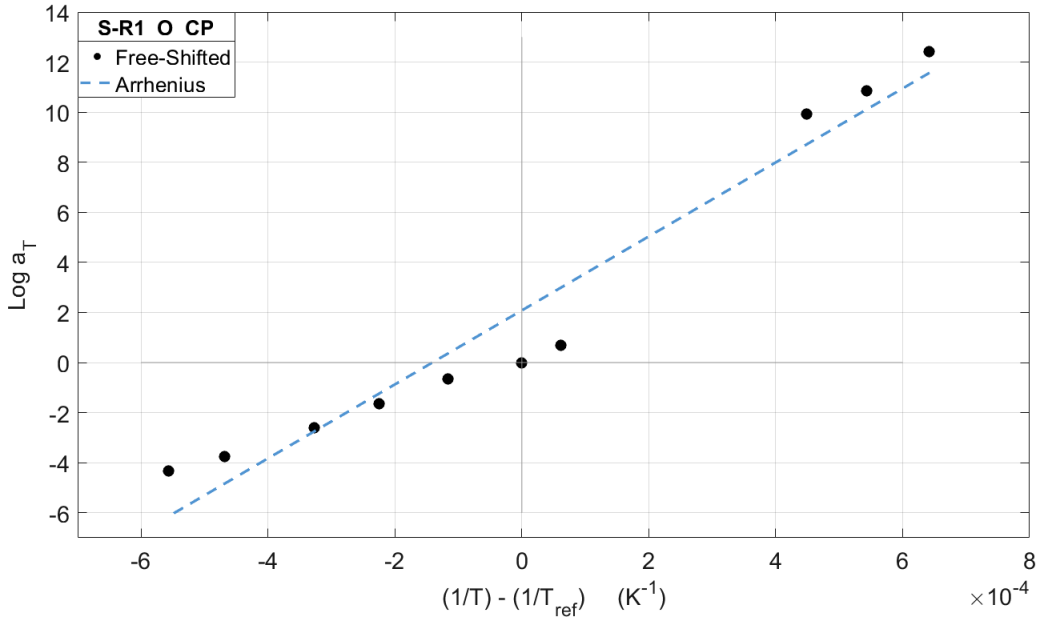

Figure 37: Arrhenius shift factor for the S-R1 Original (unaged) CP

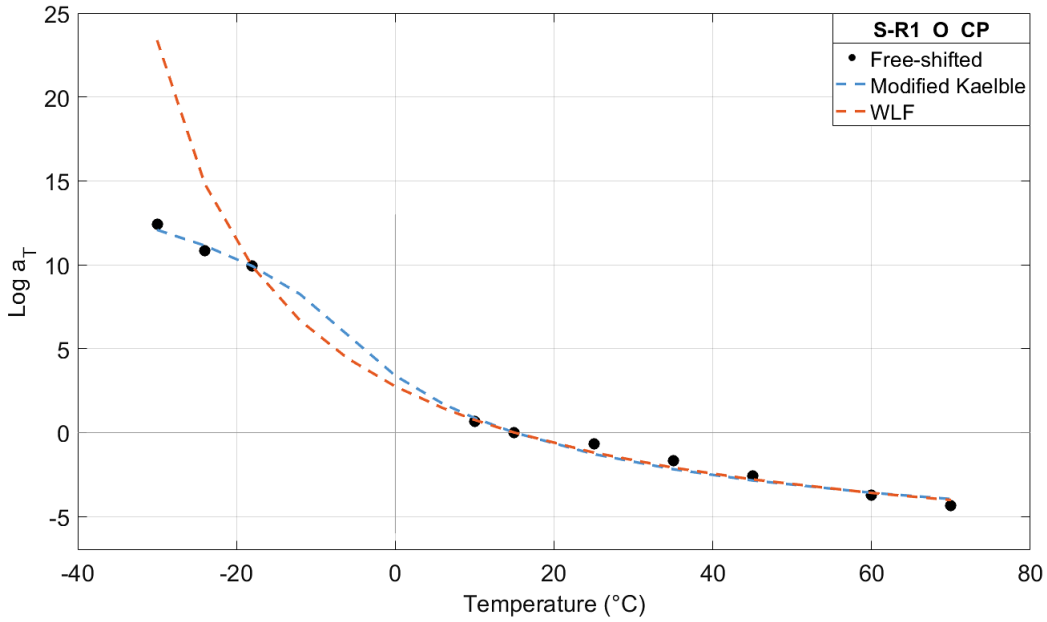

Figure 38: WLF and Modified Kaelble shift factors for the S-R1 Original (unaged) CP

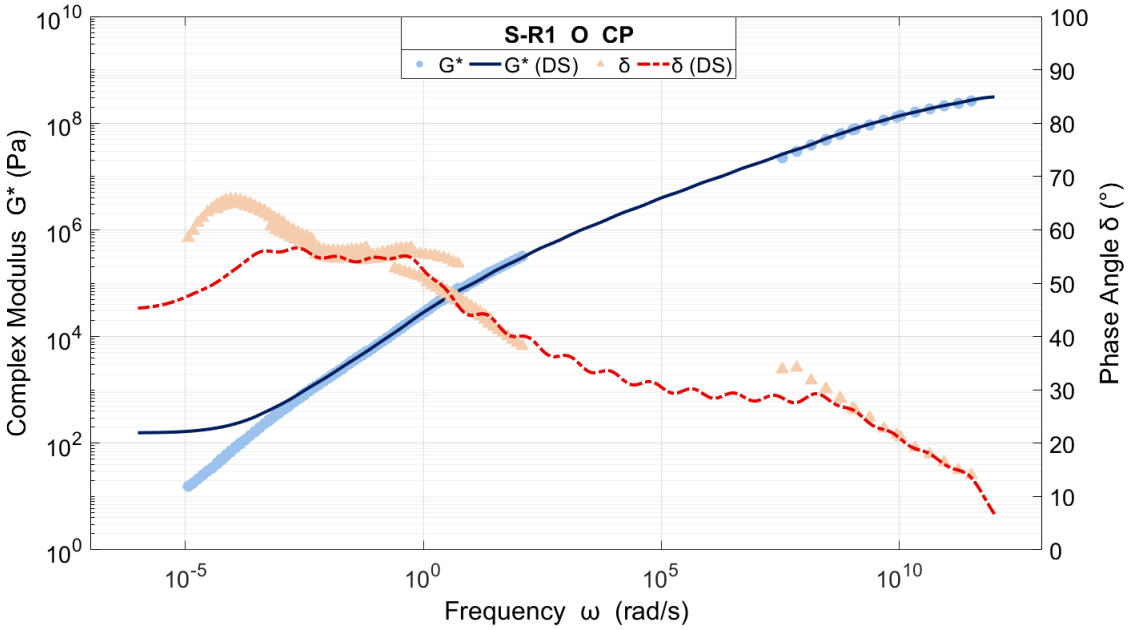

Figure 39: Master Curves with the DS model for the S-R1 Original (unaged) CP

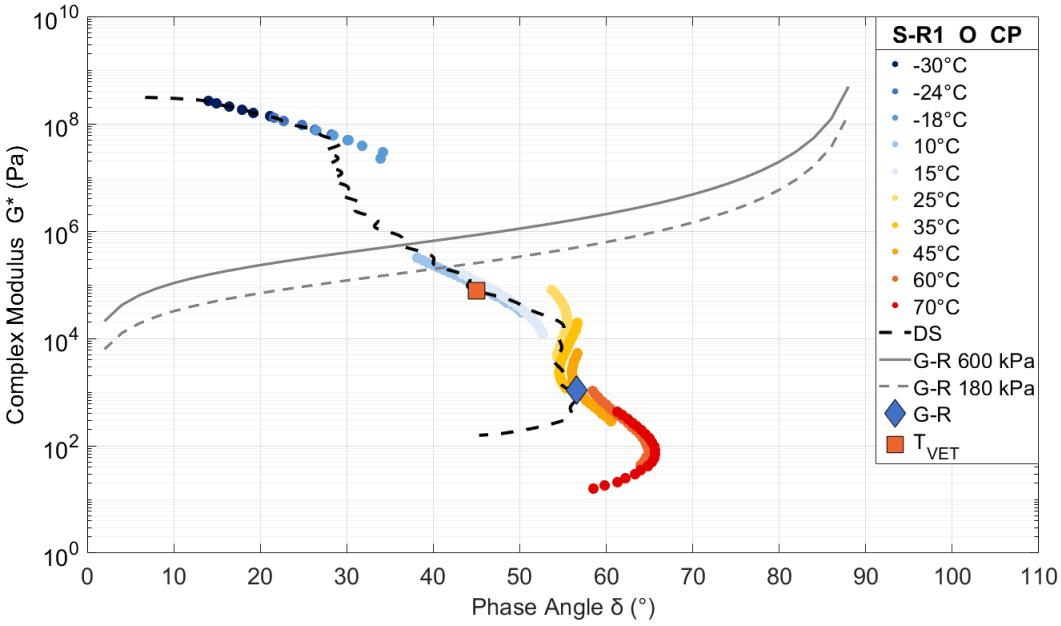

Figure 40: Black Space with the DS model for the S-R1 Original (unaged) CP

S-R1 Aged (Cone Plate)

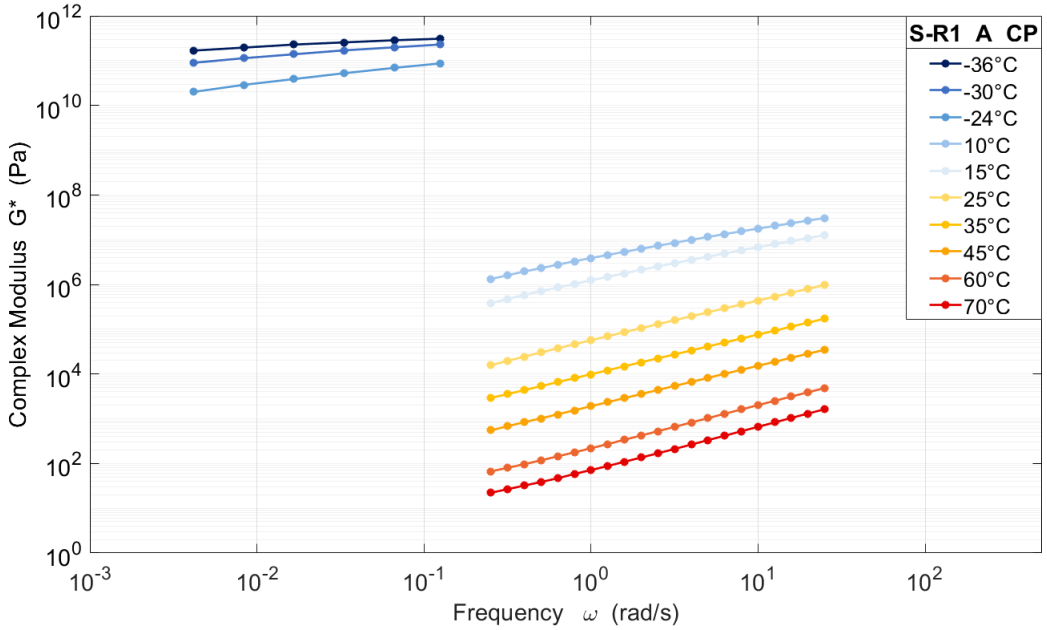

Figure 41: G* vs ω isotherms for the S-R1 Aged CP

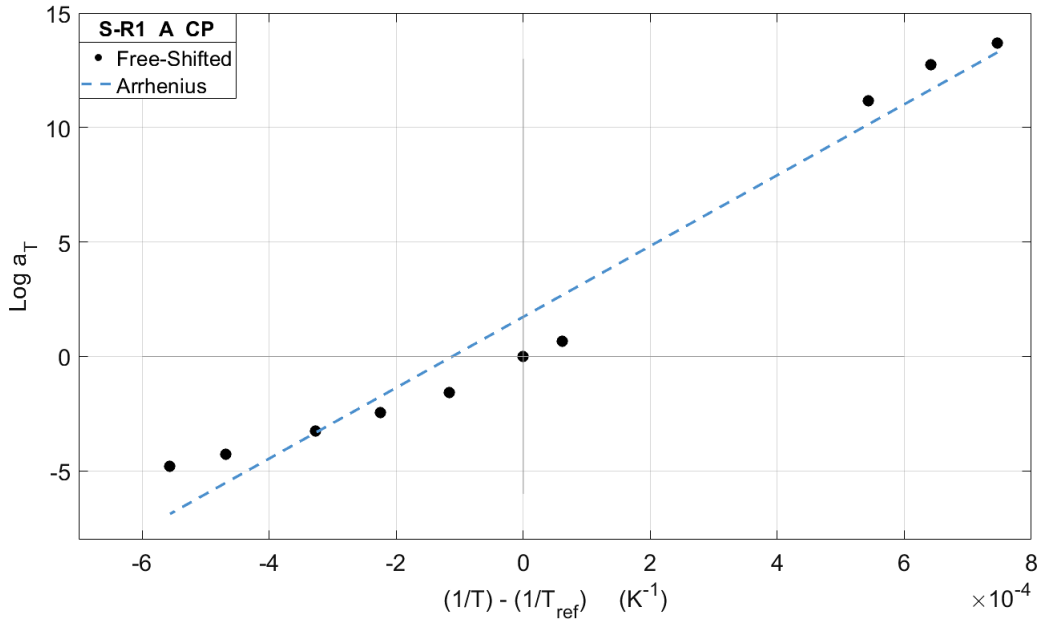

Figure 42: Arrhenius shift factor for the S-R1 Aged CP

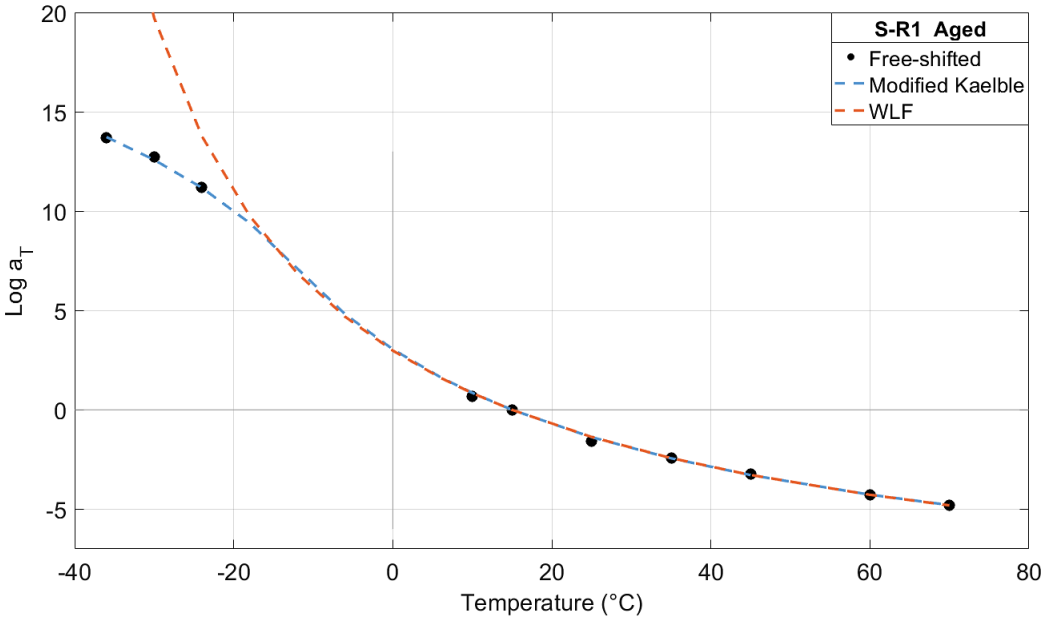

Figure 43: WLF and Modified Kaelble shift factors for the S-R1 Aged CP

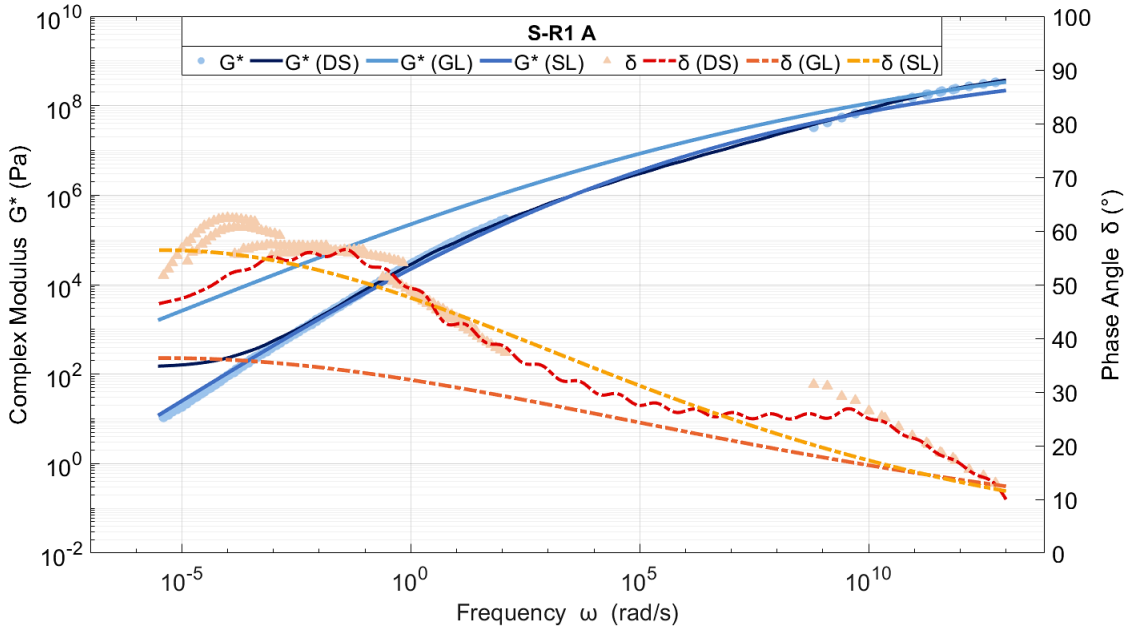

Figure 44: Master Curves with the DS, GL and SL models for the S-R1 Aged CP

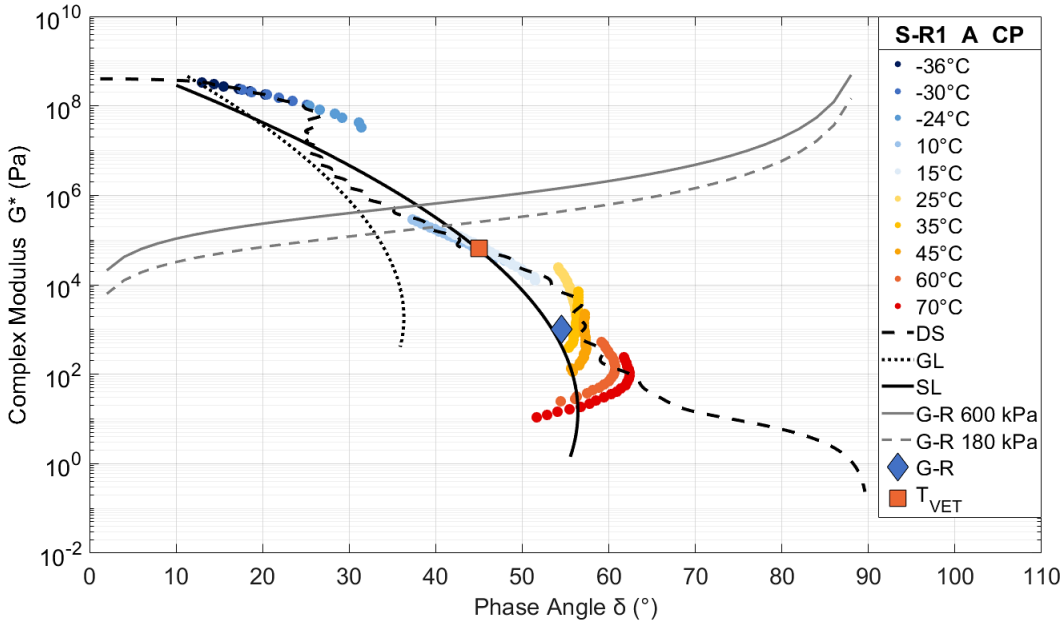

Figure 45: Black Space with the DS, GL and SL model for the S-R1 Aged CP

S-R2 Original (Parallel Plate)

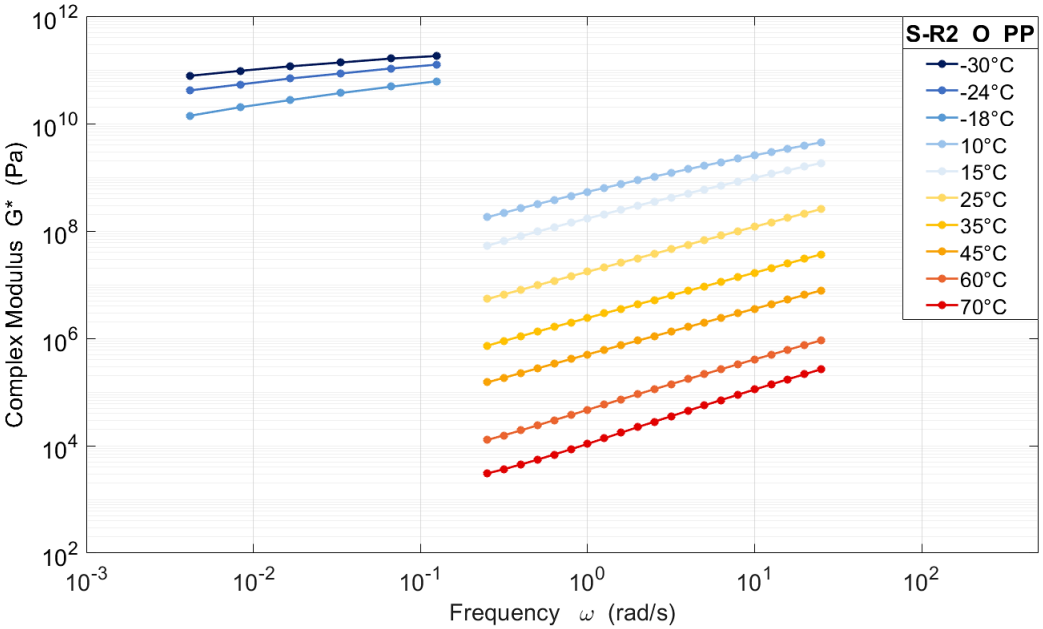

Figure 46: G* vs ω isotherms for the S-R2 Original (unaged) PP

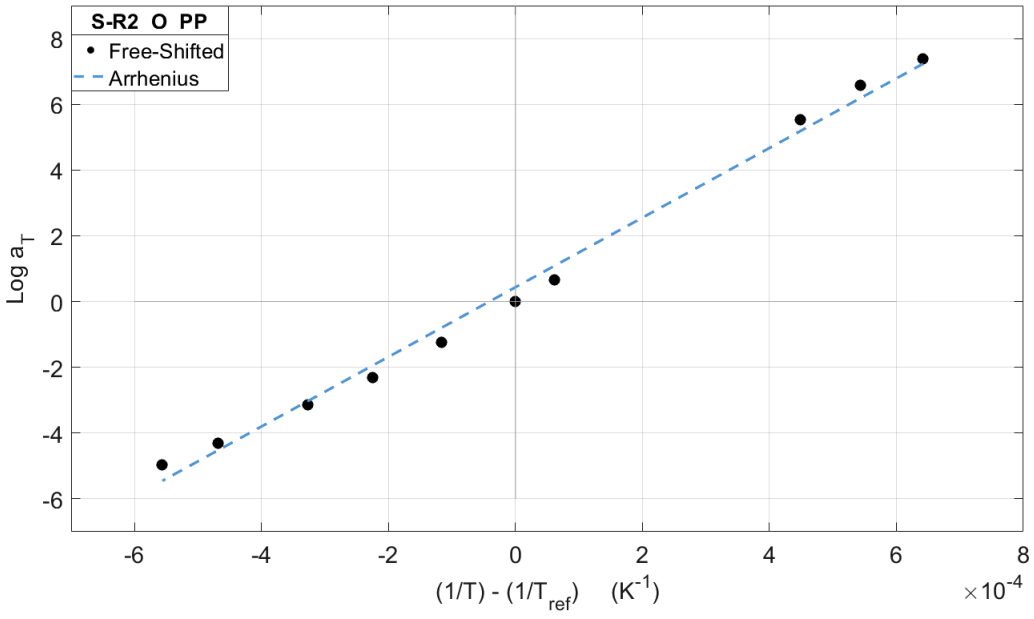

Figure 47: Arrhenius shift factor for the S-R2 Original (unaged) PP

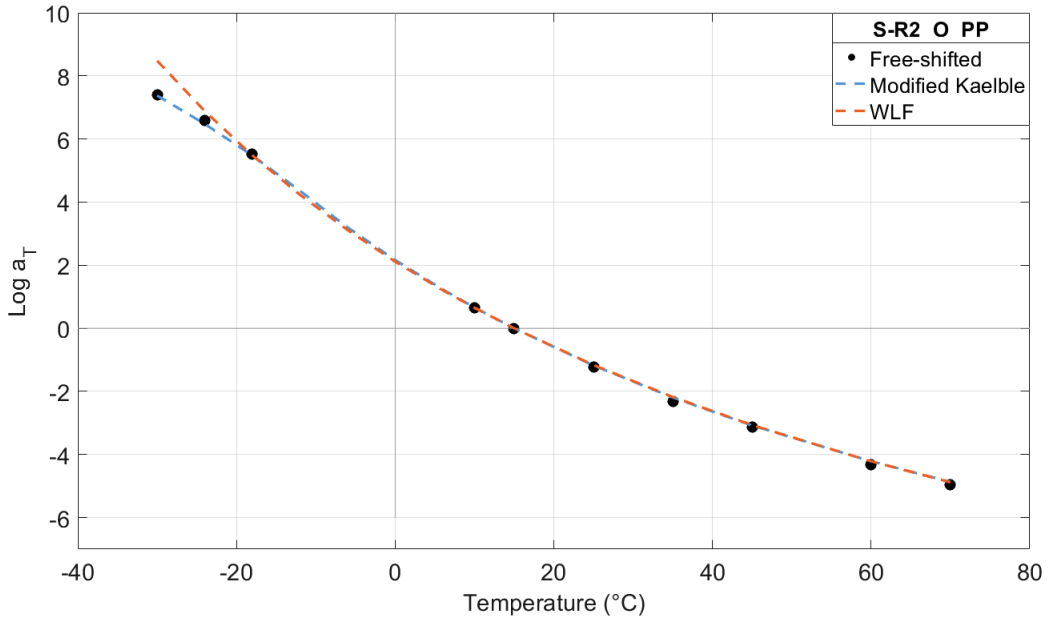

Figure 48: WLF and Modified Kaelble shift factors for the S-R2 Original (unaged) PP

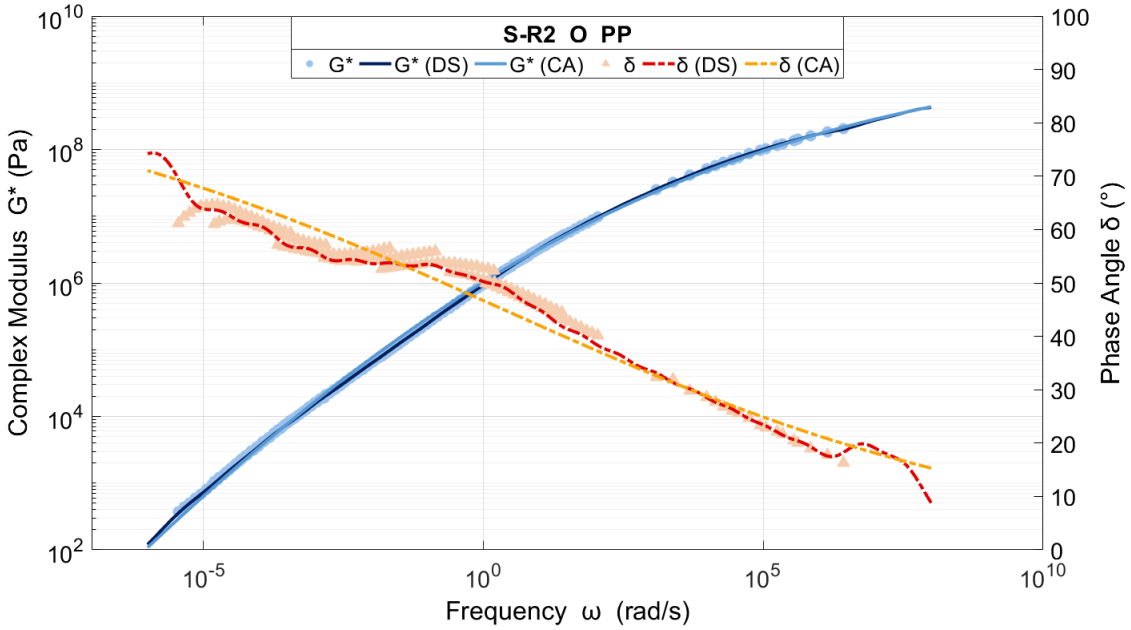

Figure 49: Master Curves with the CA and DS models for the S-R2 Original (unaged) PP

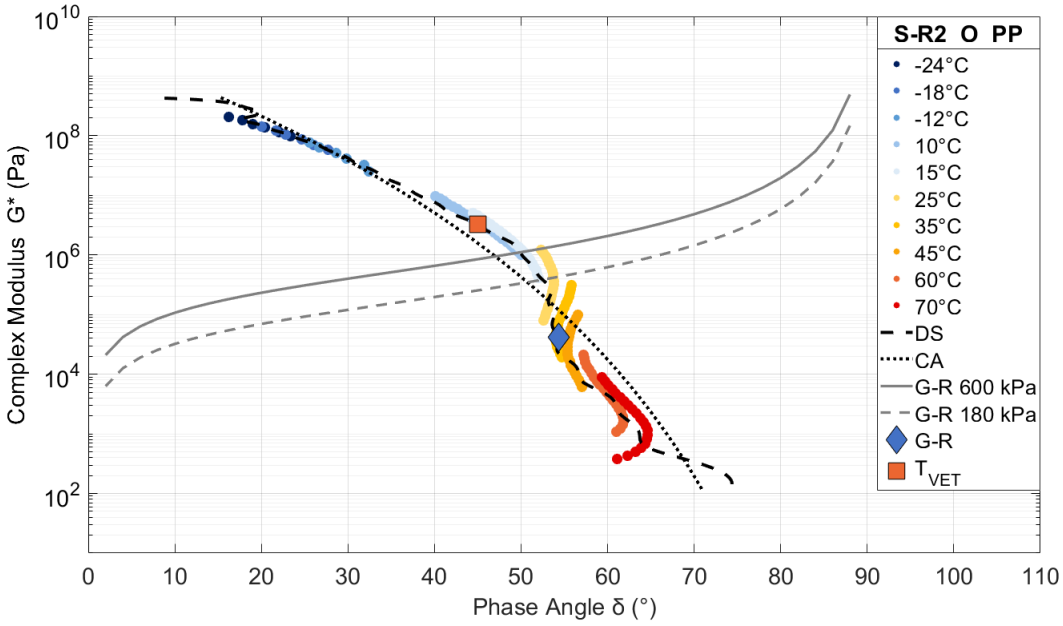

Figure 50: Black Space with the CA and DS models for the S-R2 Original (unaged) PP

S-R2 Original (Cone Plate)

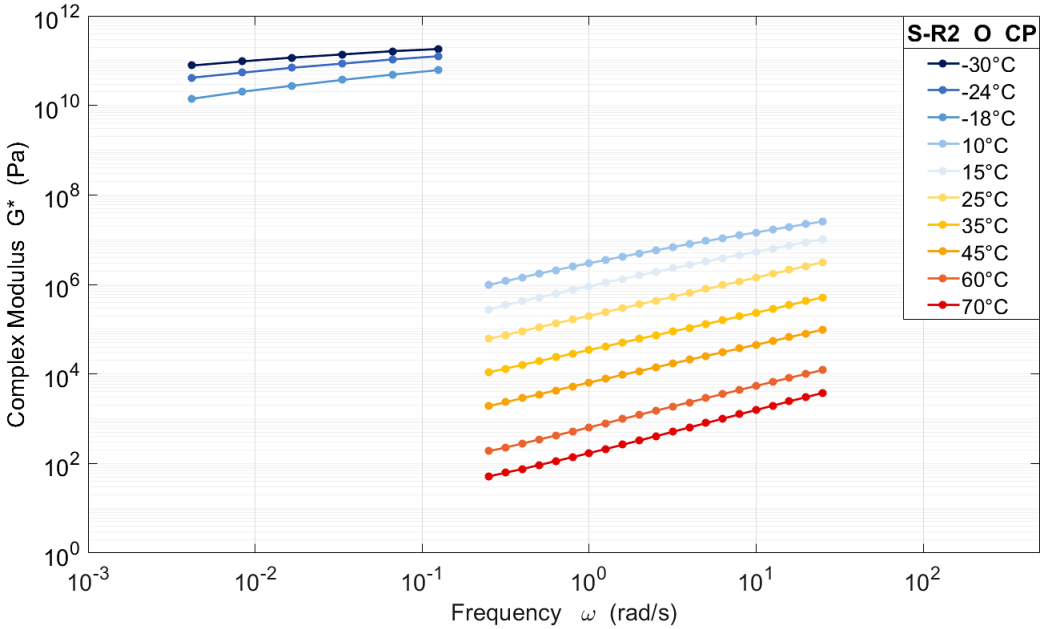

Figure 51: G* vs ω isotherms for the S-R2 Original (unaged) CP

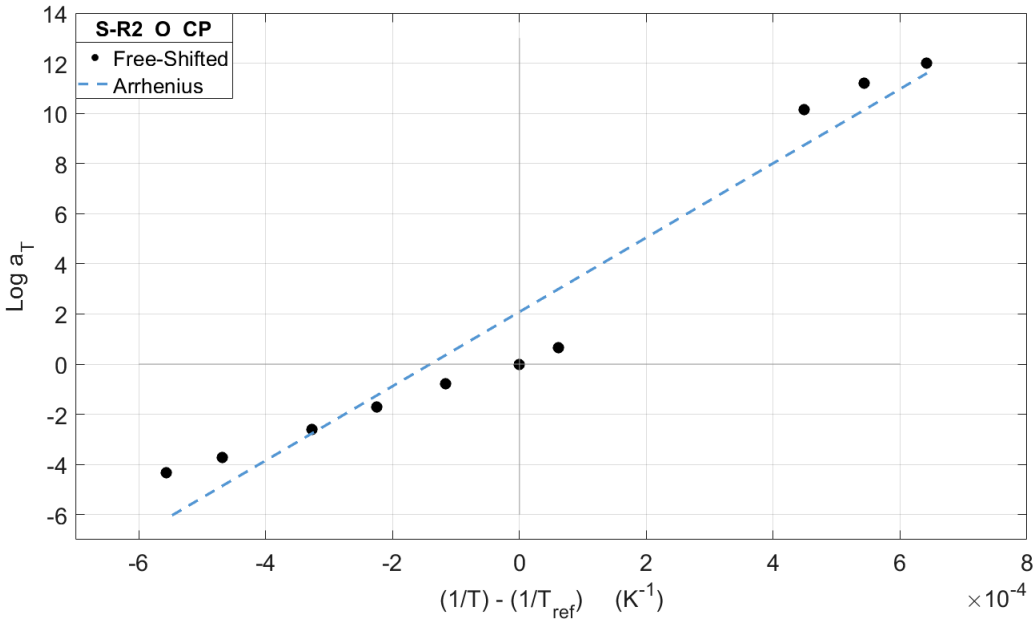

Figure 52: Arrhenius shift factor for the S-R2 Original (unaged) CP

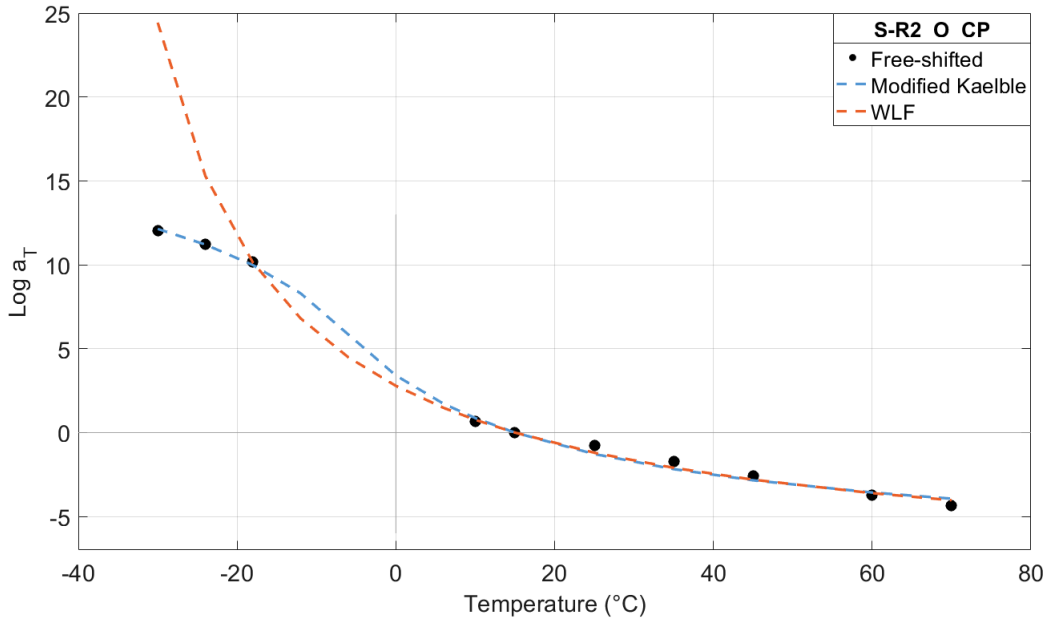

Figure 53: WLF and Modified Kaelble shift factors for the S-R2 Original (unaged) CP

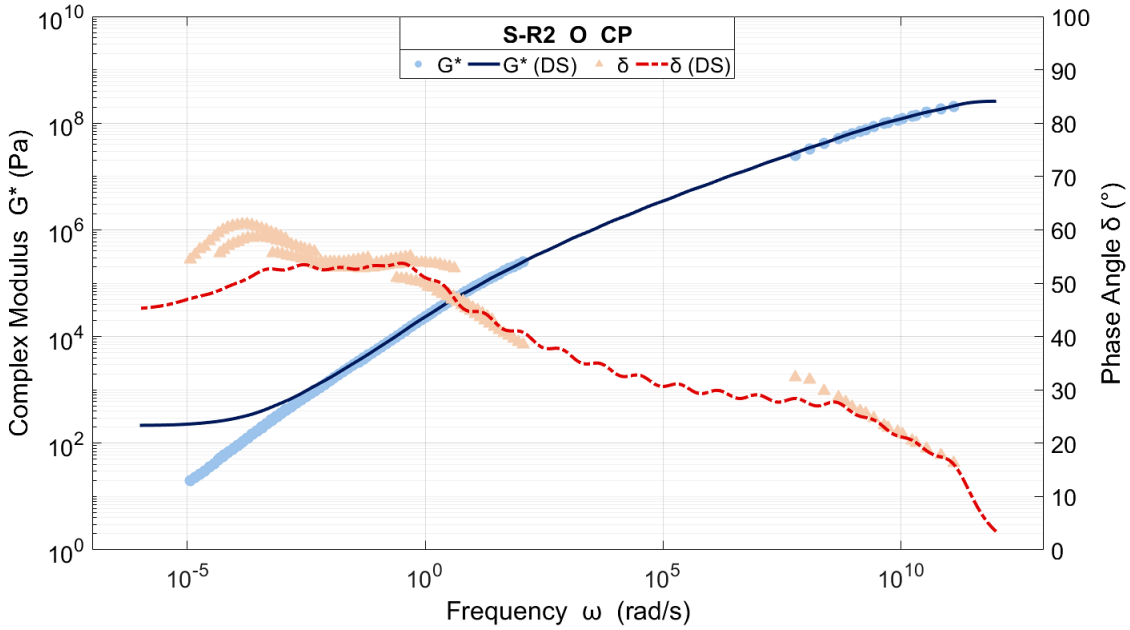

Figure 54: Master Curves with the DS model for the S-R2 Original (unaged) CP

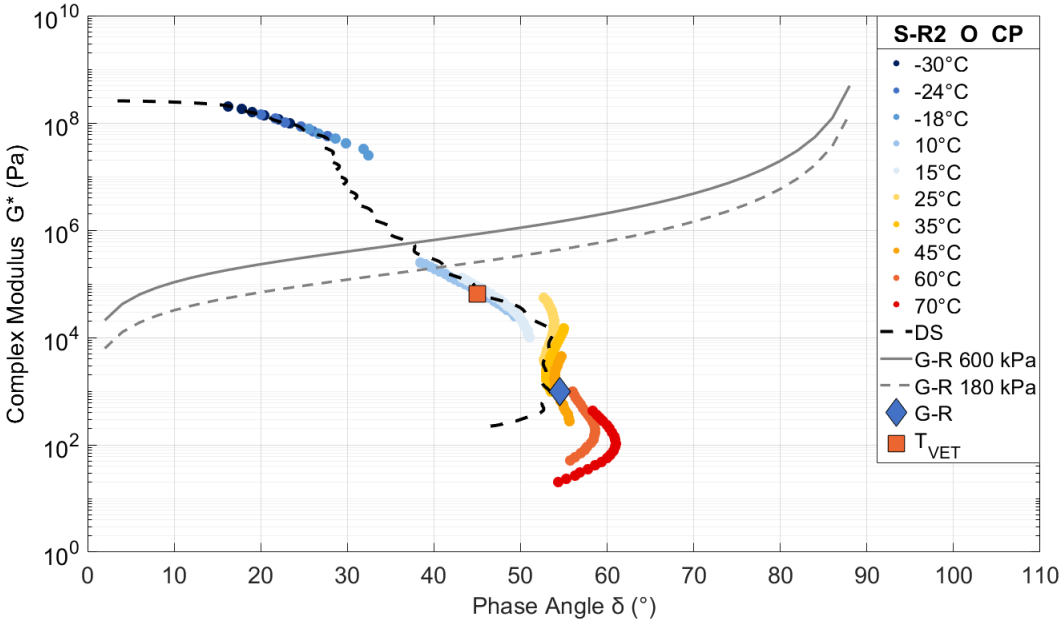

Figure 55: Black Space with the DS model for the S-R2 Original (unaged) CP

S-R2 Aged (Cone Plate)

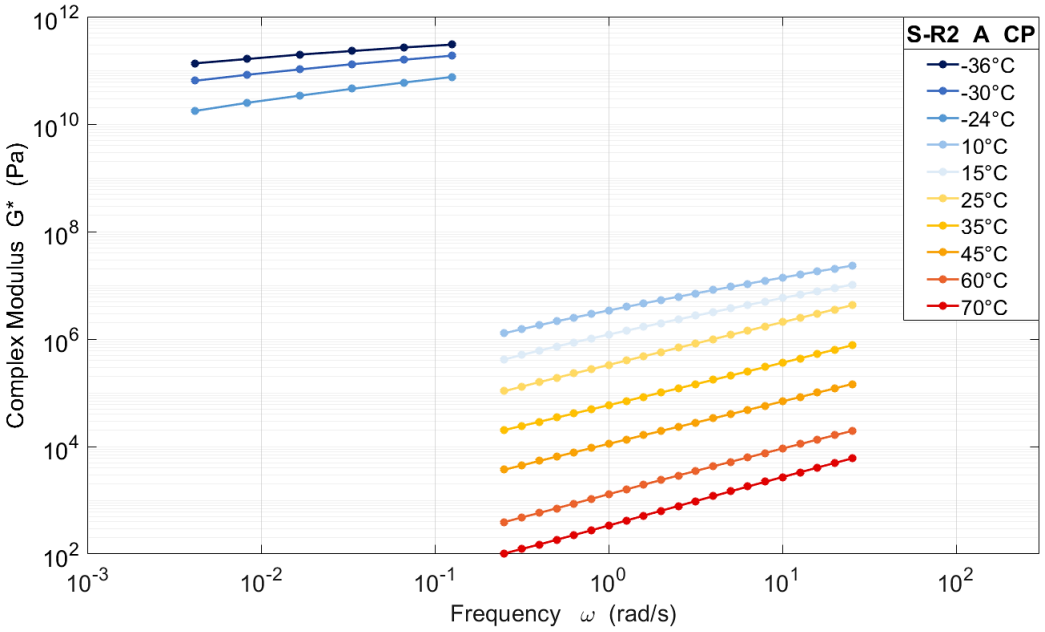

Figure 56: G* vs ω isotherms for the S-R2 Aged CP

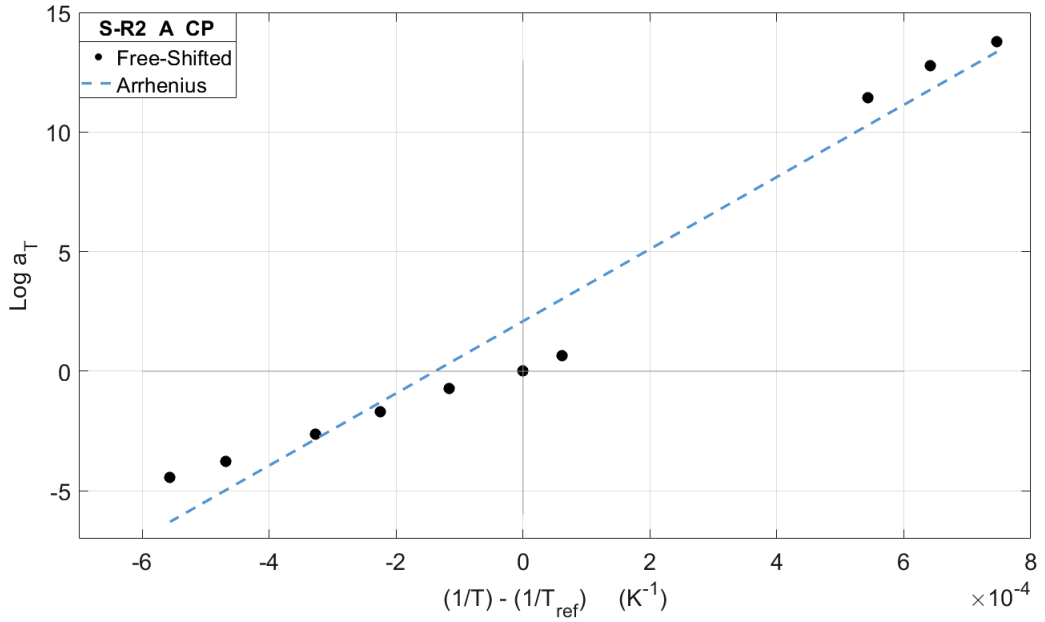

Figure 57: Arrhenius shift factor for the S-R2 Aged CP

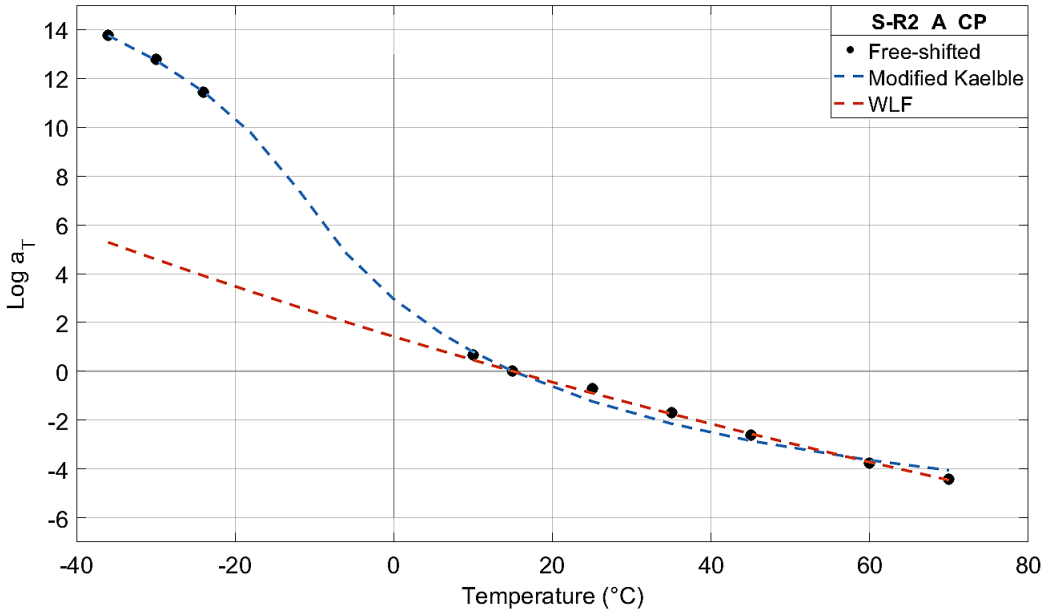

Figure 58: WLF and Modified Kaelble shift factors for the S-R2 Aged CP

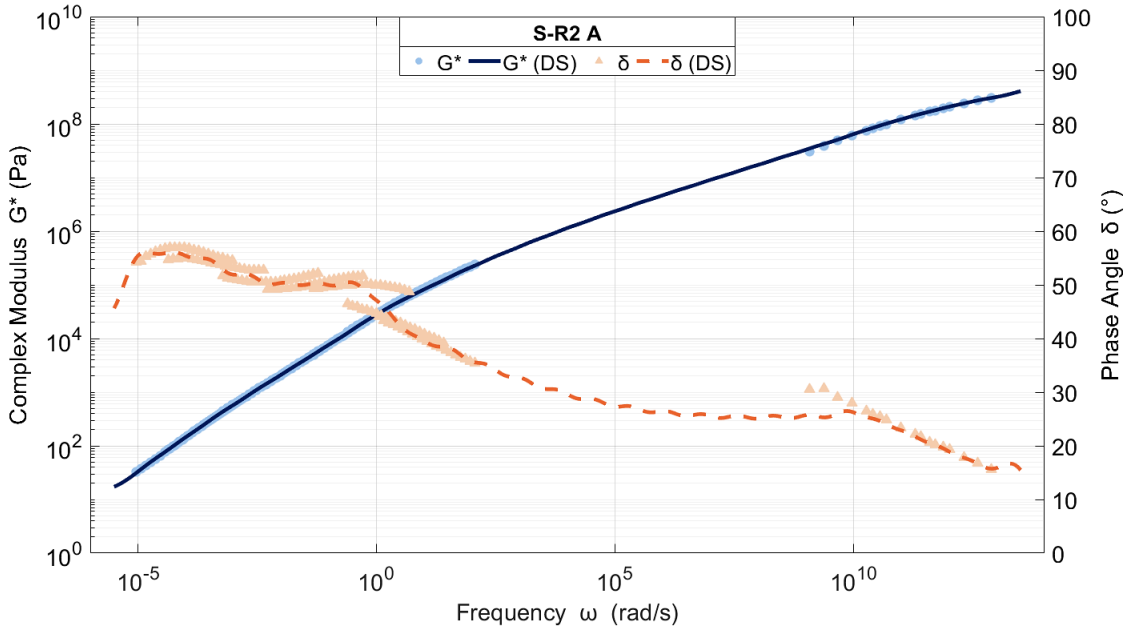

Figure 59: Master Curves with the CA and DS models for the S-R2 Aged CP

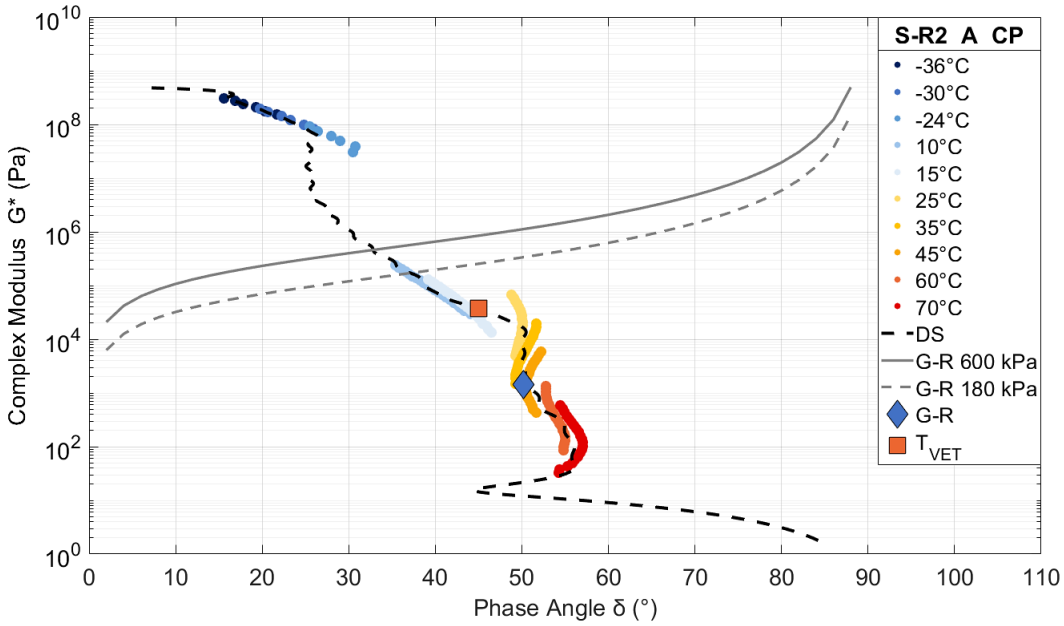

Figure 60: Black Space with the CA and DS models for the S-R1 Aged CP

MSCR

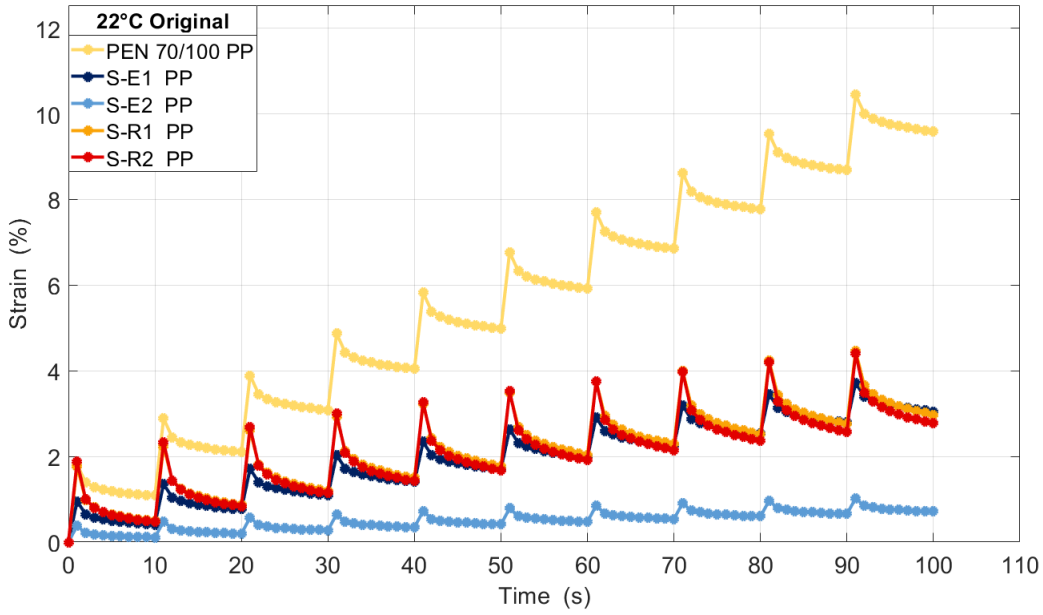

Figure 61: Strain vs time for Original binder at 22°C (only PP)

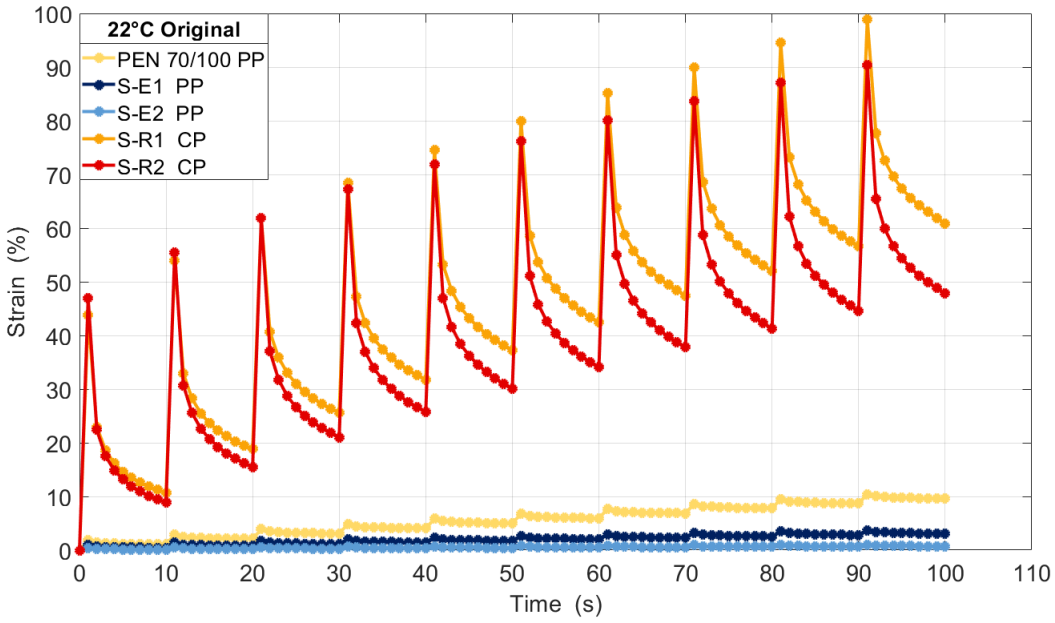

Figure 62: Strain vs time for Original binder at 22°C (PP and CP)

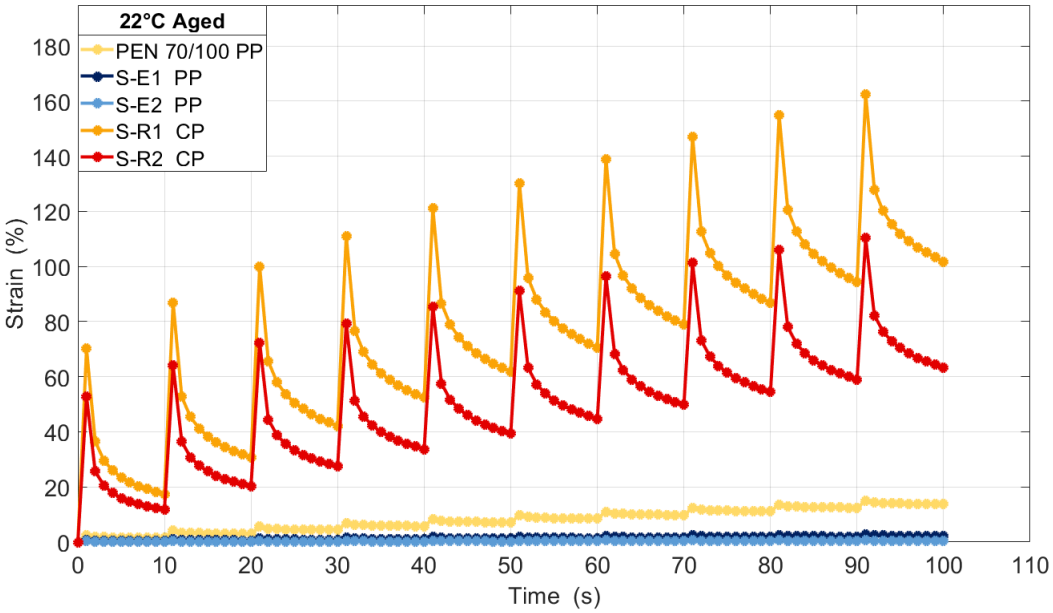

Figure 63: Strain vs time for Aged binder at 22°C

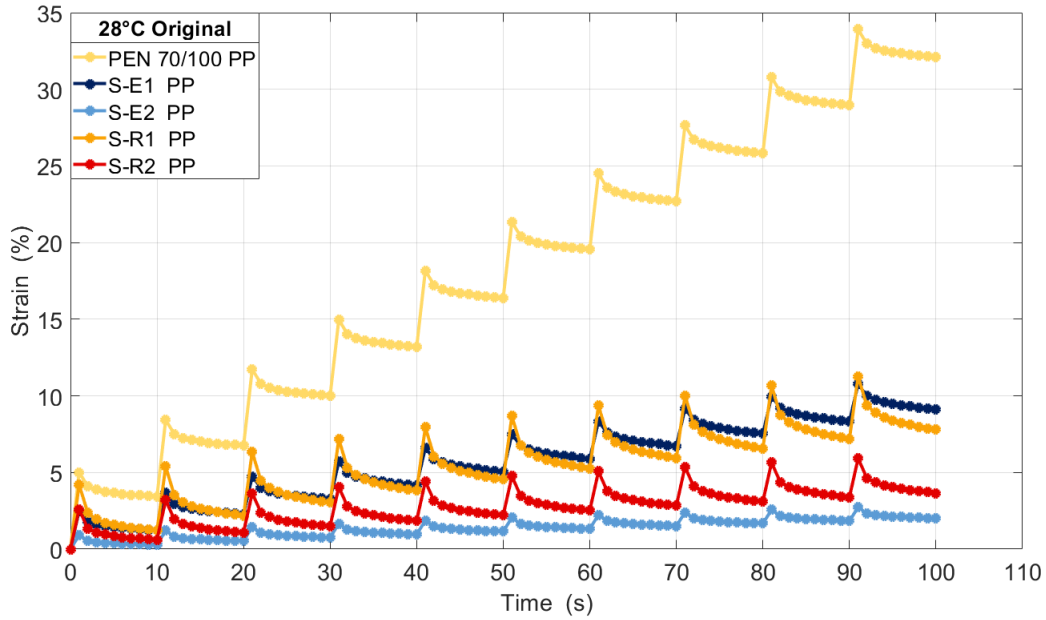

Figure 64: Strain vs time for Original binder at 28°C (only PP)

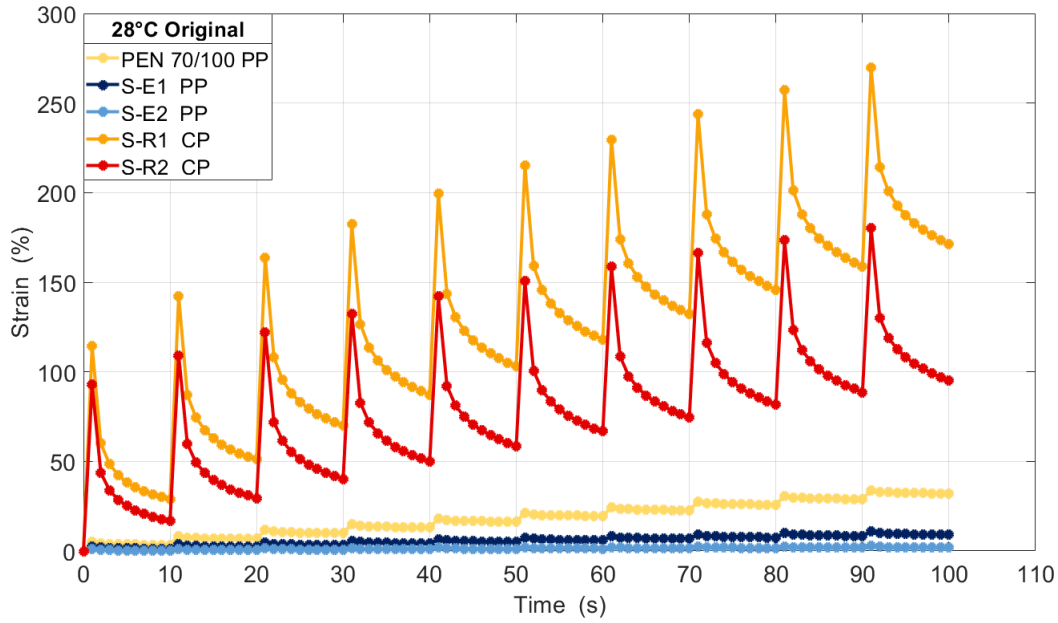

Figure 65: Strain vs time for Original binder at 28°C (PP and CP)

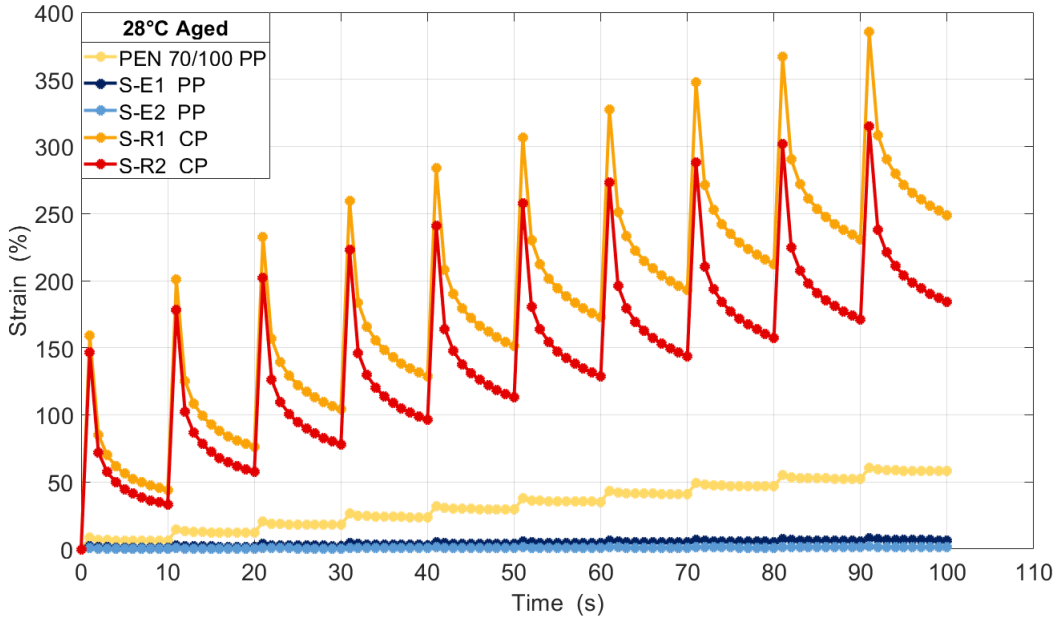

Figure 66: Strain vs time for Aged binder at 28°C

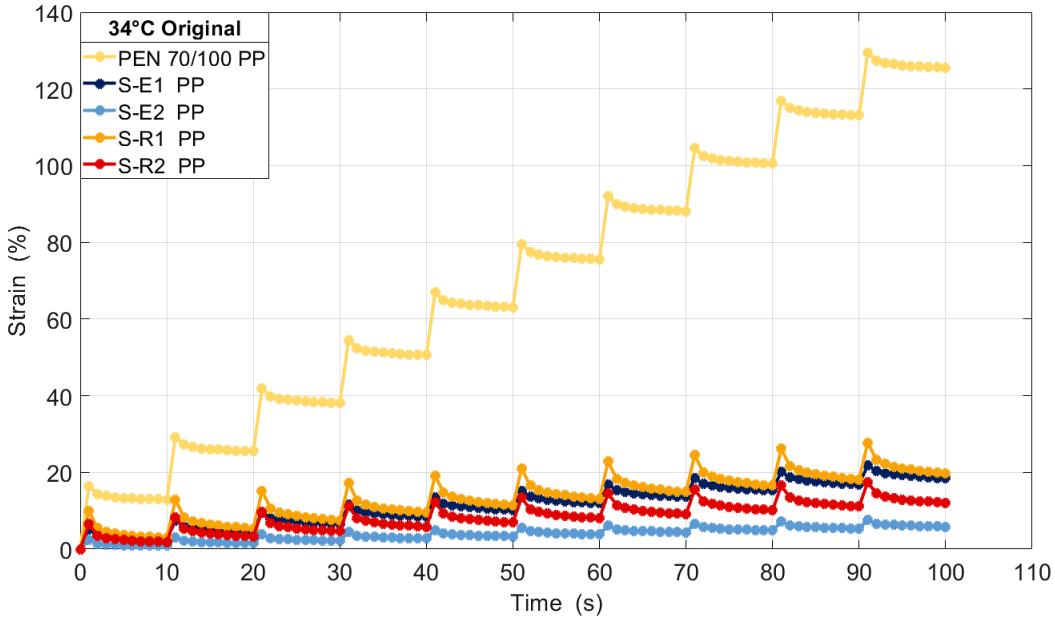

Figure 67: Strain vs time for Original binder at 34°C (only PP)

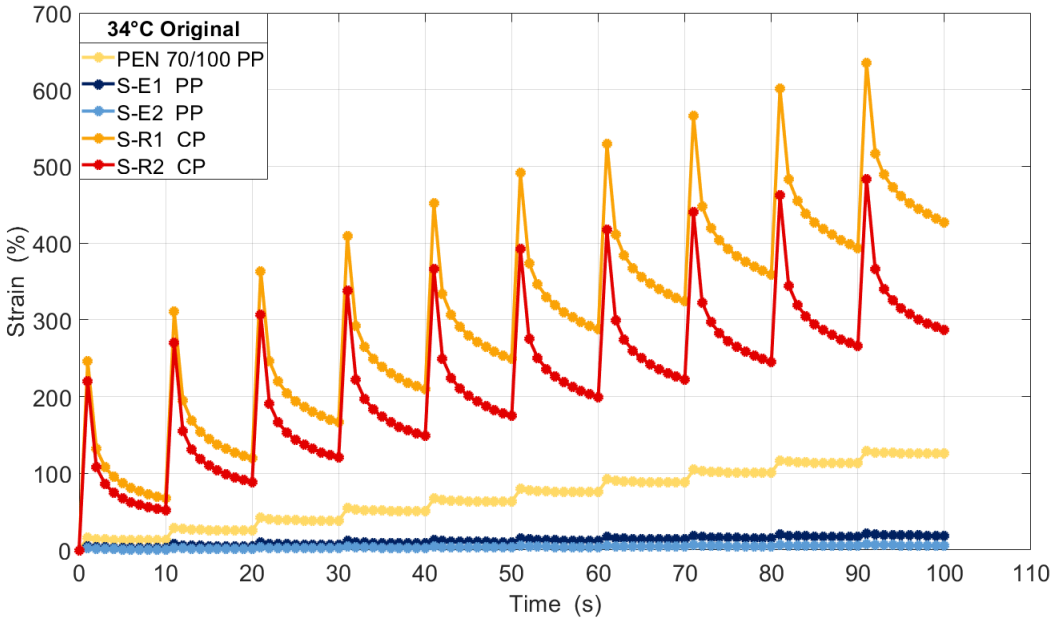

Figure 68: Strain vs time for Original binder at 34°C (PP and CP)

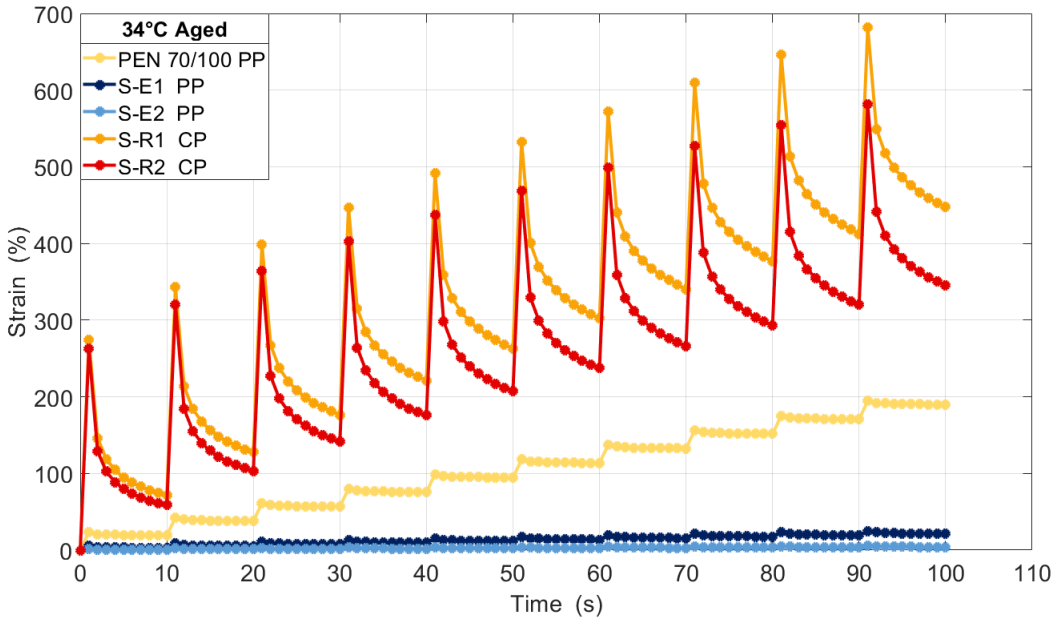

Figure 69: Strain vs time for Aged binder at 34°C